

UC San Diego

UC San Diego Electronic Theses and Dissertations

Title

Feedback, power control, and beamforming : methods for situational aware wireless networks

Permalink

<https://escholarship.org/uc/item/6751g952>

Author

Huang, Yichao

Publication Date

2012

Peer reviewed|Thesis/dissertation

UNIVERSITY OF CALIFORNIA, SAN DIEGO

**Feedback, Power Control, and Beamforming: Methods for Situational
Aware Wireless Networks**

A dissertation submitted in partial satisfaction of the
requirements for the degree
Doctor of Philosophy

in

Electrical Engineering
(Communication Theory and Systems)

by

Yichao Huang

Committee in charge:

Professor Bhaskar D. Rao, Chair
Professor Massimo Franceschetti
Professor Yoav Freund
Professor William S. Hodgkiss
Professor Laurence B. Milstein

2012

Copyright
Yichao Huang, 2012
All rights reserved.

The dissertation of Yichao Huang is approved, and it is acceptable in quality and form for publication on microfilm and electronically:

Chair

University of California, San Diego

2012

DEDICATION

To my family.

EPIGRAPH

*It is no use doing what you like;
you have got to like what you do.*

—Winston Churchill

TABLE OF CONTENTS

Signature Page	iii
Dedication	iv
Epigraph	v
Table of Contents	vi
List of Figures	ix
List of Tables	xii
Acknowledgements	xiii
Vita	xvi
Abstract of the Dissertation	xix
Chapter 1	Introduction 1
	1.1 Contributions of the Dissertation 3
	1.1.1 Adaptive Feedback Design Based on Spectral Channel Statistics 3
	1.1.2 Analytical Framework for Heterogeneous Feedback Being Aware of User Densities 3
	1.1.3 Random Beamforming with Heterogeneous Users and Selective Feedback 4
	1.1.4 Outage Balancing Based on Spatial Channel Statistics 5
	1.1.5 Efficient Algorithm Design Being Aware of Large System Structure 5
	1.2 Dissertation Outline 6
Chapter 2	Adaptive Feedback Based on Spectral Channel Statistics 8
	2.1 Introduction 8
	2.2 System Model 12
	2.2.1 Motivation for Heterogeneous Partial Feedback 12
	2.2.2 Multi-Cluster Subband Fading Model 16
	2.3 Perfect Feedback 17
	2.3.1 Derivation of Average Sum Rate 17
	2.3.2 Sum Rate Ratio and Best-M 21
	2.4 Imperfect Feedback 22
	2.4.1 Imperfect Feedback Model 22

	2.4.2	Fix Rate Strategy	24
	2.4.3	Variable Rate Strategy	25
	2.4.4	Optimization and Adaptation to Imperfections	29
2.5		Numerical Results	31
	2.5.1	Perfect Feedback Scenario	31
	2.5.2	Imperfect Feedback Scenario	35
2.6		Conclusion	37
2.7		Appendices	39
	2.7.1	Appendix A	39
	2.7.2	Appendix B	40
Chapter 3		Analytical Framework for Heterogeneous Feedback Being Aware of User Densities	44
	3.1	Introduction	44
	3.2	System Model	48
	3.3	General Sum Rate Analysis	49
	3.4	Exact Performance Analysis	54
	3.4.1	The Statistics of CQI	54
	3.4.2	Procedures to Compute $\mathcal{G}_k(\epsilon)$	55
	3.5	Asymptotic Performance Analysis	58
	3.5.1	The Type of Convergence	59
	3.5.2	Asymptotic Rate Approximation	60
	3.5.3	Determining the Minimum Required Partial Feed- back	66
	3.6	Numerical Results	67
	3.7	Conclusion	72
	3.8	Appendices	73
	3.8.1	Appendix C	73
	3.8.2	Appendix D	77
Chapter 4		Random Beamforming with Heterogeneous Users and Selective Feedback	83
	4.1	Introduction	83
	4.2	System Model	86
	4.3	Full Feedback Analysis	88
	4.3.1	Scheduling Policy and Individual Sum Rate	88
	4.3.2	Individual Scaling Laws	91
	4.4	Selective Feedback in the Spatial Dimension	92
	4.4.1	Individual Sum Rate	92
	4.4.2	Individual Scaling Laws	96
	4.5	Selective Feedback in Both Spatial and Spectral Dimension	98
	4.5.1	System Model	98
	4.5.2	Individual Sum Rate	99

	4.5.3 Individual Scaling Laws	101
	4.6 Conclusion	105
	4.7 Appendices	106
	4.7.1 Appendix E	106
	4.7.2 Appendix F	107
	4.7.3 Appendix G	108
Chapter 5	Outage Balancing Based on Spatial Channel Statistics	110
	5.1 Introduction	110
	5.2 System Model	112
	5.3 Problem Analysis	114
	5.3.1 Problem Manipulation	114
	5.3.2 Optimal Solution Under Fixed Beamformer	115
	5.4 Joint Beamforming and Power Control	117
	5.4.1 Problem Observation	117
	5.4.2 Near-Optimal Solution	118
	5.4.3 Algorithm Design	120
	5.5 Numerical Results	120
	5.6 Conclusion	122
	5.7 Appendices	124
	5.7.1 Appendix H	124
	5.7.2 Appendix I	124
Chapter 6	Efficient Algorithm Design Being Aware of Large System Struc- ture	128
	6.1 Introduction	128
	6.2 System Model	131
	6.3 Finite System Analysis	133
	6.3.1 Problem Reformulation	133
	6.3.2 Network Duality and Algorithm Design	134
	6.4 Large System Analysis	137
	6.4.1 Asymptotic Analysis for the Dual Network	138
	6.4.2 Asymptotic Analysis for the Primal Network . . .	141
	6.5 Numerical Results	144
	6.6 Conclusion	148
	6.7 Appendices	149
	6.7.1 Appendix J	149
	6.7.2 Appendix K	150
Chapter 7	Concluding Remarks	158
Bibliography	162

LIST OF FIGURES

Figure 2.1:	Comparison of average sum rate for different subband sizes ($\eta = 1, 2, 4$) and partial feedback ($M = 2, 4$) with respect to the number of users.	14
Figure 2.2:	Illustration of the multi-cluster subband fading channel model for two different clusters with 16 resource blocks. The subband sizes equal 2 and 4 for the two different clusters respectively. . .	15
Figure 2.3:	Calculating the average goodput from numerical evaluation ($M = 2, 4, 16$) and Jensen approximation ($M = 16$) for the variable rate scenario under different ρ	28
Figure 2.4:	Comparison of the required minimum M between numerically solving (2.17) and using approximation (2.19) under different γ with respect to the number of users.	31
Figure 2.5:	Computing the required minimum M with respect to different number of users when varying the ratio of the number of users in cluster \mathcal{K}_1	32
Figure 2.6:	Comparison of the average sum rate for a 4-cluster system under different feedback strategies with respect to the number of users.	33
Figure 2.7:	Comparison of average goodput between fixed rate and variable rate strategies under normalized parameter β ($\beta = \beta_1 = \beta_0/10$) for different number of users K	34
Figure 2.8:	Comparison of average outage probability between fixed rate and variable rate strategies under normalized parameter β ($\beta = \beta_1 = \beta_0/10$) for different number of users K	35
Figure 2.9:	The optimal fix rate parameter β_0 with respect to channel estimation error (σ_w^2) and feedback delay (α).	36
Figure 2.10:	The optimal variable rate parameter β_1 with respect to channel estimation error (σ_w^2) and feedback delay (α).	37
Figure 2.11:	Comparison of the average goodput for a 4-cluster system with fix rate and variable rate strategies using optimized β_0^* and β_1^*	38
Figure 3.1:	Illustration of a generic OFDMA-based multicell heterogeneous cellular networks. Each cell has users associated with it. One selected user for transmission in one resource block is shown: solid line (desired signal); dashed line (potential intercell interference).	49
Figure 3.2:	Comparison of the sum rate for best-M feedback obtained using the exact analysis and the asymptotic analysis under different symmetric large scale effects for different M with respect to the number of users: the one-dominant interference limited case ($\rho \triangleq \frac{\rho^{(0)}}{\rho^{(1)}}$).	65

Figure 3.3:	Comparison of the sum rate for best-M feedback obtained using the exact analysis and the asymptotic analysis under different symmetric large scale effects for different M with respect to the number of users: the noise limited case ($\rho \triangleq \rho^{(0)}$).	66
Figure 3.4:	The sum rate comparison of the three scheduling policies: the greedy policy, the round robin policy, and the CDF-based policy under best-M partial feedback strategy with respect to the associated users in a macrocell ($N = 16; M = 4$).	68
Figure 3.5:	The system fairness comparison of the three scheduling policies: the greedy policy, the round robin policy, and the CDF-based policy under best-M partial feedback strategy with respect to the associated users in a macrocell ($N = 16; M = 4$).	69
Figure 3.6:	Comparison of the individual sum rate obtained from simulation, analytical result, and asymptotic approximation for different partial feedback M with respect to the number of associated users for a randomly selected user in macrocell ($N = 16; M = 2, 4, 16$).	70
Figure 3.7:	Comparison of the minimum required M obtained from exact analysis and asymptotic analysis under different thresholds ($\eta = 0.9, 0.99$).	71
Figure 3.8:	Comparison of the total number of required partial feedback from exact analysis and asymptotic analysis under threshold $\eta = 0.9$	72
Figure 4.1:	Comparison of the exact CDF F_{Y_k} with the Fréchet upper bound and the negative association upper bound for spatial dimension selective feedback ($M = 4, \rho_k = 10$ dB).	94
Figure 4.2:	Comparison of the exact individual sum rate and the approximated one for a given user with different M and ρ_k with respect to the number of users ($M = 2, 4, \rho_k = 0$ dB, 10 dB, 20 dB).	95
Figure 4.3:	Illustration of the spatial and spectral dimension selective feedback and the scheduling result in an OFDMA system (different colors denote different users $K = 9, N = 5$ resource blocks, $M = 4$ beams, the spectral dimension selective feedback $L = 2$).	97
Figure 4.4:	Comparison of the exact individual sum rate and the approximated one for a given user with different spectral dimension selective feedback L with respect to the number of users ($M = 4, N = 10, \rho_k = 10$ dB, $L = 1, 2, 4, 10$).	102
Figure 4.5:	Comparison of the exact individual sum rate and the approximated one for a given user with different spectral dimension selective feedback L with respect to different ρ_k ($M = 4, N = 10, K = 20, L = 1, 2, 4, 10$).	103

Figure 4.6:	Comparison of the exact CDF F_{W_k} and its tail equivalence for different spectral dimension selective feedback L ($M = 4$, $N = 10$, $\rho_k = 10$ dB, $L = 1, 2, 4, 10$).	104
Figure 5.1:	Convergence result of the primal network transmit power for different users ($K = 4$, $N = 4$, $\bar{P} = 1$ W, SINR Threshold = -5 dB).	121
Figure 5.2:	Convergence result of the outage probability for different users ($K = 4$, $N = 4$, $\bar{P} = 1$ W, SINR Threshold = -5 dB).	122
Figure 5.3:	The effect of total power and the SINR threshold on the maximum outage probability in the network ($K = 4$, $N = 4$, SINR Threshold = $-10, -5, 0, 5$ dB).	123
Figure 6.1:	Convergence plot of the primal network power in a finite system setting employing Algorithm 6.1: ($N = 4$, $K = 4$, $J = 3$, $\bar{P} = 10$ Watt). Different marker types represent different users.	144
Figure 6.2:	Convergence plot of the primal network weighted SINR in a finite system setting employing Algorithm 6.1: ($N = 4$, $K = 4$, $J = 3$, $\bar{P} = 10$ Watt). Different marker types represent different users.	145
Figure 6.3:	Convergence plot of the primal network weighted SINR in a large system setting employing Algorithm 6.5: ($N = 50$, $K = 40$, $J = 3$, $\bar{P} = 10$ Watt). The SINR for different users are not differentiated, but use the same line style for illustration.	146
Figure 6.4:	The achieved primal network SINR for each individual user using the asymptotically optimal beamformer in a large system setting for one channel realization: ($N = 50$, $K = 40$, $J = 3$, $\bar{P} = 10$ Watt). The mean of the achieved SINR using asymptotically optimal beamformer averaged over users and the the achieved SINR using the optimal beamformer are illustrated for comparison.	147
Figure 6.5:	Comparison of the average achieved primal network SINR using asymptotically optimal beamformer and the optimal beamformer in a finite system setting with respect to different values of the power constraint \bar{P} : ($N = 4$, $K = 3$, $J = 3$).	148

LIST OF TABLES

Table 5.1: Algorithm 5.1–Decentralized algorithm to compute the optimal solution under fixed beamformer	126
Table 5.2: Algorithm 5.2–Decentralized algorithm to compute the optimal solution for (5.16)	127
Table 6.1: Algorithm 6.1–Max-min weighted SINR for multicell downlink . .	154
Table 6.2: Algorithm 6.2–Computation of $\hat{\phi}$ given $\hat{\mathbf{q}}$	155
Table 6.3: Algorithm 6.3–Computation of $\hat{\mathbf{q}}$ given $\hat{\phi}$	155
Table 6.4: Algorithm 6.4–Computation of $\hat{\mathbf{p}}$ given $\hat{\mathbf{q}}$ and $\hat{\phi}$	156
Table 6.5: Algorithm 6.5–Computation of $\hat{\mathbf{p}}$ and $\hat{\mathbf{q}}$ for multicell downlink .	157

ACKNOWLEDGEMENTS

First and foremost, I am deeply indebted to my advisor Professor Bhaskar D. Rao for his extreme patience at the beginning, his tireless encouragement throughout the duration of my Ph.D. journey, and his invaluable insight on my thesis topic. His thoughtfulness, dedication, and guidance have made this dissertation a reality. He provided me with the freedom to pursue research topics of my interest, and helped me grow up from a wandering graduate student to a professional researcher. It has been a great pleasure working under his supervision.

I am very thankful to other members on my Ph.D. committee, Professor Massimo Franceschetti, Professor Yoav Freund, Professor William S. Hodgkiss and Professor Laurence B. Milstein. I have been fortunate to have these tremendous teachers and researchers in my committee, and I enjoyed your colorful and insightful lectures. I would also like to express my gratitude to my undergraduate advisor Professor Chunming Zhao who taught me how to appreciate coding theory and provided me with the motivation to pursue a Ph.D.

It is a great pleasure to thank Professor Chee Wei Tan for his collaboration and his deep insight on optimization. I would like to express my gratitude to Professor Mung Chiang for his thoughtful host during my visiting at Princeton. I would like to thank Dr. Zhongren Cao for sharing his expertise on channel estimation at Calit2. I would also like to thank my mentors during my internships at Qualcomm, Dr. Alan Barbieri, Dr. Tingfang Ji, Dr. Yongbin Wei, Dr. Damanjit Singh, Dr. Chirag Patel and Dr. Rajat Prakash. I cherish the great opportunity to link my theoretical knowledge with practical wireless systems and I am grateful for all their supports, help, and career advices.

I gained many helpful insights and analytical perspectives from many senior lab-mate, Yogananda Isukapalli, Matthew Pugh, Seong-Ho Hur, Eddy Kwon and Liwen Yu. I would like to thank Anh Nguyen for his collaboration. I am also thankful to my lab fellows in the research group, Sagnik Ghosh, Yuzhe Jin, Nandan Das, Sheu-Sheu Tan, Alireza Masnadi-Shirazi, Zhilin Zhang, Furkan Kavasoğlu, PhuongBang Nguyen, Xiaofei Chen and Oleg Tanchuk for many constructive discussions in our group meeting. I am lucky to know many friends from ECE dur-

ing my stay in UCSD and it is my pleasure to meet Jun Zhou, Lelin Zhang, Shiyu Song, Yu Xiang, Weixin Li, Lele Wang, Minghai Qin, Dawei Wang, Chiao-Yi Chen, Ting-Lan Lin and Ashish Tawari. I am especially thankful to Feng Lu and Minghui Zhu for being incredible friends, their support, and both technical and non-technical conversations.

I owe my deep gratitude to my parents, my parents-in-law, and my family for their endless love and their unconditional support. Mom and dad, I owe everything to you and none of my dreams could be achieved without your belief, encouragement and sacrifice during all these years. I want to thank my grandmother-in-law, to whom I dedicate this dissertation, for bringing me up and teaching me about honesty and responsibility. Finally, to my loving wife, Dongyan, I am thankful beyond words for her invaluable love, company and support. I would not be where I am today without you.

This work was supported by Ericsson endowed chair funds, the Center for Wireless Communications, UC Discovery grant com09R-156561 and NSF grant CCF-1115645.

This dissertation is a collection of papers that were published or submitted for publication. The text of Chapter 2, in part, is a reprint of the paper, Y. Huang and B. D. Rao, “Performance analysis of heterogeneous feedback design in an OFDMA downlink with partial and imperfect feedback”, *IEEE Transactions on Signal Processing*, *accepted, to appear*, 2012. The text of Chapter 3, in part, is a reprint of the paper, Y. Huang and B. D. Rao, “An analytical framework for heterogeneous partial feedback design in heterogeneous multicell OFDMA networks”, *IEEE Transactions on Signal Processing*, *accepted, to appear*, 2012. The text of Chapter 3, in part, is a reprint of the paper, Y. Huang and B. D. Rao, “Random beamforming with heterogeneous users and selective feedback: individual sum rate and individual scaling laws”, *IEEE Transactions on Wireless Communications*, *submitted*, 2012. The text of Chapter 4, in part, is a reprint of the paper, Y. Huang, C. W. Tan and B. D. Rao, “Outage balancing in multiuser MISO networks: network duality and algorithms”, *IEEE Global Communications Conferences (Globecom)*, Anaheim, CA, Dec. 2012. The text of Chapter 5, in part, is

a reprint of the paper, Y. Huang, C. W. Tan, and B. D. Rao, “Joint beamforming and power control in coordinated multicell: max-min duality, effective network and large system transition”, *IEEE Transactions on Wireless Communications*, *minor revision, revised*, 2012. The dissertation author is the primary researcher and author, and the co-authors listed in these publications contributed to or supervised the research which forms the basis of this dissertation.

VITA

- 2008 B.Eng., Information Engineering
Southeast University, Nanjing, China
- 2010 Research Assistant
California Institute for Telecommunications and Information
Technology, La Jolla, CA
- 2010 M.S.
Electrical Engineering (Communication Theory and Systems)
University of California, San Diego, La Jolla, CA
- 2011 Intern
Qualcomm, Corporate R&D, San Diego, CA
- 2012 Visiting Student
Department of Electrical Engineering
Princeton University, Princeton, NJ
- 2012 Intern
Qualcomm, Corporate R&D, San Diego, CA
- 2008-2012 Research Assistant
Department of Electrical and Computer Engineering
University of California, San Diego, La Jolla, CA
- 2012 Doctor of Philosophy
Electrical Engineering (Communication Theory and Systems)
University of California, San Diego, La Jolla, CA

PUBLICATIONS

Journal Publications

Y. Huang and B. D. Rao, “An analytical framework for heterogeneous partial feedback design in heterogeneous multicell OFDMA networks”, *IEEE Transactions on Signal Processing*, *accepted, to appear*, 2012.

Y. Huang and B. D. Rao, “Performance analysis of heterogeneous feedback design in an OFDMA downlink with partial and imperfect feedback”, *IEEE Transactions on Signal Processing*, *accepted, to appear*, 2012.

Y. Huang, C. W. Tan, and B. D. Rao, "Joint beamforming and power control in coordinated multicell: max-min duality, effective network and large system transition", *IEEE Transactions on Wireless Communications*, minor revision, revised, 2012.

Y. Huang and B. D. Rao, "Random beamforming with heterogeneous users and selective feedback: individual sum rate and individual scaling laws", *IEEE Transactions on Wireless Communications*, submitted, 2012.

A. H. Nguyen, Y. Huang, and B. D. Rao, "Weighted CDF-based scheduling for an OFDMA relay downlink with partial feedback", *IEEE Transactions on Communications*, in preparation, 2012.

Y. Huang and B. D. Rao, "Awareness of channel statistics for slow cyclic prefix adaptation in an OFDMA system", *IEEE Wireless Communications Letters*, vol. 1, no. 4, pp. 332-335, Aug. 2012.

Y. Huang and B. D. Rao, "Sum rate analysis of one-pico-inside OFDMA network with opportunistic scheduling and selective feedback", *IEEE Signal Processing Letters*, vol. 19, no. 7, pp. 383-386, Jul. 2012.

Y. Huang and B. D. Rao, "Closed form sum rate of random beamforming", *IEEE Communications Letters*, vol. 16, no. 5, pp. 630-633, May 2012.

Conference Proceedings

Y. Huang, C. W. Tan and B. D. Rao, "Outage balancing in multiuser MISO networks: network duality and algorithms", *IEEE Global Communications Conferences (GLOBECOM)*, Anaheim, CA, Dec. 2012.

Y. Huang, C. W. Tan and B. D. Rao, "Cooperative beamforming in multiuser MIMO networks: fast SINR fairness algorithms", *IEEE Global Communications Conferences (GLOBECOM)*, Anaheim, CA, Dec. 2012.

Y. Huang and B. D. Rao, "A unified analysis of CDF-based distributed scheduling in a heterogeneous multicell", *IEEE Asilomar Conference on Signals, Systems and Computers*, Pacific Grove, CA, Nov. 2012.

Y. Huang and B. D. Rao, "Sum rate analysis and quantizer design for a quantized heterogeneous feedback MIMO OFDMA downlink", *IEEE Asilomar Conference on Signals, Systems and Computers*, Pacific Grove, CA, Nov. 2012.

A. H. Nguyen, Y. Huang and B. D. Rao, "Weighted CDF-based scheduling for an OFDMA relay downlink with partial feedback", *IEEE Asilomar Conference on Signals, Systems and Computers*, Pacific Grove, CA, Nov. 2012.

- Y. Huang, C. W. Tan and B. D. Rao, “Large system analysis of power minimization in multiuser MISO downlink with transmit-side channel correlation”, *International Symposium on Information Theory and its Applications (ISITA)*, Honolulu, HI, Oct. 2012.
- Y. Huang and B. D. Rao, “On rate scaling laws with CDF-based distributed scheduling in multicell networks”, *International Symposium on Information Theory and its Applications (ISITA)*, Honolulu, HI, Oct. 2012.
- Y. Huang and B. D. Rao, “Opportunistic beamforming in a downlink distributed antenna system with linear receivers”, *International Conference on Signal Processing and Communications (SPCOM)*, Bangalore, India, Jul. 2012.
- Y. Huang and B. D. Rao, “Heterogeneous partial feedback design in heterogeneous cellular OFDMA networks”, *IEEE International Conference on Communications (ICC)*, Ottawa, Canada, Jun. 2012.
- Y. Huang and B. D. Rao, “Analysis of a MIMO OFDMA heterogeneous feedback system employing joint scheduling and spatial diversity in Nakagami fading channels”, *IEEE International Conference on Communications (ICC)*, Ottawa, Canada, Jun. 2012.
- Y. Huang, C. W. Tan and B. D. Rao, “Asymptotic analysis of max-min weighted SINR in multiuser downlink”, *Conference on Information Sciences and Systems (CISS)*, Princeton, NJ, Mar. 2012 (Invited Paper).
- Y. Huang and B. D. Rao, “Performance analysis of random beamforming with heterogeneous users”, *Conference on Information Sciences and Systems (CISS)*, Princeton, NJ, Mar. 2012.
- Y. Huang, C. W. Tan and B. D. Rao, “Multicell network duality with instantaneous and statistical channel information: a nonlinear Perron-Frobenius characterization”, *Conference on Information Sciences and Systems (CISS)*, Princeton, NJ, Mar. 2012.
- Y. Huang and B. D. Rao, “Asymptotic analysis of a partial feedback OFDMA system employing spatial, spectral, and multiuser diversity”, *IEEE International Conference on Acoustics, Speech, and Signal Processing (ICASSP)*, Kyoto, Japan, Mar. 2012.
- Y. Huang and B. D. Rao, “Environmental-aware heterogeneous partial feedback design in a multiuser OFDMA system”, *IEEE Asilomar Conference on Signals, Systems and Computers*, Pacific Grove, CA, Nov. 2011.
- Y. Huang and B. D. Rao, “On using a priori channel statistics for cyclic prefix optimization in OFDM”, *IEEE Wireless Communications and Networking Conference (WCNC)*, Cancun, Mexico, Mar. 2011.

ABSTRACT OF THE DISSERTATION

**Feedback, Power Control, and Beamforming: Methods for Situational
Aware Wireless Networks**

by

Yichao Huang

Doctor of Philosophy in Electrical Engineering
(Communication Theory and Systems)

University of California, San Diego, 2012

Professor Bhaskar D. Rao, Chair

Feedback, power control and beamforming are important PHY and MAC layer issues in wireless communication systems. This dissertation is concerned with theoretical studies and algorithmic developments related to these issues in the context of and in support of the design of situational aware wireless networks. The envisioned situational aware wireless networks adapt system parameters and algorithms design to the channel attributes, user attributes, and system attributes, which constitute the wireless environment and network situations. The research topics in this dissertation regarding feedback, power control and beamforming are motivated by issues that arise from considering different types of awareness.

We first propose an adaptive feedback design based on the heterogeneous spectral channel statistics among users, which advocates the awareness of channel attributes. We leverage the multi-cluster subband fading model to develop an analytical framework to investigate the impact of partial feedback and potential imperfections including channel estimation error and feedback delay on system performance.

Next, we examine partial feedback in a heterogeneous multicell, and propose a heterogeneous feedback design based on heterogeneous user densities and large scale channel effects, which advocates the awareness of user attributes. The cumulative distribution function (CDF)-based scheduling policy is employed to obtain multiuser diversity gain while maintaining scheduling fairness. We derive a closed form expression as well as asymptotic approximation for the sum rate. In addition, the CDF-based scheduling policy is leveraged in a random beamforming framework to address several open problems. We develop the notion of individual sum rate to study the rate scaling for each individual user. We theoretically examine the randomness of multiuser diversity incurred by selective feedback to further establish the individual scaling laws under different feedback schemes.

We then investigate joint beamforming and power control in a multiuser interference network, and propose the usage of spatial channel statistics for algorithm design, which advocates the awareness of channel attributes. With the outage event induced by the utilization of spatial channel statistics, we present decentralized and fast convergent algorithms to achieve outage balancing in the interference network.

Finally, we study joint beamforming and power control in a coordinated multicell downlink and employ the max-min formulation to enforce egalitarian user fairness. In order to design efficient algorithm that scales well with the system dimension, we leverage the large system structure and advocate the awareness of system attributes. In our proposed algorithm design, the asymptotic power is computed using statistical channel information and the instantaneous beamformer is obtained in a non-iterative manner. We also establish the effective network to characterize and interpret the asymptotic solution.

Chapter 1

Introduction

Wireless communication networks continue to get more complex. Heterogeneous networks envisioned in LTE-advanced systems, self-organizing ad-hoc and peer to peer networks, decentralized cognitive radio networks, all are clear evidence of this trend. In order to efficiently use the wireless resources across a network, we envision enhanced situational awareness and high levels of cognition as playing a critical role. Existing networks already include such elements but future networks are going to need to incorporate them in a much more significant and comprehensive manner. We initiate the discussion of situational aware wireless networks with the following qualitative definition.

Situational Aware Wireless Networks: wireless networks incorporating link level awareness to network level awareness for algorithm design and for the adaptation of system parameters to better deal with varying wireless environments and network situations.

Developing a comprehensive framework for situational awareness and cognition in a wireless ecosystem is a daunting task, whose challenges are multifaceted in nature and will require long-term efforts from many research groups. In order to help in advancing the foundations of this nascent field, we initially deconstruct situational awareness into three inter-related components in the wireless ecosystem: awareness of *channel* attributes, awareness of *user* attributes, and awareness of *system* attributes. Channel attributes may include different types of channel information (both instantaneous channel information and statistical channel

information), the large-scale channel effects (i.e., path loss, shadowing, etc), various channel statistics reflected in different dimensions (i.e., delay spread, doppler spread and angular spread), among others. These channel attributes can be both location dependent and environment dependent. With the unprecedented growth of smart communication devices equipped with a number of sensory components such as GPS receiver, digital compass, and proximity sensor, such position (or location) awareness being aware of the channel attributes is very likely to emerge in next generation wireless networks. User attributes may include different user densities across cellular structures, the fairness requirements among users, different user mobilities at different periods of serving time, among others. System attributes may include the backhaul capability, the limited system resources, different traffic loads across base stations, the system dimension (large system structure), among others. The three concrete components, channel, user, and system, are inter-related and they as a whole constitute the wireless ecosystem. Our aim in the thesis is addressing algorithmic issues and analytical studies necessary towards understanding and designing situational aware wireless networks that are aware of channel attributes, user attributes, and system attributes. To approach this aim, we address important PHY and MAC layer issues for system design including feedback, power control, and beamforming. Investigating these issues is becoming more and more vital for next generation resource allocation and interference management (the detailed motivations can be referred to the introduction in each following chapter). On the conceptual side, the research problems addressed in the thesis related to feedback, power control, and beamforming, advocate the design of situational aware wireless networks from different perspectives. On the analytical side, we contributed to the research fields of feedback, power control, and beamforming by solving several open issues in each of the research problems. We now present the main contributions of the thesis by summarizing the technical contributions in each of the research topics.

1.1 Contributions of the Dissertation

In the sequel, we summarize the main contributions for each of the research topics.

1.1.1 Adaptive Feedback Design Based on Spectral Channel Statistics

Current OFDMA systems group resource blocks into subband to form the basic feedback unit. Homogeneous feedback design with a common subband size is not aware of the heterogeneous channel statistics among users. Under a general correlated channel model, we demonstrate the gain of matching the subband size to the underlying channel statistics motivating heterogeneous feedback design with different subband sizes and feedback resources across clusters of users (being aware of channel attributes). Employing the best-M partial feedback strategy, users with smaller subband size would convey more partial feedback to match the frequency selectivity. In order to develop an analytical framework to investigate the impact of partial feedback and potential imperfections, we leverage the multi-cluster subband fading model. The perfect feedback scenario is thoroughly analyzed, and the closed form expression for the average sum rate is derived for the heterogeneous partial feedback system. We proceed to examine the effect of imperfections due to channel estimation error and feedback delay, which leads to additional consideration of system outage. Two transmission strategies: the fix rate and the variable rate, are considered for the outage analysis. We also investigate how to adapt to the imperfections in order to maximize the average goodput under heterogeneous partial feedback.

1.1.2 Analytical Framework for Heterogeneous Feedback Being Aware of User Densities

The inherent heterogeneous structure resulting from user densities and large scale channel effects motivates heterogeneous partial feedback design in heteroge-

neous networks (being aware of user attributes). In such emerging networks, a distributed scheduling policy which enjoys multiuser diversity as well as maintains fairness among users is favored for individual user rate enhancement and guarantees. For a system employing the cumulative distribution function (CDF)-based scheduling, which satisfies the two above mentioned desired attributes, we develop an analytical framework to investigate heterogeneous partial feedback in a general OFDMA-based heterogeneous multicell employing the best-M partial feedback strategy. Exact sum rate analysis is first carried out and closed form expressions are obtained by a novel decomposition of the probability density function of the selected user's signal-to-interference-plus-noise ratio. To draw further insight, we perform asymptotic analysis using extreme value theory to examine the effect of partial feedback on the randomness of multiuser diversity, show the asymptotic optimality of best-1 feedback, and derive an asymptotic approximation for the sum rate in order to determine the minimum required partial feedback.

1.1.3 Random Beamforming with Heterogeneous Users and Selective Feedback

We investigate three open problems in random beamforming based communication systems: the scheduling policy with heterogeneous users, the closed form sum rate, and the randomness of multiuser diversity with selective feedback. By employing the CDF-based scheduling policy, we guarantee fairness among users as well as obtain multiuser diversity gain in the heterogeneous scenario. Under this scheduling framework, the individual sum rate, namely the average rate for a given user multiplied by the number of users, is of interest and analyzed under different feedback schemes. Firstly, under the full feedback scheme, we derive the closed form individual sum rate by employing a decomposition of the probability density function of the selected user's signal-to-interference-plus-noise ratio. This technique is employed to further obtain a closed form rate approximation with selective feedback in the spatial dimension. The analysis is also extended to random beamforming in a wideband OFDMA system with additional selective feedback in the spectral dimension wherein only the best beams for the best-L resource

blocks are fed back. We utilize extreme value theory to examine the randomness of multiuser diversity incurred by selective feedback. Finally, by leveraging the tail equivalence method, the multiplicative effect of selective feedback and random observations is observed to establish the individual rate scaling.

1.1.4 Outage Balancing Based on Spatial Channel Statistics

We study joint beamforming and power control in a multiuser MISO interference network with spatial channel statistics (being aware of channel attributes). Such information consists of the slow-varying covariance matrices in the beamforming network, and can be employed to reduce instantaneous feedback needs. With the outage event induced by the utilization of statistical channel information, we optimize signal transmission strategies to minimize the maximum outage probability under weighted sum power constraint to achieve outage balancing in the interference network. Under the condition of fixed beamformer, we use nonlinear Perron-Frobenius theory to present a decentralized algorithm with provable geometrically fast convergence rate to compute the optimal power. Since the joint beamformer and power optimization problem is non-convex, we examine its certainty-equivalent margin counterpart. By leveraging nonlinear Perron-Frobenius theory and the established network duality, we present a near-optimal decentralized algorithm to jointly optimize the beamformer and power. The algorithm converges quickly and the convergence rate of the algorithm is proven to be geometrical.

1.1.5 Efficient Algorithm Design Being Aware of Large System Structure

We investigate joint beamforming and power control in a coordinated multicell downlink system that serves multiple users per cell to maximize the minimum weighted signal-to-interference-plus-noise ratio. The optimal solution and distributed algorithm with geometrically fast convergence rate are derived by em-

ploying the nonlinear Perron-Frobenius theory and the multicell network duality. The iterative algorithm, though operating in a distributed manner, still requires instantaneous power update within the coordinated cluster through the backhaul. The backhaul information exchange and message passing may become prohibitive with increasing number of transmit antennas and increasing number of users. In order to derive asymptotically optimal solution, random matrix theory is leveraged to design a distributed algorithm that only requires statistical information (being aware of system attributes). The advantage of our approach is that there is no instantaneous power update through backhaul. Moreover, by using nonlinear Perron-Frobenius theory and random matrix theory, an effective primal network and an effective dual network are proposed to characterize and interpret the asymptotic solution.

1.2 Dissertation Outline

The remainder of the dissertation is organized as follows.

In Chapter 2, we propose the design of an adaptive (or heterogeneous) feedback strategy based on spectral channel statistics in a downlink OFDMA system. Conceptually, this design method is aware of the channel attributes in terms of the frequency domain channel statistics. We adapt the feedback amount to the different frequency selectivity of the users' channels, and we provide a thorough analysis of both perfect and imperfect feedback system performance under our proposed multi-cluster subband fading model. We also develop several approximations and near-optimal approaches to adapt and optimize the system performance.

Chapter 3 examines heterogeneous partial feedback from another perspective (different than the design philosophy proposed in Chapter 2). The highlighted heterogeneous feedback design method is adaptive to the user densities. Conceptually, this design method is aware of the user attributes in terms of the different user densities across the emerging heterogeneous multicell networks. We employ the CDF-based scheduling policy to maintain user fairness and simultaneously obtain multiuser diversity gain in a general multicell network. Under this distributed

scheduling policy, we develop an analytical framework to investigate heterogeneous partial feedback in heterogeneous multicell networks.

The scheduling policy utilized for analysis in Chapter 3 is further leveraged in Chapter 4 to study several open problems in random beamforming. We address practical considerations of random beamforming with heterogeneous users and selective feedback. We provide theoretical analysis to understand the effect of selective feedback on rate performance in both spatial and spectral dimensions. We also develop the notion of virtual users and the multiplicative effect to explain the impact of selective feedback on rate scaling.

Starting from Chapter 5, we shift our attention to power control and beamforming. We consider the use of spatial channel statistics for system design in a multiuser MISO interference network. Conceptually, the proposed algorithm design is aware of the channel attributes in terms of spatial statistical channel information. We investigate the outage balancing problem to develop efficient transmission strategies under given power constraint. We also prove the convergence of the proposed algorithm to be geometrical.

In Chapter 6, we focus on leveraging the emerging large-scale multiple antenna structure for algorithm design. Conceptually, the proposed design method is aware of the system attributes in terms of system dimension and backhaul capability. We study the problem of joint beamforming and power control in a coordinated multicell downlink. We examine the large system structure for algorithm design and establish the notion of effective network to provide insight into the power control problem with asymptotic solution.

Finally, Chapter 7 concludes the dissertation with discussion on future research directions.

Chapter 2

Adaptive Feedback Based on Spectral Channel Statistics

2.1 Introduction

Leveraging feedback to obtain the channel state information at the transmitter (CSIT) enables a wireless system to adapt its transmission strategy to the varying wireless environment. The growing number of wireless users, as well as their increasing demands for higher data rate services impose a significant burden on the feedback link. In particular for OFDMA systems, which have emerged as the core technology in 4G and future wireless systems, full CSIT feedback may become prohibitive because of the large number of resource blocks. This motivates more efficient feedback design approaches in order to achieve performance comparable to a full CSIT system with reduced feedback. In the recent years, considerable work and effort has been focused on limited or partial feedback design, e.g., see [1] and the references therein. To the best of our knowledge, most of the existing partial feedback designs are homogeneous, i.e., users' feedback consumptions do not adapt to the underlying channel statistics. In this chapter, we propose and analyze a heterogeneous feedback design, which aligns users' feedback needs to the statistical properties of their wireless environments.

Current homogeneous feedback design in OFDMA systems groups the re-

source blocks into subband [2–6] which forms the basic scheduling and feedback unit. Since the subband granularity is determined by the frequency selectivity, or the coherence bandwidth of the underlying channel, it would be beneficial to adjust the subband size of different users according to their channel statistics. Empirical measurements and analysis from the channel modeling field have shown that the root mean square (RMS) delay spread which is closely related to the coherence bandwidth, is both location and environment dependent [7–14]. The typical RMS delay spread for an indoor environment in WLAN does not exceed hundreds of nanoseconds; whereas in the outdoor environment of a cellular system, it can be up to several microseconds. Intuitively, users with lower RMS delay spread could model their channel with a larger subband size and require less feedback resource than the users with higher RMS delay spread. Herein, we investigate this heterogeneous feedback design in a multiuser opportunistic scheduling framework where the system favors the user with the best channel condition to exploit multiuser diversity [15, 16]. There are two major existing partial feedback strategies for opportunistic scheduling, one is based on thresholding where each user provides one bit of feedback per subband to indicate whether or not the particular channel gain exceeds a predetermined or optimized threshold [17–20]. The other promising strategy currently considered in practical systems such as LTE [21] is the best-M strategy, where the receivers order and convey the M best channels [22–29]. The best-M partial feedback strategy is embedded in the proposed heterogeneous feedback framework. Apart from the requirement of partial feedback to save feedback resource, the study of imperfections is also important to understand the effect of channel estimation error and feedback delay on the heterogeneous feedback framework. These imperfections are also considered in our work.

An important step towards heterogeneous feedback design is leveraging the “match” among coherence bandwidth, subband size and partial feedback. Under a given amount of partial feedback, if the subband size is much larger than the coherence bandwidth, then multiple independent channels could exist within a subband and the subband-based feedback could only be a coarse representative of the channels. On the other hand, if the subband size is much smaller than

the coherence bandwidth, then channels in adjacent subbands are likely to be highly correlated and requiring feedback on adjacent subbands could be a waste of resource; or a small amount of subband-based partial feedback may not be enough to reflect the channel quality. In order to support this heterogeneous framework, we first consider the scenario of a general correlated channel model with one cluster of users with the same coherence bandwidth. The subband size is adjustable and each user employs the best-M partial feedback strategy to convey the M best channel quality information (CQI) which is defined to be the subband average rate. The simulation result shows that a suitable chosen subband size yields higher average sum rate under partial feedback conforming the aforementioned intuition. This motivates the design of heterogeneous feedback to “match” the subband size to the coherence bandwidth. The above-mentioned study, though closely reflects the relevant mechanism, is not analytically tractable due to two main reasons. Firstly, the general correlated channel model complicates the statistical analysis of the CQI. Secondly, the use of subband average rate as CQI makes it difficult to analyze the multi-cluster scenario. Therefore, a simplified generic channel model is needed that balances the competing needs of analytical tractability and practical relevance.

In order to facilitate analysis, a subband fading channel model is developed that generalizes the widely used frequency domain block fading channel model. The subband fading model is suited for the multi-cluster analysis. According to the subband fading model, the channel frequency selectivity is flat within each subband, and independent across subbands. Since the subband sizes are different across different clusters, the number of independent channels are heterogeneous across clusters and this yields heterogeneous partial feedback design. Another benefit of the subband fading model is that the CQI becomes the channel gain and thus facilitate further statistical analysis. Under the multi-cluster subband fading model¹ and the assumption of perfect feedback, we derive a closed form expression for the average sum rate. Additionally, we approximate the sum rate ratio for heterogeneous design, i.e., the ratio of the average sum rate obtained by

¹An initial treatment of a two-cluster scenario was first presented in [30].

a partial feedback scheme to that achieved by a full feedback scheme, in order to choose different best-M for users with different coherence bandwidth. We also compare and demonstrate the potential of the proposed heterogeneous feedback design against the homogeneous case under the same feedback constraint in our simulation study.

The average sum rate helps in understanding the system performance with perfect feedback. In practical feedback systems, imperfections occur such as channel estimation error and feedback delay. These inevitable factors degrade the system performance by causing outage [31]. Therefore, rather than using average sum rate as the performance metric, we employ the notion of average goodput [32–34] to incorporate outage probability. Under the multi-cluster subband fading model, we perform analysis on the average goodput and the average outage probability with heterogeneous partial feedback. In addition to examining the impact of imperfect feedback on multiuser diversity [35, 36], we also investigate how to adapt and optimize the average goodput in the presence of these imperfections. We consider both the fixed rate and the variable rate scenarios, and utilize bounding technique and an efficient approximation to derive near-optimal strategies.

To summarize, the contributions of this chapter are threefold: a conceptual heterogeneous feedback design framework to adapt feedback amount to the underlying channel statistics, a thorough analysis of both perfect and imperfect feedback systems under the multi-cluster subband fading model, and the development of approximations and near-optimal approaches to adapt and optimize the system performance. The rest of the chapter is organized as follows. The motivation under the general correlated channel model and the development of system model is presented in Section 2.2. Section 2.3 deals with perfect feedback, and Section 2.4 examines imperfect feedback due to channel estimation error and feedback delay. Numerical results are presented in Section 2.5. Finally, Section 2.6 concludes the chapter.

2.2 System Model

2.2.1 Motivation for Heterogeneous Partial Feedback

This part provides justification for the adaptation of subband size with one cluster of users under the general correlated channel model, and motivates the design of heterogeneous partial feedback for the multi-cluster scenario in Section 2.2.2. Consider a downlink multiuser OFDMA system with one base station and K users. One cluster of user is assumed in this part and users in this cluster are assumed to experience the same frequency selectivity. The system consists of N_c subcarriers. $H_{k,n}$, the frequency domain channel transfer function between transmitter and user k at subcarrier n , can be written as:

$$H_{k,n} = \sum_{l=0}^{L-1} \sigma_l F_{k,l} \exp\left(-\frac{j2\pi(l-1)n}{N_c}\right), \quad (2.1)$$

where L is the number of channel taps, σ_l for $l = 0, \dots, L-1$ represents the channel power delay profile and is normalized, i.e., $\sum_{l=0}^{L-1} \sigma_l^2 = 1$, $F_{k,l}$ denotes the discrete time channel impulse response, which is modeled as complex Gaussian distributed random processes with zero mean and unit variance $\mathcal{CN}(0, 1)$ and is i.i.d. across k and l . Only fast fading effect is considered in this chapter, i.e., the effects of path loss and shadowing are assumed to be ideally compensated by power control². The received signal of user k at subcarrier n can be written as:

$$u_{k,n} = \sqrt{P_c} H_{k,n} s_{k,n} + v_{k,n}, \quad (2.2)$$

where P_c is the average received power per subcarrier, $s_{k,n}$ is the transmitted symbol and $v_{k,n}$ is the additive white noise distributed as $\mathcal{CN}(0, \sigma_{n_c}^2)$. From (2.1), it can be shown that $H_{k,n}$ is distributed as $\mathcal{CN}(0, 1)$. The channels at different subcarriers are correlated, and the correlation coefficient between subcarriers n_1 and n_2 can be described as follows:

$$\text{cov}(H_{k,n_1}, H_{k,n_2}) = \sum_{l=0}^{L-1} \sigma_l^2 \exp\left(-\frac{j2\pi(l-1)(n_2 - n_1)}{N_c}\right). \quad (2.3)$$

²This assumption has been employed in [20, 27, 36] to simplify the scheduling policy. With the same average SNR, the opportunistic scheduling policy is also long-term fair. When different average SNR is assumed, the proportional-fair scheduling policy [16] can be utilized.

In general, adjacent subcarriers are highly correlated. In order to reduce feedback needs, R_c subcarriers are formed as one resource block, and η resource blocks are grouped into one subband³. Thus, there are $N = \frac{N_c}{R_c}$ resource blocks and $\frac{N}{\eta}$ subbands⁴. In this manner, each user performs subband-based feedback to enable opportunistic scheduling at the transmitter. Since the channels are correlated and there is one CQI to represent a given subband, the CQI is a function of the all the individual channels within that subband. Herein, we employ the following subband (aggregate) average rate $S_{k,r}$ as the functional form⁵ [43,44] of the CQI for user k at subband r :

$$S_{k,r} \triangleq \frac{1}{\eta R_c} \sum_{n=(r-1)\eta R_c+1}^{r\eta R_c} \log_2 \left(1 + \frac{P_c |H_{k,n}|^2}{\sigma_{n_c}^2} \right). \quad (2.4)$$

Each user employs the best-M partial feedback strategy and conveys back the M best CQI values selected from $S_{k,r}$, $1 \leq r \leq \frac{N}{\eta}$. A detailed description of the best-M strategy can be found in [25,27,29]. After the base station receives feedback, it performs opportunistic scheduling and selects the user k for transmission at subband r if user k has the largest CQI at subband r . Also, it is assumed that if no user reports CQI for a certain subband, scheduling outage happens and the transmitter does not utilize it for transmission.

Now we demonstrate the need to adapt the subband size to achieve the potential ‘‘match’’ among coherence bandwidth, subband size and partial feedback through a simulation example. The channel is modeled according to the exponential power delay profile [45–47]: $\sigma_l^2 = \frac{1 - \exp(-l/\delta)}{1 - \exp(-L/\delta)} \exp(-l/\delta)$ for $0 \leq l < L$, where the parameter δ is related to the RMS delay spread. The simulation parameters are: $N_c = 256$, $N = 32$, $L = 16$, $\delta = 4$, $\frac{P_c}{\sigma_{n_c}^2} = 10$ dB. The subband size η can

³E.g., in LTE, one resource block consists of 12 subcarriers, and one subband can contain 1 to 8 resource blocks [37].

⁴Throughout this chapter, N_c , N and η are assumed to be a radix 2 number. A more general treatment is possible but this will result in edge effects making for more complex notation without much insight.

⁵This functional form employs the capacity formula and the resulting effective SNR has a geometric mean interpretation. Other functional forms of the CQI exist in practical systems such as exponential effective SNR mapping (EESM) [38–40] and mutual information per bit (MMIB) [41,42] to map the effective SNR to the block-error-rate (BLER) curve. The intuitions are similar: to obtain a representative CQI as a single performance measure corresponding to the rate performance.

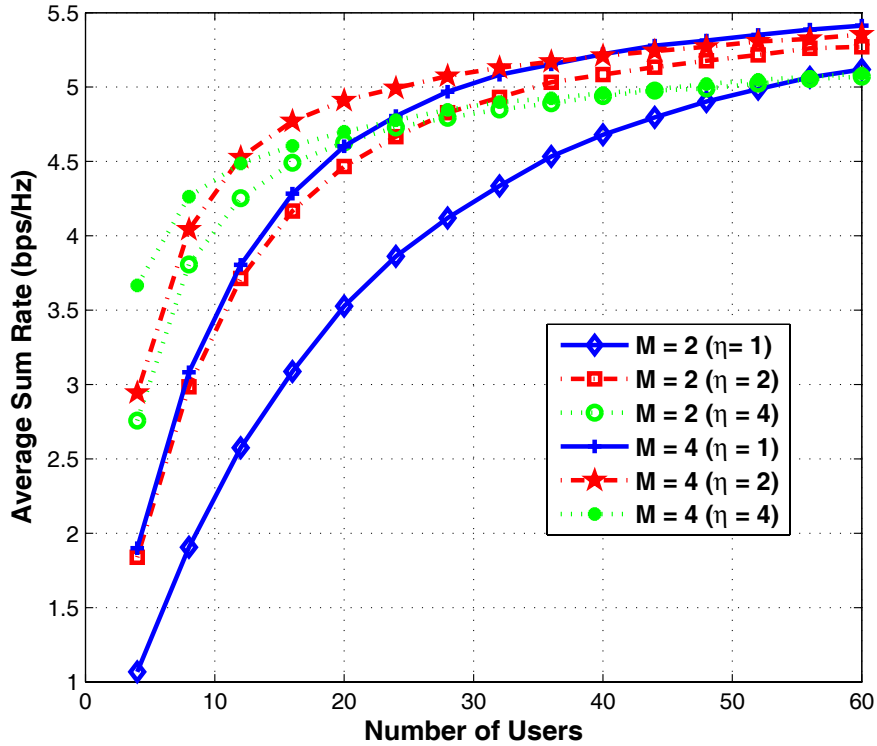


Figure 2.1: Comparison of average sum rate for different subband sizes ($\eta = 1, 2, 4$) and partial feedback ($M = 2, 4$) with respect to the number of users.

be adjusted and ranges from 1 to 4 resource blocks. We consider partial feedback with $M = 2$ and $M = 4$. The average sum rate of the system for different subband sizes and partial feedback with respect to the number of users is shown in Fig. 2.1. Under the given coherence bandwidth, several observations can be made. Firstly, the curves with $\eta = 4$ has the smallest increasing rate because a larger subband size gives a poor representation of the channel. Secondly, the curve with $\eta = 1, M = 2$ has the smallest average sum rate because a small amount of partial feedback is not enough to reflect the channel quality. Thirdly, the two curves $\eta = 1, M = 4$ and $\eta = 2, M = 2$ possess similar increasing rate. This is because the underlying channel is highly correlated within 2 resource blocks and thus having M -best feedback with $\eta = 2$ yields similar effect as having $2M$ -best feedback with $\eta = 1$. From the above observations, $\eta = 2$ matches the frequency selectivity and there would be performance loss or waste of feedback resource when a subband size is

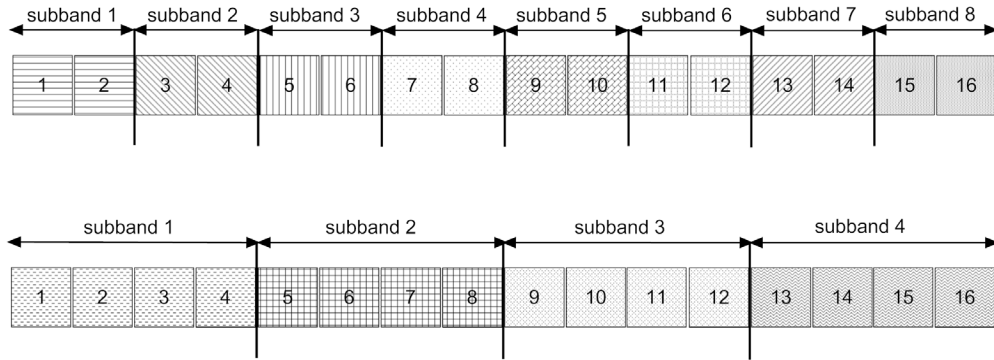


Figure 2.2: Illustration of the multi-cluster subband fading channel model for two different clusters with 16 resource blocks. The subband sizes equal 2 and 4 for the two different clusters respectively.

blindly chosen. In a multi-cluster scenario where users in different clusters experience diverse coherence bandwidth, this advocates heterogeneous subband size and heterogeneous feedback.

The general correlated channel model as well as the non-linearity of the CQI, though useful to demonstrate the need for heterogeneous feedback, does not lend itself to tractable statistical analysis. To develop a tractable analytical framework, an approximated channel model is needed. A widely used model is the block fading model in the frequency domain [48, 49] due to its simplicity and capability to provide a good approximation to actual physical channels. According to the block fading model, the channel frequency selectivity is flat within each block, and independent across blocks [19, 27, 29]. Herein, we generalize the block fading model to the subband fading model for the multi-cluster scenario. We assume that users possessing similar frequency selectivity are grouped into a cluster and the subband size is perfectly matched to the coherence bandwidth for a given cluster⁶. According to the subband fading model, for a given cluster with a perfectly matched subband size, the channel frequency selectivity is flat within each subband, and independent across subbands. Fig. 2.2 demonstrates the subband fading model for

⁶In practical systems, since the coherence bandwidth is determined by the channel statistics which vary on the order of tens of seconds or more, the cluster information can be learned and updated through infrequent user feedback. Therefore, the cluster is formed dynamically but in a slow way compared to the time variation of the fast fading effect which is on the order of milliseconds.

two different clusters with different subband sizes under a given number of resource blocks.

2.2.2 Multi-Cluster Subband Fading Model

We now present the multi-cluster subband fading model. Consider a down-link multiuser OFDMA system with one base station and G clusters of users⁷. The system consists of N resource blocks and the total number of users equals K . Users in cluster \mathcal{K}_g are indexed by the set $\mathcal{K}_g = \{1, \dots, k, \dots, K_g\}$ for $1 \leq g \leq G$, with $|\mathcal{K}_g| = K_g$ and $\sum_{g=1}^G K_g = K$. In our framework, users in the same cluster group their resource blocks into subbands in the same manner while each cluster can potentially employ a different grouping which enables the subband size to be heterogeneous between clusters. Denote η_g as the subband size for cluster \mathcal{K}_g , and $\eta_g \in \{2^0, 2^1, \dots, N\}$. The η_g 's are ordered such that $\eta_1 < \dots < \eta_G$. Based on the assumption for η_g , the number of subbands in cluster \mathcal{K}_g equals $\frac{N}{\eta_g}$.

Let $H_{k,r}^{(g)}$ be the frequency domain channel transfer function between transmitter and user k in cluster \mathcal{K}_g at subband r , where $1 \leq k \leq K_g, 1 \leq r \leq \frac{N}{\eta_g}$. $H_{k,r}^{(g)}$ is distributed as $\mathcal{CN}(0, 1)$. According to the subband fading model, $H_{k,r}^{(g)}$ is assumed to be independent across users and subbands in cluster \mathcal{K}_g . The feedback for different clusters is at different granularity, and so to model the channel for the different clusters of users at the same basic resource block level, some additional notation is needed. Let $\tilde{H}_{k,n}^{(g)} = H_{k, \lceil \frac{n}{\eta_g} \rceil}^{(g)}$ with $1 \leq n \leq N$ denote the resource block based channel transfer function. Then the received signals of user k in cluster \mathcal{K}_g at resource block n can be represented by:

$$u_{k,n}^{(g)} = \sqrt{P} \tilde{H}_{k,n}^{(g)} s_{k,n}^{(g)} + v_{k,n}^{(g)}, \quad (2.5)$$

where P is the average received power per resource block, $s_{k,n}^{(g)}$ is the transmitted symbol and $v_{k,n}^{(g)}$ is additive white noise distributed with $\mathcal{CN}(0, \sigma_n^2)$.

Let $Z_{k,r}^{(g)} \triangleq |H_{k,r}^{(g)}|^2$ denote the CQI for user k in cluster \mathcal{K}_g at subband r . In order to reduce the feedback load, users employ the best-M strategy to feed back

⁷The base station and users are equipped with one antenna each. The scenario with spatial diversity [50–54] in the heterogeneous feedback framework is examined in [55].

their CQI. In the basic best-M feedback policy, users measure CQI for each resource block at their receiver and feed back the CQI values of the M best resource blocks chosen from the total N values. For each resource block, the scheduling policy selects the user with the largest CQI among the users who fed back CQI to the transmitter for that resource block. However, in our heterogeneous partial feedback framework, since the number of independent CQI for cluster \mathcal{K}_g is $\frac{N}{\eta_g}$, a fair and reasonable way to allocate the feedback resource is to linearly scale the feedback amount for users in cluster \mathcal{K}_g . To be specific, user k in \mathcal{K}_G (i.e., the cluster with the largest subband size) is assumed to feed back the M best CQI selected from $\{Z_{k,r}^{(G)}\}, 1 \leq r \leq \frac{N}{\eta_G}$, whereas user k in \mathcal{K}_g conveys the $\frac{\eta_G}{\eta_g}M$ best CQI selected from $\{Z_{k,r}^{(g)}\}, 1 \leq r \leq \frac{N}{\eta_g}$. After receiving feedback from all the clusters, for each resource block the system schedules the user for transmission with the largest CQI. It is useful to note that the user feedback is based on the subband level, while the base station schedules transmission at the resource block level.

2.3 Perfect Feedback

In this section, the CQI are assumed to be fed back without any errors and the average sum rate is employed as the performance metric for system evaluation. We derive a closed form expression for the average sum rate in Section 2.3.1 for the multi-cluster heterogeneous feedback system. In Section 2.3.2 we analyze the relationship between the sum rate ratio and the choice of the best-M.

2.3.1 Derivation of Average Sum Rate

According to the assumption, the CQI $Z_{k,r}^{(g)}$ is i.i.d. across subbands and users, and thus let F_Z denote the CDF. Because only a subset of the ordered CQI are fed back, from the transmitter's perspective, if it receives feedback on a certain resource block from a user, it is likely to be any one of the CQI from the ordered subset. We now aim to find the CDF of the CQI seen at the transmitter side as a consequence of partial feedback. Let $\tilde{Y}_{k,n}^{(g)}$ denote the reported CQI viewed at the transmitter for user k in \mathcal{K}_g at resource block n . Also, let $Y_{k,r}^{(g)}$ represent the

subband-based CQI seen at the transmitter for user k in \mathcal{K}_g at subband r , then $\tilde{Y}_{k,n}^{(g)} = Y_{k, \lceil \frac{n}{\eta_g} \rceil}^{(2)}$. The following lemma describes the CDF of $\tilde{Y}_k^{(g)}$ (the index n is dropped for notational simplicity), which is denoted by $F_{\tilde{Y}_k^{(g)}}$.

Lemma 2.1. *The CDF of $\tilde{Y}_k^{(g)}$ is given by:*

$$F_{\tilde{Y}_k^{(g)}}(x) = \sum_{m=0}^{\frac{\eta_G M - 1}{\eta_g}} \xi_g(N, M, \boldsymbol{\eta}, m) (F_Z(x))^{\frac{N}{\eta_g} - m}, \quad (2.6)$$

where the vector $\boldsymbol{\eta} \triangleq (\eta_1, \dots, \eta_g, \dots, \eta_G)$ and

$$\xi_g(N, M, \boldsymbol{\eta}, m) = \sum_{i=m}^{\frac{\eta_G M - 1}{\eta_g}} \frac{\frac{\eta_G M - i}{\eta_g}}{\frac{\eta_G M}{\eta_g}} \binom{\frac{N}{\eta_g}}{i} \binom{i}{m} (-1)^{i-m}. \quad (2.7)$$

Proof. The proof is provided in Appendix A. □

Let k_n^* denote the selected user at resource block n , then according to the scheduling policy:

$$k_n^* = \arg \max_{k \in \mathcal{U}_n} \{\tilde{Y}_{k,n}^{(1)}, \dots, \tilde{Y}_{k,n}^{(g)}, \dots, \tilde{Y}_{k,n}^{(G)}\}, \quad (2.8)$$

where $\mathcal{U}_n \triangleq \{\mathcal{U}_n^{(1)}, \dots, \mathcal{U}_n^{(g)}, \dots, \mathcal{U}_n^{(G)}\}$ is the set of users who convey feedback for resource block n , with $|\mathcal{U}_n^{(g)}| = \tau_g$ representing the number of users belonging to \mathcal{U}_n in cluster \mathcal{K}_g . It can be easily seen that in the full feedback case, i.e., $M = M_F \triangleq \frac{N}{\eta_G}$, $|\mathcal{U}_n^{(g)}| = K_g$. For the general case when $1 \leq M < M_F$, the probability mass function (PMF) of \mathcal{U}_n is given by:

$$\begin{aligned} \mathbb{P}(\mathcal{U}_n) &= \left(\prod_{g=1}^G \binom{K_g}{\tau_g} \right) \left(\frac{\eta_G M}{N} \right)^{\sum_{g=1}^G \tau_g} \\ &\times \left(1 - \frac{\eta_G M}{N} \right)^{K - \sum_{g=1}^G \tau_g}, \quad 0 \leq \tau_g \leq K_g. \end{aligned} \quad (2.9)$$

Remark: Only the largest subband size η_G appears in the expression of $\mathbb{P}(\mathcal{U}_n)$ instead of the vector $\boldsymbol{\eta}$. This is due to our heterogeneous partial feedback design to let users in cluster \mathcal{K}_g convey back the $\frac{\eta_G M}{\eta_g}$ best CQI out of $\frac{N}{\eta_g}$ values.

Now we turn to determine the conditional CDF of the CQI for the selected user at resource block n , conditioned on the set of users providing CQI for that

resource block. Since users are equiprobable to be scheduled according to the fair scheduling policy, the condition on k_n^* is not described explicitly, and so we denote the conditional CDF as $F_{X_n|\mathcal{U}_n}$, where $X_n|\mathcal{U}_n$ is the conditional CQI of the selected user at resource block n . Notice from Lemma 2.1 that $\tilde{Y}_k^{(g)}$ possess a different distribution for different g due to the heterogeneous feedback from different clusters. Using order statistics [56] yields $F_{X_n|\mathcal{U}_n}$ as:

$$F_{X_n|\mathcal{U}_n}(x) = \prod_{g=1}^G (F_{\tilde{Y}_k^{(g)}}(x))^{\tau_g}. \quad (2.10)$$

Then the polynomial form of $F_{X_n|\mathcal{U}_n}$ can be obtained, which is stated in the following theorem.

Theorem 2.1. *The CDF of $F_{X_n|\mathcal{U}_n}$ is given by:*

$$F_{X_n|\mathcal{U}_n}(x) = \sum_{m=0}^{\Phi(M, \boldsymbol{\eta}, \boldsymbol{\tau})} \Theta_{G-1}(N, M, \boldsymbol{\eta}, \boldsymbol{\tau}, m) \times (F_Z(x))^{\sum_{g=1}^G \frac{N}{\eta_g} \tau_g - m}, \quad (2.11)$$

where the vector $\boldsymbol{\tau} \triangleq (\tau_1, \dots, \tau_g, \dots, \tau_G)$, $\Phi(M, \boldsymbol{\eta}, \boldsymbol{\tau}) \triangleq \sum_{g=1}^G \tau_g \left(\frac{\eta_G}{\eta_g} M - 1 \right)$,

$$\Theta_g(N, M, \boldsymbol{\eta}, \boldsymbol{\tau}, m) = \begin{cases} \sum_{i=0}^m \Lambda_1(N, M, \boldsymbol{\eta}, \boldsymbol{\tau}, i) \Lambda_2(N, M, \boldsymbol{\eta}, \boldsymbol{\tau}, m-i), & g=1 \\ \sum_{i=0}^m \Theta_{g-1}(N, M, \boldsymbol{\eta}, \boldsymbol{\tau}, i) \times \Lambda_{g+1}(N, M, \boldsymbol{\eta}, \boldsymbol{\tau}, m-i), & 2 \leq g < G \end{cases} \quad (2.12)$$

$$\Lambda_g(N, M, \boldsymbol{\eta}, \boldsymbol{\tau}, m) = \begin{cases} (\xi_g(N, M, \boldsymbol{\eta}, 0))^{\tau_g}, & m=0 \\ \frac{1}{m \xi_g(N, M, \boldsymbol{\eta}, 0)} \sum_{\ell=1}^{\min(m, \frac{\eta_G}{\eta_g} M - 1)} ((\tau_g + 1)\ell - m) \times \xi_g(N, M, \boldsymbol{\eta}, \ell) \Lambda_g(N, M, \boldsymbol{\eta}, \boldsymbol{\tau}, m-\ell), & 1 \leq m < \tau_g \left(\frac{\eta_G}{\eta_g} M - 1 \right) \\ (\xi_g(N, M, \boldsymbol{\eta}, \frac{\eta_G}{\eta_g} M - 1))^{\tau_g}, & m = \tau_g \left(\frac{\eta_G}{\eta_g} M - 1 \right). \end{cases} \quad (2.13)$$

Proof. The proof is provided in Appendix A. □

After obtaining the conditional CDF $F_{X_n|\mathcal{U}_n}$, let $C_P(M)$ denote the average sum rate and it can be computed using the following procedure.

$$\begin{aligned}
C_P(M) &= \frac{1}{N} \sum_{n=1}^N \mathbb{E}[\log_2(1 + X_n)] \\
&\stackrel{(a)}{=} \mathbb{E}_{\mathcal{U}} \left[\int_0^\infty \log_2(1 + \rho x) d(F_{X|\mathcal{U}}(x)) \right] \\
&\stackrel{(b)}{=} \mathbb{E}_{\mathcal{U}} \left[\sum_{m=0}^{\Phi(M, \boldsymbol{\eta}, \boldsymbol{\tau})} \Theta_{G-1}(N, M, \boldsymbol{\eta}, \boldsymbol{\tau}, m) \right. \\
&\quad \left. \times \int_0^\infty \log_2(1 + \rho x) d(F_Z(x))^{\sum_{g=1}^G \frac{N}{\eta_g} \tau_g - m} \right] \\
&\stackrel{(c)}{=} \sum_{\boldsymbol{\tau} \neq \mathbf{0}} \mathbb{P}(\mathcal{U}) \sum_{m=0}^{\Phi(M, \boldsymbol{\eta}, \boldsymbol{\tau})} \Theta_{G-1}(N, M, \boldsymbol{\eta}, \boldsymbol{\tau}, m) \\
&\quad \times \mathcal{I}_1 \left(\rho, \sum_{g=1}^G \frac{N}{\eta_g} \tau_g - m \right), \tag{2.14}
\end{aligned}$$

where $\rho \triangleq \frac{P}{\sigma_n^2}$ and $\mathbb{P}(\mathcal{U})$ is given by (2.9). (a) follows from the conditional expectation of $X_n|\mathcal{U}_n$ and the identically distributed property (let X and \mathcal{U} represent X_n and \mathcal{U}_n respectively), (b) follows from (2.11) in Theorem 2.1, (c) follows from (2.9), and define $\mathcal{I}_1(a, b) \triangleq \int_0^\infty \log_2(1 + ax) d(F_Z(x))^b$. $\mathcal{I}_1(a, b)$ is computed in Appendix A to be:

$$\mathcal{I}_1(a, b) = \frac{b}{\ln 2} \sum_{\ell=0}^{b-1} \binom{b-1}{\ell} \frac{(-1)^\ell}{\ell+1} \exp\left(\frac{\ell+1}{a}\right) E_1\left(\frac{\ell+1}{a}\right), \tag{2.15}$$

where $E_1(x) = \int_x^\infty \exp(-t)t^{-1} dt$ is the exponential integral function [57].

The average sum rate for the full feedback is a special case and is given by:

$$C_P(M_F) = \int_0^\infty \log_2(1 + \rho x) d(F_Z(x))^K = \mathcal{I}_1(\rho, K). \tag{2.16}$$

Remark: It is noteworthy to mention that the functional form of $C_P(M)$ in (2.14) consists of two main parts. The first part, which involves $\mathbb{P}(\mathcal{U})$ and $\Theta_{G-1}(\cdot, \cdot, \cdot, \cdot, \cdot)$, accounts for the randomness of the set of users who convey feedback as well as the scheduling policy. This part is inherent to the heterogeneous partial feedback strategy, and is independent of the system metric for evaluation, such as

the average sum rate employed in this chapter. The second part $\mathcal{I}_1(\cdot, \cdot)$ depends on statistical assumption of the underlying channel and the system metric, and it is impacted by partial feedback as well.

2.3.2 Sum Rate Ratio and Best-M

We now examine how to determine the smallest M that results in almost the same performance, in terms of average sum rate, as the full feedback case. Applying the same technique as in [25, 29], define γ_P as the spectral efficiency ratio and the problem can be formulated as:

$$\text{Find the minimum } M^*, \quad \text{s.t. } \gamma_P = \frac{C_P(M^*)}{C_P(M_F)} \geq \gamma. \quad (2.17)$$

The above problem can be numerically solved by substituting the expressions for $C_P(M)$ and $C_P(M_F)$. In order to obtain a simpler and tractable relationship between M and K given $\boldsymbol{\eta}$, i.e., the tradeoff between the amount of partial feedback and the number of users given existing heterogeneity of channel statistics in frequency domain, an approximation is utilized similar to that in [29], by observing that $\mathcal{I}_1(a, b)$ in (2.15) is slowly increasing in b with fixed a (This phenomenon is due to the saturation of multiuser diversity [58]). Observing $\sum_{m=0}^{\Phi(M, \boldsymbol{\eta}, \boldsymbol{\tau})} \Theta_{G-1}(N, M, \boldsymbol{\eta}, \boldsymbol{\tau}, m) = 1$ and employing the binomial theorem yields the approximation for the spectral efficiency ratio as:

$$\gamma_P \simeq 1 - \left(1 - \frac{\eta_G M^*}{N}\right)^K. \quad (2.18)$$

From (2.17) and (2.18), the minimum required M^* can be obtained as follows:

$$M^* \geq \frac{N}{\eta_G} \left(1 - (1 - \gamma)^{\frac{1}{K}}\right). \quad (2.19)$$

Remark: It can be seen that M^* depends on the system parameters (N, K, γ) as well on the largest subband size η_G . It is also a consequence of our heterogeneous partial feedback assumption to let users in cluster \mathcal{K}_g convey back the $\frac{\eta_G}{\eta_g} M$ best CQI out of $\frac{N}{\eta_g}$ values. This results in the fact that obtaining feedback information from users belonging to different clusters have almost the same statistical influence on scheduling performance.

2.4 Imperfect Feedback

After analyzing the heterogeneous partial feedback design with perfect feedback, we turn to examine the impact of feedback imperfections in this section. We develop the imperfect feedback model due to channel estimation error and feedback delay in Section 2.4.1, and investigate the influence of imperfections on two different transmission strategies in Section 2.4.2 and 2.4.3. Then we propose how to optimize the system performance to adapt to the imperfections in Section 2.4.4.

2.4.1 Imperfect Feedback Model

The imperfect feedback model is built upon the subband fading model for the perfect feedback case. To differentiate from the notation for the perfect feedback case and focus on the imperfect feedback model, the resource block index is dropped. Let h_k denote the frequency domain channel transfer function of user k (users in different clusters are not temporally distinguished to avoid notational overload). Due to channel estimation error, the user only has its estimated version \hat{h}_k , and the relationship between h_k and \hat{h}_k can be modeled as:

$$h_k = \hat{h}_k + w_k, \quad (2.20)$$

where $w_k \sim \mathcal{CN}(0, \sigma_{w_k}^2)$ is the channel estimation error. The channel of each resource block is assumed to be estimated independently, which yields the channel estimation errors w_k i.i.d. across users and resource blocks, i.e., $w_k \sim \mathcal{CN}(0, \sigma_w^2)$. It is clear that the base station makes decision on scheduling and adaptive transmission depending on CQI, a function of \hat{h}_k . Thus this information can be outdated due to delay between the instant CQI is measured and the actual instant of use for data transmission to the selected user. Let \tilde{h}_k be the actual channel transfer function and we employ a first-order Gaussian-Markov model [34, 36] to describe the time evolution and to capture the relationship with the delayed version as follows:

$$\tilde{h}_k = \alpha_k(\hat{h}_k + w_k) + \sqrt{1 - \alpha_k^2}\varepsilon_k, \quad (2.21)$$

where ε_k accounts for the innovation noise and is distributed as $\mathcal{CN}(0, 1)$. The delay time between \tilde{h}_k and \hat{h}_k is not explicitly written for notational simplicity, and

$\alpha_k \in [0, 1]$ is used to model the correlation coefficient. Since the feedback delay is mainly caused by the periodic feedback interval and processing complexity [34], the innovation noise ε_k are i.i.d. across users and a common α is assumed. Moreover, w_k and ε_k are assumed independent. Therefore, for notational simplicity, the user index k in the aforementioned parameters is dropped and $\hat{Z} \triangleq |\hat{h}|^2$ is denoted as CQI.

Let $\tilde{\chi}$, χ and $\hat{\chi}$ represent: the actual CQI of the selected user for transmission, its outdated version, and its outdated estimate respectively ($\hat{\chi}$ corresponds to X for the perfect feedback case in Section 2.3.1). Notice that the PDF of the outdated estimate $\hat{\chi}$ depends on the heterogeneous feedback design and the scheduling strategy, whereas the conditional PDF of $\tilde{\chi}|\hat{\chi}$ only depends on α and σ_w^2 . Employing the same method in [35, 36], the conditional PDF is obtained as follows:

$$f_{\tilde{\chi}|\hat{\chi}}(x|\hat{\chi}) = \frac{\alpha_w^2}{2} \exp\left(-\frac{\alpha_w^2 x + \alpha_w^2 \alpha^2 \hat{\chi}}{2}\right) I_0(\alpha_w^2 \alpha \sqrt{\hat{\chi} x}), \quad (2.22)$$

where $\alpha_w = \sqrt{\frac{2}{\alpha^2 \sigma_w^2 + 1 - \alpha^2}}$, and $I_0(\cdot)$ is the zeroth-order modified Bessel function of the first kind [57].

Since the feedback is imperfect, there are two types of issues that arise. The first is the choice of the incorrect user to serve. However, because of the i.i.d nature of the errors this does not compromise the fairness and also does not complicate the determination of the CDF. The second problem is that of outage because the rate adaptation is made by the base station based on the erroneous CQI. Because of the error in the CQI, the rate chosen may exceed the rate that the channel can support and so the base station has to take steps to mitigate this effect of outage. A conservative strategy will result in less outage but under utilization of the channel while an aggressive strategy will result in good utilization of the channel but only for a small fraction of the time. We now present two transmission strategies to address the outage issue.

2.4.2 Fix Rate Strategy

In the fix rate conservative scenario, a system parameter β_0 is chosen for rate adaptation, and outage results under the following condition:

$$\text{Declare outage if: } \{\tilde{\chi} \leq \beta_0 | \hat{\chi}\}. \quad (2.23)$$

The system average goodput is defined as the total average bps/Hz successfully transmitted [32]. We derive the average goodput and average outage probability for a given choice of system parameter β_0 in the following procedure.

Firstly the conditional outage probability is expressed as:

$$\mathbb{P}(\tilde{\chi} \leq \beta_0 | \hat{\chi}) = 1 - \mathcal{Q}_1(\alpha_w \alpha \sqrt{\hat{\chi}}, \alpha_w \sqrt{\beta_0}), \quad (2.24)$$

where $\mathcal{Q}_1(a, b) = \int_b^\infty t \exp(-\frac{t^2+a^2}{2}) I_0(at) dt$ is the first-order Marcum-Q function [59]. Denote $R_0(\beta_0, M)$ as the average goodput for the heterogeneous partial feedback system, which is written according to definition:

$$R_0(\beta_0, M) = \mathbb{E}_{\mathcal{U}} [\mathbb{E}_{\hat{\chi}|\mathcal{U}} [\mathbb{P}(\tilde{\chi} \geq \beta_0 | \hat{\chi}) \log_2(1 + \rho\beta_0)]] . \quad (2.25)$$

Then, from (2.9) and (2.14), $R_0(\beta_0, M)$ can be computed as:

$$\begin{aligned} & R_0(\beta_0, M) \\ &= \mathbb{E}_{\mathcal{U}} \left[\sum_{m=0}^{\Phi(M, \boldsymbol{\eta}, \boldsymbol{\tau})} \Theta_{G-1}(N, M, \boldsymbol{\eta}, \boldsymbol{\tau}, m) \right. \\ & \quad \times \left. \int_0^\infty \mathcal{Q}_1(\alpha_w \alpha \sqrt{x}, \alpha_w \sqrt{\beta_0}) \log_2(1 + \rho\beta_0) d(F_{\hat{Z}}(x))^{\sum_{g=1}^G \frac{N}{\eta_g} \tau_g - m} \right] \\ &= \sum_{\boldsymbol{\tau} \neq \mathbf{0}} \mathbb{P}(\mathcal{U}) \sum_{m=0}^{\Phi(M, \boldsymbol{\eta}, \boldsymbol{\tau})} \Theta_{G-1}(N, M, \boldsymbol{\eta}, \boldsymbol{\tau}, m) \\ & \quad \times \log_2(1 + \rho\beta_0) \mathcal{I}_2 \left(\beta_0, \sum_{g=1}^G \frac{N}{\eta_g} \tau_g - m \right), \end{aligned} \quad (2.26)$$

where $\mathcal{I}_2(a, b) \triangleq \int_0^\infty \mathcal{Q}_1(\alpha_w \alpha \sqrt{x}, \alpha_w \sqrt{a}) d(F_{\hat{Z}}(x))^b$. $\mathcal{I}_2(a, b)$ is computed in Appendix B to be:

$$\begin{aligned} \mathcal{I}_2(a, b) &= \frac{2b}{(1 - \sigma_w^2) \ln 2} \sum_{\ell=0}^{b-1} \binom{b-1}{\ell} (-1)^\ell \frac{1}{\zeta_\ell} \\ & \quad \times \left(\exp(-\frac{\vartheta^2}{2}) + \exp(-\frac{\zeta_\ell \vartheta^2}{2(\varpi^2 + \zeta_\ell)}) (1 - \exp(-\frac{\varpi^2 \vartheta^2}{2(\varpi^2 + \zeta_\ell)})) \right), \end{aligned} \quad (2.27)$$

where $\varpi = \alpha_w \alpha$, $\vartheta = \alpha_w \sqrt{a}$, $\zeta_\ell = \frac{2(\ell+1)}{1-\sigma_w^2}$.

The average outage probability $P_0(\beta_0, M)$ for the heterogeneous partial feedback design can be directly calculated from definition and (2.26) as follows:

$$\begin{aligned} P_0(\beta_0, M) &= \mathbb{E}_{\mathcal{U}} \left[\mathbb{E}_{\hat{\chi}|\mathcal{U}} [\mathbb{P}(\tilde{\chi} \leq \beta_0|\hat{\chi})] \right] \\ &= \sum_{\boldsymbol{\tau} \neq \mathbf{0}} \mathbb{P}(\mathcal{U}) \sum_{m=0}^{\Phi(M, \boldsymbol{\eta}, \boldsymbol{\tau})} \Theta_{G-1}(N, M, \boldsymbol{\eta}, \boldsymbol{\tau}, m) \\ &\quad \times \left(1 - \mathcal{I}_2 \left(\beta_0, \sum_{g=1}^G \frac{N}{\eta_g} \tau_g - m \right) \right). \end{aligned} \quad (2.28)$$

The average goodput and average outage probability for the full feedback scenario is a special case and is given by:

$$\begin{aligned} R_0(\beta_0, M_F) &= \log_2(1 + \rho\beta_0) \mathcal{I}_2(\beta_0, K), \\ P_0(\beta_0, M_F) &= 1 - \mathcal{I}_2(\beta_0, K). \end{aligned} \quad (2.29)$$

2.4.3 Variable Rate Strategy

Instead of choosing a conservative system parameter to account for the fix rate scenario as in the previous subsection, we consider an approach we refer to as the variable rate strategy. In the variable rate scenario, a system parameter β_1 is chosen and outage results under the following condition:

$$\text{Declare outage if : } \{ \tilde{\chi} \leq \beta_1 \hat{\chi} | \hat{\chi} \}, \quad (2.30)$$

where β_1 can be regarded as the backoff factor. The system average goodput and average outage probability can be derived utilizing the following procedure.

Now under the variable rate scenario, the conditional outage probability is expressed as:

$$\mathbb{P}(\tilde{\chi} \leq \beta_1 \hat{\chi} | \hat{\chi}) = 1 - \mathcal{Q}_1(\alpha_w \alpha \sqrt{\hat{\chi}}, \alpha_w \sqrt{\beta_1 \hat{\chi}}). \quad (2.31)$$

Using the same method as (2.25) and (2.26), let $R_1(\beta_1, M)$ denote the average

goodput for the variable rate scenario whose expression can be written as follows:

$$\begin{aligned}
R_1(\beta_1, M) &= \mathbb{E}_{\mathcal{U}} \left[\mathbb{E}_{\hat{\chi}|\mathcal{U}} \left[\mathbb{P}(\tilde{\chi} \geq \beta_1 \hat{\chi} | \hat{\chi}) \log_2(1 + \rho \beta_1 \hat{\chi}) \right] \right] \\
&= \sum_{\boldsymbol{\tau} \neq \mathbf{0}} \mathbb{P}(\mathcal{U}) \sum_{m=0}^{\Phi(M, \boldsymbol{\eta}, \boldsymbol{\tau})} \Theta_{G-1}(N, M, \boldsymbol{\eta}, \boldsymbol{\tau}, m) \\
&\quad \times \mathcal{I}_3 \left(\beta_1, \sum_{g=1}^G \frac{N}{\eta_g} \tau_g - m \right), \tag{2.32}
\end{aligned}$$

where $\mathcal{I}_3(a, b) \triangleq \int_0^\infty \mathcal{Q}_1(\alpha_w \alpha \sqrt{x}, \alpha_w \sqrt{ax}) \log_2(1 + \rho ax) d(F_{\hat{Z}}(x))^b$.

For the full feedback case, the average goodput is given by:

$$R_1(\beta_1, M_F) = \mathcal{I}_3(\beta_1, K). \tag{2.33}$$

Note that unlike $\mathcal{I}_2(a, b)$, $\mathcal{I}_3(a, b)$ can not be written in closed form. Therefore, bounding technique and suitable approximation are attractive to find closed form alternatives for $\mathcal{I}_3(a, b)$. The following proposition presents a valid closed form upper bound for $\mathcal{I}_3(a, b)$ in the low SNR regime.

Proposition 2.1. *In the low SNR regime, $\mathcal{I}_3(a, b)$ can be efficiently upper bounded by:*

$$\begin{aligned}
\mathcal{I}_3^{\text{UB}}(a, b) &= \frac{4\rho ab}{(1 - \sigma_w^2) \ln 2} \sum_{\ell=0}^{b-1} (-1)^\ell \frac{1}{\zeta_\ell^2} \left(1 + \frac{\vartheta^2}{\varphi_\ell} \left(\frac{\varpi^2}{\varphi_\ell} \right. \right. \\
&\quad \times {}_2F_1 \left(1, \frac{3}{2}; 2; \frac{4\varpi^2 \vartheta^2}{\varphi_\ell^2} \right) - {}_2F_1 \left(\frac{1}{2}, 1; 1; \frac{4\varpi^2 \vartheta^2}{\varphi_\ell^2} \right) \\
&\quad \left. \left. + \frac{2\zeta_\ell}{\varphi_\ell} \left(\frac{\varpi^2}{\varphi_\ell} {}_2F_1 \left(\frac{3}{2}, 2; 2; \frac{4\varpi^2 \vartheta^2}{\varphi_\ell^2} \right) - \frac{1}{2} {}_2F_1 \left(1, \frac{3}{2}; 1; \frac{4\varpi^2 \vartheta^2}{\varphi_\ell^2} \right) \right) \right) \right), \tag{2.34}
\end{aligned}$$

where $\varpi = \alpha_w \alpha$, $\vartheta = \alpha_w \sqrt{a}$, $\zeta_\ell = \frac{2(\ell+1)}{1-\sigma_w^2}$, $\varphi_\ell = \varpi^2 + \vartheta^2 + \zeta_\ell$, and ${}_2F_1(\cdot, \cdot; \cdot; \cdot)$ is the Gaussian hypergeometric function [57].

Proof. The proof is provided in Appendix B. □

$\mathcal{I}_3^{\text{UB}}(a, b)$ is valid and tight especially for the low SNR regime. In order to track $\mathcal{I}_3(a, b)$ over the whole SNR regimes, we propose the following approximation method by leveraging Jensen's inequality [60]. Recall the definition of $\mathcal{I}_3(a, b) =$

$\mathbb{E}[\mathcal{Q}_1(\alpha_w \alpha \sqrt{\tilde{\chi}}, \alpha_w \sqrt{a \tilde{\chi}}) \log_2(1 + \rho a \tilde{\chi})]$, where the random variable $\tilde{\chi}$ is defined to have CDF $(F_Z(x))^b$. Firstly, $\mathbb{E}[\tilde{\chi}]$ can be computed and is given by:

$$\begin{aligned} \mathbb{E}[\tilde{\chi}] &= \int_0^\infty x \frac{b}{1 - \sigma_w^2} \sum_{\ell=0}^{b-1} \binom{b-1}{\ell} (-1)^\ell \exp\left(-\frac{(\ell+1)x}{1 - \sigma_w^2}\right) dx \\ &= \frac{b}{1 - \sigma_w^2} \sum_{\ell=0}^{b-1} \binom{b-1}{\ell} (-1)^\ell \left(\frac{1 - \sigma_w^2}{\ell+1}\right)^2. \end{aligned} \quad (2.35)$$

Then plugging (2.35) into $\mathcal{Q}_1(\alpha_w \alpha \sqrt{x}, \alpha_w \sqrt{ax}) \log_2(1 + \rho ax)$ yields:

$$\mathcal{I}_3^A(a, b) = \mathcal{Q}_1\left(\alpha_w \alpha \sqrt{\mathbb{E}[\tilde{\chi}]}, \alpha_w \sqrt{a \mathbb{E}[\tilde{\chi}]}\right) \log_2(1 + \rho a \mathbb{E}[\tilde{\chi}]). \quad (2.36)$$

Note that $\mathcal{I}_3^A(a, b)$ would serve as an upper bound from Jensen's inequality if the function of interest $\mathcal{Q}_1(\alpha_w \alpha \sqrt{x}, \alpha_w \sqrt{ax}) \log_2(1 + \rho ax)$ was concave in x . Properties of this function such as monotonicity and concavity are of interest and lead to rigorous arguments in support of this bound. If outage does not occur, extensive analysis can be carried out due to the well known properties of the $\log(\cdot)$ function. However, the concavity (or log-concavity) of $\mathcal{Q}_1(\alpha_w \alpha \sqrt{x}, \alpha_w \sqrt{\beta_1 x})$ in x (notice that x appears in both entries of $\mathcal{Q}_1(\cdot, \cdot)$) still remains an important open problem [61]. Our numerical evidence suggests that $\mathcal{Q}_1(\alpha_w \alpha \sqrt{x}, \alpha_w \sqrt{\beta_1 x}) \log_2(1 + \rho \beta_1 x)$ is concave and monotonically increasing in x for practical choices of β_1 . For any given β_1 preserving the aforementioned property, Jensen's inequality yields an upper bound, whose tightness is of interest and discussed in the following proposition. The word practical is used to exclude the situation when β_1 approaches its maximum 1 which in turn enables $\mathcal{Q}_1(\cdot, \cdot)$ to dominate the goodput to incur extreme outage. This makes intuitive sense according to the definition of average goodput.

Proposition 2.2. *Let $\{\tilde{\chi}_b\}$ be the family of positive i.i.d. random variables. If $\mathcal{Q}_1(\alpha_w \alpha \sqrt{x}, \alpha_w \sqrt{\beta_1 x}) \log_2(1 + \rho \beta_1 x)$ is concave and monotonically increasing in x for any given β_1 , then the Jensen bound is asymptotically tight, i.e., as $b \rightarrow \infty$,*

$$\frac{\mathbb{E}[\mathcal{Q}_1(\alpha_w \alpha \sqrt{\tilde{\chi}_b}, \alpha_w \sqrt{\beta_1 \tilde{\chi}_b}) \log_2(1 + \rho \beta_1 \tilde{\chi}_b)]}{\mathcal{Q}_1(\alpha_w \alpha \sqrt{\mathbb{E}[\tilde{\chi}_b]}, \alpha_w \sqrt{\beta_1 \mathbb{E}[\tilde{\chi}_b]}) \log_2(1 + \rho \beta_1 \mathbb{E}[\tilde{\chi}_b])} \rightarrow 1. \quad (2.37)$$

Proof. The proof is provided in Appendix B. □

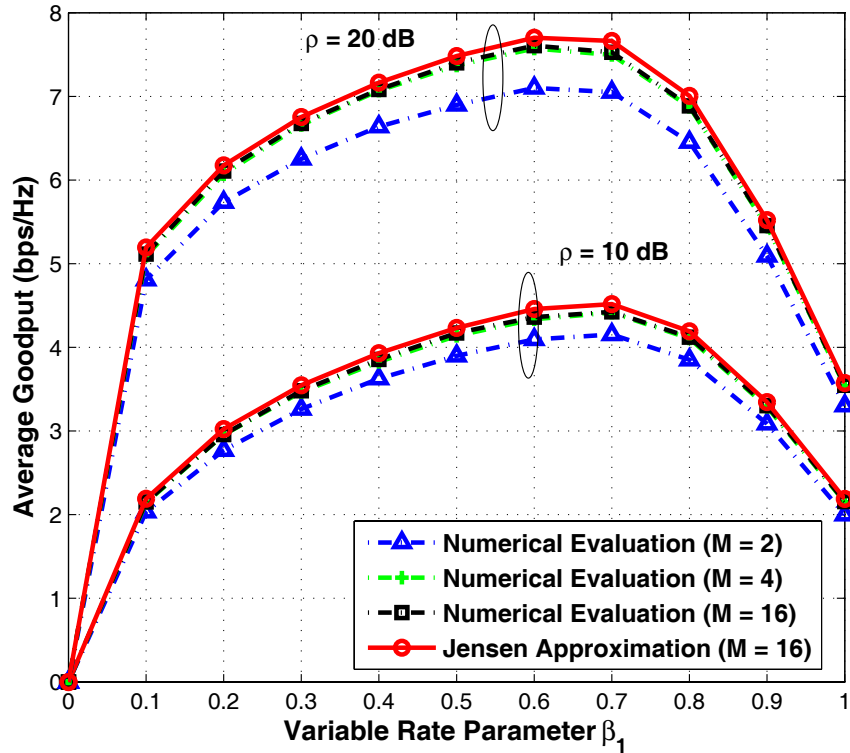


Figure 2.3: Calculating the average goodput from numerical evaluation ($M = 2, 4, 16$) and Jensen approximation ($M = 16$) for the variable rate scenario under different ρ .

Nonetheless, when the aforementioned property is not preserved (e.g., β_1 approaches 1), Jensen's inequality does not hold but the expression has been experimentally found to be a good approximation and so can still be used. Therefore, (2.36) is denoted as Jensen approximation. We conduct a numerical study and demonstrate the tightness of Jensen approximation in Fig. 2.3. It is observed that the approximation method is very tight for moderate (even small) number of users and for all values of $\beta_1 \in [0, 1]$, which shows its potential in accurately tracking the performance of average goodput.

Now we calculate the average outage probability. Since it does not involve

the $\log(\cdot)$ function, it can be computed into closed form as follows:

$$\begin{aligned}
P_1(\beta_1, M) &= \mathbb{E}_{\mathcal{U}} \left[\mathbb{E}_{\tilde{\chi}|\mathcal{U}} [\mathbb{P}(\tilde{\chi} \leq \beta_1 \hat{\chi} | \hat{\chi})] \right] \\
&= \sum_{\tau \neq \mathbf{0}} \mathbb{P}(\mathcal{U}) \sum_{m=0}^{\Phi(M, \boldsymbol{\eta}, \boldsymbol{\tau})} \Theta_{G-1}(N, M, \boldsymbol{\eta}, \boldsymbol{\tau}, m) \\
&\quad \times \left(1 - \mathcal{I}_4 \left(\beta_1, \sum_{g=1}^G \frac{N}{\eta_g} \tau_g - m \right) \right), \tag{2.38}
\end{aligned}$$

where

$$\begin{aligned}
\mathcal{I}_4(a, b) &\triangleq \int_0^\infty \mathcal{Q}_1(\alpha_w \alpha \sqrt{x}, \alpha_w \sqrt{ax}) d(F_{\hat{\chi}}(x))^b \\
&\stackrel{(a)}{=} \frac{2b}{(1 - \sigma_w^2)} \sum_{\ell=0}^{b-1} \binom{b-1}{\ell} (-1)^\ell \\
&\quad \times \int_0^\infty \mathcal{Q}_1(\alpha_w \alpha x, \alpha_w \sqrt{ax}) \exp\left(-\frac{(\ell+1)x^2}{1 - \sigma_w^2}\right) x dx \\
&\stackrel{(b)}{=} \frac{b}{(1 - \sigma_w^2)} \sum_{\ell=0}^{b-1} \binom{b-1}{\ell} (-1)^\ell \frac{1}{\zeta_\ell} \left(1 + \frac{\psi_\ell}{\varsigma_\ell} \right), \tag{2.39}
\end{aligned}$$

$\varpi = \alpha_w \alpha$, $\vartheta = \alpha_w \sqrt{a}$, $\zeta_\ell = \frac{2(\ell+1)}{1 - \sigma_w^2}$, $\varphi_\ell = \varpi^2 + \vartheta^2 + \zeta_\ell$, $\psi_\ell = \varpi^2 - \vartheta^2 + \zeta_\ell$, $\varsigma_\ell = \sqrt{\varphi_\ell^2 - 4\varpi^2\vartheta^2}$. (a) follows from change of variables; (b) follows from applying [62, B.48].

In the case of full feedback, the average outage probability $P_1(\beta_1, M_F)$ becomes:

$$P_1(\beta_1, M_F) = 1 - \mathcal{I}_4(\beta_1, K). \tag{2.40}$$

2.4.4 Optimization and Adaptation to Imperfections

We have obtained the relationship between the system parameter (β_0 or β_1) and the system average goodput, and we now aim to maximize the average goodput by adapting the system parameters.

Consider the optimization of $R_1(\beta_1, M)$ to obtain the optimal backoff factor β_1^* . It is observed from (2.32) that directly optimizing $R_1(\beta_1, M)$ is tedious, and a near-optimal method is now proposed to obtain β_1^* . This method is inspired by the results in Section 2.3.2, which show that the minimum required M^* can be chosen

to achieve almost the same performance as a system with full feedback. Thus an optimal β_1^* for the full feedback scenario can be optimized first, and then M^* is obtained to “match” the system performance. Looking again at Fig. 2.3 with emphasis on different number M of partial feedback, as M gets larger, the optimal β_1 converges to the full feedback case. In this example, $M^* = 4$ is adequate to match the system performance. It is noteworthy to mention that this adaptation philosophy can be applied to partial feedback systems wherein system parameters are optimized according to full feedback assumption first and minimum required partial feedback is chosen subsequently.

Note that a closed form approximation has been obtained to track $R_1(\beta_1, M_F)$ in Section 2.4.3, which is denoted as $R_1^A(\beta_1, M_F) \triangleq \mathcal{I}_3^A(\beta_1, K)$. The following proposition demonstrates the optimal property of β_1 when optimizing $R_1^A(\beta_1, M_F)$.

Proposition 2.3. *There exists a unique global optimal β_1 maximizing $R_1^A(\beta_1, M_F)$.*

Proof. The proof is provided in Appendix B. □

From the above analysis, the optimization strategy can be described as:

$$\beta_1^* = \arg \max_{0 \leq \beta_1 \leq 1} R_1^A(\beta_1, M_F) \simeq \arg \max_{0 \leq \beta_1 \leq 1} R_1(\beta_1, M_F). \quad (2.41)$$

Since it is proved in Proposition 2.3 that $R_1^A(\beta_1, M_F)$ is quasiconcave [60] in β_1 , numerical approach such as Newton-Raphson method can be applied to obtain β_1^* . As discussed before, once β_1^* is found, the minimum required M^* can be obtained by solving (2.17) or relying on (2.19).

The same strategy can be carried over to the optimization of β_0 , which is presented as follows:

$$\beta_0^* = \arg \max_{\beta_0} R_0(\beta_0, M_F). \quad (2.42)$$

The impact of imperfections on system parameter adaptation, and the comparison between the fixed rate and variable rate strategies will be examined through simulations in Section 2.5.2.

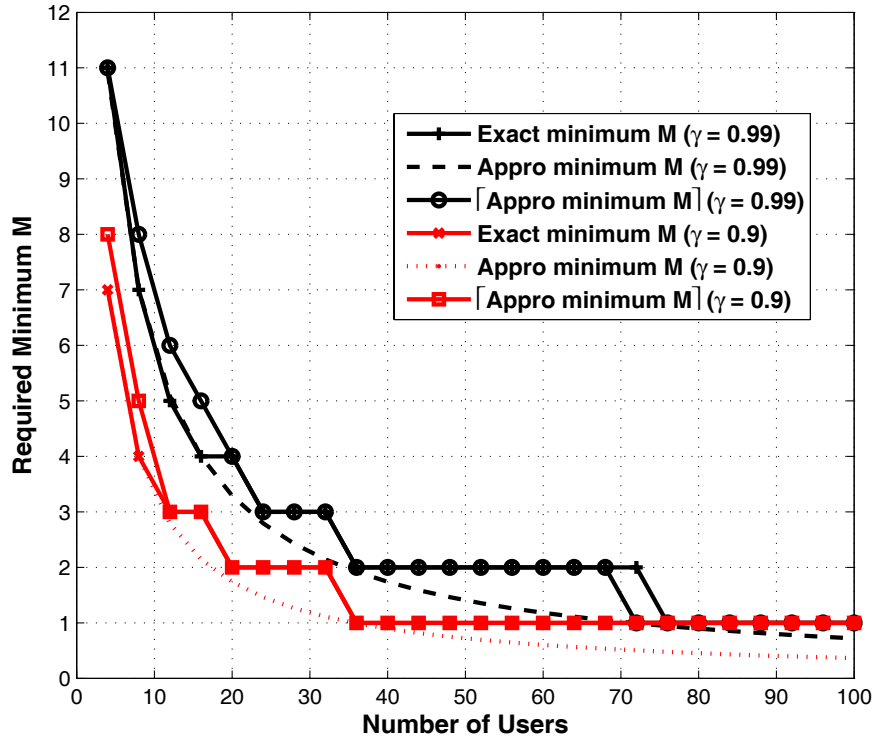


Figure 2.4: Comparison of the required minimum M between numerically solving (2.17) and using approximation (2.19) under different γ with respect to the number of users.

2.5 Numerical Results

In this section, we conduct a numerical study to verify the results developed and to draw some insight.

2.5.1 Perfect Feedback Scenario

The number of resource blocks N is assumed to be 64 for simulations throughout this section. We first consider a 2-cluster system. Fig. 2.4 plots the minimum required M obtained by directly solving (2.17) and alternatively by the approximation (2.19) for two thresholds: $\gamma = 0.99$ and 0.9. Note that the result from (2.19) is rounded with the ceiling function since the required M is an integer. The other simulation parameters are $\boldsymbol{\eta} = (1, 4)$ (i.e., $M_F = 16$), and $\rho = 10$ dB.

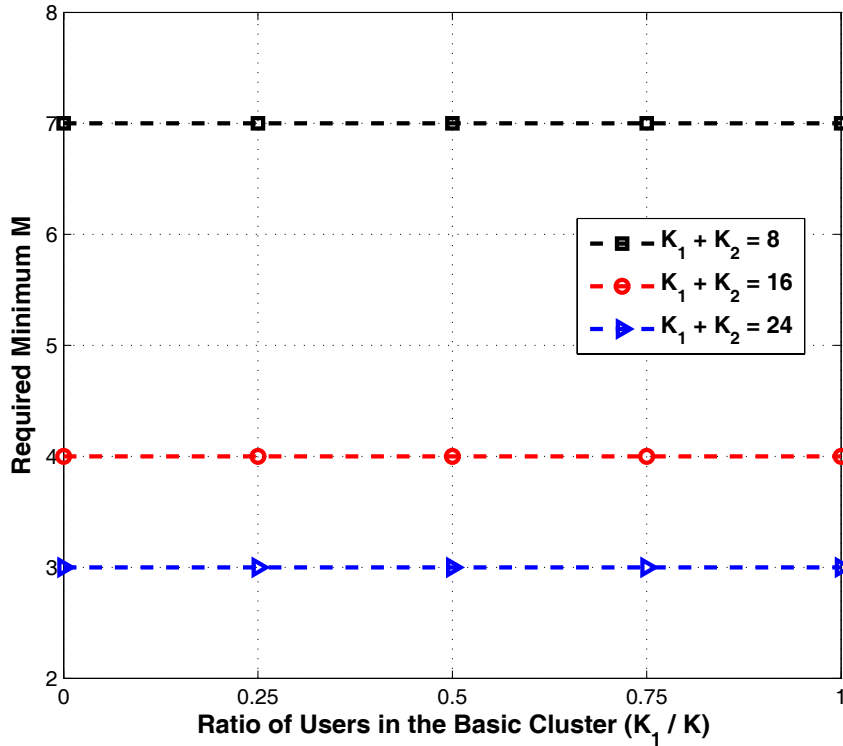


Figure 2.5: Computing the required minimum M with respect to different number of users when varying the ratio of the number of users in cluster \mathcal{K}_1 .

It is observed that the results from the approximate expression matches quite well with the exact computation. The question of whether the required M is sensitive to the partition of users in the system is examined in Fig. 2.5 wherein the ratio of the number of users in cluster \mathcal{K}_1 is changed and the minimum required M is depicted for different total number of users with threshold $\gamma = 0.99$. Interestingly, the result turns out to be “uniform”. As discussed in Section 2.3, it is due to the heterogenous feedback design assumption to let users in cluster \mathcal{K}_1 consume $\frac{\eta G}{\eta_1} M$ ($4M$ in this simulation) feedback which results in the fact that obtaining feedback information from users belonging to different clusters have almost the same influence on scheduling performance. Therefore, the representative simulation setup $K_g = K/G$ can be employed when the system performance metric is investigated with respect to the total number of users.

We now consider a 4-cluster system with subband size vector $\boldsymbol{\eta} = (1, 2, 4, 8)$

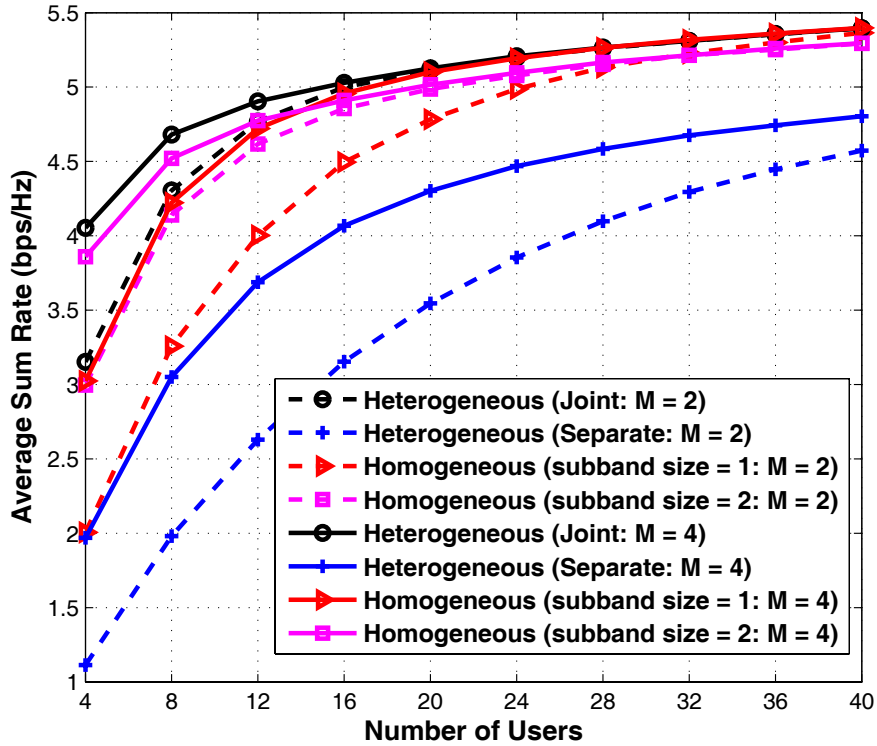


Figure 2.6: Comparison of the average sum rate for a 4-cluster system under different feedback strategies with respect to the number of users.

(i.e., $M_F = 8$). Fig. 2.6 demonstrates the benefit of using heterogeneous feedback design. One of the competing strategies is also heterogeneous, but treats users from each cluster separately. In particular, the system firstly clusters the users based on their channel statistics, and then serves the clusters one by one requiring feedback only from the served cluster of users. In this way, the feedback amount is varying over time depending on the partition of users. This strategy is denoted as *separate* heterogeneous feedback compared to our *joint* heterogeneous feedback design. The other competing strategies are homogeneous without taking advantage of the channel statistics of different users. To maintain at least the same feedback amount for fair comparison, each user in the homogeneous case is assumed to feed back $\lceil \sum_{g=1}^G \frac{\eta_G}{\eta_g} \frac{M}{G} \rceil$ CQI values. Two subband sizes are assumed for the homogeneous feedback. It is clear that for the homogeneous case, users in cluster \mathcal{K}_1 have more independent feedback while users in cluster \mathcal{K}_4 suffer from redundant feedback.

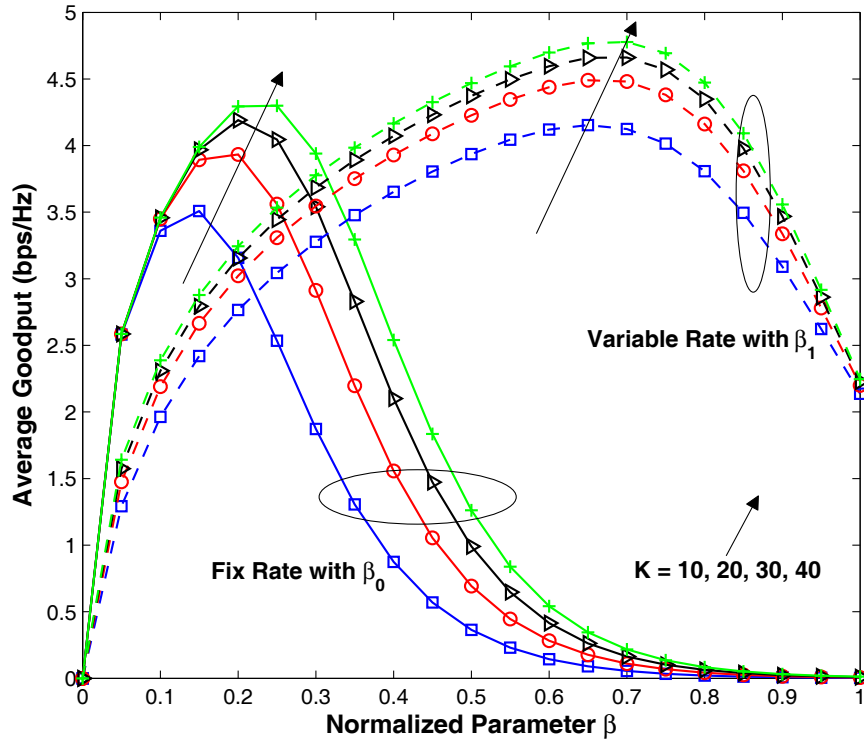


Figure 2.7: Comparison of average goodput between fixed rate and variable rate strategies under normalized parameter β ($\beta = \beta_1 = \beta_0/10$) for different number of users K .

The average sum rate for two different values of M are shown in Fig. 2.6. The separate heterogeneous feedback is observed to have the worst performance from a sum rate perspective because it does not fully exploit multiuser diversity, but it consumes the least feedback. Our joint heterogeneous feedback design is shown to perform much better than the two homogeneous strategies for the 4-cluster system. It is due to the fact that by considering the existing heterogeneity among users, the proposed heterogeneous design can make the best use of the degrees of freedom in the frequency domain in order to enhance the system performance as well as reduce feedback needs.

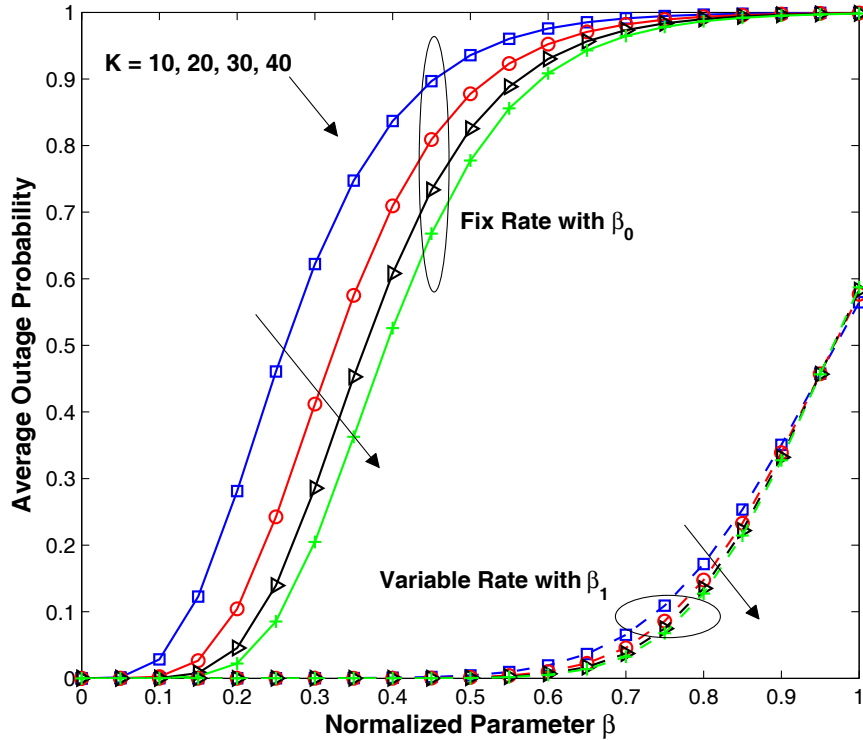


Figure 2.8: Comparison of average outage probability between fixed rate and variable rate strategies under normalized parameter β ($\beta = \beta_1 = \beta_0/10$) for different number of users K .

2.5.2 Imperfect Feedback Scenario

Fig. 2.7 and Fig. 2.8 exhibit the comparison between the fix rate and variable rate outage scenarios as well as the effect of the number of users on the optimization of β_0 and β_1 . In order to show the system performance of the two scenarios in one figure, a normalized parameter β is defined. While examining the variable rate plots $\beta = \beta_1$, and when considering the fixed rate plots $\beta = \beta_0/10$. The system parameters are: $\alpha = 0.98$, $\sigma_w^2 = 0.01$, and $\rho = 10$ dB. It can be seen that for both scenarios, larger number of users K yields better system performance, i.e., higher average goodput and lower average outage probability. This is a consequence of increased multiuser diversity gain to combat the imperfections in the feedback system.

Fig. 2.9 and Fig. 2.10 illustrate the effect of channel estimation error σ_w^2

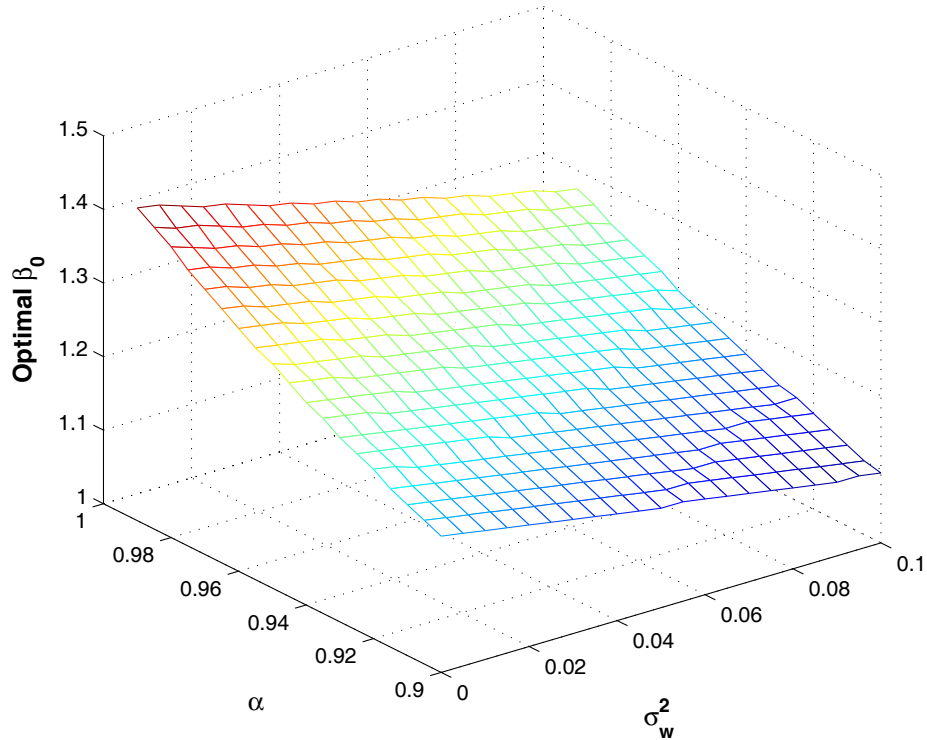


Figure 2.9: The optimal fix rate parameter β_0 with respect to channel estimation error (σ_w^2) and feedback delay (α).

and feedback delay α on the optimal value of β_0 and β_1 . Here σ_w^2 is varied from 0 to 0.1, and α is varied from 0.9 to 0.99 in steps of 0.005. It can be observed from the changing profiles that both the optimal values of β_0 and β_1 get smaller as the imperfections become worse. Therefore, the system should adjust the system parameters to adapt to the encountered imperfections.

Now we consider the adaptation of system parameters (β_0 or β_1) and partial feedback in a 4-cluster heterogeneous feedback system. The system parameters are: $\boldsymbol{\eta} = (1, 2, 4, 8)$, $\alpha = 0.98$, $\sigma_w^2 = 0.01$, and $\rho = 10$ dB. For both transmission strategies and for a given number of users K , the optimal value of β_0^* or β_1^* is first optimized according to the full feedback case discussed in Section 2.4.4. Then, a minimum required M^* is obtained by matching the system performance to that in the full feedback case. Fig. 2.11 demonstrates the average goodput for both transmission strategies with M^* and β_0^* (or β_1^*). We observe that there is almost

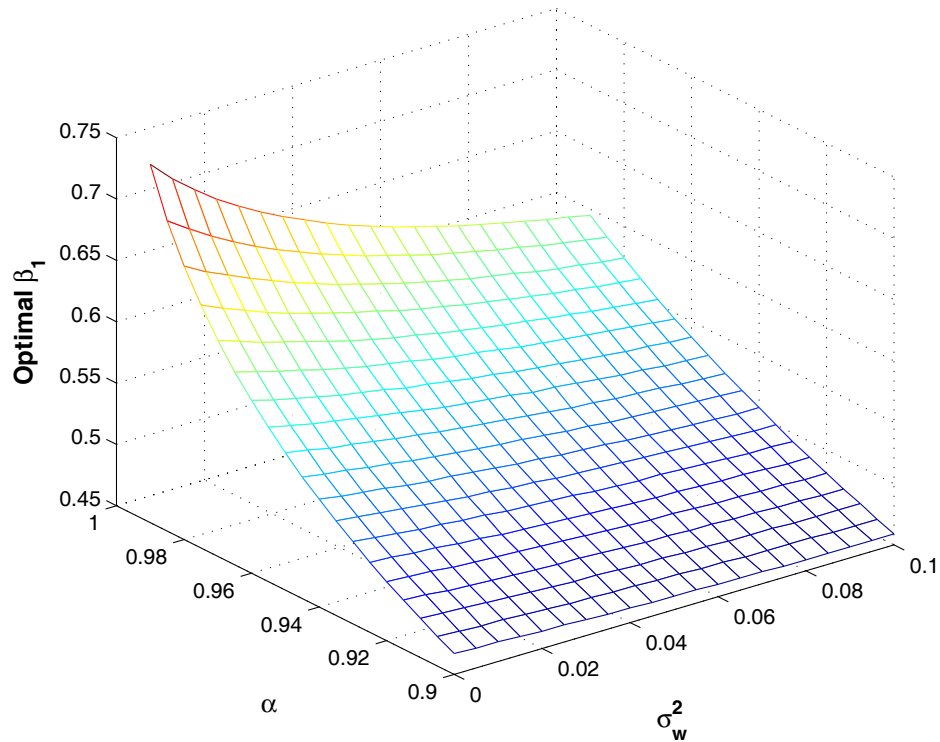


Figure 2.10: The optimal variable rate parameter β_1 with respect to channel estimation error (σ_w^2) and feedback delay (α).

a constant performance gain for the variable rate strategy compared with the fix rate one. This is due to the fact that for the variable rate scenario, the system is adapting the transmission parameters conditioned on the past memory even if it is the outdated one. If the channel estimation error and feedback delay are not severe, the imperfections can be compensated by multiplying with the backoff factor and relying on the past feedback.

2.6 Conclusion

In this chapter, we propose and analyze a heterogeneous feedback design adapting the feedback resource according to users' frequency domain channel statistics. Under the general correlated channel model, we demonstrate the gain by achieving the potential match among coherence bandwidth, subband size and par-

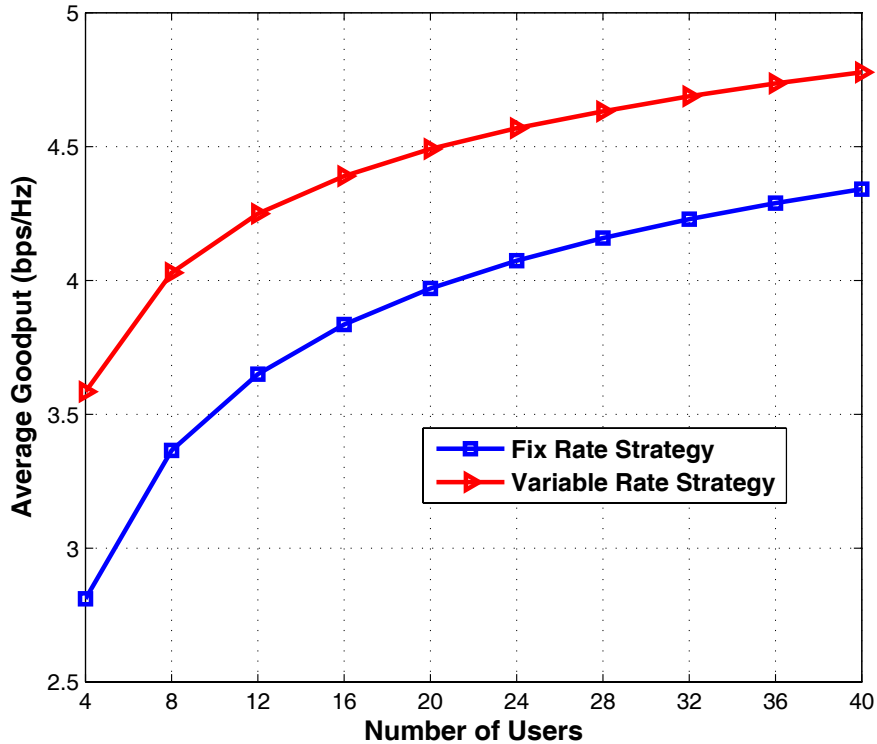


Figure 2.11: Comparison of the average goodput for a 4-cluster system with fix rate and variable rate strategies using optimized β_0^* and β_1^* .

tial feedback. To facilitate statistical analysis, we employ the subband fading model for the multi-cluster heterogeneous feedback system. We derive a closed form expression of the average sum rate under perfect partial feedback assumption, and provide a method to obtain the minimum heterogeneous partial feedback required to obtain performance comparable to a scheme using full feedback. We also analyze the effect of imperfections on the heterogeneous partial feedback system. We obtain a closed form expression for the average goodput of the fix rate scenario, and utilize a bounding technique and tight approximation to track the performance of the variable rate scenario. Methods adapting the system parameters to maximize the average system goodput are proposed. The heterogeneous feedback design is shown to outperform the homogeneous one with the same feedback resource. With imperfections, the system adjusting the transmission strategy and the amount of partial feedback is shown to yield better performance. The

developed analysis provides a theoretical reference to understand the approximate behavior of the proposed heterogeneous feedback system and its interplay with practical imperfections.

The text of this chapter, in part, is a reprint of the paper [63], Y. Huang and B. D. Rao, “Performance analysis of heterogeneous feedback design in an OFDMA downlink with partial and imperfect feedback”, *IEEE Transactions on Signal Processing*, *accepted, to appear*, 2012. The dissertation author is the primary researcher and author, and the co-author listed in this publication directed and supervised the research which forms the basis of this chapter.

2.7 Appendices

2.7.1 Appendix A

Proof of Lemma 2.1: The methodology is an extension of the work in [29] which deals with the homogeneous feedback case with one cluster of users and one specific subband size.

Let $F_{Y_k^{(g)}}$ denote the CDF of $Y_k^{(g)} \triangleq Y_{k,r}^{(g)}$. Substituting the subband size $\frac{N}{\eta_g}$ and the number of reported CQI $\frac{\eta_g}{\eta_g}M$ for user k in cluster \mathcal{K}_g makes $F_{Y_k^{(g)}}$ satisfy (2.6). It can be shown that $F_{\tilde{Y}_k^{(g)}}(x) = \mathbb{P}(\tilde{Y}_{k,n}^{(g)} \leq x) = \mathbb{P}(Y_{k, \lceil \frac{n}{\eta_g} \rceil}^{(g)} \leq x) = F_{Y_k^{(g)}}(x)$, which concludes the proof.

Proof of Theorem 2.1: Substituting the expressions of $F_{\tilde{Y}_k^{(g)}}$ from Lemma 2.1 and combining (2.10) yield:

$$F_{X_n|\mathcal{U}_n}(x) = (F_Z(x))^{\sum_{g=1}^G \frac{N}{\eta_g} \tau_g} \times \prod_{g=1}^G \left(\sum_{m=0}^{\frac{\eta_g}{\eta_g} M - 1} \frac{\xi_g(N, M, \boldsymbol{\eta}, 0)}{(F_Z(x))^m} \right)^{\tau_g}. \quad (2.43)$$

Applying [64, 0.314] to a finite-order power series in (2.43), the expression $\left(\sum_{m=0}^{\frac{\eta_g}{\eta_g} M - 1} \frac{\xi_g(N, M, \boldsymbol{\eta}, 0)}{(F_Z(x))^m} \right)^{\tau_g}$ can be written as $\sum_{m=0}^{\tau_g (\frac{\eta_g}{\eta_g} M - 1)} \frac{\Lambda_g(N, M, \boldsymbol{\eta}, \boldsymbol{\tau}, m)}{(F_Z(x))^m}$, where the expression for $\Lambda_g(N, M, \boldsymbol{\eta}, \boldsymbol{\tau}, m)$ is described in Theorem 2.1. Note that the coefficients of $\frac{1}{(F_Z(x))^m}$ can be computed in a recursive manner.

Then we employ [64, 0.316] for the multiplication of power series. For $g = 1$, $\Theta_1(N, M, \boldsymbol{\eta}, \boldsymbol{\tau}, m)$ can be calculated from $\Lambda_1(N, M, \boldsymbol{\eta}, \boldsymbol{\tau}, m)$ and $\Lambda_2(N, M, \boldsymbol{\eta}, \boldsymbol{\tau}, m)$ as:

$$\begin{aligned}\Theta_1(N, M, \boldsymbol{\eta}, \boldsymbol{\tau}, m) &= \sum_{i=0}^m \Lambda_1(N, M, \boldsymbol{\eta}, \boldsymbol{\tau}, i) \\ &\quad \times \Lambda_2(N, M, \boldsymbol{\eta}, \boldsymbol{\tau}, m - i).\end{aligned}$$

For $2 \leq g < G$, $\Theta_g(N, M, \boldsymbol{\eta}, \boldsymbol{\tau}, m)$ can be computed from $\Theta_{g-1}(N, M, \boldsymbol{\eta}, \boldsymbol{\tau}, m)$ and $\Lambda_{g+1}(N, M, \boldsymbol{\eta}, \boldsymbol{\tau}, m)$ in the following manner:

$$\begin{aligned}\Theta_g(N, M, \boldsymbol{\eta}, \boldsymbol{\tau}, m) &= \sum_{i=0}^m \Theta_{g-1}(N, M, \boldsymbol{\eta}, \boldsymbol{\tau}, i) \\ &\quad \times \Lambda_{g+1}(N, M, \boldsymbol{\eta}, \boldsymbol{\tau}, m - i).\end{aligned}$$

This concludes the proof.

Derivation of $\mathcal{I}_1(a, b)$: From the definition of Z , $F_Z(x) = 1 - \exp(-x)$ and $f_Z(x) = \exp(-x)$. Thus:

$$\begin{aligned}d(F_Z(x))^b &= b(F_Z(x))^{b-1} f_Z(x) dx \\ &= b \sum_{\ell=0}^{b-1} \binom{b-1}{\ell} (-1)^\ell \exp(-(\ell+1)x) dx,\end{aligned}$$

where the last equality follows from the binomial theorem.

Therefore,

$$\begin{aligned}\int_0^\infty \log_2(1+ax) d(F_Z(x))^b &= \frac{b}{\ln 2} \sum_{\ell=0}^{b-1} \binom{b-1}{\ell} (-1)^\ell \\ &\quad \times \int_0^\infty \ln(1+ax) \exp(-(\ell+1)x) dx.\end{aligned}$$

Applying [64, 4.337.2] yields (2.15).

2.7.2 Appendix B

Derivation of $\mathcal{I}_2(a, b)$: From the definition of \hat{Z} , it can be shown that $F_{\hat{Z}}(x) = 1 - \exp(-\frac{1}{1-\sigma_w^2}x)$ and $f_{\hat{Z}}(x) = \frac{1}{1-\sigma_w^2} \exp(-\frac{1}{1-\sigma_w^2}x)$. Then $\mathcal{I}_2(a, b)$ can be

calculated as:

$$\begin{aligned}
& \mathcal{I}_2(a, b) \\
& \stackrel{(a)}{=} \frac{2b}{(1 - \sigma_w^2) \ln 2} \sum_{\ell=0}^{b-1} \binom{b-1}{\ell} (-1)^\ell \\
& \quad \times \int_0^\infty \mathcal{Q}_1(\alpha_w \alpha x, \alpha_w \sqrt{a}) \exp\left(-\frac{(\ell+1)x^2}{1 - \sigma_w^2}\right) x dx \\
& \stackrel{(b)}{=} \frac{2b}{(1 - \sigma_w^2) \ln 2} \sum_{\ell=0}^{b-1} \binom{b-1}{\ell} (-1)^\ell \frac{1}{\zeta_\ell} \\
& \quad \times \left(\mathcal{Q}_1(0, \vartheta) + \exp\left(-\frac{\zeta_\ell \vartheta^2}{2(\varpi^2 + \zeta_\ell)}\right) \left(1 - \mathcal{Q}_1\left(0, \frac{\varpi \vartheta}{\sqrt{\varpi^2 + \zeta_\ell}}\right)\right) \right) \\
& \stackrel{(c)}{=} \frac{2b}{(1 - \sigma_w^2) \ln 2} \sum_{\ell=0}^{b-1} \binom{b-1}{\ell} (-1)^\ell \frac{1}{\zeta_\ell} \\
& \quad \times \left(\exp\left(-\frac{\vartheta^2}{2}\right) + \exp\left(-\frac{\zeta_\ell \vartheta^2}{2(\varpi^2 + \zeta_\ell)}\right) \left(1 - \exp\left(-\frac{\varpi^2 \vartheta^2}{2(\varpi^2 + \zeta_\ell)}\right)\right) \right), \quad (2.44)
\end{aligned}$$

where $\varpi = \alpha_w \alpha$, $\vartheta = \alpha_w \sqrt{a}$, $\zeta_\ell = \frac{2(\ell+1)}{1-\sigma_w^2}$. (a) is obtained by substituting the expression of $d(F_{\hat{z}}(x))^b$ and using change of variables; (b) follows from applying [62, B.18]; (c) follows from using the fact that $\mathcal{Q}_1(0, \vartheta) = \exp(-\frac{\vartheta^2}{2})$.

Proof of Proposition 2.1:

$$\begin{aligned}
& \mathcal{I}_3(a, b) \\
& \stackrel{(a)}{=} \frac{b}{(1 - \sigma_w^2) \ln 2} \sum_{\ell=0}^{b-1} \binom{b-1}{\ell} (-1)^\ell \\
& \quad \times \int_0^\infty \mathcal{Q}_1(\alpha_w \alpha \sqrt{x}, \alpha_w \sqrt{ax}) \ln(1 + \rho ax) \exp\left(-\frac{(\ell+1)x}{1 - \sigma_w^2}\right) dx \\
& \stackrel{(b)}{<} \frac{2\rho ab}{(1 - \sigma_w^2) \ln 2} \sum_{\ell=0}^{b-1} \binom{b-1}{\ell} (-1)^\ell \\
& \quad \times \int_0^\infty \mathcal{Q}_1(\alpha_w \alpha x, \alpha_w \sqrt{ax}) \exp\left(-\frac{(\ell+1)x^2}{1 - \sigma_w^2}\right) x^3 dx \\
& \stackrel{(c)}{=} \frac{4\rho ab}{(1 - \sigma_w^2) \ln 2} \sum_{\ell=0}^{b-1} (-1)^\ell \frac{1}{\zeta_\ell^2} \left(1 + \frac{\vartheta^2}{\varphi_\ell} \left(\frac{\varpi^2}{\varphi_\ell}\right.\right. \\
& \quad \times {}_2F_1\left(1, \frac{3}{2}; 2; \frac{4\varpi^2\vartheta^2}{\varphi_\ell^2}\right) - {}_2F_1\left(\frac{1}{2}, 1; 1; \frac{4\varpi^2\vartheta^2}{\varphi_\ell^2}\right) \\
& \quad \left.\left. + \frac{2\zeta_\ell}{\varphi_\ell} \left(\frac{\varpi^2}{\varphi_\ell} {}_2F_1\left(\frac{3}{2}, 2; 2; \frac{4\varpi^2\vartheta^2}{\varphi_\ell^2}\right) - \frac{1}{2} {}_2F_1\left(1, \frac{3}{2}; 1; \frac{4\varpi^2\vartheta^2}{\varphi_\ell^2}\right)\right)\right)\right), \quad (2.45)
\end{aligned}$$

where $\varpi = \alpha_w \alpha$, $\vartheta = \alpha_w \sqrt{a}$, $\zeta_\ell = \frac{2(\ell+1)}{1-\sigma_w^2}$, $\varphi_\ell = \varpi^2 + \vartheta^2 + \zeta_\ell$, and ${}_2F_1(\cdot, \cdot; \cdot; \cdot)$ is the Gaussian hypergeometric function [57]. (a) is obtained by substituting the expression of $d(F_{\check{Z}}(x))^b$; (b) follows from the fact that when $\rho \ll 1$, ρax is a tight upper bound for $\ln(1 + \rho ax)$; note that change of variables are used; (c) follows from applying [62, B.60].

Proof of Proposition 2.2: Define $s(\check{\chi}_b) \triangleq \mathcal{Q}_1(\alpha_w \alpha \sqrt{\check{\chi}_b}, \alpha_w \sqrt{\beta_1 \check{\chi}_b}) \log_2(1 + \rho \beta_1 \check{\chi}_b)$. Firstly it must be shown that $\frac{s(\check{\chi}_b)}{s(\mathbb{E}[\check{\chi}_b])}$ converges to 1 in probability. For $\forall \epsilon > 0$, it is now shown that:

$$\begin{aligned}
\mathbb{P}\left(\left|\frac{s(\check{\chi}_b)}{s(\mathbb{E}[\check{\chi}_b])} - 1\right| \geq \epsilon\right) &= \mathbb{P}\left(\left|\frac{s(\check{\chi}_b) - s(\mathbb{E}[\check{\chi}_b])}{s(\mathbb{E}[\check{\chi}_b])}\right| \geq \epsilon\right) \\
&\stackrel{(a)}{\leq} \mathbb{P}\left(\frac{s(|\check{\chi}_b - \mathbb{E}[\check{\chi}_b]|)}{s(\mathbb{E}[\check{\chi}_b])} \geq \epsilon\right) \stackrel{(b)}{\rightarrow} 0, \quad (2.46)
\end{aligned}$$

where (a) follows from the concave and monotonically increasing property of $s(\cdot)$: $|s(x) - s(y)| < s(|x - y|)$; (b) follows from the asymptotic scaling rate of $\mathbb{E}[\check{\chi}_b]$ and $|\check{\chi}_b - \mathbb{E}[\check{\chi}_b]|$, and the utilization of the Chebyshev's inequality. From extreme value

theory and asymptotic analysis of order statistics [56, 58], it is known that the tail behavior of $\check{\chi}_b$ converges to type 3 Gumbel distribution, which enables $\mathbb{E}[\check{\chi}_b]$ to scale as $\log b$ and $|\check{\chi}_b - \mathbb{E}[\check{\chi}_b]|$ to scale as $\log \log b$.

Then a method similar to that in [17] can be employed to prove the uniformly integrable property [65] of $\frac{s(\check{\chi}_b)}{s(\mathbb{E}[\check{\chi}_b])}$. By combining the above property along with the convergence in probability leads to convergence in the mean [65], which concludes the proof.

Proof of Proposition 2.3: It must be shown that the following defined function $\mathcal{I}_3^A(\beta_1, K) = \mathcal{Q}_1\left(\alpha_w \alpha \sqrt{\mathbb{E}[\check{\chi}]}, \alpha_w \sqrt{\beta_1 \mathbb{E}[\check{\chi}]}\right) \log_2(1 + \rho \beta_1 \mathbb{E}[\check{\chi}])$ is strictly quasi-concave in β_1 .

This property can be proved by log-concavity [60]. It is shown in [61, 66] that $\mathcal{Q}_1(\sqrt{a}, \sqrt{b})$ is log-concave in $b \in [0, \infty)$ for $a \geq 0$. Also, $\log(1+b)$ is concave thus log-concave in $b \in [0, \infty)$. Since log-concavity is maintained in multiplication, $\mathcal{Q}_1(\sqrt{a}, \sqrt{b}) \log(1+b)$ is log-concave in $b \in [0, \infty)$. From the definition of $\mathcal{I}_3^A(\beta_1, K)$, it is now proved to be log-concave in $\beta_1 \in [0, \infty)$ since $\mathbb{E}[\check{\chi}]$ is irrelevant to β_1 . Therefore, it is quasiconcave in $\beta_1 \in [0, \infty)$ because log-concave functions are also quasiconcave.

In addition, it is clear that $\lim_{\beta_1 \rightarrow 0} \mathcal{I}_3^A(\beta_1, K) = 0$. Also, it is now shown that:

$$\begin{aligned}
0 &\leq \lim_{\beta_1 \rightarrow \infty} \mathcal{I}_3^A(\beta_1, K) \\
&\stackrel{(a)}{\leq} \lim_{\beta_1 \rightarrow \infty} \exp\left(-\frac{(\alpha_w \sqrt{\beta_1 \mathbb{E}[\check{\chi}]} - \alpha_w \alpha \sqrt{\mathbb{E}[\check{\chi}]})^2}{2}\right) \\
&\quad \times \log_2(1 + \rho \beta_1 \mathbb{E}[\check{\chi}]) \\
&\stackrel{(b)}{=} \lim_{\beta_1 \rightarrow \infty} \frac{\rho}{2\alpha_w^2 \ln 2} \frac{1}{(1 + \rho \beta_1 \mathbb{E}[\check{\chi}]) \left(1 - \frac{\alpha}{\sqrt{\beta_1}}\right)} \\
&\quad \times \exp\left(-\frac{(\alpha_w \sqrt{\beta_1 \mathbb{E}[\check{\chi}]} - \alpha_w \alpha \sqrt{\mathbb{E}[\check{\chi}]})^2}{2}\right) = 0, \tag{2.47}
\end{aligned}$$

where (a) follows from the upper bound $\mathcal{Q}_1(a, b) \leq \exp\left(-\frac{(b-a)^2}{2}\right)$ for $b > a \geq 0$ [62]; (b) follows from applying L'Hospital's rule. Therefore, there exists a unique global optimal β_1 which maximizes $\mathcal{I}_3^A(\beta_1, K)$.

Chapter 3

Analytical Framework for Heterogeneous Feedback Being Aware of User Densities

3.1 Introduction

The growing dependence of users on wireless services will require wireless systems to become ubiquitous and offer seamless support. The demands of video and other high data rate applications have placed increasing requirements on networks to support high data rate services in a cost effective manner leading to heterogeneous networks. With the advent of OFDMA-based heterogeneous networks [67, 68] which incorporate lower power pico [69, 70], femto base stations [71–73], and fixed relays [74–76] to coexist with the traditional macrocell, the spectrum reuse has grown aggressively to full usage pattern across different tiers [77] of the heterogeneous structure. One challenging feature of heterogeneous networks is the self-created “cell edges” within the macrocell, which requires advanced techniques both in theory and in practice to model [78], manage [79], and even make use of the cross-tier intercell interference. Among the recent approaches that have been developed such as subcarrier allocation and power control to carefully adapt the system resource in a centralized way [80–82], and utilization of

spatial domain for cooperative multicell processing to cancel, coordinate, and align the interference [83–88], a significant impediment is the NP-hardness of the problem [89], the limited resource constraints, as well as the need for extensive backhaul capability. These challenges favor the development of distributed solutions. All the aforementioned techniques in the downlink assume the availability of channel state information at the transmitter (CSIT) via feedback¹ [1] to adapt the network transmission strategy to the varying wireless environment. With the rapidly growing number of wireless users, the amount of feedback for the OFDMA-based networks may become prohibitive which motivates the design of efficient feedback schemes without significantly degrading system performance.

In addition to the usual challenges, there are two new issues that arise when investigating partial feedback in heterogeneous networks. Firstly, due to the different locations of the users and different ranges of transmit powers, users' large scale channel effects are highly asymmetric. Therefore, it is equally important to guarantee fairness among users as well as leveraging multiuser diversity [15, 16] in an opportunistic scheduling framework. Secondly, since the number of users or user densities are diverse in a heterogeneous network, it would be beneficial to adapt the feedback and require less feedback when a serving base station has more users associated with it. We refer to this methodology as heterogeneous partial feedback² and we aim to provide an analytical framework to identify its benefits under a fair and distributed opportunistic scheduling policy to fulfill the vision of location awareness [14, 90] and situational awareness.

The first step towards examining the aforementioned issues is developing an opportunistic scheduling policy, which exploits multiuser diversity and also preserves scheduling fairness among heterogeneous users. Traditional scheduling policies such as round robin strategy [91] and greedy strategy [15] are easy to implement, yet only achieve one of the desired features. In this chapter, we consider a

¹For the purpose of scheduling or optimization in a multicell network, the feedback is often needed in a frequency division duplex (FDD) system, or in a time division duplex (TDD) system when the channel reciprocity can not be observed due to intercell interference or duplexing time delay.

²Note that achieving adaptive feedback according to the number of users, the users' channel condition, and users' data rate requirements etc is an important issue in practical systems such as LTE [21, 37].

system that employs the cumulative distribution function (CDF) based scheduling policy [92, 93]. According to the basic CDF-based scheduling strategy, an user is selected whose rate is high enough, but least probable to grow higher. Therefore, this scheduling strategy possesses properties similar to the proportional fair scheduler [16, 24, 94–96], and additionally enables a user’s rate to be independent of the statistics of other users. Herein, the CDF-based scheduling policy is analyzed for a general OFDMA downlink in a multicell environment to examine heterogeneous partial feedback design. Currently, in an OFDMA-based system which groups sub-carriers into resource blocks [6, 19, 36] to form the basic scheduling and feedback unit, two partial feedback strategies are appealing: the thresholding-based partial feedback [17, 18, 20] and the best-M partial feedback [22, 23, 25, 27–29, 97]. The latter strategy, which is considered in practical systems such as LTE [21, 37], requires the users to order and convey the M best channels. Herein, we employ the best-M partial feedback strategy for further analysis. Intuitively, M would be chosen to be small when the user density in a given cell is large, which motivates the utilization of heterogeneous feedback resource across different cells in the heterogeneous networks.

Rigorous development of the analytical framework requires investigation of the interplay between the scheduling policy, partial feedback, and the statistical property of the user’s signal-to-interference-plus-noise ratio (SINR). There are limited results available in the literature on this topic and the available results analyzing the best-M partial feedback are for the single cell scenario without intercell interference [22, 23, 25, 27–29]. A detailed treatment of the best-M partial feedback is provided in [29] and a convenient polynomial form for the CDF of selected user’s SINR is presented for analytical evaluation. Though it is derived for the single cell scenario, it forms the building block for our heterogeneous network analysis which takes into account the cross-tier intercell interference. In this chapter, the analytical framework is treated first from the perspective of exact system performance. We derive the closed form expression for the sum rate with the CDF-based scheduling policy and best-M partial feedback strategy. One key technique developed and utilized is the decomposition of the probability density

function (PDF) of the selected user's SINR, which is amenable for further integration needed to determine system performance. The derived closed form results are directly applicable to further system evaluation.

In order to gain additional insight, we investigate the system performance from the asymptotic perspective utilizing extreme value theory [56, 98] when the number of users in a given cell grows large [58, 99–103]. Different from the special case of full feedback, examining the general best-M partial feedback incurs additional difficulties due to the two-stage maximization resulting from partial feedback and scheduling policy, with the first stage maximization being performed at the user side to provide selective feedback and the second stage maximization being performed at the scheduler side for user selection. Herein, we analyze the tail behavior of the selected user's SINR and establish the type of convergence in order to examine the effect of partial feedback on the randomness of multiuser diversity, show the optimality of best-1 feedback in the asymptotic sense, and more importantly, provide the asymptotic approximation for the sum rate of the general best-M partial feedback. The established asymptotic results further help in analytically tracking and determining the minimum required partial feedback.

To summarize, the contributions of this chapter are threefold: a conceptual framework for situational-aware heterogeneous partial feedback design in an OFDMA-based heterogeneous multicell network, a thorough analysis and derivation of closed form results for the sum rate, and a detailed investigation of the partial feedback based on extreme value theory. All these contributions foster the understanding of heterogeneous feedback design in future systems. Furthermore, the analytical tools developed promise to have broad applicability and can be applied to many related problems. The remainder of the chapter is organized as follows. The system model is provided in Section 3.2. The general treatment without specific channel models is examined in Section 3.3. By assuming standard channel models, Section 3.4 carries out exact performance analysis, and Section 3.5 presents asymptotic analysis. Numerical results are provided in Section 3.6, and Section 3.7 concludes the chapter.

3.2 System Model

We consider the downlink of an OFDMA-based heterogeneous network. The model assumed is generic and sufficiently general to be applicable to a multitier multicell network³, e.g., see Fig. 3.1 for illustration. The system consists of N resource blocks, with one resource block as the basic feedback and scheduling unit. Full spectrum reuse is assumed and it is also assumed that there is no advanced technique employed to suppress interference such as multiuser detection at the receiver side. The process of cell association is assumed to be performed in advance. Without loss of generality, one base station B_0 from the base station set \mathcal{B} and its associated users $\mathcal{K}_0 = \{1, \dots, k, \dots, K_0\}$ with $|\mathcal{K}_0| = K_0$ are considered.

The received signal $y_{k,n}^{(0)}$ of user k at resource block n is represented by

$$y_{k,n}^{(0)} = \sqrt{G_k^{(0)}} H_{k,n}^{(0)} s_{k,n}^{(0)} + \sum_{b=1}^{J_k} \sqrt{G_k^{(b)}} H_{k,n}^{(b)} s_n^{(b)} + v_{k,n}^{(0)}, \quad k \in \mathcal{K}_0, \quad (3.1)$$

where the superscript indicates the base station, i.e., the serving cell and the interfering cells; J_k denotes the number of effective interfering cells for user k , with the influence of other interfering cells, namely the residual interference, included in the additive white noise $v_{k,n}^{(0)}$ distributed with $\mathcal{CN}(0, \sigma_k^2)$. $s_{k,n}^{(0)}$ and $s_n^{(b)}$ are the transmitted symbols by the serving cell and the interfering cell B_b with $\mathbb{E} [|s_{k,n}^{(0)}|^2] = p^{(0)}$ and $\mathbb{E} [|s_n^{(b)}|^2] = p^{(b)}$. $H_{k,n}^{(0)}$ and $H_{k,n}^{(b)}$, which are assumed to be independent across users and resource blocks⁴, denote the small scale frequency domain channel transfer function between the serving cell and user k at resource block n , and between the interfering cell B_b and user k at resource block n , respectively. $G_k^{(0)}$ and $G_k^{(b)}$ represent the large scale channel gain between the serving cell and user k , and between the interfering cell B_b and user k respectively. Based on the aforementioned assumption, the SINR of user k at resource block n can be written as

$$\text{SINR}_{k,n}^{(0)} = \frac{G_k^{(0)} p^{(0)} |H_{k,n}^{(0)}|^2}{\sum_{b=1}^{J_k} G_k^{(b)} p^{(b)} |H_{k,n}^{(b)}|^2 + \sigma_k^2} = \frac{\rho_k^{(0)} |H_{k,n}^{(0)}|^2}{\sum_{b=1}^{J_k} \rho_k^{(b)} |H_{k,n}^{(b)}|^2 + 1}, \quad (3.2)$$

³The special case with one picocell inside a macrocell under symmetric large scale channel effects is studied in [104].

⁴This assumption corresponds to the frequency domain block fading channel model [19, 28, 29] due to its simplicity and capability to provide a good approximation to actual physical channels.

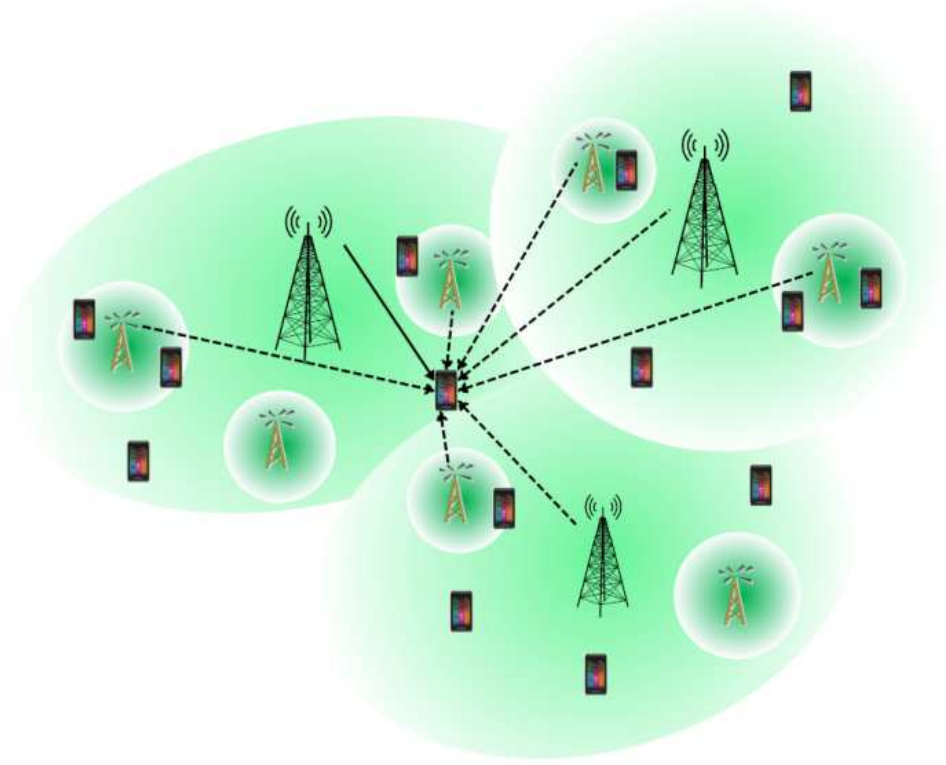


Figure 3.1: Illustration of a generic OFDMA-based multicell heterogeneous cellular networks. Each cell has users associated with it. One selected user for transmission in one resource block is shown: solid line (desired signal); dashed line (potential intercell interference).

where $\rho_k^{(0)} \triangleq \frac{G_k^{(0)} p^{(0)}}{\sigma_k^2}$, $\rho_k^{(b)} \triangleq \frac{G_k^{(b)} p^{(b)}}{\sigma_k^2}$. The SINR is the channel quality information (CQI) that will be fed back and used for scheduling as discussed next.

3.3 General Sum Rate Analysis

This section is devoted to the analysis of the interplay between the scheduling policy and partial feedback for a general channel model (note that no assumption on the distribution of the large and small scale channel gains has been made so far), with treatment of specific channel model in Section 3.4.

Let $Z_{k,n}^{(0)}$ represent $\text{SINR}_{k,n}^{(0)}$ for notational simplicity and denote it as the CQI of user k at resource block n with CDF $F_{Z_k^{(0)}}$. The CDF does not depend on

the resource block index n because the $\text{SINR}_{k,n}^{(0)}$'s are independent and identically distributed (i.i.d.) across resource blocks n for a given user k . Now consider the feedback procedure utilizing the best- M partial feedback strategy. According to the best- M partial feedback strategy, users measure CQI for each resource block at their receiver and feed back the CQI values of the M best resource blocks chosen from the total of N values⁵. More details on the best- M partial feedback approach can be found in [25,27–29,97]. This selective feedback procedure involves a maximization stage at each user. Because only a subset of the ordered CQI are fed back, from the perspective of the scheduler (i.e., the serving base station B_0), if it receives feedback on a certain resource block from a user, it is likely to be any one of the CQI from the ordered subset. We now aim to find the CDF of the CQI seen at the scheduler side as a consequence of partial feedback. Denote $Y_{k,n,M}^{(0)}$ as the received CQI at the scheduler for user k at resource block n under best- M partial feedback, which is the outcome of the user side maximization. Let $F_{Y_{k,M}^{(0)}}$ be its CDF, with resource block index n dropped due to the i.i.d. property across resource blocks for a given user. It is easy to see that for the full feedback case, i.e., $M = N$, $F_{Y_{k,N}^{(0)}} = F_{Z_k^{(0)}}$, and for the best-1 feedback case, i.e., $M = 1$, $F_{Y_{k,1}^{(0)}} = (F_{Z_k^{(0)}})^N$. Utilizing the results in [29], the CDF for the general best- M feedback case can be expressed as

$$F_{Y_{k,M}^{(0)}}(x) = \sum_{m=0}^{M-1} \xi_1(N, M, m) (F_{Z_k^{(0)}}(x))^{N-m}, \quad (3.3)$$

where $\xi_1(N, M, m) = \sum_{i=m}^{M-1} \frac{M-i}{M} \binom{N}{i} \binom{i}{m} (-1)^{i-m}$.

After the scheduler receives feedback from its serving users, it is ready to perform scheduling. It is clear that for the single cell scenario without intercell interference, the scheduling policy is easier to implement and analyze. For instance, in the single cell scenario with homogeneous users, namely same large scale effects, the greedy scheduler or the max-SNR scheduler makes full use of multiuser diversity as well as guarantees fairness due to the same statistics of the user's CQI. In the single cell scenario with heterogeneous users, i.e., different large scale effects [29],

⁵We assume the CQI is fed back without feedback delay. Analyzing the effect of feedback delay [105] on the scheduling framework is beyond the scope of this chapter.

the normalized greedy scheduler which selects user according to their normalized CQI has the same desired property. However, in the general multicell scenario with intercell interference, the $\text{SINR}_{k,n}^{(0)}$'s are independent but non-identically distributed (i.n.i.d.) across users. Therefore, the received CQI at the scheduler for different users $Y_{k,n,M}^{(0)}$ are i.n.i.d. across users. In order to leverage multiuser diversity and guarantee fairness⁶, we employ the CDF-based scheduling policy [92,93]. According to the CDF-based scheduling policy, the scheduler will utilize the distribution of the received CQI for each user, i.e., $F_{Y_{k,M}^{(0)}}$. Herein, it is assumed that the scheduler perfectly knows the CDF⁷, and it conducts the following transformation

$$\tilde{Y}_{k,n,M}^{(0)} = F_{Y_{k,M}^{(0)}}(Y_{k,n,M}^{(0)}). \quad (3.4)$$

The transformed random variable $\tilde{Y}_{k,n,M}^{(0)}$ is uniformly distributed over the range from 0 to 1 and can be regarded as the virtual received CQI of user k at resource block n . The transformed random variables $\tilde{Y}_{k,n,M}^{(0)}$'s are i.i.d. across users, which enables the maximization at the scheduler side to perform fair scheduling. Denoting k_n^* as the random variable representing the selected user for transmission at resource block n , then

$$k_n^* = \arg \max_{k \in \mathcal{U}_{n,M}} \tilde{Y}_{k,n,M}^{(0)}, \quad (3.5)$$

where $\mathcal{U}_{n,M}$ denotes the set of users who convey feedback for resource block n . It can be easily seen that when $M = N$, $\mathbb{P}(|\mathcal{U}_{n,N}| = K_0) = 1$. For the general case when $1 \leq M < N$, the probability mass function (PMF) of $|\mathcal{U}_{n,M}|$ can be shown to be

$$\mathbb{P}(|\mathcal{U}_{n,M}| = \tau_0) = \binom{K_0}{\tau_0} \left(\frac{M}{N}\right)^{\tau_0} \left(1 - \frac{M}{N}\right)^{K_0 - \tau_0}, \quad 0 \leq \tau_0 \leq K_0. \quad (3.6)$$

After the user k_n^* is selected according to (3.5), the scheduler utilizes the corresponding $Y_{k_n^*,n,M}^{(0)}$ for rate matching of the selected user. We denote the random

⁶Note that the motivations as well as the fairness for the proportional-fair (PF) scheduling policy and CDF-based scheduling policy are very different. The PF policy targets the system utility as the definition of system fairness. The CDF-based policy targets the long-term user fairness and each user on average is equiprobable to be scheduled. In the single cell case, it can be shown that these two scheduling policies have similar effects. However, in the general multicell case, users' rates are coupled under the PF policy, and independent under the CDF-based policy.

⁷This is the only system requirement to perform CDF-based scheduling, and the CDF can be obtained by infrequent feedback from users and learned by the system. Methods to estimate the CDF can be found in [92].

variable $X_{n,M}^{(0)}$ as the selected user's CQI for resource block n , and use the sum rate as the system performance metric⁸. The sum rate $C^{(0)}(M)$ for a given base station B_0 employing the CDF-based scheduling and best-M partial feedback is defined as follows

$$C^{(0)}(M) = \frac{1}{N} \sum_{n=1}^N \mathbb{E} \left[\log_2 \left(1 + X_{n,M}^{(0)} \right) \right]. \quad (3.7)$$

From the aforementioned analysis, the sum rate can be formulated, with appropriate conditioning, as⁹

$$\begin{aligned} & C^{(0)}(M) \\ &= \frac{1}{N} \sum_{n=1}^N \mathbb{E}_{k_n^*} \mathbb{E}_{|\mathcal{U}_{n,M}|} \left[\mathbb{E}_{X_{n,M}^{(0)}} \left[\log_2 \left(1 + X_{n,M}^{(0)} \right) \mid |\mathcal{U}_{n,M}| \neq 0 \right] \right. \\ & \quad \left. + \mathbb{E}_{X_{n,M}^{(0)}} \left[\log_2 \left(1 + X_{n,M}^{(0)} \right) \mid |\mathcal{U}_{n,M}| = 0 \right] \right] \\ &= \frac{1}{N} \sum_{n=1}^N \mathbb{E}_{k_n^*} \mathbb{E}_{|\mathcal{U}_{n,M}|} \left[\int_0^1 \log_2 \left(1 + F_{Y_{k_n^*,M}^{(0)}}^{-1}(x) \right) dx^{\tau_0} \mid |\mathcal{U}_{n,M}| \neq 0 \right] \\ &\stackrel{(a)}{=} \mathbb{E}_{k^*} \mathbb{E}_{|\mathcal{U}_M|} \left[\int_0^\infty \log_2(1+t) d(F_{Y_{k^*,M}^{(0)}}(t))^{\tau_0} \mid |\mathcal{U}_M| \neq 0 \right], \end{aligned} \quad (3.8)$$

where (a) follows from the identical distributed property across resource blocks and the change of variable $x = F_{Y_{k^*,M}^{(0)}}^{-1}(t)$. The conditional statistical property of $X_{n,M}^{(0)}$ conditioned on the selected user k_n^* and the set of users who have conveyed feedback $\mathcal{U}_{n,M}$ can be expressed as

$$F_{X_M^{(0)} | k^*=k, |\mathcal{U}_M|=\tau_0}(x) = (F_{Y_{k,M}^{(0)}}(x))^{\tau_0}. \quad (3.9)$$

Using (3.3), it can be expressed in the following power series expansion [29, 64]

$$\begin{aligned} & F_{X_M^{(0)} | k^*=k, |\mathcal{U}_M|=\tau_0}(x) \\ &= \sum_{m=0}^{\tau_0(M-1)} \xi_2(N, M, \tau_0, m) (F_{Z_k^{(0)}}(x))^{N\tau_0-m}, \end{aligned} \quad (3.10)$$

⁸The sum rate is employed as the performance metric in this chapter. Dealing with a more general performance metric representing certain QoS can be referred to [106].

⁹In order to maintain full frequency reuse for analytical tractability, it is assumed that if no user provides CQI for a certain resource block, then that resource block would be in outage and would not contribute to the sum rate calculation.

where

$$\xi_2(N, M, \tau_0, m) = \begin{cases} (\xi_1(N, M, 0))^{\tau_0}, & m = 0 \\ \frac{1}{m\xi_1(N, M, 0)} \sum_{\ell=1}^{\min(m, M-1)} ((\tau_0 + 1)\ell - m) \\ \quad \times \xi_1(N, M, \ell) \xi_2(N, M, \tau_0, m - \ell), & 1 \leq m < \tau_0(M - 1) \\ (\xi_1(N, M, M - 1))^{\tau_0}, & m = \tau_0(M - 1). \end{cases} \quad (3.11)$$

Using (3.6) and (3.10), the sum rate (3.8) can be expressed in the following form

$$\begin{aligned} C^{(0)}(M) &= \mathbb{E}_{k^*} \mathbb{E}_{|\mathcal{U}_M|} \left[\int_0^\infty \log_2(1+x) dF_{X_M^{(0)} | k^*=k, |\mathcal{U}_M|=\tau_0}(x) \mid |\mathcal{U}_M| \neq 0 \right] \\ &\stackrel{(a)}{=} \frac{1}{K_0} \sum_{k=1}^{K_0} \sum_{\tau_0=1}^{K_0} \binom{K_0}{\tau_0} \left(\frac{M}{N}\right)^{\tau_0} \left(1 - \frac{M}{N}\right)^{K_0 - \tau_0} \\ &\quad \times \sum_{m=0}^{\tau_0(M-1)} \xi_2(N, M, \tau_0, m) \mathcal{G}_k(N\tau_0 - m), \end{aligned} \quad (3.12)$$

where where (a) follows from the fair property of the CDF-based scheduling policy: $\mathbb{P}(k^* = k, |\mathcal{U}_M| = \tau_0) = \frac{1}{K_0} \mathbb{P}(|\mathcal{U}_M| = \tau_0)$. The integration $\mathcal{G}_k(\epsilon)$ for $\epsilon \in \mathbb{N}_+$ is defined as

$$\mathcal{G}_k(\epsilon) \triangleq \int_0^\infty \log_2(1+x) d(F_{Z_k^{(0)}}(x))^\epsilon. \quad (3.13)$$

From (3.12), the individual user rate for user k can be expressed as

$$\begin{aligned} C_k^{(0)}(M) &= \frac{1}{K_0} \sum_{\tau_0=1}^{K_0} \binom{K_0}{\tau_0} \left(\frac{M}{N}\right)^{\tau_0} \left(1 - \frac{M}{N}\right)^{K_0 - \tau_0} \\ &\quad \times \sum_{m=0}^{\tau_0(M-1)} \xi_2(N, M, \tau_0, m) \mathcal{G}_k(N\tau_0 - m). \end{aligned} \quad (3.14)$$

For the special full feedback case, the sum rate becomes $C^{(0)}(N) = \frac{1}{K_0} \sum_{k=1}^{K_0} \mathcal{G}_k(K_0)$, and the individual user rate for user k becomes $C_k^{(0)}(N) = \frac{1}{K_0} \mathcal{G}_k(K_0)$.

Remark: A few remarks are in order. Firstly, the effect of best-M partial feedback and the CDF-scheduling policy result in a two stage maximization. The first stage maximization occurs at each user side to select the M best CQI for feedback. The second stage maximization is conducted at the scheduler side by

performing CDF-based transformation and user scheduling. Secondly, with the help of CDF-based scheduling, each user feels as if the other users had the same CDF for scheduling competition [92]. In other words, each individual user's rate is independent of other users. This important feature not only enables the distributed system to enjoy multiuser diversity, but also makes it possible to consider or predict each user's rate by only considering its own CDF. Thirdly, users are equiprobable to be scheduled despite of their heterogeneous channels (e.g., different statistics due to diverse propagation environments and interference levels), and so the scheduling policy maintains fairness among users.

Up to now, we have obtained the general form of the sum rate and individual user rate with the help of $\mathcal{G}_k(\epsilon)$ without assuming specific distributions on the channel models. In the next section, we derive the closed form expression for $\mathcal{G}_k(\epsilon)$ with standard channel models.

3.4 Exact Performance Analysis

In this section, we perform exact analysis to derive the closed form sum rate with standard Rayleigh fading channel models. Section 3.4.1 examines the PDF and CDF of the SINR for each user and uses them to derive a closed form expression for $\mathcal{G}_k(\epsilon)$ in Section 3.4.2.

3.4.1 The Statistics of CQI

In a practical system setting, the time scale for the large scale and small scale channel effects are much different. The variation of the small scale channel gain H occurs on the order of millisecond; whereas the large scale channel gain G which may consist of path loss, antenna gain, and shadowing, varies usually on the order of tens of seconds. Therefore, the large scale channel effect is assumed to be known in advance by the system, through infrequent feedback or location awareness. The small scale channel effect is modeled as complex Gaussian distributed random variables with zero mean and unit variance $\mathcal{CN}(0, 1)$. From the definition of SINR in (3.2), it can be seen that the numerator is a scaled $\chi^2(2)$ (i.e., chi-square

random variable with 2 degrees of freedom) random variable, and the denominator is a weighted sum of $\chi^2(2)$ random variables plus a constant. The following lemma provides the density function of $\text{SINR}_k^{(0)}$, namely $f_{Z_k^{(0)}}$.

Lemma 3.1. *The PDF of $Z_k^{(0)}$ can be expressed as*

$$f_{Z_k^{(0)}}(x) = \sum_{b=1}^{J_k} \varpi_k^{(b)} e^{-\frac{x}{\rho_k^{(0)}}} \times \left(\frac{1}{\rho_k^{(0)} + \rho_k^{(b)} x} + \frac{\rho_k^{(0)} \rho_k^{(b)}}{\left(\rho_k^{(0)} + \rho_k^{(b)} x\right)^2} \right) u(x), \quad (3.15)$$

where $\varpi_k^{(b)} = \prod_{\substack{i=1 \\ i \neq b}} \frac{\rho_k^{(b)}}{\rho_k^{(b)} - \rho_k^{(i)}}$, and $u(\cdot)$ is the Heaviside step function.

Proof. The proof is given in Appendix C. □

From Lemma 3.1, the CDF of $Z_k^{(0)}$, namely $F_{Z_k^{(0)}}$ can be computed as

$$\begin{aligned} F_{Z_k^{(0)}}(x) &= \int_0^x \sum_{b=1}^{J_k} \varpi_k^{(b)} e^{-\frac{y}{\rho_k^{(0)}}} \\ &\quad \times \left(\frac{1}{\rho_k^{(0)} + \rho_k^{(b)} y} + \frac{\rho_k^{(0)} \rho_k^{(b)}}{\left(\rho_k^{(0)} + \rho_k^{(b)} y\right)^2} \right) dy \\ &= \left(1 - \sum_{b=1}^{J_k} \frac{\varpi_k^{(b)} e^{-\frac{x}{\rho_k^{(0)}}} \rho_k^{(0)}}{\rho_k^{(0)} + \rho_k^{(b)} x} \right) u(x). \end{aligned} \quad (3.16)$$

3.4.2 Procedures to Compute $\mathcal{G}_k(\epsilon)$

Now we consider the computation of $\mathcal{G}_k(\epsilon) = \int_0^\infty \log_2(1+x) d(F_{Z_k^{(0)}}(x))^\epsilon$, which will be carried out in three steps. Step 1 provides a suitable PDF decomposition of $d(F_{Z_k^{(0)}}(x))^\epsilon$ by examining the expression for the PDF. In Step 2, the decomposed PDF is further expanded for integration. Finally, Step 3 employs the outcome of Step 1 and 2 to derive the closed form expression for $\mathcal{G}_k(\epsilon)$ by standard integration techniques. The details are presented next.

Step 1: We are interested in the exact formulation of $d(F_{Z_k^{(0)}}(x))^\epsilon$, where the exponent $\epsilon \in \mathbb{N}_+$. In the following lemma, an amenable decomposition is proposed for the statistical form of $d(F_{Z_k^{(0)}}(x))^\epsilon$.

Lemma 3.2. *The PDF $d(F_{Z_k^{(0)}}(x))^\epsilon$ with $\epsilon \in \mathbb{N}_+$ can be decomposed as*

$$d(F_{Z_k^{(0)}}(x))^\epsilon = \epsilon \sum_{\ell=0}^{\epsilon-1} \binom{\epsilon-1}{\ell} \frac{(-1)^\ell}{\ell+1} \times d \left(1 - e^{-\frac{(\ell+1)x}{\rho_k^{(0)}}} \left(\sum_{b=1}^{J_k} \varpi_k^{(b)} \frac{\rho_k^{(0)}}{\rho_k^{(b)}} \frac{1}{x + \frac{\rho_k^{(0)}}{\rho_k^{(b)}}} \right)^{\ell+1} \right). \quad (3.17)$$

Proof. The proof is given in Appendix C. \square

Step 2: Even though the complicated form of $d(F_{Z_k^{(0)}}(x))^\epsilon$ is decomposed into (3.17), its formulation still prevents direct integration. The following lemma provides an expanded form for one of the terms to facilitate further integration.

Lemma 3.3.

$$\begin{aligned} & \left(\sum_{b=1}^{J_k} \varpi_k^{(b)} \frac{\rho_k^{(0)}}{\rho_k^{(b)}} \frac{1}{x + \frac{\rho_k^{(0)}}{\rho_k^{(b)}}} \right)^{\ell+1} \\ &= \sum_{j_1 + \dots + j_{J_k} = \ell+1} \binom{\ell+1}{j_1, \dots, j_{J_k}} \sum_{b=1}^{J_k} \sum_{i=0}^{j_b} \frac{\psi_{k,i}^{(b)} \prod_{b=1}^{J_k} \left(\frac{\varpi_k^{(b)} \rho_k^{(0)}}{\rho_k^{(b)}} \right)^{j_b}}{\left(x + \frac{\rho_k^{(0)}}{\rho_k^{(b)}} \right)^i}, \end{aligned} \quad (3.18)$$

where

$$\psi_{k,i}^{(b)} = \begin{cases} 0, & i = 0 \\ \frac{1}{(j_b - i)!} \frac{d^{j_b - i}}{dx^{j_b - i}} \left[\left(x + \frac{\rho_k^{(0)}}{\rho_k^{(b)}} \right)^{j_b} \prod_{b=1}^{J_k} \left(x + \frac{\rho_k^{(0)}}{\rho_k^{(b)}} \right)^{-j_b} \right] \Big|_{x = -\frac{\rho_k^{(0)}}{\rho_k^{(b)}}}, & i \geq 1. \end{cases} \quad (3.19)$$

Proof. The proof is given in Appendix C. \square

For illustration purpose, the formulation of Lemma 3.3 is discussed and provided for the special $J_k = 2$ case in Appendix C.

Step 3: The following theorem completes the final step by utilizing the outcomes of the above two steps to derive the closed form expression for $\mathcal{G}_k(\epsilon)$.

Theorem 3.1. $\mathcal{G}_k(\epsilon)$ can be computed as

$$\begin{aligned} \mathcal{G}_k(\epsilon) = & \epsilon \sum_{\ell=0}^{\epsilon-1} \binom{\epsilon-1}{\ell} \frac{(-1)^\ell}{\ell+1} \sum_{j_1+\dots+j_{J_k}=\ell+1} \binom{\ell+1}{j_1, \dots, j_{J_k}} \\ & \times \sum_{b=1}^{J_k} \sum_{i=0}^{j_b} \psi_{k,i}^{(b)} \prod_{b=1}^{J_k} \left(\frac{\varpi_k^{(b)} \rho_k^{(0)}}{\rho_k^{(b)}} \right)^{j_b} \mathcal{I}_1 \left(\frac{(\ell+1)}{\rho_k^{(0)}}, \frac{\rho_k^{(0)}}{\rho_k^{(b)}}, i \right), \end{aligned} \quad (3.20)$$

where $\mathcal{I}_1(\alpha, \beta, \gamma) \triangleq \int_0^\infty \frac{e^{-\alpha x}}{(1+x)(\beta+x)^\gamma} dx$ whose closed form expression is presented in Appendix C.

Proof. The proof is given in Appendix C. \square

The three-step procedure yields the closed form expression for $\mathcal{G}_k(\epsilon)$, which can be substituted into (3.12) and (3.14) to compute the closed form sum rate and individual user rate. The exact closed form expressions only involves finite sums and factorials making it computationally tractable and useful for system evaluation. In the following, the treatment of two simplified special cases are provided: the one-dominant interference limited case and the noise limited case.

One-Dominant Interference Limited Case: This case approximates the scenario when there is one dominant interferer. Without loss of generality, assume $\rho_k^{(1)} \gg \rho_k^{(b)}$ for $b \neq 1$ and the effect of noise is omitted. Then the SINR can be approximated as $\text{SINR}_{k,n}^{(0)} \simeq \text{SIR}_{k,n}^{(0)} = \frac{\rho_k^{(0)} |H_{k,n}^{(0)}|^2}{\rho_k^{(1)} |H_{k,n}^{(1)}|^2}$, which is the F distributed random variable. The CDF of the CQI can be written as

$$F_{Z_k^{(0)}}(x) = \left(1 - \frac{\rho_k^{(0)}}{\rho_k^{(1)} x + \rho_k^{(0)}} \right) u(x). \quad (3.21)$$

In this case, the computation of $\mathcal{G}_k(\epsilon)$ can be reduced to

$$\begin{aligned} \mathcal{G}_k(\epsilon) \stackrel{(a)}{=} & \frac{\epsilon}{\ln 2} \frac{\rho_k^{(0)}}{\rho_k^{(1)}} \sum_{\ell=0}^{\epsilon-1} \binom{\epsilon-1}{\ell} \frac{(-1)^\ell}{\ell+1} \\ & \times \text{Beta}(1, \ell+1) {}_2F_1 \left(1, 1; \ell+2; 1 - \frac{\rho_k^{(0)}}{\rho_k^{(1)}} \right), \end{aligned} \quad (3.22)$$

where (a) follows from [64, 3.197.5], $\text{Beta}(x, y) = \int_0^1 t^{x-1}(1-t)^{y-1}dt$ is the Beta function [64, 8.38] and ${}_2F_1(\cdot, \cdot; \cdot; \cdot)$ is the Gaussian hypergeometric function [57].

Noise Limited Case: This case approximates the scenario when the impact of intercell interference is negligible, i.e., $\rho_k^{(b)} \ll 1$. The SINR can be approximated as $\text{SINR}_{k,n}^{(0)} \simeq \text{SNR}_{k,n}^{(0)} = \rho_k^{(0)} |H_{k,n}^{(0)}|^2$, which is the $\chi^2(2)$ distributed random variable. The CDF of the CQI can be written as

$$F_{Z_k^{(0)}}(x) = \left(1 - e^{-\frac{x}{\rho_k^{(0)}}}\right) u(x). \quad (3.23)$$

In this case, the computation of $\mathcal{G}_k(\epsilon)$ can be reduced to

$$\mathcal{G}_k(\epsilon) \stackrel{(a)}{=} \frac{\epsilon}{\ln 2} \sum_{\ell=0}^{\epsilon-1} \binom{\epsilon-1}{\ell} \frac{(-1)^\ell}{\ell+1} e^{\frac{\ell+1}{\rho_k^{(0)}}} E_1\left(\frac{\ell+1}{\rho_k^{(0)}}\right), \quad (3.24)$$

where (a) follows from [64, 4.337.2] and $E_1(x) = \int_x^\infty \frac{e^{-t}}{t} dt$ is the exponential integral function of the first order [57]. The noise limited case is equivalent to the single cell problem which has been addressed extensively in [25, 27, 29].

Remark: It can be easily seen that the CDF-based scheduling for the two simplified cases has the same effect as the “normalized” CQI based scheduling, which is normalized by $\frac{\rho_k^{(0)}}{\rho_k^{(1)}}$ for the one-dominant interference limited case and normalized by $\rho_k^{(0)}$ for the noise limited case. The general CDF-based scheduling policy enables the general analysis for the multicell scenario, whose closed form expressions have been obtained by the aforementioned procedures. The exact expression, though computable, is not easy to interpret and draw insights. We now use asymptotic analysis to develop results that have the potential of providing further insights.

3.5 Asymptotic Performance Analysis

This section is devoted to the asymptotic analysis when the associated users in a given cell grows large. Section 3.5.1 proves the type of convergence exhibited by the received CQI under best-M partial feedback. A brief summary on the different types of convergence is provided in Appendix D for easy reference. In Section 3.5.2, the asymptotic rate approximation is derived and is employed to

determine the minimum required partial feedback in Section 3.5.3. The results are presented with the proofs relegated to the appendix.

3.5.1 The Type of Convergence

The first step towards performing asymptotic analysis is examining the tail behavior of the received CQI at the scheduler side under partial feedback, namely $Y_{k,M}^{(0)}$ for user k . In the full feedback case, $F_{Y_{k,N}^{(0)}} = F_{Z_k^{(0)}}$, which means the tail behavior of the CQI at the user side $Z_k^{(0)}$ is equivalent to that of the $Y_{k,N}^{(0)}$. However, for the general best-M partial feedback, the relationship between $Y_{k,M}^{(0)}$ and $Z_k^{(0)}$ is given by (3.3) and is recalled here for easy reference as $F_{Y_{k,M}^{(0)}}(x) = \sum_{m=0}^{M-1} \xi_1(N, M, m)(F_{Z_k^{(0)}}(x))^{N-m}$. One natural question is concerning the relationship between the tail behavior of $Y_{k,M}^{(0)}$ and $Z_k^{(0)}$, or formulated in a rigorous way: how to infer the type of convergence of $F_{Y_{k,M}^{(0)}}$ from the type of convergence of $F_{Z_k^{(0)}}$ under the condition of best-M partial feedback? The following theorem addresses this issue.

Theorem 3.2. (*Type of Convergence under Partial Feedback*) $F_{Y_{k,M}^{(0)}}$ has the same type of convergence property as $F_{Z_k^{(0)}}$ under the best-M partial feedback strategy.

Proof. The proof is given in Appendix D. □

Theorem 3.2 states that the best-M partial feedback does not affect the type of convergence. In other words, once the type of convergence for $F_{Z_k^{(0)}}$ is proven, the same property is established for $F_{Y_{k,M}^{(0)}}$. Note that so far no specific statistical property has been assumed for $F_{Z_k^{(0)}}$. In the following, the statistical model expressed in (3.16) will be utilized for further analysis. The following corollary describes the tail behavior of $F_{Z_k^{(0)}}$.

Corollary 3.1. *For the general SINR case in the multicell scenario, $F_{Z_k^{(0)}}$ and $F_{Y_{k,M}^{(0)}}$ belong to the domain of attraction of the Gumbel distribution [98], i.e., $F_{Z_k^{(0)}} \in \mathcal{D}(G_3)$ and $F_{Y_{k,M}^{(0)}} \in \mathcal{D}(G_3)$.*

Proof. The proof is given in Appendix D. □

For completeness, the tail behavior of $F_{Z_k^{(0)}}$ for the special simplified one-dominant interference limited case and the noise limited case is also provided in the following corollary.

Corollary 3.2. *For the one-dominant interference limited case, $F_{Z_k^{(0)}}$ and $F_{Y_{k,M}^{(0)}}$ belong to the domain of attraction of the Fréchet distribution [98], i.e., $F_{Z_k^{(0)}} \in \mathcal{D}(G_1)$ and $F_{Y_{k,M}^{(0)}} \in \mathcal{D}(G_1)$. For the noise limited case, $F_{Z_k^{(0)}}$ and $F_{Y_{k,M}^{(0)}}$ belong to the domain of attraction of Gumbel distribution [98], i.e., $F_{Z_k^{(0)}} \in \mathcal{D}(G_3)$ and $F_{Y_{k,M}^{(0)}} \in \mathcal{D}(G_3)$.*

Proof. The proof is given in Appendix D. □

These established type of convergence results will be used to obtain the asymptotic rate approximation.

3.5.2 Asymptotic Rate Approximation

We now investigate the asymptotic approximation for the exact sum rate whose closed form expression has been derived in Section 3.4. Two additional issues arise in the heterogeneous multicell setting under partial feedback when compared with the standard homogeneous setting under full feedback.

The first issue regards the heterogeneous statistics of the SINR for different users. In the homogeneous setting, the maximization or the order statistics is over the same CDF. Recall that the use of CDF-based scheduling in this chapter has enabled each user to virtually feel that the other associated users are experiencing the same CDF for scheduling competition. Therefore, for a given user k , the order statistics is over the CDF of user k 's received CQI, which makes the individual user rate more interesting than the sum rate.

The second issue arises due to the effect of partial feedback. In the full feedback case, the number of CQI values to maximize over at the scheduler is fixed and equals the number of the associated users K . However, due to partial feedback, the number of CQI values to maximize over at the scheduler is a random quantity. In other words, partial feedback results in a random effect on multiuser diversity. In the exact analysis in Section 3.3, this effect is reflected in the use of $\mathcal{U}_{n,M}$.

We are interested in the asymptotic effect when the number of users grows large. To examine this random effect in the asymptotic analysis, denote the sequence of random variables $\kappa_n(K)$ as the number of CQI values fed back for resource block n with K associated users. It is easy to see from (3.3) and (3.6) that $\kappa_n(K)$ are binomial distributed with probability of success $\frac{M}{N}$ under best-M partial feedback. Thus by the strong law of large numbers, as K grows, the number of CQI values fed back for each resource block becomes $\frac{KM}{N}$. Moreover, the convergence property of the sequence $\kappa_n(K)$ can be shown by invoking the central limit theorem [107]:

$$\lim_{K \rightarrow \infty} \sqrt{K} \left(\frac{\kappa_n(K)}{K} - \frac{M}{N} \right) \xrightarrow{d} \mathcal{N} \left(0, \frac{M}{N} \left(1 - \frac{M}{N} \right) \right), \quad (3.25)$$

where d indicates convergence in distribution. Therefore, by employing the techniques which study the extremes over random sample size [98, 108], we have the following lemma.

Lemma 3.4. *When the number of associated users K goes large, the extreme order statistics [98] of the received CQI for a given user k can be efficiently approximated by $\left(F_{Y_{k,M}^{(0)}} \right)^{\frac{KM}{N}}$.*

Proof. The proof is given in Appendix D. □

Now consider the limiting distribution of the maximum rate in order to derive the asymptotic approximation for the exact rate. Specially, we examine the limiting distribution of the rate $R_{k,M}$,

$$R_{k,M} = T(Y_{k,M}) = \log_2(1 + Y_{k,M}), \quad (3.26)$$

where the superscript (0) is temporally dropped for representation simplicity, and will be added later to tailor the results for specific K_0 and $Y_{k,M}^{(0)}$. Note that the function $T(\cdot)$ in (3.26) makes it tedious to directly check the conditions needed to enable finding the form of the asymptotic distribution. In [99], a limiting throughput distribution theorem is proposed for the full feedback single cell case for a narrowband system. Herein, we generalize the result to be applicable to the general SINR case in the general partial feedback OFDMA scenario with the following best-M limiting throughput distribution (LTD-M) theorem.

Theorem 3.3. (*LTD-M Theorem*) Assume that under the best- M partial feedback strategy with N resource blocks and K associated users, the CQI received at the scheduler for user k , $Y_{k,M}$ is a nonnegative random variable with CDF $F_{Y_{k,M}}(x)$ such that $f_{Y_{k,M}}(x) = F'_{Y_{k,M}}(x) > 0$ and $\omega(F_{Y_{k,M}}) \triangleq \sup\{x : F_{Y_{k,M}}(x) < 1\} = \infty$. If $\lim_{x \rightarrow \infty} \frac{x f_{Y_{k,M}}(x)}{1 - F_{Y_{k,M}}(x)} = \phi > 0$, $F_{Y_{k,M}} \in \mathcal{D}(G_1)$, i.e., $F_{Y_{k,M}}$ belongs to the domain of attraction of the Fréchet distribution, or if $\lim_{x \rightarrow \infty} \frac{d}{dx} \left[\frac{1 - F_{Y_{k,M}}(x)}{f_{Y_{k,M}}(x)} \right] = 0$, $F_{Y_{k,M}} \in \mathcal{D}(G_3)$, i.e., $F_{Y_{k,M}}$ belongs to the domain of attraction of the Gumbel distribution, then the distribution of the throughput for user k , $F_{R_{k,M}}(r) = F_{Y_{k,M}}(T^{-1}(r)) \in \mathcal{D}(G_3)$, i.e., $F_{R_{k,M}}$ belongs to the domain of attraction of the Gumbel distribution. Moreover, the normalizing constants [98] for user k are given by

$$\begin{aligned} a_{k:K}(M) &= \log_2 \left(1 + F_{Y_{k,M}}^{-1} \left(1 - \frac{N}{KM} \right) \right), \\ b_{k:K}(M) &= \log_2 \left(\frac{1 + F_{Y_{k,M}}^{-1} \left(1 - \frac{N}{KM} \right)}{1 + F_{Y_{k,M}}^{-1} \left(1 - \frac{N}{KM} \right)} \right). \end{aligned} \quad (3.27)$$

Proof. The proof is given in Appendix D. □

Remark: The LTD-M theorem enables us to study the distribution of $Y_{k,M}$ instead of directly examining $F_{R_{k,M}}$. Also, note that the relationship of the type of convergence between $Y_{k,M}$ and Z_k has been revealed in Theorem 3.2. Thus the connection between Z_k and $R_{k,M}$ can be established by combining the two theorems.

The normalizing constants in Theorem 3.3 can be used to obtain the asymptotic rate approximation. Denote $\mathcal{C}_k^{(0)}(M)$ as the asymptotic approximation for the individual rate of user k in cell B_0 with total associated users K_0 . Then according to the property that convergence in distribution for the maximum nonnegative random variables results in moment convergence [99, 109], $\mathcal{C}_k^{(0)}(M)$ can be evaluated

by the normalizing constants as follows¹⁰

$$\begin{aligned} \mathcal{C}_k^{(0)}(M) &= \frac{1}{K_0} \left(1 - \left(1 - \frac{M}{N} \right)^{K_0} \right) \\ &\quad \times \left(a_{k:K_0}^{(0)}(M) + E_0 b_{k:K_0}^{(0)}(M) \right), \end{aligned} \quad (3.28)$$

where E_0 is the Euler constant, and $(1 - \frac{M}{N})^{K_0}$ is the probability of scheduling outage. According to the CDF-based scheduling policy, the asymptotic approximation for the sum rate, denoted by $\mathcal{C}^{(0)}(M)$, can be computed as

$$\begin{aligned} \mathcal{C}^{(0)}(M) &= \frac{1}{K_0} \left(1 - \left(1 - \frac{M}{N} \right)^{K_0} \right) \\ &\quad \times \sum_{k=1}^{K_0} \left(a_{k:K_0}^{(0)}(M) + E_0 b_{k:K_0}^{(0)}(M) \right). \end{aligned} \quad (3.29)$$

The form in (3.29) is simpler than the exact analytic expression derived in Section 3.4 and can be an alternate basis for studying heterogeneous networks. Looking again at the normalizing constants in (3.27), the specific expressions involve the inverse of the distribution function, $F_{Y_{k,M}}^{-1}(\cdot)$. In general, due to the complicated form of the SINR as well as the procedure to evaluate $F_{Y_{k,M}}$, this inverse function can not be expressed in simple closed form except in some simplified cases. Since the CDF is a function of a scalar and is monotonically increasing, standard iterative algorithms are well suited for its computation. Now we consider the two aforementioned simplified cases: the one-dominant interference limited case and the noise limited case for illustration. For these two special cases with full feedback and best-1 feedback, the inverse of the distribution function can be computed in closed form, which are summarized in the following corollaries.

Corollary 3.3. *In the one-dominant interference limited case under full feedback,*

¹⁰This form of asymptotic approximation leverages the first and second order moments of the extreme order statistics. Dealing with higher order moments and eventually the rate of convergence can be referred to [110].

the specific form for the normalizing constants are given by:

$$\begin{aligned} a_{k:K_0}^{(0)}(N) &= \log_2 \left(1 + \frac{\rho_k^{(0)}}{\rho_k^{(1)}} (K_0 - 1) \right), \\ b_{k:K_0}^{(0)}(N) &= \log_2 \left(\frac{1 + \frac{\rho_k^{(0)}}{\rho_k^{(1)}} (K_0 e - 1)}{1 + \frac{\rho_k^{(0)}}{\rho_k^{(1)}} (K_0 - 1)} \right). \end{aligned} \quad (3.30)$$

In the noise limited case under full feedback, the specific form for the normalizing constants are given by:

$$\begin{aligned} a_{k:K_0}^{(0)}(N) &= \log_2 \left(1 + \rho_k^{(0)} \ln K_0 \right), \\ b_{k:K_0}^{(0)}(N) &= \log_2 \left(1 + \frac{\rho_k^{(0)}}{1 + \rho_k^{(0)} \ln K_0} \right). \end{aligned} \quad (3.31)$$

Proof. The proof is given in Appendix D. \square

Corollary 3.4. *In the one-dominant interference limited case under best-1 feedback, the specific form for the normalizing constants are given by:*

$$\begin{aligned} a_{k:K_0}^{(0)}(1) &= \log_2 \left(1 + \frac{\rho_k^{(0)}}{\rho_k^{(1)}} \frac{(K_0 - N)^{\frac{1}{N}}}{K_0^{\frac{1}{N}} - (K_0 - N)^{\frac{1}{N}}} \right), \\ b_{k:K_0}^{(0)}(1) &= \log_2 \left(\frac{1 + \frac{\rho_k^{(0)}}{\rho_k^{(1)}} \frac{(K_0 e - N)^{\frac{1}{N}}}{(K_0 e)^{\frac{1}{N}} - (K_0 e - N)^{\frac{1}{N}}}}{1 + \frac{\rho_k^{(0)}}{\rho_k^{(1)}} \frac{(K_0 - N)^{\frac{1}{N}}}{K_0^{\frac{1}{N}} - (K_0 - N)^{\frac{1}{N}}}} \right). \end{aligned} \quad (3.32)$$

In the noise limited case under best-1 feedback, the specific form for the normalizing constants are given by:

$$\begin{aligned} a_{k:K_0}^{(0)}(1) &= \log_2 \left(1 + \rho_k^{(0)} \ln \frac{K_0^{\frac{1}{N}}}{K_0^{\frac{1}{N}} - (K_0 - N)^{\frac{1}{N}}} \right), \\ b_{k:K_0}^{(0)}(1) &= \log_2 \left(\frac{1 + \rho_k^{(0)} \ln \frac{(K_0 e)^{\frac{1}{N}}}{(K_0 e)^{\frac{1}{N}} - (K_0 e - N)^{\frac{1}{N}}}}{1 + \rho_k^{(0)} \ln \frac{K_0^{\frac{1}{N}}}{K_0^{\frac{1}{N}} - (K_0 - N)^{\frac{1}{N}}}} \right). \end{aligned} \quad (3.33)$$

Proof. The proof is given in Appendix D. \square

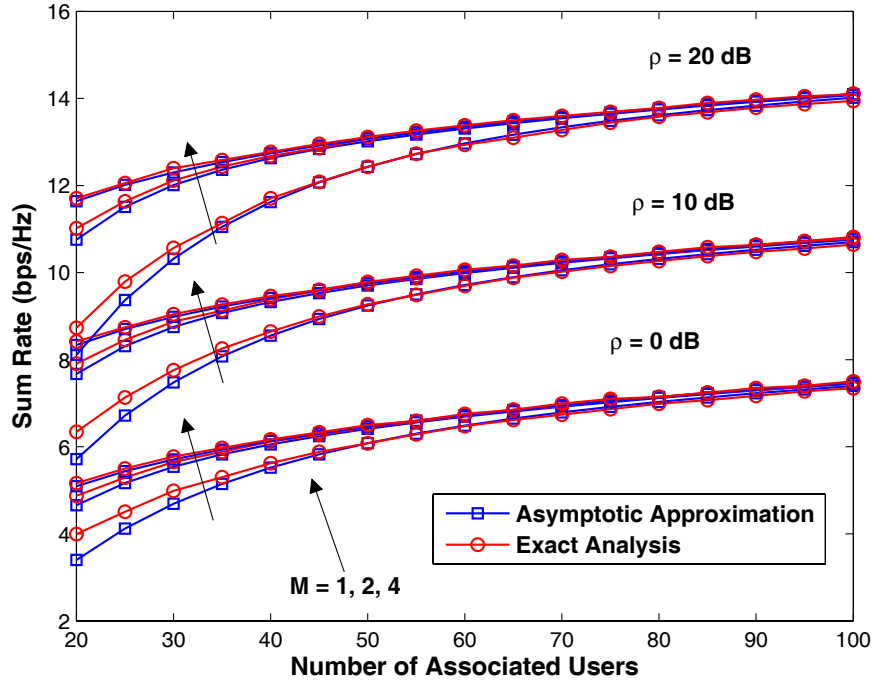


Figure 3.2: Comparison of the sum rate for best- M feedback obtained using the exact analysis and the asymptotic analysis under different symmetric large scale effects for different M with respect to the number of users: the one-dominant interference limited case ($\rho \triangleq \frac{\rho^{(0)}}{\rho^{(1)}}$).

For the general best- M partial feedback case, the normalizing constants can be obtained using (3.27) and the specific CDF for the corresponding case. To illustrate the benefit of asymptotic analysis for the two simplified cases, we conduct a numerical study to compare the sum rate obtained using the exact analysis and the asymptotic one under different symmetric large scale effects in Fig. 3.2 and Fig. 3.3. It is interesting to note that the asymptotic expressions hold well even for small number of users, which means the convergence to the limiting distribution is fast.

Up to now, we have leveraged exact analysis and asymptotic analysis to derive useful closed form results for the exact sum rate and the asymptotic approximation. In the next part, the procedure to determine the minimum required partial feedback is examined.

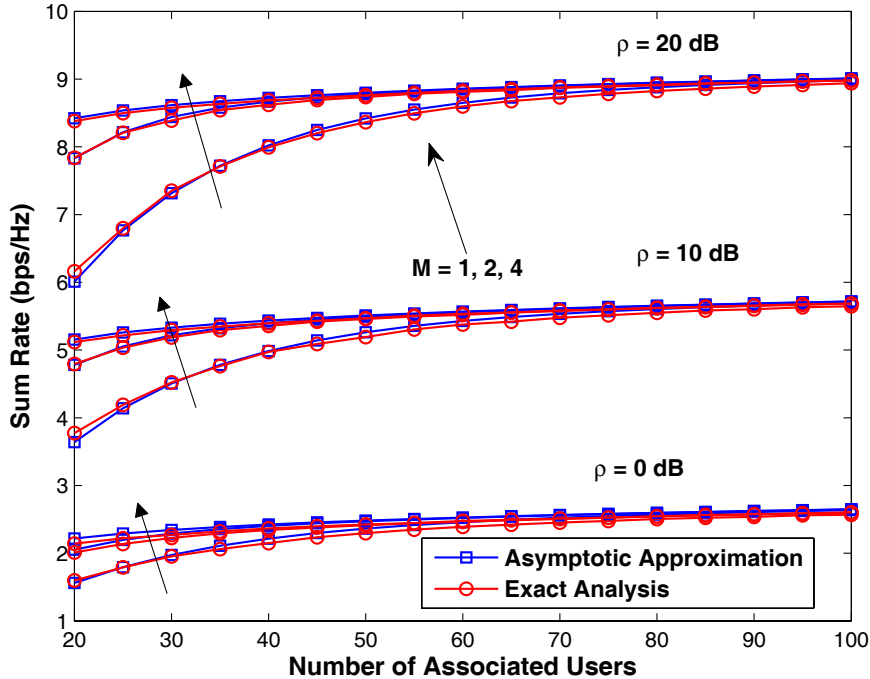


Figure 3.3: Comparison of the sum rate for best- M feedback obtained using the exact analysis and the asymptotic analysis under different symmetric large scale effects for different M with respect to the number of users: the noise limited case ($\rho \triangleq \rho^{(0)}$).

3.5.3 Determining the Minimum Required Partial Feedback

Firstly, the asymptotic optimality of the best-1 feedback is presented in the following corollary.

Corollary 3.5. *When the number of associated users $K \rightarrow \infty$, the performance loss of using best-1 feedback in terms of sum rate approaches zero.*

Proof. The proof is given in Appendix D. □

We are more interested in the pre-asymptotic user regime where the simple best-1 strategy is no longer optimal. The goal is to choose the minimum required M without seriously degrading system sum rate when compared to a system with full feedback. The selection of M can be formulated as the solution to the following

optimization problem:

$$\text{Find the minimum } M^*, \quad \text{s.t. } \frac{C^{(0)}(M^*)}{C^{(0)}(N)} \geq \eta, \quad (3.34)$$

where $C^{(0)}(M)$ refers to the exact analytic expression derived in Section 3.4 and η is a system defined threshold. As mentioned previously, the established asymptotic expressions are more computationally efficient than the exact one. By leveraging the asymptotic approximation, the problem (3.34) can be reformulated as

$$\text{Find the minimum } \tilde{M}^*, \quad \text{s.t. } \frac{\mathcal{C}^{(0)}(\tilde{M}^*)}{\mathcal{C}^{(0)}(N)} \geq \eta, \quad (3.35)$$

where $\mathcal{C}^{(0)}(M)$ refers to the asymptotic approximation in (3.29).

We see from (3.34) and (3.35) that M^* or \tilde{M}^* depends on the number of users associated with the base station and the corresponding large scale channel effects. Since these factors can be highly diverse in a heterogeneous network, the minimum required partial feedback is inherently different across different cells. Therefore, by employing the established asymptotic results, \tilde{M}^* can be quickly determined to track M^* in order to design situational-aware heterogeneous partial feedback.

3.6 Numerical Results

In this section, we conduct a numerical study to support our analysis. A simple heterogeneous network is modeled with two macrocells each with two picocells inside. The locations of the picocells are randomly placed and then fixed for simulation. The system bandwidth is 5 MHz, the noise power spectral density is -170 dBm/Hz, and the number of resource blocks $N = 16$. The transmit powers of the macrocell and picocell are 43 dBm and 30 dBm respectively. The path loss (in dB) model in [111] with 2 GHz central frequency is employed: the path loss from the macrocell base station to users is $15.3 + 37.6 \log_{10} d$ for distance d in meters; the path loss from the picocell base station to users is $30.6 + 36.7 \log_{10} d$ for distance d in meters. Log-normal shadowing is assumed with standard deviation of 8 dB. The radius of the macrocell and picocell is assumed to be 500 m and 100

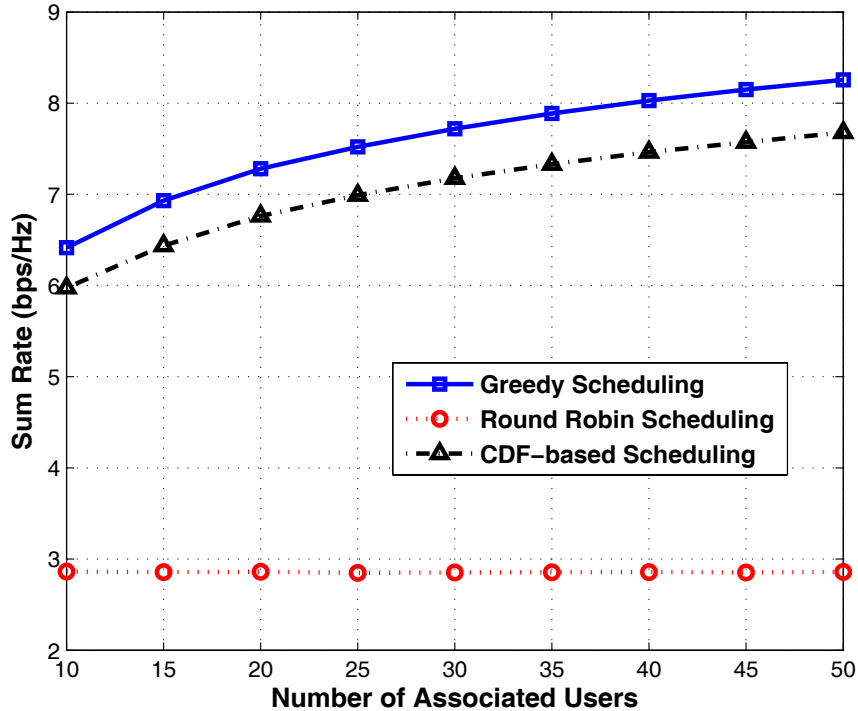


Figure 3.4: The sum rate comparison of the three scheduling policies: the greedy policy, the round robin policy, and the CDF-based policy under best-M partial feedback strategy with respect to the associated users in a macrocell ($N = 16$; $M = 4$).

m respectively. For each drop in simulation, users are randomly placed and the cell association is determined by the large scale effects and fixed.

Firstly, the performance of CDF-based scheduling is compared with the greedy scheduling policy and the round robin scheduling policy in Fig. 3.4 and Fig. 3.5. In this simulation, users are assumed to employ the best-M partial feedback with $M = 4$. In Fig. 3.4, the sum rate with respect to the number of associated users in a macrocell is shown, which is averaged by performing 1000 independent drops. It can be seen that the round robin policy does not invoke multiuser diversity at all, and the sum rate performance of the CDF-based policy is close to the greedy policy. Fig. 3.5 compares the system fairness for the three policies. The system fairness Θ is defined and discussed in [112, 113] using the following form: $\Theta \triangleq - \sum_{k=1}^K \mathbb{P}_k \frac{\ln(\mathbb{P}_k)}{\ln K}$, where \mathbb{P}_k refers to the proportion of resources

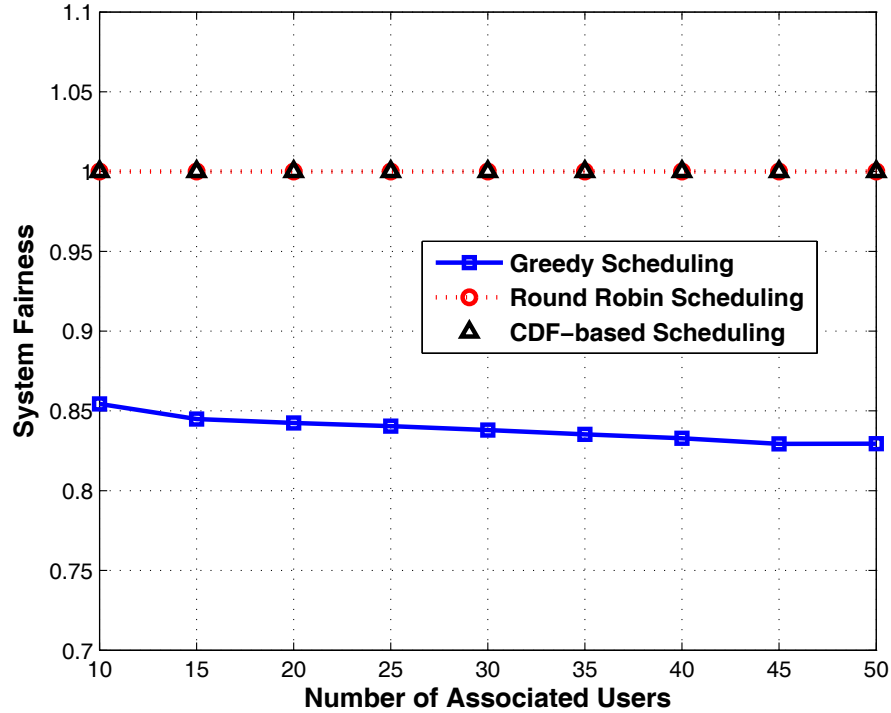


Figure 3.5: The system fairness comparison of the three scheduling policies: the greedy policy, the round robin policy, and the CDF-based policy under best-M partial feedback strategy with respect to the associated users in a macrocell ($N = 16$; $M = 4$).

assigned to user k with the normalization factor $\ln K$. The system fairness for the round robin policy and the CDF-based policy is 1 despite the number of associated users and the heterogeneous channel effects. However, the system fairness for the greedy policy is decreasing when more users are associated. This is due to the fact that some high geometry users occupy the system resources with high probability when the greedy system has more serving users. Therefore, the CDF-based scheduling policy enjoys the multiuser diversity while guaranteeing fairness at the same time, which makes it well suited for the heterogeneous framework.

Next, in order to evaluate the derived closed form results from exact analysis and the corresponding asymptotic approximation, one individual user is randomly selected for demonstration. To illustrate the scaling performance with respect to the number of associated users, the so called individual sum rate for this user is of

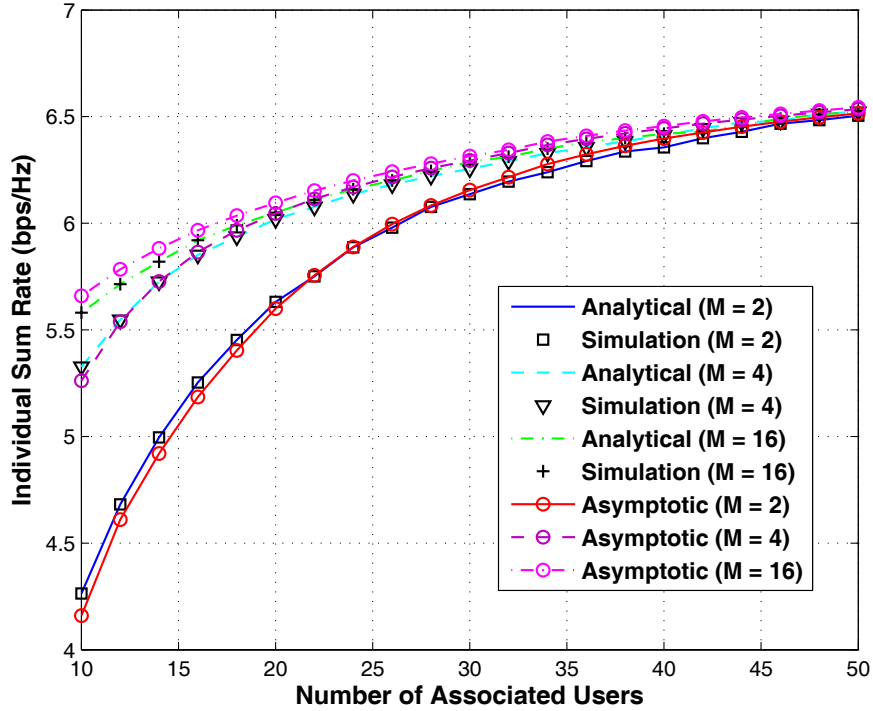


Figure 3.6: Comparison of the individual sum rate obtained from simulation, analytical result, and asymptotic approximation for different partial feedback M with respect to the number of associated users for a randomly selected user in macrocell ($N = 16$; $M = 2, 4, 16$).

interest. The individual sum rate is the individual user rate multiplied by the number of associated users. Fig. 3.6 plots the individual sum rate obtained from the analytical expression by exact analysis, from simulation, and from the established asymptotic approximation using normalizing constants. Different partial feedback cases are also shown for comparison. It can be observed that the analytical expression and the simulation results are in full agreement. Also, the asymptotic approximation tracks the system performance very well. Furthermore, the rate gap between the partial feedback case and full feedback case becomes negligible when the number of associated users increases.

Finally, Fig. 3.7 examines the minimum required partial feedback M^* obtained by using the expression for the sum rate from the exact analysis and the asymptotic approximation for a macrocell. Two different thresholds are set for

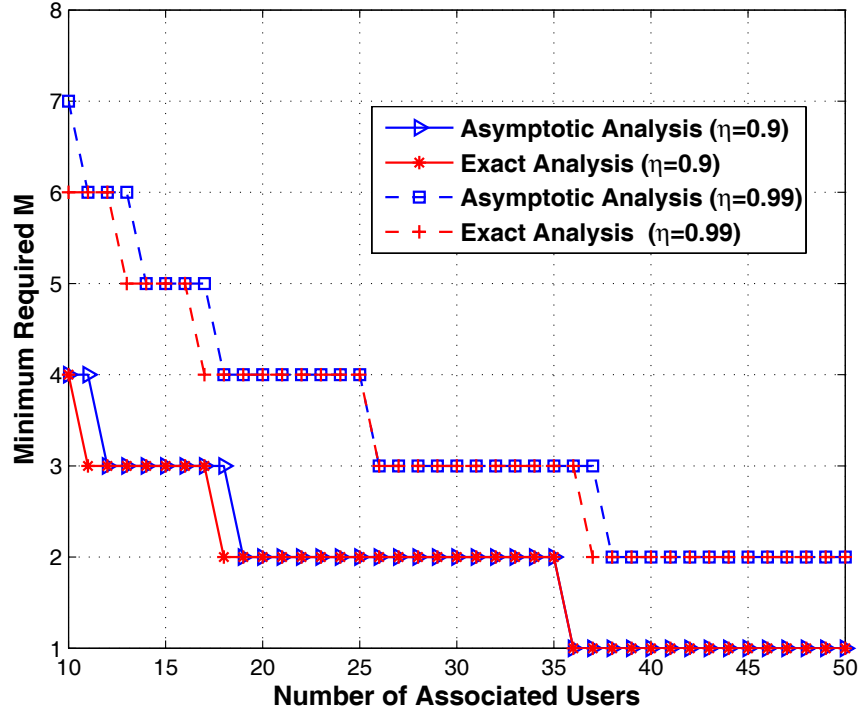


Figure 3.7: Comparison of the minimum required M obtained from exact analysis and asymptotic analysis under different thresholds ($\eta = 0.9, 0.99$).

evaluation: $\eta = 0.9, 0.99$. It can be seen that the results obtained using asymptotic analysis track the results from exact analysis very well, especially for lower threshold and larger number of users. Since the number of users associated with each cell as well as the large scale channel effects can lie in diverse ranges, this results in heterogeneous partial feedback in heterogeneous multicell networks. The total number of partial feedback with respect to the number of associated users for a macrocell is illustrated in Fig. 3.8 under the threshold $\eta = 0.9$. The total number of partial feedback is calculated by multiplying the minimum required partial feedback M^* with a given number of associated users. It can be seen that the range of variation for the total number of partial feedback is limited. Even though the number of associated users is 5 times larger, the total number of partial feedback does not change much. This is due to the heterogeneous partial feedback design to adapt the number of partial feedback to the number of users as well as

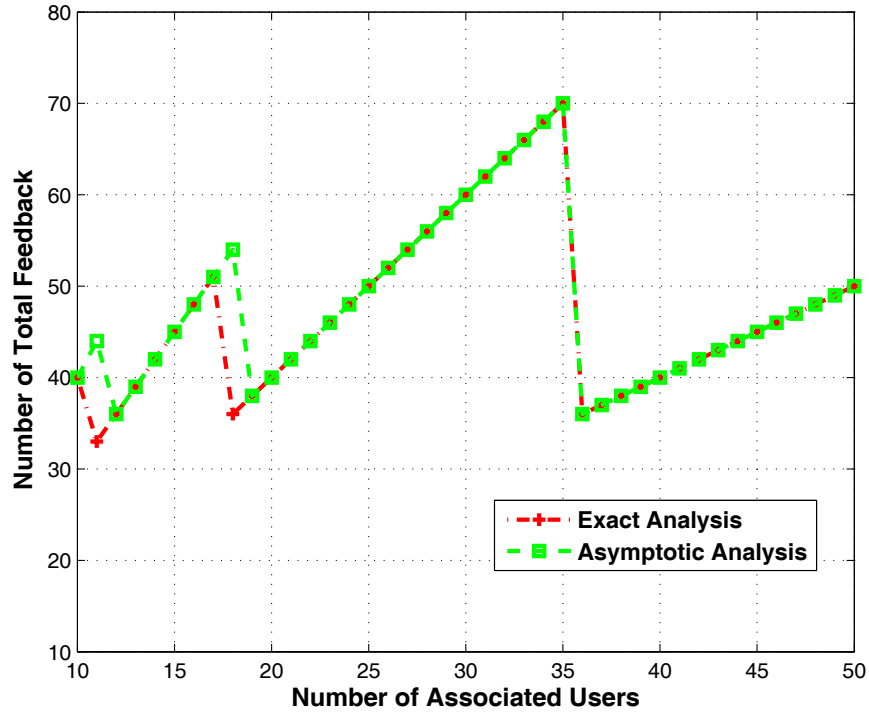


Figure 3.8: Comparison of the total number of required partial feedback from exact analysis and asymptotic analysis under threshold $\eta = 0.9$.

the channel conditions.

3.7 Conclusion

In this chapter, an analytical framework is proposed and developed to investigate the performance of situational-aware heterogeneous partial feedback in an OFDMA-based heterogeneous multicell using the best-M partial feedback strategy. The system model is general and thus the obtained results can be generalized and applied to conduct system evaluation with alternate statistical models. The CDF-based scheduling policy employed in this chapter has the desired property of supporting multiuser diversity while maintaining scheduling fairness among the contending users to guarantee each user's data rate despite of different locations and large scale channel effects. The exact closed form sum rate is obtained for the

multicell model by suitable decomposition and expansion of the received CQI at the scheduler side. Asymptotic analysis is carried out to draw further insight into the multicell model with partial feedback. Interestingly, the effect of partial feedback does not alter the type of convergence of the received CQI. The random effect of multiuser diversity caused by partial feedback is also examined and asymptotic approximations are derived by utilizing the normalizing constants. The established asymptotic approximation tracks the exact system performance well even for small number of users. Therefore, it can be leveraged to quickly determine the minimum required partial feedback in a given cell.

The text of this chapter, in part, is a reprint of the paper [114], Y. Huang and B. D. Rao, “An analytical framework for heterogeneous partial feedback design in heterogeneous multicell OFDMA networks”, *IEEE Transactions on Signal Processing*, *accepted, to appear*, 2012. The dissertation author is the primary researcher and author, and the co-author listed in this publication directed and supervised the research which forms the basis of this chapter.

3.8 Appendices

3.8.1 Appendix C

Proof of Lemma 3.1: Denote $\zeta = \sum_{b=1}^{J_k} \rho_k^{(b)} |H_{k,n}^{(b)}|^2$, which is a weighted sum of $\chi^2(2)$ random variable. In practical system setting, the large scale effects from the interfering cells are distinct, the PDF of ζ is derived to be [115, 116]:

$$f_\zeta(\zeta) = \left(\sum_{b=1}^{J_k} \frac{\varpi_k^{(b)}}{\rho_k^{(b)}} e^{-\frac{\zeta}{\rho_k^{(b)}}} \right) u(x), \quad (3.36)$$

where $\varpi_k^{(b)} = \prod_{\substack{i=1 \\ i \neq b}} \frac{\rho_k^{(b)}}{\rho_k^{(b)} - \rho_k^{(i)}}$. Then the PDF of $Z_k^{(0)}$ can be obtained as follows

$$\begin{aligned}
f_{Z_k^{(0)}}(x) &= \int_0^\infty f_{Z_k^{(0)}|\zeta}(x|\zeta) f_\zeta(\zeta) d\zeta \\
&= \frac{1}{\rho_k^{(0)}} e^{-\frac{x}{\rho_k^{(0)}}} \sum_{b=1}^{J_k} \frac{\varpi_k^{(b)}}{\rho_k^{(b)}} \int_0^\infty (1+\zeta) e^{-\left(\frac{x}{\rho_k^{(0)}} + \frac{1}{\rho_k^{(b)}}\right)\zeta} d\zeta \\
&= \frac{1}{\rho_k^{(0)}} e^{-\frac{x}{\rho_k^{(0)}}} \sum_{b=1}^{J_k} \frac{\varpi_k^{(b)}}{\rho_k^{(b)}} \left(\frac{\rho_k^{(0)}}{x + \frac{\rho_k^{(0)}}{\rho_k^{(b)}}} + \frac{\left(\rho_k^{(0)}\right)^2}{\left(x + \frac{\rho_k^{(0)}}{\rho_k^{(b)}}\right)^2} \right) u(x). \tag{3.37}
\end{aligned}$$

Proof of Lemma 3.2: It is clear that $d(F_{Z_k^{(0)}}(x))^\epsilon = \epsilon(F_{Z_k^{(0)}}(x))^{\epsilon-1} f_{Z_k^{(0)}}(x) dx$. Employing the binomial theorem [117], and substituting the expressions for $F_{Z_k^{(0)}}(x)$ and $f_{Z_k^{(0)}}(x)$ yield

$$\begin{aligned}
d(F_{Z_k^{(0)}}(x))^\epsilon &= \epsilon \sum_{\ell=0}^{\epsilon-1} \binom{\epsilon-1}{\ell} (-1)^\ell \left(\sum_{b=1}^{J_k} \frac{\varpi_k^{(b)} e^{-\frac{x}{\rho_k^{(0)}}} \rho_k^{(0)}}{\rho_k^{(0)} + \rho_k^{(b)} x} \right)^\ell \\
&\quad \times \left(\sum_{b=1}^{J_k} \frac{\varpi_k^{(b)} e^{-\frac{x}{\rho_k^{(0)}}}}{\rho_k^{(0)} + \rho_k^{(b)} x} + \frac{\rho_k^{(0)} \rho_k^{(b)} \varpi_k^{(b)} e^{-\frac{x}{\rho_k^{(0)}}}}{\left(\rho_k^{(0)} + \rho_k^{(b)} x\right)^2} \right) dx \\
&\stackrel{(a)}{=} \epsilon \sum_{\ell=0}^{\epsilon-1} \binom{\epsilon-1}{\ell} \frac{(-1)^\ell}{\ell+1} \\
&\quad \times d \left(1 - \left(\sum_{b=1}^{J_k} \frac{\varpi_k^{(b)} e^{-\frac{x}{\rho_k^{(0)}}} \rho_k^{(0)}}{\rho_k^{(0)} + \rho_k^{(b)} x} \right)^{\ell+1} \right), \tag{3.38}
\end{aligned}$$

where (a) follows from the differentiation property of $(1 - F_{Z_k^{(0)}}(x))^{\ell+1}$.

Proof of Lemma 3.3: Applying the multinomial theorem [117] yields

$$\begin{aligned}
&\left(\sum_{b=1}^{J_k} \varpi_k^{(b)} \frac{\rho_k^{(0)}}{\rho_k^{(b)}} \frac{1}{x + \frac{\rho_k^{(0)}}{\rho_k^{(b)}}} \right)^{\ell+1} \\
&= \sum_{j_1 + \dots + j_{J_k} = \ell+1} \binom{\ell+1}{j_1, \dots, j_{J_k}} \prod_{b=1}^{J_k} \frac{\left(\frac{\varpi_k^{(b)} \rho_k^{(0)}}{\rho_k^{(b)}} \right)^{j_b}}{\left(x + \frac{\rho_k^{(0)}}{\rho_k^{(b)}} \right)^{j_b}}. \tag{3.39}
\end{aligned}$$

Exploiting the partial fraction expansion [64] generates the expanded form in (3.18) with specific expression for $\psi_{k,i}^{(b)}$ defined in (3.19).

For illustration purpose, the expansion for $J_k = 2$ case, which corresponds to two major interferers is now presented. In this case, applying binomial theorem is sufficient for expansion, which yields

$$\begin{aligned}
& \left(\frac{\varpi_k^{(1)} \rho_k^{(0)}}{\rho_k^{(1)}} \frac{1}{x + \frac{\rho_k^{(0)}}{\rho_k^{(1)}}} + \frac{\varpi_k^{(2)} \rho_k^{(0)}}{\rho_k^{(2)}} \frac{1}{x + \frac{\rho_k^{(0)}}{\rho_k^{(2)}}} \right)^{\ell+1} \\
&= \sum_{j=0}^{\ell+1} \binom{\ell+1}{j} \left(\rho_k^{(0)} \right)^{\ell+1} \left(\frac{\varpi_k^{(1)}}{\rho_k^{(1)}} \right)^{\ell+1-j} \left(\frac{\varpi_k^{(2)}}{\rho_k^{(2)}} \right)^j \\
&\quad \times \frac{1}{\left(x + \frac{\rho_k^{(0)}}{\rho_k^{(1)}} \right)^{\ell+1-j} \left(x + \frac{\rho_k^{(0)}}{\rho_k^{(2)}} \right)^j} \\
&= \sum_{j=0}^{\ell+1} \binom{\ell+1}{j} \left(\rho_k^{(0)} \right)^{\ell+1} \left(\frac{\varpi_k^{(1)}}{\rho_k^{(1)}} \right)^{\ell+1-j} \left(\frac{\varpi_k^{(2)}}{\rho_k^{(2)}} \right)^j \\
&\quad \times \left(\sum_{i=0}^{\ell+1-j} \frac{\psi_{k,i}^{(1)}}{\left(x + \frac{\rho_k^{(0)}}{\rho_k^{(1)}} \right)^i} + \sum_{i=0}^j \frac{\psi_{k,i}^{(2)}}{\left(x + \frac{\rho_k^{(0)}}{\rho_k^{(2)}} \right)^i} \right), \tag{3.40}
\end{aligned}$$

where $\psi_{k,i}^{(1)} = (-1)^{\ell+1-j-i} \binom{\ell-i}{j-i} \frac{1}{\left(\frac{\rho_k^{(0)}}{\rho_k^{(2)}} - \frac{\rho_k^{(0)}}{\rho_k^{(1)}} \right)^{\ell+1-i}}$ and $\psi_{k,i}^{(2)} = (-1)^{j-i} \binom{\ell-i}{j-i} \frac{1}{\left(\frac{\rho_k^{(0)}}{\rho_k^{(1)}} - \frac{\rho_k^{(0)}}{\rho_k^{(2)}} \right)^{\ell+1-i}}$

for the nontrivial $i > 0$ case.

Proof of Theorem 3.1: The outcomes of Step 1 and Step 2 lead to direct

integration to calculate $\mathcal{G}_k(\epsilon)$ as follows

$$\begin{aligned}
\mathcal{G}_k(\epsilon) &= \frac{\epsilon}{\ln 2} \sum_{\ell=0}^{\epsilon-1} \binom{\epsilon-1}{\ell} \frac{(-1)^\ell}{\ell+1} \\
&\quad \times \int_0^\infty \ln(1+x) d \left(1 - \left(\sum_{b=1}^{J_k} \frac{\varpi_k^{(b)} e^{-\frac{x}{\rho_k^{(0)}}} \rho_k^{(0)}}{\rho_k^{(0)} + \rho_k^{(b)} x} \right)^{\ell+1} \right) \\
&\stackrel{(a)}{=} \frac{\epsilon}{\ln 2} \sum_{\ell=0}^{\epsilon-1} \binom{\epsilon-1}{\ell} \frac{(-1)^\ell}{\ell+1} \\
&\quad \times \sum_{j_1+\dots+j_{J_k}=\ell+1} \binom{\ell+1}{j_1, \dots, j_{J_k}} \sum_{b=1}^{J_k} \sum_{i=0}^{j_b} \psi_{k,i}^{(b)} \\
&\quad \times \prod_{b=1}^{J_k} \left(\frac{\varpi_k^{(b)} \rho_k^{(0)}}{\rho_k^{(b)}} \right)^{j_b} \int_0^\infty \frac{e^{-\frac{(\ell+1)x}{\rho_k^{(0)}}}}{(1+x) \left(x + \frac{\rho_k^{(0)}}{\rho_k^{(b)}}\right)^i} dx, \tag{3.41}
\end{aligned}$$

where (a) follows from integration by parts. The form of (3.20) is expressed by the definition $\mathcal{I}_1(\alpha, \beta, \gamma) \triangleq \int_0^\infty \frac{e^{-\alpha x}}{(1+x)(\beta+x)^\gamma} dx$. In order to compute $\mathcal{I}_1(\alpha, \beta, \gamma)$ into closed form, firstly apply partial fraction expansion [64] to $\frac{1}{(1+x)(\beta+x)^\gamma}$, and then define the auxiliary integration $\mathcal{I}_2(\alpha, \beta, \gamma) \triangleq \int_0^\infty \frac{e^{-\alpha x}}{(\beta+x)^\gamma} dx$. It is clear that when $\gamma = 0$, $\mathcal{I}_1(\alpha, \beta, \gamma) = \mathcal{I}_2(\alpha, 1, 1)$. For the non-trivial case when $\gamma \geq 1$, employing the partial fraction expansion and after some manipulation the following relationship is revealed between $\mathcal{I}_1(\cdot, \cdot, \cdot)$ and $\mathcal{I}_2(\cdot, \cdot, \cdot)$:

$$\begin{aligned}
\mathcal{I}_1(\alpha, \beta, \gamma) &= \frac{1}{(\beta-1)^\gamma} \mathcal{I}_2(\alpha, 1, 1) \\
&\quad + \sum_{\iota=1}^{\gamma} \frac{(-1)^{\iota-1}}{(1-\beta)^\iota} \mathcal{I}_2(\alpha, \beta, \gamma - \iota + 1). \tag{3.42}
\end{aligned}$$

$\mathcal{I}_2(\alpha, \beta, \gamma)$ can be further computed by noting from [64, 3.352.2] that $\mathcal{I}_2(\alpha, \beta, 1) = e^{\alpha\beta} E_1(\alpha\beta)$, where $E_1(x) = \int_x^\infty \frac{e^{-t}}{t} dt$ is the exponential integral function of the first order [57], and utilizing integration by parts. The closed form result for $\mathcal{I}_2(\alpha, \beta, \gamma)$ is presented as follows

$$\mathcal{I}_2(\alpha, \beta, \gamma) = \begin{cases} \frac{(-1)^{\gamma-1} \alpha^{\gamma-1} e^{\alpha\beta} E_1(\alpha\beta)}{(\gamma-1)!} \\ \quad + \sum_{\iota=1}^{\gamma-1} \frac{(\iota-1)!}{(\gamma-1)!} (-1)^{\gamma-\iota-1} \alpha^{\gamma-\iota-1}, & \gamma \geq 2 \\ e^{\alpha\beta} E_1(\alpha\beta), & \gamma = 1 \end{cases} \tag{3.43}$$

3.8.2 Appendix D

Lemma 3.5. (*Sufficient Conditions for Type of Convergence [56, 58, 98, 99]*) Let $\lambda_1, \lambda_2, \dots, \lambda_K$ be i.i.d. random variables with CDF $F_\lambda(x)$. We denote $\Lambda_K = \max_i \lambda_i$. If there exists some distribution function G which is nondegenerate and some constant $a_K \in \mathbb{R}, b_K > 0$ such that the distribution of $\frac{\Lambda_K - a_K}{b_K}$ converges to G , then G must be one of just three types: G_1 : Fréchet distribution; G_2 : Weibull distribution; G_3 : Gumbel distribution.

The CDF of λ_i , i.e., F_λ determines one of the exact types. If F_λ results in one limiting distribution, then we say F_λ belongs to the domain of attraction of this type, i.e., $F_\lambda \in \mathcal{D}(G_i)$. The well-known sufficient conditions for $F_\lambda \in \mathcal{D}(G_1)$ and $F_\lambda \in \mathcal{D}(G_3)$ are as follows: Define $\omega(F_\lambda) = \sup\{x : F_\lambda(x) < 1\}$. $F_\lambda(x)$ is absolutely continuous and $f_\lambda(x) = F'_\lambda(x)$ and $f'_\lambda(x) = F''_\lambda(x)$ exist, then

(a) $F_\lambda \in \mathcal{D}(G_1)$ if $f_\lambda(x) > 0$ for all large x and for some $\phi > 0$,

$$\lim_{x \rightarrow \infty} \frac{x f_\lambda(x)}{1 - F_\lambda(x)} = \phi. \quad (3.44)$$

(b) $F_\lambda \in \mathcal{D}(G_2)$ if $\mu < \infty$ and for some $\phi > 0$,

$$\lim_{x \rightarrow \mu} \frac{(\mu - x) f_\lambda(x)}{1 - F_\lambda(x)} = \phi. \quad (3.45)$$

(c) $F_\lambda \in \mathcal{D}(G_3)$ if $f_\lambda(x) > 0$ and is differentiable for all x in $(x_1, \omega(F_\lambda))$ for some x_1 , and

$$\lim_{x \rightarrow \omega(F_\lambda)} \frac{d}{dx} \left[\frac{1 - F_\lambda(x)}{f_\lambda(x)} \right] = 0. \quad (3.46)$$

Further, we can choose the normalizing constants $a_K = F_\lambda^{-1}(1 - \frac{1}{K})$ and $b_K = F_\lambda^{-1}(1 - \frac{1}{Ke}) - F_\lambda^{-1}(1 - \frac{1}{K})$, where $F_\lambda^{-1}(x) = \inf\{y : F_\lambda(y) \geq x\}$.

Proof of Theorem 3.2: Assume $Z_k^{(0)}$ is a nonnegative random variable with CDF $F_{Z_k^{(0)}}(x)$ such that $f_{Z_k^{(0)}}(x) > 0$ and $f'_{Z_k^{(0)}}(x)$ exist. The random variable $Y_{k,M}^{(0)}$ is related to $Z_k^{(0)}$ by the following equation:

$$F_{Y_{k,M}^{(0)}}(x) = \sum_{m=0}^{M-1} \xi_1(N, M, m) (F_{Z_k^{(0)}}(x))^{N-m}.$$

$$\begin{aligned}
\lim_{x \rightarrow \infty} \frac{x f_{Y_{k,M}^{(0)}}(x)}{1 - F_{Y_{k,M}^{(0)}}(x)} &= \lim_{x \rightarrow \infty} \frac{x \sum_{m=0}^{M-1} \xi_1(N, M, m)(N-m)(F_{Z_k^{(0)}}(x))^{N-m-1} f_{Z_k^{(0)}}(x)}{1 - \sum_{m=0}^{M-1} \xi_1(N, M, m)(F_{Z_k^{(0)}}(x))^{N-m}} \\
&\stackrel{(a)}{=} \lim_{x \rightarrow \infty} \frac{\sum_{m=0}^{M-1} \xi_1(N, M, m)(N-m) \left(f_{Z_k^{(0)}}(x) + x f'_{Z_k^{(0)}}(x) \right)}{- \sum_{m=0}^{M-1} \xi_1(N, M, m)(N-m)(F_{Z_k^{(0)}}(x))^{N-m-1} f_{Z_k^{(0)}}(x)} \\
&\stackrel{(b)}{=} \frac{N - \sum_{m=0}^{M-1} \xi_1(N, M, m)m}{N - \sum_{m=0}^{M-1} \xi_1(N, M, m)m} \phi = \phi, \tag{3.47}
\end{aligned}$$

$$\begin{aligned}
&\lim_{x \rightarrow \mu} \frac{(\mu - x) f_{Y_{k,M}^{(0)}}(x)}{1 - F_{Y_{k,M}^{(0)}}(x)} \\
&= \lim_{x \rightarrow \mu} \frac{(\mu - x) \sum_{m=0}^{M-1} \xi_1(N, M, m)(N-m)(F_{Z_k^{(0)}}(x))^{N-m-1} f_{Z_k^{(0)}}(x)}{1 - \sum_{m=0}^{M-1} \xi_1(N, M, m)(F_{Z_k^{(0)}}(x))^{N-m}} \\
&\stackrel{(a)}{=} \lim_{x \rightarrow \mu} \frac{\sum_{m=0}^{M-1} \xi_1(N, M, m)(N-m)(F_{Z_k^{(0)}}(x))^{N-m-1} \left(f_{Z_k^{(0)}}(x) - (\mu - x) f'_{Z_k^{(0)}}(x) \right)}{\sum_{m=0}^{M-1} \xi_1(N, M, m)(N-m)(F_{Z_k^{(0)}}(x))^{N-m-1} f_{Z_k^{(0)}}(x)} \\
&\stackrel{(b)}{=} \lim_{x \rightarrow \mu} \frac{\sum_{m=0}^{M-1} \xi_1(N, M, m)(N-m)(F_{Z_k^{(0)}}(x))^{N-m-1}}{\sum_{m=0}^{M-1} \xi_1(N, M, m)(N-m)(F_{Z_k^{(0)}}(x))^{N-m-1}} \phi = \phi, \tag{3.48}
\end{aligned}$$

In order to show that $F_{Y_{k,M}^{(0)}}$ has the same type of convergence property as $F_{Z_k^{(0)}}$, the proof in the sequel will be conducted for each of the three types.

(i) If for some $\phi > 0$, $\lim_{x \rightarrow \infty} \frac{x f_{Z_k^{(0)}}(x)}{1 - F_{Z_k^{(0)}}(x)} = \phi$, then $F_{Z_k^{(0)}} \in \mathcal{D}(G_1)$. It must be

shown that $\lim_{x \rightarrow \infty} \frac{x f_{Y_{k,M}^{(0)}}(x)}{1 - F_{Y_{k,M}^{(0)}}(x)} = \tilde{\phi}$ for some $\tilde{\phi} > 0$. Substituting the expression for $F_{Y_{k,M}^{(0)}}$ and $f_{Y_{k,M}^{(0)}}$ yields (3.47), where (a) holds by applying the L'Hospital's rule; (b) follows from the type of convergence of $Z_k^{(0)}$. Therefore, $\tilde{\phi} = \phi$, and $F_{Y_{k,M}^{(0)}} \in \mathcal{D}(G_1)$.

(ii) If $\mu < \infty$ and for some $\phi > 0$, $\lim_{x \rightarrow \mu} \frac{(\mu - x) f_{Z_k^{(0)}}(x)}{1 - F_{Z_k^{(0)}}(x)} = \phi$, then $F_{Z_k^{(0)}} \in \mathcal{D}(G_2)$.

It must be shown that $\lim_{x \rightarrow \mu} \frac{(\mu - x) f_{Y_{k,M}^{(0)}}(x)}{1 - F_{Y_{k,M}^{(0)}}(x)} = \tilde{\phi}$ for some $\tilde{\phi} > 0$. Substituting the

$$\begin{aligned}
& \lim_{x \rightarrow \infty} \frac{\left(F_{Y_{k,M}}^{(0)}(x) - 1 \right) f'_{Y_{k,M}}(x)}{\left(f_{Y_{k,M}}^{(0)}(x) \right)^2} \\
&= \lim_{x \rightarrow \infty} \frac{\left(\sum_{m=0}^{M-1} \xi_1(N, M, m) (F_{Z_k}^{(0)}(x))^{N-m-1} \right)}{\left(\sum_{m=0}^{M-1} \xi_1(N, M, m) (N-m) (F_{Z_k}^{(0)}(x))^{N-m-1} f_{Z_k}^{(0)}(x) \right)^2} \\
&\quad \times \left(\sum_{m=0}^{M-1} \xi_1(N, M, m) (N-m) (F_{Z_k}^{(0)}(x))^{N-m-1} f'_{Z_k}{}^{(0)}(x) \right) \\
&\quad + \lim_{x \rightarrow \infty} \frac{\left(\sum_{m=0}^{M-1} \xi_1(N, M, m) (F_{Z_k}^{(0)}(x))^{N-m-1} \right)}{\left(\sum_{m=0}^{M-1} \xi_1(N, M, m) (N-m) (F_{Z_k}^{(0)}(x))^{N-m-1} f_{Z_k}^{(0)}(x) \right)^2} \\
&\stackrel{(a)}{=} \frac{\left(\sum_{m=0}^{M-1} \xi_1(N, M, m) (N-m) \right)^2 \left(\sum_{m=0}^{M-1} \xi_1(N, M, m) (F_{Z_k}^{(0)}(x))^{N-m-1} \right)}{\left(\sum_{m=0}^{M-1} \xi_1(N, M, m) (N-m) \right)^2 \left(f_{Z_k}^{(0)}(x) \right)^2} \\
&\quad \times \left(\sum_{m=0}^{M-1} \xi_1(N, M, m) (N-m) (F_{Z_k}^{(0)}(x))^{N-m-1} f'_{Z_k}{}^{(0)}(x) \right) \\
&\stackrel{(b)}{=} 1,
\end{aligned} \tag{3.49}$$

expression for $F_{Y_{k,M}}^{(0)}$ and $f_{Y_{k,M}}^{(0)}$ yields (3.48), where (a) holds by considering the term that dominant the limit and applying the L'Hospital's rule; (b) follows from the type of convergence of $Z_k^{(0)}$. Therefore, $\tilde{\phi} = \phi$, and $F_{Y_{k,M}}^{(0)} \in \mathcal{D}(G_2)$.

(iii) If $\lim_{x \rightarrow \infty} \frac{d}{dx} \left[\frac{1 - F_{Z_k}^{(0)}(x)}{f_{Z_k}^{(0)}(x)} \right] = 0$, and $\lim_{x \rightarrow \infty} \frac{1 - F_{Z_k}^{(0)}(x)}{f_{Z_k}^{(0)}(x)}$ exists, then $F_{Z_k}^{(0)} \in \mathcal{D}(G_3)$. It must be shown that $\lim_{x \rightarrow \infty} \frac{d}{dx} \left[\frac{1 - F_{Y_{k,M}}^{(0)}(x)}{f_{Y_{k,M}}^{(0)}(x)} \right] = 0$. Carrying out the differen-

tiation, another equivalent condition is the following: $\lim_{x \rightarrow \infty} \frac{\left(F_{Y_{k,M}}^{(0)}(x) - 1 \right) f'_{Y_{k,M}}(x)}{\left(f_{Y_{k,M}}^{(0)}(x) \right)^2} = 1$.

Substituting the expression for $F_{Y_{k,M}}^{(0)}$ and $f_{Y_{k,M}}^{(0)}$ yields (3.49), where (a) comes from the fact that $\sum_{m=0}^{M-1} \xi_1(N, M, m) = 1$, (b) holds by applying the L'Hospital's rule and the type of convergence of $Z_k^{(0)}$. Therefore, $F_{Y_{k,M}}^{(0)} \in \mathcal{D}(G_3)$.

Proof of Corollary 3.1: For the general SINR case, in order to prove that $F_{Z_k}^{(0)} \in \mathcal{D}(G_3)$, it must be shown that $\lim_{x \rightarrow \infty} \frac{d}{dx} \left[\frac{1 - F_{Z_k}^{(0)}(x)}{f_{Z_k}^{(0)}(x)} \right] = 0$. Substituting the

expression for $f_{Z_k^{(0)}}$ and $F_{Z_k^{(0)}}$ in (3.15) and (3.16) yields

$$\begin{aligned}
& \lim_{x \rightarrow \infty} \frac{1 - F_{Z_k^{(0)}}(x)}{f_{Z_k^{(0)}}(x)} \\
&= \lim_{x \rightarrow \infty} \frac{\sum_{b=1}^{J_k} \frac{\varpi_k^{(b)} e^{-\frac{x}{\rho_k^{(0)}}} \rho_k^{(0)}}{\rho_k^{(0)} + \rho_k^{(b)} x}}{\sum_{b=1}^{J_k} \varpi_k^{(b)} e^{-\frac{x}{\rho_k^{(0)}}} \left(\frac{1}{\rho_k^{(0)} + \rho_k^{(b)} x} + \frac{\rho_k^{(0)} \rho_k^{(b)}}{(\rho_k^{(0)} + \rho_k^{(b)} x)^2} \right)} \\
&\stackrel{(a)}{=} \frac{\rho_k^{(0)} \sum_{b=1}^{J_k} \varpi_k^{(b)} \frac{1}{\rho_k^{(b)}}}{\sum_{b=1}^{J_k} \varpi_k^{(b)} \frac{1}{\rho_k^{(b)}}} = \rho_k^{(0)}, \tag{3.50}
\end{aligned}$$

where (a) follows from applying the L'Hospital's rule. It can be shown that

$$\begin{aligned}
f'_{Z_k^{(0)}}(x) &= \sum_{b=1}^{J_k} \varpi_k^{(b)} e^{-\frac{x}{\rho_k^{(0)}}} \\
&\times \left(\frac{-\rho_k^{(0)}}{\rho_k^{(0)} + \rho_k^{(b)} x} + \frac{-2\rho_k^{(b)}}{(\rho_k^{(0)} + \rho_k^{(b)} x)^2} + \frac{-2\rho_k^{(0)} \rho_k^{(b)}}{(\rho_k^{(0)} + \rho_k^{(b)} x)^3} \right). \tag{3.51}
\end{aligned}$$

Utilizing the same technique as in (3.50), it can be easily shown that

$$\lim_{x \rightarrow \infty} \frac{f'_{Z_k^{(0)}}(x)}{f_{Z_k^{(0)}}(x)} = -\frac{1}{\rho_k^{(0)}}. \tag{3.52}$$

By combining the results of (3.50) and (3.52), the following equation holds

$$\lim_{x \rightarrow \infty} \frac{(F_{Z_k^{(0)}}(x) - 1) f'_{Z_k^{(0)}}(x)}{(f_{Z_k^{(0)}}(x))^2} = \frac{-\rho_k^{(0)}}{-\rho_k^{(0)}} = 1,$$

which proves the type of convergence of $F_{Z_k^{(0)}}$. Applying Theorem 3.2 yields $F_{Y_{k,M}^{(0)}} \in \mathcal{D}(G_3)$.

Proof of Corollary 3.2: In the one-dominant interference limited case, it is easy to verify that

$$\lim_{x \rightarrow \infty} \frac{x f_{Z_k^{(0)}}(x)}{1 - F_{Z_k^{(0)}}(x)} = \lim_{x \rightarrow \infty} \frac{\rho_k^{(1)} x}{\rho_k^{(1)} x + \rho_k^{(0)}} = 1. \tag{3.53}$$

Thus, $F_{Z_k^{(0)}} \in \mathcal{D}(G_1)$. Applying Theorem 3.2 yields $F_{Y_{k,M}^{(0)}} \in \mathcal{D}(G_1)$.

In the noise limited case, it is easy to verify that $F_{Z_k^{(0)}} \in \mathcal{D}(G_3)$, e.g., see [99]. Applying Theorem 3.2 yields $F_{Y_{k,M}^{(0)}} \in \mathcal{D}(G_3)$.

Proof of Lemma 3.4: To prove this lemma, the following theorem which discusses the extremes over random sample size is called upon.

Theorem 3.4. (*Random Observations Theorem [98, 108]*) *Let, as $K \rightarrow \infty$, $\frac{\kappa(K)}{K} \rightarrow \vartheta$ in probability, where ϑ is a positive random variable. Assume that there are sequences $a_K \in \mathbb{R}, b_K > 0$ such that $\frac{\Lambda_K - a_K}{b_K}$ converges weakly to a nondegenerate distribution function G . Then, as $K \rightarrow \infty$,*

$$\lim \mathbb{P}(\Lambda_{\kappa(K)} < a_K + b_K x) = \int_{-\infty}^{\infty} G^y(x) d\mathbb{P}(\vartheta < y). \quad (3.54)$$

From the analysis in Section 3.5.2, when $K \rightarrow \infty$, $\frac{\kappa(K)}{K} \rightarrow \frac{M}{N}$. Thus from the above random observations theorem, the extreme order statistics of the received CQI for a given user k can be efficiently approximated by $\left(F_{Y_{k,M}^{(0)}}\right)^{\frac{KM}{N}}$.

Proof of Theorem 3.3: According to the condition of domain of attraction, it must be shown that

$$\lim_{r \rightarrow \infty} \frac{d}{dr} \left[\frac{1 - F_{R_{k,M}}(r)}{f_{R_{k,M}}(r)} \right] = 0. \quad (3.55)$$

if $\lim_{x \rightarrow \infty} \frac{x f_{Y_{k,M}}(x)}{1 - F_{Y_{k,M}}(x)} = \phi > 0$ or $\lim_{x \rightarrow \infty} \frac{d}{dx} \left[\frac{1 - F_{Y_{k,M}}(x)}{f_{Y_{k,M}}(x)} \right] = 0$.

It is derived in [99] that

$$\begin{aligned} & \lim_{r \rightarrow \infty} \frac{d}{dr} \left[\frac{1 - F_{R_{k,M}}(r)}{f_{R_{k,M}}(r)} \right] \\ &= \lim_{r \rightarrow \infty} \left(-1 - \frac{(1 - F_{Y_{k,M}}(T^{-1}(r))) f'_{Y_{k,M}}(T^{-1}(r))}{(f_{Y_{k,M}}(T^{-1}(r)))^2} \right) \\ & \quad - \lim_{r \rightarrow \infty} \left(\frac{(1 - F_{Y_{k,M}}(T^{-1}(r))) (T^{-1})''(r)}{f_{Y_{k,M}}(T^{-1}(r)) ((T^{-1})'(r))^2} \right) \\ &= \lim_{x \rightarrow \infty} \frac{d}{dx} \left[\frac{1 - F_{Y_{k,M}}(x)}{f_{Y_{k,M}}(x)} \right] - \lim_{x \rightarrow \infty} \frac{1 - F_{Y_{k,M}}(x)}{x f_{Y_{k,M}}(x)}. \end{aligned} \quad (3.56)$$

If $\lim_{x \rightarrow \infty} \frac{1 - F_{Y_{k,M}}(x)}{x f_{Y_{k,M}}(x)} = \frac{1}{\phi}$, then $F_{Y_{k,M}} \in \mathcal{D}(G_1)$. Using L'Hospital's rule, for a function $\theta(x)$ such as $\theta(x) \rightarrow \infty$ as $x \rightarrow \infty$, if $\lim_{x \rightarrow \infty} \frac{\theta(x)}{x} = \frac{1}{\phi}$, then $\lim_{x \rightarrow \infty} \theta'(x) = \frac{1}{\phi}$.

This leads to $\lim_{r \rightarrow \infty} \frac{d}{dr} \left[\frac{1 - F_{R_{k,M}}(r)}{f_{R_{k,M}}(r)} \right] = 0$.

If $\lim_{x \rightarrow \infty} \frac{d}{dx} \left[\frac{1 - F_{Y_{k,M}}(x)}{f_{Y_{k,M}}(x)} \right] = 0$, then $F_{Y_{k,M}} \in \mathcal{D}(G_3)$. Similarly, we can apply L'Hospital's rule to yield $\lim_{r \rightarrow \infty} \frac{d}{dr} \left[\frac{1 - F_{R_{k,M}}(r)}{f_{R_{k,M}}(r)} \right] = 0$.

Up to now, the sufficient conditions have been proved. From the analysis in Section 3.5.2 on the random effect of multiuser diversity due to partial feedback, the number of CQI values fed back for each resource block becomes $\frac{KM}{N}$ with high probability. Additionally, note that

$$F_{R_{k,M}}^{-1}(x) = T(F_{Y_{k,M}}^{-1}(x)) = \log_2 \left(1 + F_{Y_{k,M}}^{-1}(x) \right), \quad (3.57)$$

thus the normalizing constants (3.27) can be obtained.

Proof of Corollary 3.3: In the one-dominant interference limited case with full feedback, the normalizing constants can be obtained by using $F_{Y_{k,N}^{(0)}}^{-1}(x) = \frac{\rho_k^{(0)} x}{\rho_k^{(1)} (1-x)}$.

In the noise limited case with full feedback, the normalizing constants can be obtained by using $F_{Y_{k,N}^{(0)}}^{-1}(x) = \rho_k^{(0)} \ln \frac{1}{1-x}$.

Proof of Corollary 3.4: In the one-dominant interference limited case with full feedback, the normalizing constants can be obtained by using $F_{Y_{k,N}^{(0)}}^{-1}(x) = \frac{\rho_k^{(0)} x^{\frac{1}{N}}}{\rho_k^{(1)} (1-x)^{\frac{1}{N}}}$ and the number of CQI values fed back per resource block equaling $\frac{K}{N}$.

In the noise limited case with full feedback, the normalizing constants can be obtained by using $F_{Y_{k,N}^{(0)}}^{-1}(x) = \rho_k^{(0)} \ln \frac{1}{1-x^{\frac{1}{N}}}$ and the number of CQI values fed back per resource block equaling $\frac{K}{N}$.

Proof of Corollary 3.5: When $K \rightarrow \infty$, the probability of scheduling outage $(1 - \frac{1}{N})^K \rightarrow 0$. Therefore, from (3.27) it should be shown that $\lim_{K \rightarrow \infty} \frac{1 - \frac{1}{K}}{(1 - \frac{N}{K})^{\frac{1}{N}}} \rightarrow 1$. By applying the L'Hospital's rule, the following equivalent equation holds:

$$\lim_{K \rightarrow \infty} \frac{\frac{1}{K}}{1 - (1 - \frac{N}{K})^{\frac{1}{N}}} = 1. \quad (3.58)$$

Chapter 4

Random Beamforming with Heterogeneous Users and Selective Feedback

4.1 Introduction

In multi-antenna downlink systems, transmission strategies which require less feedback resources [1, 100, 118, 119] to fully utilize multiuser diversity [15, 16], but with asymptotic sum capacity comparable to dirty paper coding [120–124], are favored. The idea of random beamforming [58], which satisfies the two aforementioned features has drawn much interest in recent years [125–131]. In the basic random beamforming strategy suggested in [58], the transmitter with M transmit antennas generates M random orthonormal beams and requires each user to feed back the SINR experienced by them for each beam. Then the transmitter schedules users for transmission that currently have the best channel for each random beam. Despite the considerable literature on this topic, there are three existing open problems:

1. How to address heterogeneous users with diverse large scale channel effects and the impact on scheduling policy?

2. What is the closed form sum rate by exact¹ performance analysis?
3. What is the effect of selective feedback, both spatial and spectral, on the randomness of multiuser diversity?

The first problem is related to a practical downlink system setting with asymmetrically located users having heterogeneous large scale channel effects. This near-far effect was first treated in [58] by observing that the system becomes interference dominated when M is large enough. In the large M setting, the authors prove that users are asymptotically equiprobable to be scheduled. However, when M is finite and not increasing simultaneously with the number of users, the greedy scheduling policy employed in [58] can not maintain fairness among users. Also, if a round robin scheduling policy was utilized, fairness can be guaranteed, but no multiuser diversity gain could be achieved for capacity growth. Therefore, an alternate scheduling policy is needed to maintain fairness while exploiting multiuser diversity at the same time. In this chapter, the cumulative distribution function (CDF)-based scheduling policy [92] is leveraged and analyzed in the random beamforming framework, wherein the user whose rate for a given beam is high enough but least probable to become higher is selected. Under this scheduling policy, each user can be equivalently viewed as competing with other users with the same CDF, thus making the study of individual user rate more relevant and interesting than that of the sum rate. In this chapter, we develop the notion of individual sum rate, which is the individual user rate multiplied by the number of users, in order to demonstrate the multiuser diversity gain with user growth for a given user.

The second problem addresses exact system analysis, namely deriving closed form expression for the sum rate for arbitrary but finite number of users. Note that even with full feedback, wherein each user conveys back the signal-to-interference-plus-noise ratio (SINR) for M beams, the closed form sum rate has not been derived. This is partially due to the complicated form of SINR and its interplay with multiuser diversity. In this work, the problem is tackled and solved by a novel probability density function (PDF) decomposition [132] which decomposes and interprets the selected user's SINR. In [132], the homogeneous setting is considered

¹We use the term exact to denote results valid for arbitrary but finite number of users.

and in this chapter, the technique is extended to the heterogeneous user setting and the closed form individual sum rate is derived. The closed form result under full feedback helps in evaluating the system performance and acts as the building block for exact analysis with selective feedback.

The third problem is concerned with standard selective feedback in the spatial dimension, wherein each user feeds back the SINR for the best beam among the M beams and the corresponding beam index. This selective feedback is fundamentally different than full feedback in two aspects. The first difference is the two-stage maximization with the first stage maximization carried out by each user for feedback selection and the second stage maximization carried out by the scheduler to perform user selection. Since the best beam is selected by each user, the first stage maximization is over M correlated SINR. This correlation issue has been addressed in [20, 133], and the CDF for the selected SINR at the user side is derived. In this chapter, we propose an approximation for the CDF and utilize it to derive closed form rate approximation. The other fundamental difference is the number of the SINR values that the scheduler has to maximize over for each beam. This number is fixed and equals the number of users in the full feedback case. However, with selective feedback, it becomes a random quantity. In other words, selective feedback results in a random effect on the multiuser diversity. This effect was first observed in [20]. In this chapter, we investigate the randomness of multiuser diversity by extremes over random samples and provide a rigorous argument on the rate scaling.

The third problem is further extended to include spectral selectivity by examining a wideband OFDMA system, which groups the subcarriers into resource blocks [6] to form the basic scheduling and feedback unit. In order to save feedback resource while not significantly degrading the system performance, additional selective feedback in the spectral dimension is necessary. The effect of random beamforming in a wideband system is examined in [134] by extensive simulations, and further studied from a utility function perspective with the proportional-fair scheduler in [135]. In [136], analytical results on the asymptotic cluster size is provided. Apart from the thresholding-based partial feedback strategy [17], the

best- L selective feedback strategy [29] is appealing and utilized in practical systems such as LTE [37]. In this chapter, we employ the best- L selective feedback strategy to investigate random beamforming and the effect of spectral dimension selective feedback, which calls for an additional maximization stage at the user side to perform feedback selection. In this feedback strategy, only the best beams from the best L resource blocks along with the beam and resource block index are fed back from each user. In this chapter, we first derive a closed form rate approximation with exact analysis, i.e., valid for arbitrary but finite number of users. Then, the influence of the additional spectral dimension selective feedback on the type of convergence is investigated with the technique of tail equivalence. Moreover, the multiplicative effect of selective feedback and random observations is observed to establish the rate scaling.

To summarize, the main contributions of this chapter are threefold: the utilization of CDF-based scheduling policy to address heterogeneous users with random beamforming, the obtained closed form rate results with different selective feedback assumptions, and the asymptotic analysis on the randomness of multiuser diversity incurred by selective feedback. These three contributions analytically examine the raised open problems, and foster further understanding on random beamforming with heterogeneous users and selective feedback. The organization of this chapter is as follows. Section 4.2 reviews the basic narrowband system model for random beamforming. The analysis for the full feedback case is carried out in Section 4.3, and for the spatial dimension selective feedback in Section 4.4. Section 4.5 provides the model for the wideband OFDMA with random beamforming, and examines the effect of additional spectral dimension selective feedback on rate performance. Finally, Section 4.6 concludes the chapter.

4.2 System Model

We consider a multi-antenna narrowband Gaussian downlink channel with K single antenna receivers and a transmitter equipped with M antennas. A block fading channel model with coherence interval T is assumed. The random

beamforming strategy employs M random orthonormal vectors $\phi_m \in \mathbb{C}^{M \times 1}$ for $m = 1, \dots, M$, where the ϕ_i 's are drawn from an isotropic distribution independently every T channel uses [58]. Denoting $s_m(t)$ as the m th transmission symbol at time t , the transmitted vector of symbols at time t , represented by $\mathbf{s}(t) \in \mathbb{C}^{M \times 1}$, is given as

$$\mathbf{s}(t) = \sum_{m=1}^M \phi_m(t) s_m(t), \quad t = 1, \dots, T. \quad (4.1)$$

Let $y_k(t)$ be the received signal at the k th user, then

$$y_k(t) = \sum_{m=1}^M \sqrt{\rho_k} \mathbf{h}_k^\dagger(t) \phi_m(t) s_m(t) + v_k(t), \quad (4.2)$$

where $\mathbf{h}_k \in \mathbb{C}^{M \times 1}$ is the complex channel vector which is assumed to be known at the receiver, v_k is the additive white noise, and the elements of \mathbf{h}_k and v_k are i.i.d. complex Gaussian with zero mean and unit variance $\mathcal{CN}(0, 1)$. Note that this channel assumption corresponds to the Rayleigh fading assumption for the small scale channel effect. From now on, the time variable t will be dropped for notational convenience. The total transmit power is chosen to be 1, i.e., $\mathbb{E}[\mathbf{s}^\dagger \mathbf{s}] = 1$, and thus the received signal-to-noise ratio (SNR) of user k is ρ_k . In a practical downlink setting, due to different locations of users, the large scale channel effects ρ_k which may consist of path loss and shadowing vary across users. From (4.2), the SINR of the k th user for the m th transmit beam can be computed as

$$\text{SINR}_{k,m} = \frac{|\mathbf{h}_k^\dagger \phi_m|^2}{M/\rho_k + \sum_{i \neq m} |\mathbf{h}_k^\dagger \phi_i|^2}, \quad m = 1, \dots, M. \quad (4.3)$$

Denote $Z_{k,m} \triangleq \text{SINR}_{k,m}$ for notational simplicity. Then for a given beam m , the $Z_{k,m}$'s are independent across users k but non-identically distributed due to different ρ_k . For a given user k , the $Z_{k,m}$'s are identically distributed and correlated. Thus the beam index m can be dropped in the expression for the PDF, which is computed in [58] as

$$f_{Z_k}(x) = \frac{e^{-\frac{M}{\rho_k}x}}{(1+x)^M} \left(\frac{M}{\rho_k}(1+x) + M - 1 \right) u(x), \quad (4.4)$$

where $u(\cdot)$ is the Heaviside step function. The CDF of Z_k is shown in [58] to be

$$F_{Z_k}(x) = \left(1 - \frac{e^{-\frac{M}{\rho_k}x}}{(1+x)^{M-1}} \right) u(x). \quad (4.5)$$

4.3 Full Feedback Analysis

This section is devoted to the analysis for the full feedback case wherein each user feeds back the SINR for M beams. Since under full feedback, all the beams are fed back, the order statistics for each beam is over K independent random variables. Thus this case is well suited for illustration of the scheduling policy and the derivation of the individual sum rate.

4.3.1 Scheduling Policy and Individual Sum Rate

After receiving the $\text{SINR}_{k,m}$ from user k for beam m , the scheduler is ready to perform user selection. In a homogeneous setting, selecting the user with the largest SINR for a given beam maintains fairness and obtains multiuser diversity gain. This system was analyzed in our recent work [132]. The work is now expanded to the more complex heterogeneous case. In a heterogeneous setting, the greedy scheduling policy would be highly unfair for finite M . The round robin scheduling policy can maintain scheduling fairness, but no multiuser diversity gain can be obtained. The proportional-fair scheduling policy [16, 135] achieves the system fairness in terms of system utility. However, under the scenario of inter-beam interference, the users' rates are coupled under the proportional-fair scheduling policy. This coupled effect makes it very difficult, if not impossible, to develop further analytical results². Therefore, to tackle this problem it is useful to consider alternate scheduling policies that decouple each user's rate. In this chapter, we employ the CDF-based scheduling policy [92] for further analysis. According to this policy, the scheduler will utilize the distribution of the received SINR, i.e., F_{Z_k} . It is assumed that the scheduler perfectly knows the CDF³, and it performs the

²Note that extensive simulation results have been provided regarding the use of proportional-fair scheduling policy under random beamforming in existing literature such as [135]. However, the coupled effect of user's rate prevents further analysis and it remains an open problem to theoretically understand the system performance of proportional-fair scheduling policy under the heterogeneous user setting with inter-beam interference.

³This is the only system requirement to conduct the CDF-based scheduling, and the CDF can be obtained by infrequent feedback from users and learned by the system.

following transformation [92]:

$$\tilde{Z}_{k,m} = F_{Z_k}(Z_{k,m}). \quad (4.6)$$

The transformed random variable $\tilde{Z}_{k,m}$ is uniformly distributed ranging from 0 to 1, and independent and identically distributed (i.i.d.) across users for a given beam. Denote k_m^* as the random variable representing the selected user for beam m , then

$$k_m^* = \max_{\mathcal{U}_m} \tilde{Z}_{k,m}, \quad (4.7)$$

where \mathcal{U}_m denotes the set of users conveying feedback for beam m . In the full feedback case, $|\mathcal{U}_m| = K$. After user k_m^* is selected per (4.7), the scheduler utilizes the corresponding $Z_{k_m^*,m}$ for rate matching of the selected user. Let X_m be the SINR of the selected user for beam m and now consider the sum rate of the system defined as follows,

$$R = \mathbb{E} \left[\sum_{m=1}^M \log_2(1 + X_m) \right]. \quad (4.8)$$

From the aforementioned formulation, the sum rate can be computed in the following procedure

$$\begin{aligned} R &\stackrel{(a)}{\simeq} M \mathbb{E}_{k_m^*} \left[\int_0^1 \log_2 \left(1 + F_{Z_{k_m^*,m}}^{-1}(x) \right) dx^K \right] \\ &\stackrel{(b)}{=} \frac{M}{K} \sum_{k=1}^K \int_0^\infty \log_2(1+t) d(F_{Z_k}(t))^K = \frac{M}{K} \sum_{k=1}^K \mathcal{J}_k(K), \end{aligned} \quad (4.9)$$

where (a) follows from the sufficient small probability that multiple beams are assigned to the same user; (b) follows from the change of variable $x = F_{Z_{k_m^*,m}}^{-1}(t)$, the fair property of the CDF-based scheduling, and the following definition for $\mathcal{J}_k(\epsilon)$ with exponent $\epsilon \in \mathbb{N}_+$:

$$\mathcal{J}_k(\epsilon) \triangleq \int_0^\infty \log_2(1+x) d(F_{Z_k}(x))^\epsilon. \quad (4.10)$$

With the help of the CDF-based scheduling, each user feels as if the other users have the same CDF for scheduling competition [92]. Therefore, each user's rate is independent of other users making it possible to consider or predict individual user's rate by only examining its own CDF. It is clear that the scheduling policy

is not only fair, but also acknowledges multiuser diversity at the same time. If we denote the sum rate as the “macro” level understanding of the system performance, then the individual user rate can be seen as the “micro” level understanding of the system performance since this performance metric examines the rate for any specific user and the sum rate can be directly computed from the individual user rate from all the users. Thus, under the CDF-based scheduling policy, each user’s rate can be examined separately and this property serves as one building block for further analysis with selective feedback.

In order to demonstrate the multiuser diversity gain for each individual user, we define the individual sum rate \hat{R}_k for user k which is the individual user rate R_k multiplied by the number of users, as follows

$$\hat{R}_k \triangleq KR_k = M\mathcal{J}_k(K). \quad (4.11)$$

The definition of the individual sum rate under the CDF-based scheduling policy makes it natural to examine the rate scaling for each user separately, and also provide a “micro” level understanding of the sum rate scaling. Compared with the sum rate and the individual user rate which can be treated as performance metrics, the notion of individual sum rate can be regarded as the analytic metric for further scaling analysis.

Note that in the homogeneous setting, $\mathcal{J}_k(\epsilon)$ reduces to $\mathcal{J}(\epsilon) \triangleq \int_0^\infty \log_2(1+x)d(F_Z(x))^\epsilon$. It is mentioned in previous works that the exact closed form for $\mathcal{J}(\epsilon)$ is hard to obtain due to the coupled effect of SINR and multiuser scheduling. In the sequel, the closed form expression for $\mathcal{J}_k(\epsilon)$ is obtained which is the key to computing the sum rate given by (4.9). The main technique is employing the following proposed PDF decomposition which readily follows from [132].

Lemma 4.1. *(PDF Decomposition) $d(F_{Z_k}(x))^\epsilon$ can be decomposed as*

$$d(F_{Z_k}(x))^\epsilon = \epsilon \sum_{i=0}^{\epsilon-1} \binom{\epsilon-1}{i} \frac{(-1)^i}{i+1} d \left(1 - \frac{e^{-\frac{M(i+1)x}{\rho_k}}}{(1+x)^{(M-1)(i+1)}} \right). \quad (4.12)$$

With the help of this PDF decomposition, $\mathcal{J}_k(\epsilon)$ can be computed in closed form using standard integration techniques whose expression is presented in the following theorem.

Theorem 4.1. (*Closed Form of \mathcal{J}_k*)

$$\mathcal{J}_k(\epsilon) = \frac{\epsilon}{\ln 2} \sum_{i=0}^{\epsilon-1} \binom{\epsilon-1}{i} \frac{(-1)^i}{i+1} \mathcal{I} \left(\frac{M(i+1)}{\rho_k}, (M-1)(i+1) + 1 \right), \quad (4.13)$$

where $\mathcal{I}(\alpha, \beta) \triangleq \int_0^\infty \frac{e^{-\alpha x}}{(1+x)^\beta} dx$ whose closed form expression is presented in Appendix E.

Proof. The proof is given in Appendix E. □

Remark: A few remarks are in order. Firstly, the analytically useful PDF decomposition decouples the effect of multiuser diversity and random beamforming, which facilitates the integration. The decomposition is general in that it can be applied to other channel models, though in this chapter the simple Rayleigh channel model is assumed to obtain the SINR statistics in (4.5). Secondly, the derived closed form results for the individual sum rate and the sum rate only involve finite sums and factorials, which can readily be computed. Moreover, the derived $\mathcal{J}_k(\epsilon)$ will be employed as a building block for rate computation in Section 4.4 and Section 4.5 with selective feedback.

4.3.2 Individual Scaling Laws

With homogeneous setting, the asymptotic sum rate scaling is of interest and has been established as $M \log_2 \log_2 K$ [58] given the SINR statistics in (4.5). It can be easily seen that the multiuser diversity gain is linear with respect to the number of transmit antennas. With heterogeneous setting employing the CDF-based scheduling, the same technique can be applied to obtain the asymptotic scaling for the individual sum rate \hat{R}_k of user k . We now develop the notion of individual rate scaling and state the individual scaling laws under full feedback through the following theorem.

Theorem 4.2. (*Individual Scaling Laws Under Full Feedback*)

$$\lim_{K \rightarrow \infty} \frac{\hat{R}_k}{M \log_2 \log_2 K} = 1. \quad (4.14)$$

Remark: It is seen from Theorem 4.2 that users asymptotically follow the same scaling laws in the CDF-based scheduling policy. The large scale channel effect ρ_k is not written explicitly in (4.14) since it is a constant inside the log term. It should briefly be noted that the rate scaling only measures the asymptotic trend when $K \rightarrow \infty$ and thus can not accurately match the exact performance⁴ for finite regions of K .

4.4 Selective Feedback in the Spatial Dimension

This section examines selective feedback in the spatial dimension wherein each user only conveys the best beam. This standard user side selection requires the handling of correlated random variables and the random effect on observations, which are pursued in Section 4.4.1 and Section 4.4.2.

4.4.1 Individual Sum Rate

With selective feedback, each user selects and feeds back the largest SINR among M beams. As discussed in Section 4.2, the $Z_{k,m}$'s are correlated random variables given k . Thus simple order statistics result can not be used to characterize the selected SINR at user side. Denote $Y_{k,m^*(k)} = \max_m Z_{k,m}$ representing the selected SINR for user k with $m^*(k)$ as the selected beam index. Then according to the derivation in [20, 133], the CDF of $Y_{k,m^*(k)}$ is shown to be

$$F_{Y_{k,m^*(k)}}(x) = \left(1 - \sum_{\iota=1}^M \frac{[d_\iota(x)]_+^M e^{-\frac{2Mx}{\rho_k d_\iota(x)}}}{A_\iota(x)} \right) u(x), \quad (4.15)$$

where $d_\iota(x) = \frac{2(1-(M-\iota)x)}{M-\iota+1}$, $A_\iota(x) = d_\iota(x) \prod_{i \neq \iota}^M (d_i(x) - d_i(x))$, and $[\cdot]_+$ is the positive part of the argument. Note that the distribution does not depend on the selected beam index $m^*(k)$ due to the identically distributed property across beams and is dropped to simplify notation, i.e., $F_{Y_{k,m^*(k)}}(x) = F_{Y_k}(x)$. Using a similar procedure to that described in Section 4.3.1, after receiving feedback, the scheduler performs

⁴Using asymptotic approximation method to approximate the exact rate performance is examined in [137].

the transformation for user selection:

$$\tilde{Y}_{k,m^*(k)} = F_{Y_k}(Y_{k,m^*(k)}). \quad (4.16)$$

Compared with (4.6), it is clear that $F_{Y_k} = F_{Z_k}$ for the full feedback case. Denote k_m^* as the random variable representing the selected user for beam m , then

$$k_m^* = \max_{\mathcal{U}_m} \tilde{Y}_{k,m^*(k)}, \quad (4.17)$$

where $\mathcal{U}_m = \{k : m^*(k) = m\}$ denotes the set of users conveying feedback for beam m . \mathcal{U}_m is a set of random size and the probability mass function (PMF) can be shown to be given by

$$\mathbb{P}(|\mathcal{U}_m| = \tau_1) = \binom{K}{\tau_1} \left(\frac{1}{M}\right)^{\tau_1} \left(1 - \frac{1}{M}\right)^{K-\tau_1}, \quad 0 \leq \tau_1 \leq K. \quad (4.18)$$

Following the derivation in Section 4.3.1, let X_m be the selected SINR for beam m at the scheduler side, then conditioned on k_m^* and $|\mathcal{U}_m| = \tau_1$, the conditional CDF of X_m can be written as $F_{X_m|k_m^*,|\mathcal{U}_m|=\tau_1}(x) = (F_{Y_{k_m^*,m}}(x))^{\tau_1}$. By averaging over the randomness of $|\mathcal{U}_m|$, the conditional CDF is expressed as

$$F_{X_m|k_m^*}(x) = \sum_{\tau_1=0}^K \binom{K}{\tau_1} \left(\frac{1}{M}\right)^{\tau_1} \left(1 - \frac{1}{M}\right)^{K-\tau_1} (F_{Y_{k_m^*,m}}(x))^{\tau_1}. \quad (4.19)$$

From (4.9) and (4.11), the individual sum rate of user k is derived as⁵

$$\hat{R}_k = M \sum_{\tau_1=1}^K \binom{K}{\tau_1} \left(\frac{1}{M}\right)^{\tau_1} \left(1 - \frac{1}{M}\right)^{K-\tau_1} \int_0^\infty \log_2(1+x) d(F_{Y_k}(x))^{\tau_1}. \quad (4.20)$$

Due to the complicated form of F_{Y_k} , the exact closed form expression for (4.20) is hard to obtain. We now aim to provide an approximate expression for the closed form by examining the property of F_{Y_k} and utilizing the established result in Section 4.3.1. Recall that Y_k is the maximization over M correlated random variables $Z_{k,m}$, thus alternative approximation for F_{Y_k} would lead to rate approximation. One simple approach is to use the Fréchet upper bound [98] for the $Z_{k,m}$'s. Since the $Z_{k,m}$'s are identically distributed across m , the Fréchet upper bound yields F_{Z_k} . This upper bound is very loose empirically for F_{Y_k} . One

⁵In this chapter, it is assumed that if no user feeds back SINR for a certain beam, that beam would be in scheduling outage and would not contribute to rate calculation.

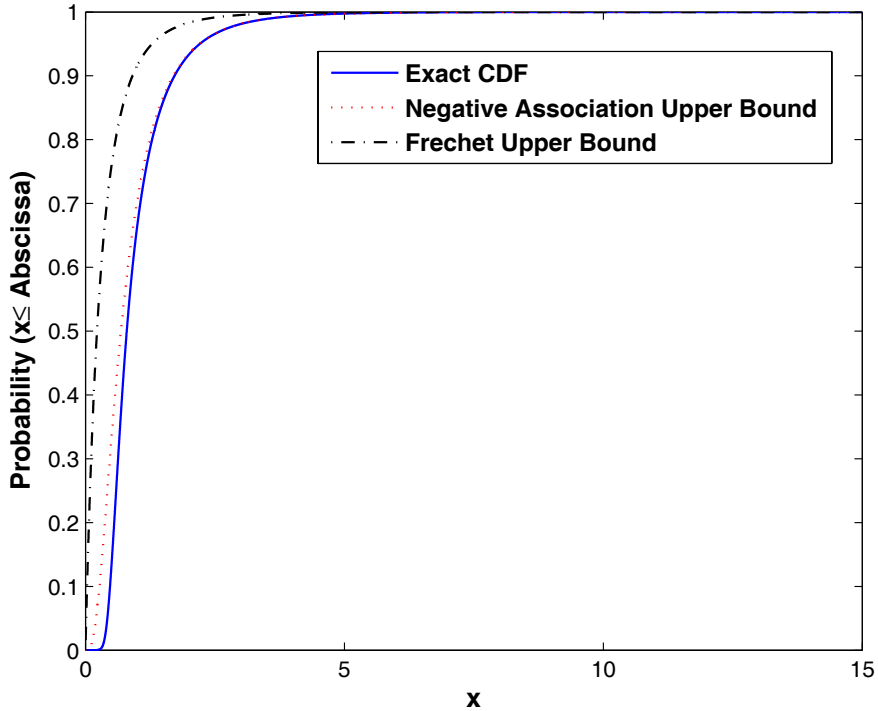


Figure 4.1: Comparison of the exact CDF F_{Y_k} with the Fréchet upper bound and the negative association upper bound for spatial dimension selective feedback ($M = 4$, $\rho_k = 10$ dB).

suitable approach is inspired by the conjectured negative associated upper bound proposed in [20] to deal with the minimum mean square error (MMSE) receiver. Our empirical evidence shows that even with single antenna receiver, the $Z_{k,m}$'s are negative associated [138], thus the upper bound produced by the negative association property can be utilized to approximate F_{Y_k} , namely

$$F_{Y_k}(x) \simeq (F_{Z_k}(x))^M. \quad (4.21)$$

Fig. 4.1 illustrates the bounds and the empirical CDF F_{Y_k} for $M = 4$, $\rho_k = 10$ dB. It can be seen that the proposed upper bound in (4.21) approximates the exact one in (4.15) well, especially when the SINR is large. By using the CDF approximation, the individual sum rate can be approximated by a closed form expression presented in the following corollary.

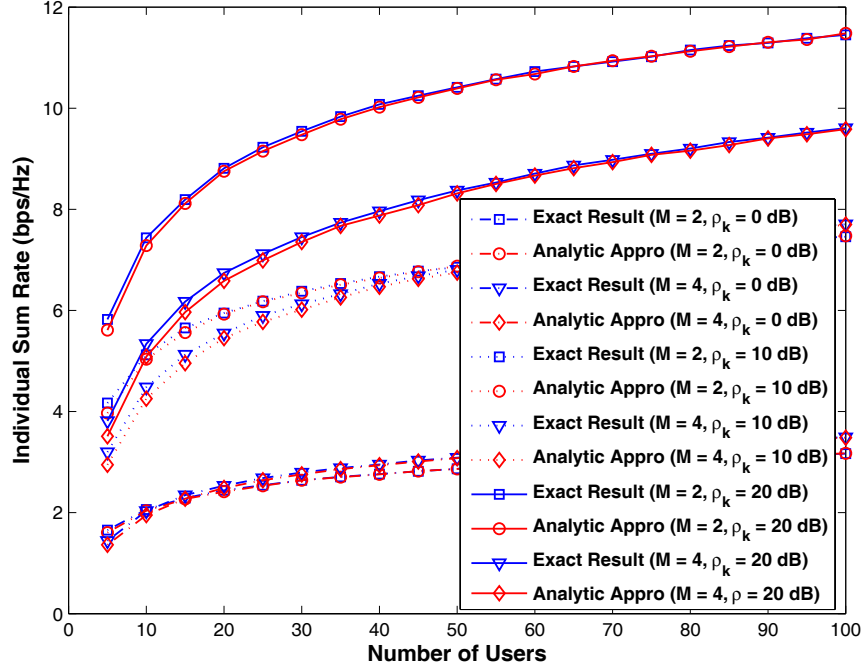


Figure 4.2: Comparison of the exact individual sum rate and the approximated one for a given user with different M and ρ_k with respect to the number of users ($M = 2, 4$, $\rho_k = 0$ dB, 10 dB, 20 dB).

Corollary 4.1. (*Closed Form Approximation of Individual Sum Rate*)

$$\hat{R}_k \simeq \hat{R}_k^{\text{App}} = M \sum_{\tau_1=1}^K \binom{K}{\tau_1} \left(\frac{1}{M}\right)^{\tau_1} \left(1 - \frac{1}{M}\right)^{K-\tau_1} \mathcal{J}_k(M\tau_1). \quad (4.22)$$

Proof. The proof is given in Appendix F. □

In order to demonstrate the rate approximation in Corollary 4.1, we conduct a numerical study in Fig. 4.2 for different M and ρ_k with respect to the number of users. The exact \hat{R}_k in (4.20) can be calculated by numerical integration. It is observed that (4.22) approximates the exact rate very well, which makes the rate approximation valuable due to its efficient computational form.

4.4.2 Individual Scaling Laws

The difficulty of dealing with rate scaling with selective feedback is two-fold. Firstly, due to selective feedback of the best beam, the number of SINR to maximize over at the scheduler side for each beam is a random quantity. This random effect is reflected in the random set \mathcal{U}_m in Section 4.4.1. Secondly, the normalizing constants for establishing the type of convergence [56, 98] have to be obtained for a quantity ϑ other than the number of users K in the full feedback case. In [20], the first issue was tackled by the Delta method. In this chapter, we solve the first issue by referring to the extremes over random samples, and rigorously solve the second one by using the normalizing constants theorem. The proof is provided in Appendix F.

To examine the random effect on multiuser diversity, denote the sequence of random variables $\kappa_m(K)$ as the number of SINR fed back for beam m with K users. It is easy to see that $\kappa_m(K)$ are binomial distributed with probability of success $\frac{1}{M}$. Thus by the strong law of large numbers, as K grows, the number of SINR fed back for each beam becomes $\frac{K}{M}$. The following theorem is called upon to deal with this random effect.

Theorem 4.3. (*Extremes with Random Sample Size [98, 108]*) *Let, as $K \rightarrow \infty$, $\frac{\kappa(K)}{K} \rightarrow \vartheta$ in probability, where ϑ is a positive random variable. Assume that there are sequences $a_K \in \mathbb{R}, b_K > 0$ such that $\frac{\Lambda_K - a_K}{b_K}$ converges weakly to a nondegenerate distribution function G . Then, as $K \rightarrow \infty$,*

$$\lim \mathbb{P}(\Lambda_{\kappa(K)} < a_K + b_K x) = \int_{-\infty}^{\infty} G^y(x) d\mathbb{P}(\vartheta < y). \quad (4.23)$$

Therefore, if we denote $\Lambda_{k:\kappa(K)}$ as the extreme order statistics of the received SINR for each beam of a given user k , then from Theorem 4.3, its CDF can be efficiently approximated by $(F_{Y_k})^{\frac{K}{M}}$. Combining this with the normalizing constants theorem in Appendix F yields the following corollary.

Corollary 4.2. (*Individual Scaling Laws Under Spatial Dimension Selective Feedback*)

$$\lim_{K \rightarrow \infty} \frac{\hat{R}_k}{M \log_2 \log_2 \frac{K}{M}} = 1, \quad \lim_{K \rightarrow \infty} \frac{\hat{R}_k^{\text{App}}}{M \log_2 \log_2 K} = 1. \quad (4.24)$$

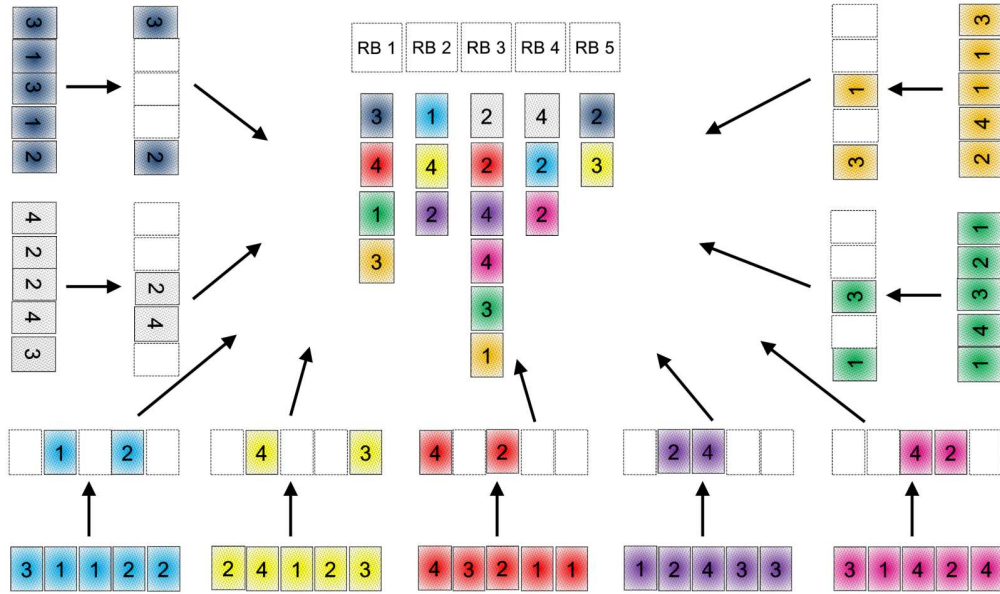


Figure 4.3: Illustration of the spatial and spectral dimension selective feedback and the scheduling result in an OFDMA system (different colors denote different users $K = 9$, $N = 5$ resource blocks, $M = 4$ beams, the spectral dimension selective feedback $L = 2$).

Proof. The proof is given in Appendix F. \square

Remark: The scaling for the exact rate \hat{R}_k and approximated rate \hat{R}_k^{APP} differs in the factor $\frac{1}{M}$. The rate scaling for \hat{R}_k^{APP} does not have this factor because intuitively the exponent M in the approximated CDF $(F_{Z_k}(x))^M$ counteracts the reduction in the number of SINR values for maximization, i.e., $\frac{K}{M}$, due to selective feedback. We call this effect as the *multiplicative effect*. The detailed proof can be found in Appendix F. To draw further insights, we can think of the exponent of $F_{Z_k}(x)$ as the *virtual users*. In the full feedback case, the exponent equals K . In the selective feedback case with the approximated CDF, the exponent asymptotically equals K by the aforementioned multiplicative effect⁶. The notion of virtual users and the multiplicative effect will be investigated further with both spatial and spectral dimension selective feedback in Section 4.5.3.

⁶Note that even though the scaling laws are the same for the full feedback and the selective feedback case, this metric only measures the asymptotic performance when K is large. The exact rate performance is different due to the randomness of multiuser diversity and the scheduling outage event.

4.5 Selective Feedback in Both Spatial and Spectral Dimension

In this section, random beamforming is embedded in a wideband OFDMA system. The system model is presented in Section 4.5.1, the exact analysis and the asymptotic analysis are examined in Section 4.5.2 and Section 4.5.3 respectively.

4.5.1 System Model

The system model described in Section 4.2 is extended to an OFDMA system with N resource blocks. Each resource block is regarded as the basic scheduling and feedback unit. The random beamforming strategy generates M orthonormal beams $\phi_{m,n}$ for each resource block. Denote $s_{m,n}$ as the m th transmission symbol at resource block n , then the received signal $y_{k,n}$ for user k at resource block n can be expressed as

$$y_{k,n} = \sum_{m=1}^M \sqrt{\rho_k} \mathbf{H}_{k,n}^\dagger \phi_{m,n} s_{m,n} + v_{k,n}, \quad (4.25)$$

where $\mathbf{H}_{k,n} \in \mathbb{C}^{M \times 1}$ is the frequency domain channel transfer function of user k at resource block n with i.i.d. $\mathcal{CN}(0, 1)$ elements. To facilitate analysis, $\mathbf{H}_{k,n}$ is assumed to be i.i.d. across resource blocks for a given user. This corresponds to the widely used block fading approximation in the frequency domain [48, 49] due to its simplicity and capability to provide a good approximation to actual physical channels. The transmit power for a resource block is assumed to be 1. From (4.25), the SINR $_{k,n,m}$ of user k at resource block n for beam m is $\text{SINR}_{k,n,m} = \frac{|\mathbf{H}_{k,n}^\dagger \phi_{m,n}|^2}{M/\rho_k + \sum_{i \neq m} |\mathbf{H}_{k,n}^\dagger \phi_{i,n}|^2}$, and is denoted by $Z_{k,n,m}$ for notational simplicity. For a given user k , the $Z_{k,n,m}$'s are i.i.d. across resource blocks for a given beam m , and for a given resource block n , the $Z_{k,n,m}$'s are identically distributed and correlated across beams. The CDF of $Z_{k,n,m}$ is given by $F_{Z_k}(x) = \left(1 - \frac{e^{-\frac{M}{\rho_k}x}}{(1+x)^{M-1}}\right) u(x)$, where the index n and m can be dropped due to the identically distributed property.

4.5.2 Individual Sum Rate

With the extra degrees of freedom in the spectral dimension, additional selective feedback at each user side can be made possible by the following two-stage feedback selection. The first stage selection is in the spatial dimension, where each user selects the best beam with the largest SINR for each of the resource block. This process is similar to the narrowband feedback selection discussed in Section 4.4.1. Let $Y_{k,n,m}$ be the outcome of the first stage selection, thus from (4.15), its CDF can be written as $F_{Y_k}(x) = \left(1 - \sum_{i=1}^M \frac{[d_i(x)]_+^M e^{-\frac{2Mx}{\rho_k d_i(x)}}}{A_i(x)}\right) u(x)$, where again the resource block index n and the beam index m can be dropped due to the identically distributed property across resource blocks and beams. The second stage selection occurs in the spectral dimension, where each user feeds back the SINR values of the best L resource blocks among the total N resource blocks. Let $W_{k,n,m}$ denote the outcome of the second stage selection of user k at resource block n for beam m . Thus this random variable represents the selected SINR at the user side, whose CDF is of interest for further analysis. It is easy to see that for the case of full feedback in the spectral dimension, i.e., $L = N$, $F_{W_k} = F_{Y_k}$. For the best-1 feedback case, i.e., $L = 1$, $F_{W_k} = (F_{Y_k})^N$ due to the independent property of Y_k across resource blocks. For the general best- L feedback case, utilizing the results in [29], the CDF can be shown as

$$F_{W_k}(x) = \sum_{\ell=0}^{L-1} \xi_1(N, L, \ell) (F_{Y_k}(x))^{N-\ell}, \quad (4.26)$$

where $\xi_1(N, L, \ell) = \sum_{i=\ell}^{L-1} \frac{L-i}{L} \binom{N}{i} \binom{i}{\ell} (-1)^{i-\ell}$. The two-stage feedback selection is demonstrated in Fig. 4.3 with nine users denoted by different colors, five resource blocks, and four beams. In the illustrated example, we use best-2 spectral dimension feedback, i.e., $L = 2$.

After receiving feedback, the scheduler performs the CDF-based scheduling by first conducting the transformation on the received SINR,

$$\tilde{W}_{k,n,m} = F_{W_k}(W_{k,n,m}). \quad (4.27)$$

Denote $k_{n,m}^*$ as the random variable representing the selected user at resource block

n for beam m , then

$$k_{n,m}^* = \max_{\mathcal{U}_{n,m}} \tilde{W}_{k,n,m}, \quad (4.28)$$

where $\mathcal{U}_{n,m}$ denotes the set of users conveying feedback for beam m at resource block n . Following the derivation in Section 4.4.1, let $X_{n,m}$ be the selected SINR for beam m at resource block n at the scheduler side. Then averaging over the randomness of $|\mathcal{U}_{n,m}|$, the conditional CDF conditioned on $k_{n,m}^*$ can be written as

$$\begin{aligned} F_{X_{n,m}|k_{n,m}^*}(x) &= \sum_{\tau_1=0}^K \binom{K}{\tau_1} \left(\frac{1}{M}\right)^{\tau_1} \left(1 - \frac{1}{M}\right)^{K-\tau_1} \\ &\quad \times \sum_{\tau_2=0}^{\tau_1} \binom{\tau_1}{\tau_2} \left(\frac{L}{N}\right)^{\tau_2} \left(1 - \frac{L}{N}\right)^{\tau_1-\tau_2} (F_{W_{k_{n,m}^*,n,m}}(x))^{\tau_2}. \end{aligned} \quad (4.29)$$

For further derivation, $(F_{W_k}(x))^{\tau_2}$ is manipulated into the following form by the power series expansion [29, 64]:

$$(F_{W_k}(x))^{\tau_2} = \sum_{\ell=0}^{\tau_2(L-1)} \xi_2(N, L, \tau_2, \ell) (F_{Y_k}(x))^{N\tau_2-\ell}, \quad (4.30)$$

where

$$\xi_2(N, L, \tau_2, \ell) = \begin{cases} (\xi_1(N, L, 0))^{\tau_2}, & \ell = 0 \\ \frac{1}{\ell \xi_1(N, L, 0)} \sum_{i=1}^{\min(\ell, L-1)} ((\tau_2 + 1)i - \ell) \\ \quad \times \xi_1(N, L, i) \xi_2(N, L, \tau_2, \ell - i), & 1 \leq \ell < \tau_2(L-1) \\ (\xi_1(N, L, L-1))^{\tau_2}, & \ell = \tau_2(L-1). \end{cases} \quad (4.31)$$

Following the same procedure as in Section 4.4.1, the individual sum rate for user k can be derived as

$$\begin{aligned} \hat{R}_k &= \frac{1}{N} \sum_{n=1}^N \mathbb{E} \left[\sum_{m=1}^M \log_2(1 + X_{n,m}|k_{n,m}^* = k) \right] \\ &= M \sum_{\tau_1=1}^K \binom{K}{\tau_1} \left(\frac{1}{M}\right)^{\tau_1} \left(1 - \frac{1}{M}\right)^{K-\tau_1} \sum_{\tau_2=1}^{\tau_1} \binom{\tau_1}{\tau_2} \left(\frac{L}{N}\right)^{\tau_2} \left(1 - \frac{L}{N}\right)^{\tau_1-\tau_2} \\ &\quad \times \sum_{\ell=0}^{\tau_2(L-1)} \xi_2(N, L, \tau_2, \ell) \int_0^\infty \log_2(1+x) d(F_{Y_k}(x))^{N\tau_2-\ell}. \end{aligned} \quad (4.32)$$

In order to obtain the closed form rate approximation for \hat{R}_k , the CDF approximation proposed in (4.21) by the negative association property is utilized to approximate F_{Y_k} . The closed form result is presented in the following corollary.

Corollary 4.3. (*Closed Form Approximation of Individual Sum Rate*)

$$\begin{aligned} \hat{R}_k \simeq \hat{R}_k^{\text{App}} &= M \sum_{\tau_1=1}^K \binom{K}{\tau_1} \left(\frac{1}{M}\right)^{\tau_1} \left(1 - \frac{1}{M}\right)^{K-\tau_1} \sum_{\tau_2=1}^{\tau_1} \binom{\tau_1}{\tau_2} \left(\frac{L}{N}\right)^{\tau_2} \left(1 - \frac{L}{N}\right)^{\tau_1-\tau_2} \\ &\quad \times \sum_{\ell=0}^{\tau_2(L-1)} \xi_2(N, L, \tau_2, \ell) \mathcal{J}_k(M(N\tau_2 - \ell)). \end{aligned} \quad (4.33)$$

To understand the impact of spectral dimension selective feedback, we conduct a numerical study assuming $N = 10$, $M = 4$. Fig. 4.4 plots the exact and approximated rate for different L under $\rho_k = 10$ dB with respect to the number of users. It can be seen that when the number of users is small, there is a certain rate gap between selective feedback and full feedback. However, the gap becomes negligible when the number of users increases. In Fig. 4.5, the performance is observed for different ρ_k for $K = 20$. From the two figures, we can see that the proposed rate approximation tracks the exact performance very well.

4.5.3 Individual Scaling Laws

We now examine the rate scaling with selective feedback in both spatial and spectral dimension. In Section 4.4.2 with spatial dimension selective feedback, the CDF of interest is F_{Y_k} and the number of SINR to maximize over at the scheduler side for each beam approaches $\frac{K}{M}$. With additional spectral dimension feedback, the CDF of F_{W_k} is of primary interest. To get a handle on the randomness of multiuser diversity for this case, an approach similar to that in Section 4.4.2 can be utilized. Let the sequence of random variables $\kappa_{n,m}(K)$ be the number of SINR values fed back for beam m at resource block n with K users. It is easy to see that $\kappa_{n,m}(K)$ are binomial distributed with probability of success $\frac{L}{MN}$. Therefore, by the strong law of large numbers, as K grows, the number of SINR values fed back for each beam at each resource block becomes $\frac{KL}{MN}$. Moreover, the convergence property of the sequence $\kappa_{n,m}(K)$ can be shown by invoking the central limit theorem:

$$\lim_{K \rightarrow \infty} \sqrt{K} \left(\frac{\kappa_{n,m}(K)}{K} - \frac{L}{MN} \right) \xrightarrow{d} \mathcal{N} \left(0, \frac{L}{MN} \left(1 - \frac{L}{MN} \right) \right), \quad (4.34)$$

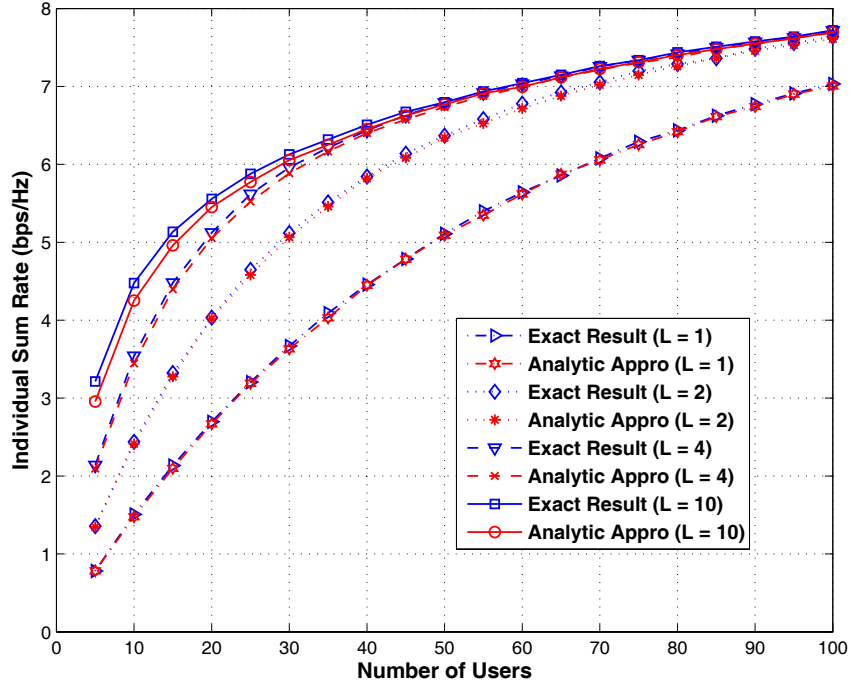


Figure 4.4: Comparison of the exact individual sum rate and the approximated one for a given user with different spectral dimension selective feedback L with respect to the number of users ($M = 4$, $N = 10$, $\rho_k = 10$ dB, $L = 1, 2, 4, 10$).

where d indicates convergence in distribution. By applying Theorem 4.3, the extreme order statistics of the received SINR for each beam at each resource block for a given user k can be efficiently approximated by $(F_{W_k})^{\frac{KL}{MN}}$.

Now the remaining problem is to examine the type of convergence of F_{W_k} . Recall the formulation of F_{W_k} as: $F_{W_k}(x) = \sum_{\ell=0}^{L-1} \xi_1(N, L, \ell)(F_{Y_k}(x))^{N-\ell}$. It is known that F_{Y_k} converges weakly to the type 3 Gumbel distribution. Due to the complicated form of $\xi_1(\cdot, \cdot, \cdot)$, it is tedious to directly check the conditions for proving the type of convergence. In order to investigate the tail behavior of F_{W_k} which dominates the type of convergence [56], the following tail equivalence theorem is called upon.

Theorem 4.4. (*The Tail Equivalence Theorem [139]*) $U(\cdot)$ and $V(\cdot)$ are distribu-

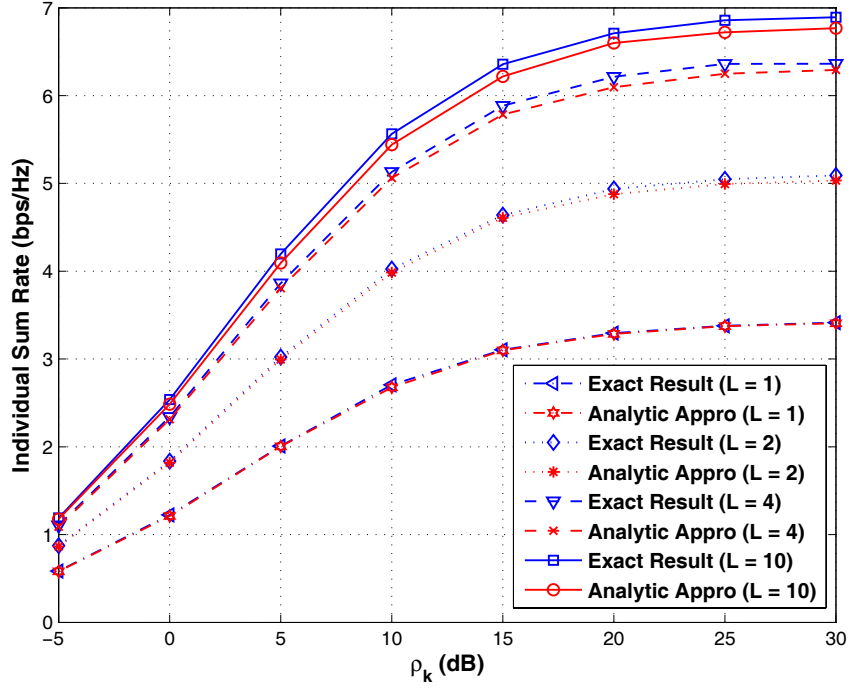


Figure 4.5: Comparison of the exact individual sum rate and the approximated one for a given user with different spectral dimension selective feedback L with respect to different ρ_k ($M = 4$, $N = 10$, $K = 20$, $L = 1, 2, 4, 10$).

tion functions such that

$$\lim_{x \rightarrow \infty} \frac{1 - U(x)}{1 - V(x)} = 1. \quad (4.35)$$

If there exist normalizing constants $a_K, b_K > 0$ such that $U^K(a_K + b_K x) \rightarrow G(x)$, where $G(x)$ is non-degenerate, then $V^K(a_K + b_K x) \rightarrow G(x)$.

From Theorem 4.4 one can infer that if two distribution functions are tail equivalent, then they belong to the domain of attraction of the same type. Employing Theorem 4.4, a tail equivalent formulation can be obtained for F_{W_k} expressed in the following corollary.

Corollary 4.4. (Tail Equivalent CDF) $F_{W_k}(x)$ and $(F_{Y_k}(x))^{N - \sum_{\ell=0}^{L-1} \xi_1(N, L, \ell)}$ are tail equivalent.

Proof. The proof is given in Appendix G. □

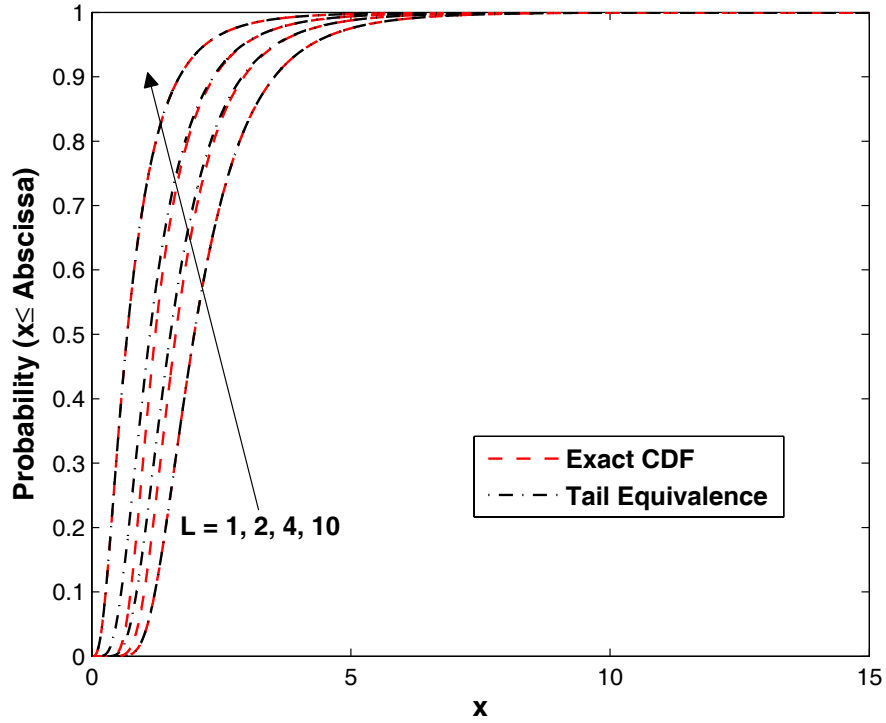


Figure 4.6: Comparison of the exact CDF F_{W_k} and its tail equivalence for different spectral dimension selective feedback L ($M = 4$, $N = 10$, $\rho_k = 10$ dB, $L = 1, 2, 4, 10$).

Fig. 4.6 compares the exact CDF and the corresponding tail equivalence for different selective feedback L under $M = 4$, $N = 10$, and $\rho_k = 10$ dB. The tail equivalent CDF is observed to track the exact one even when x is small, which supports and lends confidence in the power of the tail equivalence theorem. Therefore, the tail equivalence is used to study the type of convergence, which is expressed in the following lemma.

Lemma 4.2. (*Type of Convergence of Selective Feedback*) *Given the statistical property of F_{Y_k} in (4.15), F_{W_k} belongs to the domain of attraction of type 3 Gumbel distribution.*

Proof. The proof is given in Appendix G. □

Having obtained the type of convergence for F_{W_k} , the rate scaling result

can be derived by referring to the normalizing constants theorem in Appendix F. The individual rate scaling is provided below.

Theorem 4.5. (*Individual Scaling Laws Under Spatial and Spectral Dimension Selective Feedback*)

$$\begin{aligned} \lim_{K \rightarrow \infty} \frac{\hat{R}_k}{M \log_2 \log_2 \frac{(N - \sum_{\ell=0}^{L-1} \xi_1(N, L, \ell) L) K}{MN}} &= 1, \\ \lim_{K \rightarrow \infty} \frac{\hat{R}_k^{\text{App}}}{M \log_2 \log_2 \frac{(N - \sum_{\ell=0}^{L-1} \xi_1(N, L, \ell) L) K}{N}} &= 1. \end{aligned} \quad (4.36)$$

Proof. The proof is given in Appendix G. \square

Remark: For the exact rate \hat{R}_k , the ultimate equivalent CDF of interest is $F_{Y_k}^{\frac{(N - \sum_{\ell=0}^{L-1} \xi_1(N, L, \ell) L) K}{MN}}$, thus the exponent $\frac{(N - \sum_{\ell=0}^{L-1} \xi_1(N, L, \ell) L) K}{MN}$ due to multiplicative effect can be seen as the virtual users for scheduling competition. This exponent is for the general best-L spectral dimension feedback. For the full feedback $L = N$, since $\xi_1(N, N, \ell)$ equals 1 for $\ell = N - 1$ and 0 otherwise, the CDF becomes $F_{Y_k}^{\frac{K}{M}}$. For the best-1 feedback $L = 1$, since $\xi_1(N, 1, \ell)$ is 1 for $\ell = 0$ and 0 otherwise, the CDF becomes $F_{Y_k}^{\frac{K}{M}}$. Intuitively, the best-1 feedback is asymptotically optimal due to the same number of virtual users. In other words, even though additional maximization reduces the average number of variables for feedback, it counteracts this reduction by increasing the exponent of the CDF. The number of virtual users is the limiting factor that dominates rate scaling. For the approximated rate \hat{R}_k^{App} , since the approximated CDF compensates for the spatial dimension selection by increasing the exponent, the rate scaling differs by a factor of M .

4.6 Conclusion

In this chapter, an analytical approach is used to investigate the problem of random beamforming with heterogeneous users and selective feedback. The heterogeneous user scenario corresponds to the practical scenario of potentially different large scale channel effects for different users. We leverage the CDF-based scheduling policy to decouple each user's rate and thus theoretically examine the

individual user rate. We develop the notion of individual sum rate to analyze the rate scaling for each individual user. We focus our analysis in this work on theoretically understanding the effect of selective feedback in both spatial and spectral dimensions. On the exact analysis part, extensive numerical results show that our approximate expression for the rate under selective feedback is effective and provides an efficient expression for computing the exact rate. On the asymptotic analysis part, we develop the notion of virtual users and the multiplicative effect to explain the impact of selective feedback on rate scaling. We further discover that the limiting factor for the rate scaling is the exponent for the ultimate CDF of the selected SINR at the scheduler side.

The text of this chapter, in part, is a reprint of the paper [140], Y. Huang and B. D. Rao, “Random beamforming with heterogeneous users and selective feedback: individual sum rate and individual scaling laws”, *IEEE Transactions on Wireless Communications*, *submitted*, 2012. The dissertation author is the primary researcher and author, and the co-author listed in this publication directed and supervised the research which forms the basis of this chapter.

4.7 Appendices

4.7.1 Appendix E

Proof of Theorem 4.1: With the help of Lemma 4.1, $\mathcal{J}_k(\epsilon)$ can be computed as

$$\begin{aligned} \mathcal{J}_k(\epsilon) &\stackrel{(a)}{=} \frac{\epsilon}{\ln 2} \sum_{i=0}^{\epsilon-1} \binom{\epsilon-1}{i} \frac{(-1)^i}{i+1} \int_0^\infty \ln(1+x) d \left(1 - \frac{e^{-\frac{M(i+1)x}{\rho_k}}}{(1+x)^{(M-1)(i+1)}} \right) \\ &\stackrel{(b)}{=} \frac{\epsilon}{\ln 2} \sum_{i=0}^{\epsilon-1} \binom{\epsilon-1}{i} \frac{(-1)^i}{i+1} \int_0^\infty \frac{e^{-\frac{M(i+1)x}{\rho_k}}}{(1+x)^{(M-1)(i+1)+1}} dx, \end{aligned} \quad (4.37)$$

where (a) follows from applying Lemma 4.1; (b) follows from integration by parts. The closed form result for $\mathcal{I}(\alpha, \beta)$ in Theorem 4.1 can be computed in a recursive

manner [64] and is presented as follows

$$\mathcal{I}(\alpha, \beta) = \begin{cases} \frac{(-1)^{\beta-1} \alpha^{\beta-1} e^\alpha E_1(\alpha)}{(\beta-1)!} + \sum_{i=1}^{\beta-1} \frac{(i-1)!}{(\beta-1)!} (-1)^{\beta-i-1} \alpha^{\beta-i-1}, & \beta \geq 2 \\ e^\alpha E_1(\alpha), & \beta = 1 \end{cases} \quad (4.38)$$

where $E_1(x) = \int_x^\infty \frac{e^{-t}}{t} dt$ is the exponential integral function of the first order [57].

4.7.2 Appendix F

Proof of Corollary 4.1:

$$\begin{aligned} \hat{R}_k^{\text{App}} &\stackrel{(a)}{=} M \sum_{\tau_1=1}^K \binom{K}{\tau_1} \left(\frac{1}{M}\right)^{\tau_1} \left(1 - \frac{1}{M}\right)^{K-\tau_1} \int_0^\infty \log_2(1+x) d(F_{Z_k}(x))^{M\tau_1} \\ &\stackrel{(b)}{=} M \sum_{\tau_1=1}^K \binom{K}{\tau_1} \left(\frac{1}{M}\right)^{\tau_1} \left(1 - \frac{1}{M}\right)^{K-\tau_1} \mathcal{J}_k(M\tau_1), \end{aligned} \quad (4.39)$$

where (a) follows from the CDF approximation in (4.21); (b) follows from the definition and computation of $\mathcal{J}_k(\epsilon)$.

Proof of Corollary 4.2: It is shown in [20] that F_{Y_k} belongs to the domain of attraction of type 3 Gumbel distribution [56]. Thus if the number of SINR to maximize over for each beam is fixed and equals the number of users K , then the following equation holds: $\lim_{K \rightarrow \infty} (F_{Y_k}(a_{k:K} + b_{k:K}x))^K = \Psi(x)$, where $\Psi(x) = e^{-e^{-x}}$ is the type 3 Gumbel distribution, $a_{k:K}$ and $b_{k:K}$ represent the normalizing constants for user k . From Theorem 4.3, the number of SINR to maximize over for each beam approaches $\frac{K}{M}$. Let $c_{k:K}$ and $d_{k:K}$ denote the normalizing constants for user k under the selective feedback case. Then the following equation holds: $\lim_{K \rightarrow \infty} (F_{Y_k}(c_{k:K} + d_{k:K}x))^{\frac{K}{M}} = \Psi(x)$. In order to obtain $c_{k:K}$ and $d_{k:K}$, the following theorem is called upon.

Theorem 4.6. (*The Normalizing Constants Theorem [98]*) *Let $F_K(y)$ be a sequence of distribution functions. Let $a_K, b_K > 0$, c_K , and $d_K > 0$ be sequences of real numbers such that, as $K \rightarrow \infty$,*

$$\lim F_K(a_K + b_Kx) = U(x), \quad \lim F_K(c_K + d_Kx) = V(x) \quad (4.40)$$

for all continuity points x of the limits, where $U(x)$ and $V(x)$ are nondegenerate distribution functions. Then, as $K \rightarrow \infty$, the limits: $\lim \frac{d_K}{b_K} = B \neq 0$, $\lim \frac{c_K - a_K}{b_K} = A$ are finite, and $V(x) = U(A + Bx)$.

The spatial dimension selective feedback case possesses the following situation in Theorem 4.6: $F_K(x) = (F_{Y_k}(x))^K$, $a_K = a_{k:K}$, $b_K = b_{k:K}$, $c_K = c_{k:K}$, $d_K = d_{k:K}$, $U(x) = \Psi(x)$, and $V(x) = (\Psi(x))^M$. The sequence of $a_{k:K}$ has been derived in [58] as: $a_{k:K} = \rho_k \log_2 K - \rho_k(M-1) \log_2 \log_2 K + o(1)$. A suitable choice of $b_{k:K}$ for type 3 is $g_k(b_{k:K})$, where $g_k(x)$ is the growth function for user k defined by $g_k(x) \triangleq \frac{1 - F_{Z_k}(x)}{f_{Z_k}(x)}$. Thus a suitable sequence is $b_{k:K} = \rho_k$ for all K . Solving $(\Psi(x))^M = \Psi(A + Bx)$ yields $A = -\log M$, $B = 1$. Therefore, by referring to Theorem 4.6, the normalizing constants can be derived to be: $c_{k:K} = \rho_k \log_2 \frac{K}{M} - \rho_k(M-1) \log_2 \log_2 K + o(1)$, and $d_{k:K} = \rho_k$ for all K . Then by employing the Corollary A.1. in [58], the individual rate for user k , namely \hat{R}_k scales as $M \log_2 \log_2 \frac{K}{M}$.

Regarding the approximated rate \hat{R}_k^{APP} , since the approximated CDF by negative association is $(F_{Z_k}(x))^M$ and the number of SINR to maximize over approaches $\frac{K}{M}$, we have $\lim_{K \rightarrow \infty} (F_{Z_k}(c_{k:K} + d_{k:K}x))^{M \frac{K}{M}} = \lim_{K \rightarrow \infty} (F_{Z_k}(c_{k:K} + d_{k:K}x))^K = \Psi(x)$. Thus the normalizing constants $c_{k:K} = a_{k:K}$, and $d_{k:K} = b_{k:K}$, which enables the approximated rate \hat{R}_k^{APP} to scale as $M \log_2 \log_2 K$.

4.7.3 Appendix G

Proof of Corollary 4.4: Given Theorem 4.4, the following equality holds:

$$\begin{aligned} & \lim_{x \rightarrow \infty} \frac{1 - \sum_{\ell=0}^{L-1} \xi_1(N, L, \ell) (F_{Y_k}(x))^{N-\ell}}{1 - (F_{Y_k}(x))^{N - \sum_{\ell=0}^{L-1} \xi_1(N, L, \ell) \ell}} \\ & \stackrel{(a)}{=} \lim_{x \rightarrow \infty} \frac{\sum_{\ell=0}^{L-1} \xi_1(N, L, \ell) (N - \ell) (F_{Y_k}(x))^{N-\ell-1} f_{Y_k}(x)}{(N - \sum_{\ell=0}^{L-1} \xi_1(N, L, \ell) \ell) (F_{Y_k}(x))^{N - \sum_{\ell=0}^{L-1} \xi_1(N, L, \ell) \ell - 1} f_{Y_k}(x)} \stackrel{(b)}{=} 1, \quad (4.41) \end{aligned}$$

where (a) follows from the L'Hospital's rule; (b) follows from the following fact that $\sum_{\ell=0}^{L-1} \xi_1(N, L, \ell) = 1$.

Proof of Lemma 4.2: F_{Y_k} with statistics in (4.15) belongs to the domain of attraction of type 3. It can be shown that for any distribution function $F(x)$ which

converges weakly to the limiting distribution, then its exponent form $F^\epsilon(x)$ has the same type of convergence [98], $(F_{Y_k}(x))^{N-\sum_{\ell=0}^{L-1} \xi_1(N,L,\ell)\ell}$ belongs to the domain of attraction of type 3. Then by Theorem 4.4, F_{W_k} belongs to the domain of attraction of type 3.

Proof of Theorem 4.5: A procedure similar to that used in proving Corollary 4.2 can be used here. Since the number of SINR to maximize over for each beam at each resource block approaches $\frac{KL}{MN}$, and F_{W_k} belongs to the domain of attraction of type 3, the following equation holds: $\lim_{K \rightarrow \infty} (F_{W_k}(c_{k:K} + d_{k:K}x))^{\frac{KL}{MN}} = \Psi(x)$. By referring to the tail equivalence theorem, the equivalent equation is: $\lim_{K \rightarrow \infty} (F_{Y_k}(c_{k:K} + d_{k:K}x))^{\frac{KL(N-\sum_{\ell=0}^{L-1} \xi_1(N,L,\ell)\ell)}{MN}} = \Psi(x)$. Applying Theorem 4.6 yields the normalizing constants: $c_{k:K} = \rho_k \log_2 \frac{KL(N-\sum_{\ell=0}^{L-1} \xi_1(N,L,\ell)\ell)}{MN} - \rho_k(M-1) \log_2 \log_2 K + o(1)$, and $d_{k:K} = \rho_k$ for all K . Therefore, \hat{R}_k scales as $M \log_2 \log_2 \frac{KL(N-\sum_{\ell=0}^{L-1} \xi_1(N,L,\ell)\ell)}{MN}$.

For the approximated rate \hat{R}_k^{APP} using the approximated CDF $(F_{Z_k}(x))^M$ for F_{Y_k} , the following equation holds: $\lim_{K \rightarrow \infty} (F_{Z_k}(c_{k:K} + d_{k:K}x))^{\frac{KL(N-\sum_{\ell=0}^{L-1} \xi_1(N,L,\ell)\ell)}{N}} = \Psi(x)$. Using the same line of arguments, it can be shown that \hat{R}_k^{APP} scales as $M \log_2 \log_2 \frac{KL(N-\sum_{\ell=0}^{L-1} \xi_1(N,L,\ell)\ell)}{N}$.

Chapter 5

Outage Balancing Based on Spatial Channel Statistics

5.1 Introduction

In a multiuser interference network, intelligent power control helps in energy saving and interference reduction thereby enabling cost-effective usage of the wireless spectrum [141]. With the additional antenna arrays at the transmitter side, efficient beamforming technique can be employed jointly with power control to exploit the spatial resources in multiuser MISO networks and improve spectrum usage. In such interference networks, instantaneous channel state information (CSI) regarding the wireless environment has to be made available to all the transmit nodes in order to achieve maximum throughput. To obtain the instantaneous CSI, each receive node has to estimate the channel and conveys such information via feedback. The feedback requirement may become prohibitive and even infeasible in a mobile network when there are many transmit-receive links and the channel changes rapidly. Therefore, much work has focused on efficient transmission strategies with limited feedback or partial feedback, e.g., see [1] and the references therein.

In this work, we examine the usage of statistical channel information, or channel distribution information (CDI) for system design. In a MISO interference

network, the CDI reflects the existing correlation information at antenna side [142], and is known to be slowly varying on the order of tens of seconds or more. Algorithms based on CDI are triggered only when the statistical channel information has changed. Thus, CDI can be incorporated into system design to achieve stable and robust performance compared with design schemes relying on CSI [143]. However, in a CDI-based system, reliable transmission can not be guaranteed all the time due to the statistical variation of the instantaneous channel. In other words, the outage event occurs when the received signal-to-interference-plus-noise ratio (SINR) is less than a pre-determined threshold, which depends on specific modulation type and other design parameters. Herein, we focus on joint optimization of beamformer and power to minimize the maximum outage probability in order to achieve outage balancing in a generic MISO interference network.

Briefly reviewing the literature, earlier work on performing power control to optimize outage without multiple antennas is addressed in [144], wherein a geometric programming formulation of the worst outage problem in the interference-limited special case is formulated and a heuristic iterative algorithm is proposed to compute the optimal power. In [145], the total power minimization problem with outage constraints in a multiuser uplink is examined and an iterative algorithm is presented whose convergence is proven based on the standard interference function framework [146]. In [147], the total power minimization problem is extended to a MIMO network with antennas at both the transmitters and receivers, and an iterative algorithm similar to [145] is presented for power updates. In [148], the worst outage problem [144] is analyzed using a nonlinear Perron-Frobenius theory [149], and the convergence problem of the heuristic algorithm in [144] is resolved. However, the analysis in [148] focuses on the single antenna model. In this chapter, we study the outage balancing problem in a multiuser MISO network, where all the links experience correlated Rayleigh fading. This is a much harder problem due to correlation coupling and non-convexity in the power vector and beamforming weights. Based on the derived expression of the outage probability, we present the optimal solution under the fixed set of beamformer. Since jointly optimizing beamformer and power for the outage balancing problem is non-convex, we an-

alyze its certainty-equivalent margin counterpart [144, 145, 147] for near-optimal algorithm design. We present a Perron-Frobenius characterization of the network duality [121, 122, 150–152], and utilize it to propose an iterative algorithm for computing the near-optimal power vector and beamforming weights. The geometrically fast convergence rate of the proposed algorithm is further proven using nonlinear Perron-Frobenius theory.

The chapter is organized as follows. Section 5.2 presents the system model and the outage balancing problem. In Section 5.3, we examine the problem structure and derive the optimal solution given a fixed set of beamformer. Section 5.4 provides a near-optimal solution by analyzing the certainty-equivalent margin of the original problem. The numerical results are shown in Section 5.5. Finally, Section 5.6 concludes the chapter.

Notations in this chapter are presented as follows. Boldface upper-case letters denote matrices, boldface lower-case letters denote vectors, and italics denote scalars. The Perron-Frobenius eigenvalue of a nonnegative matrix \mathbf{F} is denoted as $\rho(\mathbf{F})$. Let $\mathbf{x}(\mathbf{F})$ and $\mathbf{y}(\mathbf{F})$ denote the Perron (right) and left eigenvectors of \mathbf{F} associated with $\rho(\mathbf{F})$ respectively. $\text{diag}(\mathbf{a})$ denotes the diagonal matrix having the vector \mathbf{a} on its diagonal. Let $\mathbf{a} \circ \mathbf{b} \triangleq (a_1 b_1, \dots, a_K b_K)^\top$ (the Schur product). Let \mathbb{C} , \mathbb{R}_+ , and \mathbb{R}_{++} represent the set of complex numbers, the set of nonnegative real numbers, and the set of positive real numbers respectively. Let $(\cdot)^\top$ and $(\cdot)^\dagger$ denote the transpose operation and conjugate transpose operation respectively. $\|\cdot\|$ denotes the Euclidean norm for vectors.

5.2 System Model

Consider a multiuser MISO interference network with K transmit-receive pairs. The transmitter is assumed to be equipped with N antennas. The received signal y_k for user (receiver) k is written as

$$y_k = \mathbf{h}_{k,k}^\dagger \mathbf{x}_k + \sum_{j \neq k} \mathbf{h}_{k,j}^\dagger \mathbf{x}_j + z_k, \quad (5.1)$$

where $\mathbf{h}_{k,j} \in \mathbb{C}^{N \times 1}$ denotes the channel vector between transmitter j and user k , $\mathbf{x}_k \in \mathbb{C}^{N \times 1}$ is the transmitted signal vector of transmitter k , and z_k characterizes the additive white noise effect, which is distributed as $\mathcal{CN}(0, \sigma_k)$ with $\sigma_k \in \mathbb{R}_{++}$.

Linear beamforming strategy is assumed at the transmitter, and thus the transmit signal vector \mathbf{x}_k can be expressed as $\mathbf{x}_k = \sqrt{p_k} s_k \mathbf{u}_k$, where s_k and p_k denote the information signal and the transmit power for link k , and $\mathbf{u}_k \in \mathbb{C}^{N \times 1}$ denotes the normalized transmit beamformer for user k , i.e., $\|\mathbf{u}_k\|^2 = 1$. The SINR for user k can be written as

$$\text{SINR}_k(\mathbf{p}, \mathbb{U}) = \frac{p_k |\mathbf{h}_{k,k}^\dagger \mathbf{u}_k|^2}{\sum_{j \neq k} p_j |\mathbf{h}_{k,j}^\dagger \mathbf{u}_j|^2 + \sigma_k}, \quad (5.2)$$

where $\mathbf{p} = (p_1, \dots, p_K)^\top$, $\mathbb{U} = (\mathbf{u}_1, \dots, \mathbf{u}_K)$.

If instantaneous CSI is available at transmitter side, instantaneous adaptation of beamformer and power is possible to optimize the SINR. This approach consumes a large amount of feedback resource, and is not feasible when the channel changes fast. Herein, the statistical channel information, namely the CDI characterizing the channel covariance matrix, is assumed to be available at transmitter side. In this chapter, correlated Rayleigh fading is assumed for all the links in the interference network and is modeled as

$$\mathbf{h}_{k,j} \sim \mathcal{CN}(0, \Sigma_{k,j}), \quad (5.3)$$

where $\Sigma_{k,j}$ represents the covariance matrix for $\mathbf{h}_{k,j}$.

Since only CDI is known, the instantaneous SINR becomes a random variable. Denote the SINR threshold for link k as β_k , then SINR_k can fall below β_k with some probability due to channel fading. Thus, transmission strategies based on CDI experience the fading-induced outage event. The outage probability for link k can be expressed as $\mathbb{P}(\text{SINR}_k(\mathbf{p}, \mathbb{U}) < \beta_k)$.

Let w_k denote the weight associated with p_k for user k illustrating different power prices with $\mathbf{w} = (w_1, \dots, w_K)^\top$. Denote the threshold vector $\boldsymbol{\beta} = (\beta_1, \dots, \beta_K)^\top$ and the noise vector $\boldsymbol{\sigma} = (\sigma_1, \dots, \sigma_K)^\top$. The outage balancing

problem subject to the weighted sum power constraint can be written as follows:

$$\begin{aligned}
& \text{minimize} && \max_k \mathbb{P}(\text{SINR}_k(\mathbf{p}, \mathbb{U}) < \beta_k) \\
& \text{subject to} && \mathbf{w}^\top \mathbf{p} \leq \bar{P}, \quad p_k > 0, \quad \|\mathbf{u}_k\|^2 = 1, \quad \forall k \\
& \text{variables :} && \mathbf{p}, \mathbb{U}.
\end{aligned} \tag{5.4}$$

5.3 Problem Analysis

5.3.1 Problem Manipulation

In order to analyze the optimization problem (5.4), the expression for the outage probability is needed. Based on the results developed in [147,153], the closed form expression for $\mathbb{P}(\text{SINR}_k(\mathbf{p}, \mathbb{U}) < \beta_k)$ can be obtained and is summarized in the following lemma.

Lemma 5.1. *In a multiuser MISO interference network where all the links experience correlated Rayleigh fading, the closed form expression of the outage probability for link k is written as¹*

$$\mathbb{P}(\text{SINR}_k(\mathbf{p}, \mathbb{U}) < \beta_k) = 1 - e^{-\frac{\beta_k \sigma_k}{p_k c_{k,k}}} \prod_{j \neq k} \left(1 + \frac{\beta_k p_j c_{k,j}}{p_k c_{k,k}} \right)^{-1}, \tag{5.5}$$

where $c_{k,j}$ represents the statistical beamforming channel gain, whose expression is given by

$$c_{k,j} \triangleq \mathbf{u}_j^\dagger \boldsymbol{\Sigma}_{k,j} \mathbf{u}_j. \tag{5.6}$$

Remark: The expression in (5.5) consists of the product of two major parts: $e^{-\frac{\beta_k \sigma_k}{p_k c_{k,k}}}$ and $\prod_{j \neq k} \left(1 + \frac{\beta_k p_j c_{k,j}}{p_k c_{k,k}} \right)^{-1}$. The former is due solely to additive white Gaussian noise, while the latter is due to the effect of interference from other links².

¹This lemma corrects an error in [147, Theorem 1] where a constant 2 should not appear in $e^{-\frac{\beta_k \sigma_k}{p_k c_{k,k}}}$.

²This chapter provides an outage characterization of the optimization problem. An ergodic characterization in the system setting of a cooperative MIMO beamforming can be referred to [154].

Using the results from Lemma 5.1, (5.4) is transformed to a deterministic optimization problem:

$$\begin{aligned}
& \text{minimize} && \max_k 1 - e^{-\frac{\beta_k \sigma_k}{p_k c_{k,k}}} \prod_{j \neq k} \left(1 + \frac{\beta_k p_j c_{k,j}}{p_k c_{k,k}}\right)^{-1} \\
& \text{subject to} && \mathbf{w}^\top \mathbf{p} \leq \bar{P}, \quad p_k > 0, \quad \|\mathbf{u}_k\|^2 = 1, \quad \forall k \\
& \text{variables :} && \mathbf{p}, \mathbb{U}.
\end{aligned} \tag{5.7}$$

To perform further manipulation, we introduce the auxiliary variable τ and transform (5.7) into an epigraph formulation as

$$\begin{aligned}
& \text{minimize} && \tau \\
& \text{subject to} && \frac{\beta_k \sigma_k}{p_k c_{k,k}} + \sum_{j \neq k} \log \left(1 + \frac{\beta_k p_j c_{k,j}}{p_k c_{k,k}}\right) \leq \tau, \quad \forall k \\
& && \mathbf{w}^\top \mathbf{p} \leq \bar{P}, \quad p_k > 0, \quad \|\mathbf{u}_k\|^2 = 1, \quad \forall k \\
& \text{variables :} && \mathbf{p}, \mathbb{U}, \tau.
\end{aligned} \tag{5.8}$$

The problem (5.8) is non-convex in $(\mathbf{p}, \mathbb{U}, \tau)$. However, for any fixed \mathbb{U} , it can be shown that (5.8) is convex in (\mathbf{p}, τ) and thus the optimal solution exists, which is denoted by $(\mathbf{p}^*(\mathbb{U}), \tau^*(\mathbb{U}))$. In the next part, we will analyze the optimal solution under given beamformer to draw insights.

5.3.2 Optimal Solution Under Fixed Beamformer

For a given set of beamformer \mathbb{U} , a simpler optimization problem can be formulated from (5.8):

$$\begin{aligned}
& \text{minimize} && \tau(\mathbb{U}) \\
& \text{subject to} && \sum_{j \neq k} \log \left(1 + \frac{\beta_k p_j(\mathbb{U}) c_{k,j}(\mathbb{U})}{p_k(\mathbb{U}) c_{k,k}(\mathbb{U})}\right) \\
& && \quad + \frac{\beta_k \sigma_k}{p_k(\mathbb{U}) c_{k,k}(\mathbb{U})} \leq \tau(\mathbb{U}), \quad \forall k \\
& && \mathbf{w}^\top \mathbf{p}(\mathbb{U}) \leq \bar{P}, \quad p_k(\mathbb{U}) > 0, \quad \forall k \\
& \text{variables :} && \mathbf{p}(\mathbb{U}), \tau(\mathbb{U}).
\end{aligned} \tag{5.9}$$

Now we will examine (5.9) using nonlinear Perron-Frobenius theory (some relevant lemma and theorem are briefly reviewed in Appendix H). We denote the first K constraints of (5.9) as the outage constraints. Then, by observing that the left-hand side of the k th outage constraint is monotonically decreasing in $p_k(\mathbb{U})$,

and monotonically increasing in $p_j(\mathbb{U})$ for $j \neq k$, it can be shown that at optimality, the outage constraints as well as the weighted sum power constraint become active which is utilized next.

For compact representation, we define the non-negative matrix $\Psi(\mathbf{p}) \in \mathbb{R}_+^{K \times K}$ as follows:

$$\Psi_{k,j}(\mathbf{p}) = \begin{cases} 0, & \text{if } k = j \\ \frac{p_k c_{k,k}}{\beta_k p_j} \log \left(1 + \frac{\beta_k p_j c_{k,j}}{p_k c_{k,k}} \right), & \text{if } k \neq j \end{cases} \quad (5.10)$$

Also, we define the auxiliary vector $\mathbf{g} \triangleq \left(\frac{1}{c_{1,1}}, \dots, \frac{1}{c_{K,K}} \right)^\top$. Then the optimal power vector satisfies the following conditional eigenvalue problem:

$$\tau^*(\mathbb{U}) \mathbf{p}^*(\mathbb{U}) = \text{diag}(\boldsymbol{\beta} \circ \mathbf{g}(\mathbb{U})) \left(\Psi(\mathbf{p}^*(\mathbb{U})) + \frac{1}{\bar{P}} \boldsymbol{\sigma} \mathbf{w}^\top \right) \mathbf{p}^*(\mathbb{U}). \quad (5.11)$$

From (5.11), it can be shown from non-negative matrix theory that $\mathbf{p}^*(\mathbb{U})$ is the Perron (right) eigenvector (up to a scaling factor) of the non-negative matrix $\text{diag}(\boldsymbol{\beta} \circ \mathbf{g}(\mathbb{U})) (\Psi(\mathbf{p}^*(\mathbb{U})) + (1/\bar{P}) \boldsymbol{\sigma} \mathbf{w}^\top)$, and $\tau^*(\mathbb{U})$ is related to its spectral radius by the following:

$$\tau^*(\mathbb{U}) = \rho \left(\text{diag}(\boldsymbol{\beta} \circ \mathbf{g}(\mathbb{U})) (\Psi(\mathbf{p}^*(\mathbb{U})) + (1/\bar{P}) \boldsymbol{\sigma} \mathbf{w}^\top) \right). \quad (5.12)$$

In order to derive a fast algorithm to compute the optimal solution $\mathbf{p}^*(\mathbb{U})$ and operate in a decentralized manner, we employ nonlinear Perron-Frobenius theory to present *Algorithm 5.1*, which is given in Table 5.1.

The geometrically fast convergence rate of *Algorithm 5.1* is presented in the following theorem.

Theorem 5.1. Define the norm $\|\cdot\|_{\text{PN}}$ on $\mathbb{R}_+^{K \times 1}$ as: $\|\mathbf{p}\|_{\text{PN}} = (1/\bar{P}) \sum_k w_k |p_k|$, and the mapping $f^{(1)}: \mathbb{R}_+^{K \times 1} \rightarrow \mathbb{R}_+^{K \times 1}$ as

$$f_k^{(1)}(\mathbf{p}, \mathbb{U}) = \frac{\beta_k \sigma_k}{c_{k,k}(\mathbb{U})} + \sum_{j \neq k} p_j \log \left(1 + \frac{\beta_k p_j c_{k,j}(\mathbb{U})}{p_k c_{k,k}(\mathbb{U})} \right), \forall k. \quad (5.13)$$

Then the normalized fixed-point iteration

$$\hat{f}_k^{(1)}(\mathbf{p}[\ell + 1], \mathbb{U}) = (1/\|\hat{f}_k^{(1)}(\mathbf{p}[\ell], \mathbb{U})\|_{\text{PN}}) \hat{f}_k^{(1)}(\mathbf{p}[\ell], \mathbb{U})$$

for any given \mathbb{U} converges to the optimal solution of (5.9), i.e., $\mathbf{p}^*(\mathbb{U})$, geometrically fast.

Proof. The proof is given in Appendix I. \square

We have shown the optimal power given a fixed \mathbb{U} . However, due to the coupled property of the interference in the outage constraint, it is difficult if not impossible to minimize $f_k^{(1)}(\mathbf{p}^*(\mathbb{U}), \mathbb{U})$ to obtain the optimal beamformer. As mentioned before, the outage balancing problem (5.7) is non-convex in (\mathbf{p}, \mathbb{U}) . Even though finding the optimal beamformer for the problem is still an open problem, we provide a near-optimal approach in the next section.

5.4 Joint Beamforming and Power Control

5.4.1 Problem Observation

Now we consider the joint optimization problem (5.8). One key observation of (5.8) is that the coupled effect inside the $\log(\cdot)$ function in the outage constraint causes the non-linearity and non-convexity of joint optimization. To overcome these barriers, bounding techniques are proposed in [144] by exploiting the so-called certainty-equivalent margin counterpart of the original problem. This approach is employed in [145, 147] for the power minimization problem. Herein, we leverage this approach in the outage balancing problem to derive near-optimal solution.

Utilizing the bounding technique in [144], upper and lower bound for the left-hand side of the k th outage constraint can be derived as

$$\begin{aligned} \log \left(1 + \frac{\beta_k \left(\sum_{j \neq k} p_j c_{k,j} + \sigma_k \right)}{p_k c_{k,k}} \right) &\leq \\ \frac{\beta_k \sigma_k}{p_k c_{k,k}} + \sum_{j \neq k} \log \left(1 + \frac{\beta_k p_j c_{k,j}}{p_k c_{k,k}} \right) &\leq \frac{\beta_k \left(\sum_{j \neq k} p_j c_{k,j} + \sigma_k \right)}{p_k c_{k,k}}. \end{aligned} \quad (5.14)$$

The upper bound in (5.14) will be utilized since its solution is also feasible to the original problem. In order to present the corresponding certainty-equivalent margin problem, we define $\Gamma_k^{\text{PN}}(\mathbf{p}, \mathbb{U})$ as

$$\Gamma_k^{\text{PN}}(\mathbf{p}, \mathbb{U}) = \frac{p_k c_{k,k}}{\sum_{j \neq k} p_j c_{k,j} + \sigma_k}, \quad (5.15)$$

where the superscript $(\cdot)^{\text{PN}}$ represents the primal network. It can be easily seen that $\Gamma_k^{\text{PN}}(\mathbf{p}, \mathbb{U})$ denotes the average SINR when the statistical variation of the signal as well as the interference are replaced by their expected values. The certainty-equivalent margin problem is formulated as follows:

$$\begin{aligned} & \text{maximize} && \min_k \frac{\Gamma_k^{\text{PN}}(\mathbf{p}, \mathbb{U})}{\beta_k} \\ & \text{subject to} && \mathbf{w}^\top \mathbf{p} \leq \bar{P}, \quad \mathbf{p} > 0, \quad \|\mathbf{u}_k\|^2 = 1 \\ & \text{variables :} && \mathbf{p}, \mathbb{U} \end{aligned} \quad (5.16)$$

To explicitly express the relationship between the original outage balancing problem (5.7) and its certainty-equivalent margin counterpart (5.16), denote the optimal value of (5.16) as ζ^* . Then using the bounds (5.14) and after some manipulation, we have

$$\frac{1}{\zeta^* + 1} \leq O^* \leq 1 - e^{-\frac{1}{\zeta^*}}, \quad (5.17)$$

where O^* represents the optimal solution for (5.7) and $O^* = 1 - e^{-\tau^*}$. Moreover, it is known that $\log(1+x) \simeq x$ for small x . Thus the upper and lower bound become very tight for small outage probabilities. In other words, the optimal solution for (5.16) provides a near-optimal solution for the outage balancing problem (5.7). This near-optimal effect is observed in [144, 145, 147]. In the following, we will use Perron-Frobenius theory to examine (5.16) and provide a fast iterative algorithm to compute the optimal value ζ^* .

5.4.2 Near-Optimal Solution

For any beamformer \mathbb{U} , a simpler optimization problem for (5.7) can be formulated by only optimizing the power vector. It can be shown that at optimality, the weighted power constraint becomes tight, and the weighted average SINR for different users are the same [155]. Define the nonnegative matrix $\mathbf{C} \in \mathbb{R}_+^{K \times K}$ as:

$$C_{k,j} = \begin{cases} 0, & \text{if } k = j \\ c_{k,j}, & \text{if } k \neq j \end{cases} \quad (5.18)$$

We can interpret \mathbf{C} as the average cross channel interference matrix. With the definition of \mathbf{C} , the optimal power vector satisfies the following eigenvalue problem:

$$\frac{1}{\zeta^*(\mathbb{U})} \mathbf{p}^*(\mathbb{U}) = \text{diag}(\boldsymbol{\beta} \circ \mathbf{g}(\mathbb{U})) (\mathbf{C}(\mathbb{U}) + (1/\bar{P}) \boldsymbol{\sigma} \mathbf{w}^\top) \mathbf{p}^*(\mathbb{U}). \quad (5.19)$$

Therefore, $\mathbf{p}^*(\mathbb{U})$ is the Perron (right) eigenvector (up to a scaling factor) of the non-negative matrix $\text{diag}(\boldsymbol{\beta} \circ \mathbf{g}(\mathbb{U})) (\mathbf{C}(\mathbb{U}) + (1/\bar{P})\boldsymbol{\sigma}\mathbf{w}^\top)$, and $\zeta^*(\mathbb{U})$ is related to its spectral radius by the following:

$$\zeta^*(\mathbb{U}) = \frac{1}{\rho(\text{diag}(\boldsymbol{\beta} \circ \mathbf{g}(\mathbb{U})) (\mathbf{C}(\mathbb{U}) + (1/\bar{P})\boldsymbol{\sigma}\mathbf{w}^\top))}. \quad (5.20)$$

Now we establish the hypothesized dual network for further analysis. Denote the dual network transmit power vector $\mathbf{q} \in \mathbb{R}_{++}^{K \times 1}$, where q_k denotes the transmit power for user k . Let the weight vector \mathbf{w} in the primal network be the noise vector in the dual network, and conversely let the noise vector $\boldsymbol{\sigma}$ in the primal network be the weight vector in the dual network, then given receive beamformer \mathbb{U} , the optimization for the dual network can be formulated as

$$\begin{aligned} & \text{maximize} \quad \min_k \frac{\Gamma_k^{\text{DN}}(\mathbf{q}, \mathbb{U})}{\beta_k} = \frac{q_k(\mathbb{U})}{(\text{diag}(\boldsymbol{\beta} \circ \mathbf{g}(\mathbb{U})) (\mathbf{C}^\top(\mathbb{U})\mathbf{q}(\mathbb{U}) + \mathbf{w}))_k} \\ & \text{subject to} \quad \boldsymbol{\sigma}^\top \mathbf{q}(\mathbb{U}) \leq \bar{P}, \quad \mathbf{q}(\mathbb{U}) > 0 \\ & \text{variables :} \quad \mathbf{q}(\mathbb{U}) \end{aligned} \quad (5.21)$$

where the superscript $(\cdot)^{\text{DN}}$ denotes the dual uplink network.

By leveraging the following properties of non-negative matrices: $\rho(\mathbf{A}) = \rho(\mathbf{A}^\top)$ and $\rho(\mathbf{AB}) = \rho(\mathbf{BA})$, the optimal solution for (5.21) equals the following expression: $\frac{1}{\rho(\text{diag}(\boldsymbol{\beta} \circ \mathbf{g}(\mathbb{U})) (\mathbf{C}^\top(\mathbb{U}) + (1/\bar{P})\mathbf{w}\boldsymbol{\sigma}^\top))}$. Comparing with the optimal solution for the primal network in (5.19), the network duality is observed by employing \mathbf{C}^\top as the average cross channel interference matrix for the dual network and reversing the role of \mathbf{w} and $\boldsymbol{\sigma}$. Note that the network duality holds for any given \mathbb{U} .

The benefit of the established network duality is the decoupled property of the dual network which enables beamformer optimization. The optimal beamformer \mathbb{U}^* depends on the power vector \mathbf{q} . For any given \mathbf{q} , the optimal beamformer $\mathbf{u}_k^*(\mathbf{q})$ for link k can be determined from the following equation:

$$\mathbf{u}_k^*(\mathbf{q}) = \arg \max_{\mathbf{u}_k(\mathbf{q})} \frac{\mathbf{u}_k^\dagger(\mathbf{q}) \boldsymbol{\Sigma}_{k,k} \mathbf{u}_k(\mathbf{q})}{\mathbf{u}_k^\dagger(\mathbf{q}) (\sum_{j \neq k} q_j \boldsymbol{\Sigma}_{j,k} + w_k \mathbf{I}) \mathbf{u}_k(\mathbf{q})}. \quad (5.22)$$

Therefore, the optimal beamformer is the dominant eigenvector of the generalized eigenvalue problem, which is well studied [156]. In specific, $\mathbf{u}_k^*(\mathbf{q})$ is the normalized

vector satisfying the following equation with the largest λ :

$$\Sigma_{k,k}\mathbf{x} = \lambda \left(\sum_{j \neq k} q_j \Sigma_{j,k} + w_k \mathbf{I} \right) \mathbf{x}. \quad (5.23)$$

The optimal solution for the beamformer, the power of the dual network and the primal network, and the optimal value for (5.16) can be written as: $\mathbf{u}_k^* = \mathbf{u}_k^*(\mathbf{q}^*)$, $\mathbf{q}^* = \mathbf{q}^*(\mathbb{U}^*)$, $\mathbf{p}^* = \mathbf{p}^*(\mathbb{U}^*)$, and $\zeta^* = \zeta^*(\mathbb{U}^*)$. As mentioned before, ζ^* can be used to bound the optimal outage probability, and the optimal solution for (5.16) serve as a near-optimal solution for the original outage balancing problem. In the next part, we will present an iterative algorithm to compute the optimal solution for (5.16) whose fast convergence property is also given.

5.4.3 Algorithm Design

From the aforementioned analysis, we present a decentralized algorithm denoted by *Algorithm 5.2*, which is given in Table 5.2, to compute the optimal solution for (5.16).

The geometrically fast convergence rate of *Algorithm 5.2* is presented in the following theorem.

Theorem 5.2. *Starting from any initial point $\mathbf{q}[0]$, $\mathbf{p}[0]$, and $\mathbb{U}[0]$, the $\mathbf{q}[\ell]$, $\mathbf{p}[\ell]$, and $\mathbb{U}[\ell]$ in *Algorithm 5.2* converge geometrically fast to the optimal solution \mathbf{q}^* , \mathbf{p}^* , and \mathbb{U}^* of the certainty-equivalent margin problem (5.16).*

Proof. The proof is given in Appendix I. □

5.5 Numerical Results

In this section, we conduct a numerical study to understand the efficiency of the developed algorithm for the outage balancing problem. We employ the angular spread model [147,157] to generate the covariance matrices for the multiuser MISO interference network. Transmit angular spreads varying from 5 to 20 degrees across the links are assumed and the number of scatters is assumed to be 100. The desired

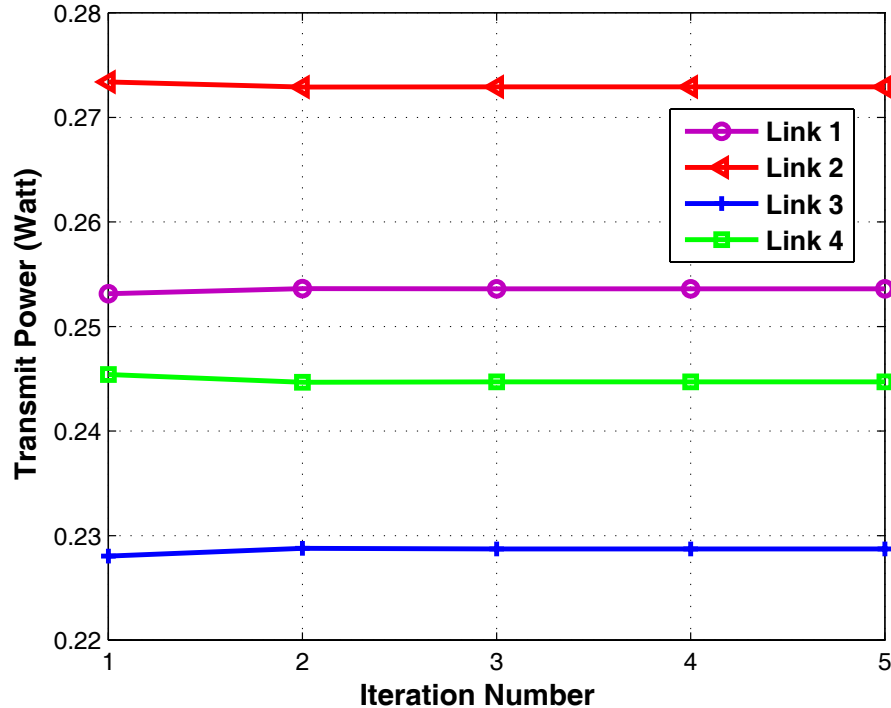


Figure 5.1: Convergence result of the primal network transmit power for different users ($K = 4$, $N = 4$, $\bar{P} = 1$ W, SINR Threshold = -5 dB).

signal links are centered at broadside, while the interfering links are centered at incident angles [147]. We assume $N = 4$ transmit antennas and the number of links $K = 4$. The signal-to-noise ratio (SNR) is kept constant at 10 dB. Also, the same weight and same SINR threshold are assumed.

We first consider the convergence property of designed algorithm. The total power \bar{P} is held constant at 1 Watt and the SINR threshold is set to be -5 dB. In Fig. 5.1, the convergence result of the primal network power is illustrated for different users. Then in Fig. 5.2, the convergence result of the outage probabilities is shown by using the near-optimal solution. It can be observed that the proposed algorithm converges with 3 runs of computation. Empirically, the algorithm converges within 5 – 10 runs with different system parameter settings, which indicate the practical applicability of the algorithm. Also, from Fig. 5.2, we observe that the maximum outage probability monotonically decreases with the iteration number.

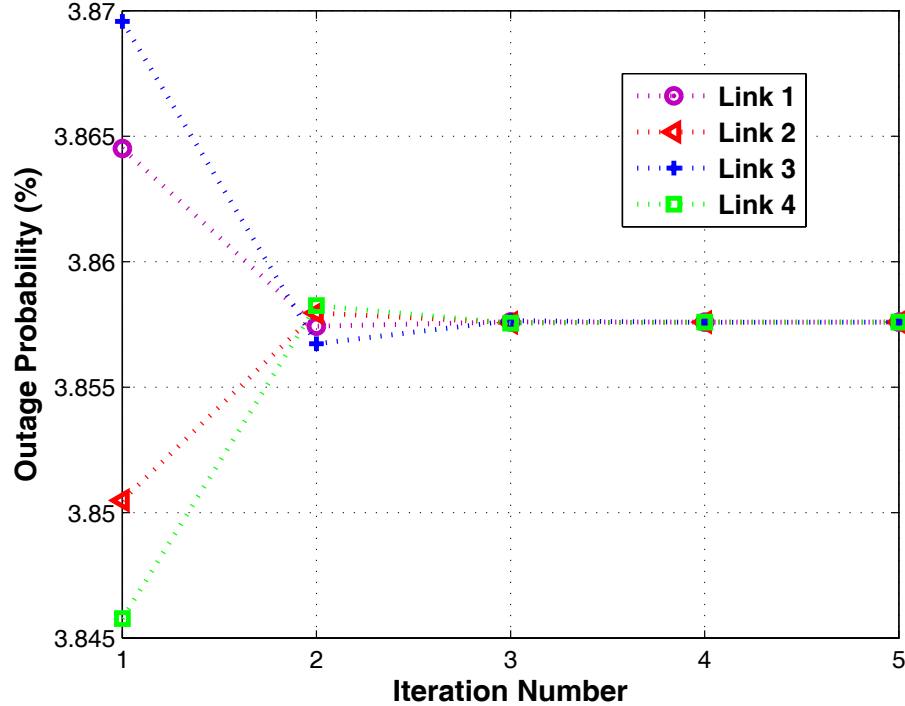


Figure 5.2: Convergence result of the outage probability for different users ($K = 4$, $N = 4$, $\bar{P} = 1$ W, SINR Threshold = -5 dB).

We next demonstrate the effect of the total transmit power \bar{P} and the SINR threshold on the maximum outage probability in the multiuser network. We average the maximum outage probability by considering 100 independent realizations of the covariance matrices in the network. From Fig. 5.3, we observe that by using the intelligent joint power control and beamformer design, a small maximum outage probability can be achieved for reasonable SINR thresholds. When the network has a high pre-defined threshold, the total transmit power has to be increased to bring down the outage probability.

5.6 Conclusion

In this chapter, we consider the use of statistical channel information for system design in a multiuser MISO interference network to reduce instantaneous feedback needs. We investigate the outage balancing problem to develop efficient

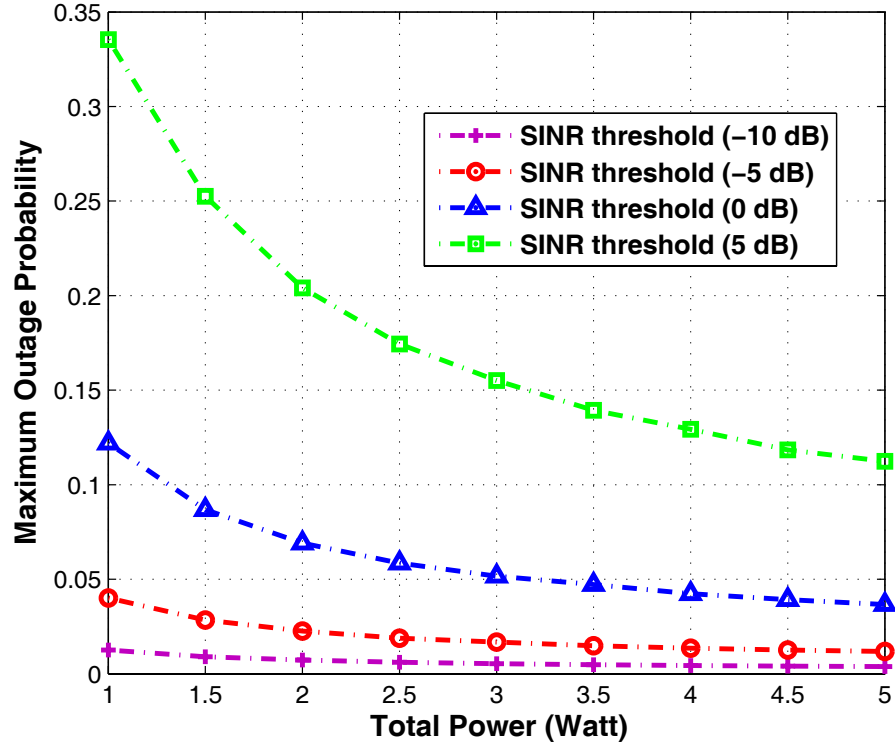


Figure 5.3: The effect of total power and the SINR threshold on the maximum outage probability in the network ($K = 4$, $N = 4$, SINR Threshold = -10 , -5 , 0 , 5 dB).

transmission strategies under a weighted sum power constraint. Under the fixed set of beamformer, we present a fast and decentralized algorithm to obtain the optimal power. Since the original outage balancing problem is non-convex when jointly optimizing power and beamformer, we analyze the certainty-equivalent margin counterpart and propose a near-optimal iterative algorithm based on network duality and non-negative matrix theory. The fast convergence of the algorithm is also proven by using nonlinear Perron-Frobenius theory, which makes it suitable for practical implementation.

The text of this chapter, in part, is a reprint of the paper [158], Y. Huang, C. W. Tan and B. D. Rao, “Outage balancing in multiuser MISO networks: network duality and algorithms”, *IEEE Global Communications Conferences (Globecom)*, Anaheim, CA, Dec. 2012. The dissertation author is the primary researcher and

author, and the co-authors listed in these publications contributed to or supervised the research which forms the basis of this chapter.

5.7 Appendices

5.7.1 Appendix H

Lemma 5.2. (*Concave Self-Mapping [149]*) A mapping $T : K \rightarrow K$ is concave if

$$T(a\mathbf{x} + (1 - a)\mathbf{y}) \geq aT\mathbf{x} + (1 - a)T\mathbf{y},$$

for all $\mathbf{x}, \mathbf{y} \in K$ and $a \in [0, 1]$, and monotone if $\mathbf{0} \leq \mathbf{x} \leq \mathbf{y}$ implies $\mathbf{0} \leq T\mathbf{x} \leq T\mathbf{y}$.

Theorem 5.3. (*Krause's theorem [149]*) Let $\|\cdot\|$ be a monotone norm on \mathbb{R}^L . For a concave mapping $f : \mathbb{R}_+^L \rightarrow \mathbb{R}_+^L$ with $f(\mathbf{z}) > \mathbf{0}$ for $\mathbf{z} \geq \mathbf{0}$, the following statements hold.

The conditional eigenvalue problem:

$$f(\mathbf{z}) = \lambda\mathbf{z},$$

with $\lambda \in \mathbb{R}$, $\mathbf{z} \geq \mathbf{0}$, $\|\mathbf{z}\| = 1$ has a unique solution $(\lambda^*, \mathbf{z}^*)$, where $\lambda^* > 0$, $\mathbf{z}^* > \mathbf{0}$. Furthermore, $\lim_{k \rightarrow \infty} \tilde{f}^k(\mathbf{z})$ converges geometrically fast to \mathbf{z}^* , where $\tilde{f}(\mathbf{z}) = f(\mathbf{z})/\|\mathbf{z}\|$.

5.7.2 Appendix I

Proof of Theorem 5.1: Following similar technique as in [148], we can prove that $f^{(1)}(\mathbf{p}, \mathbb{U})$ is a concave self-mapping of \mathbf{p} given \mathbb{U} . Also, we have $f_k^{(1)}(\mathbf{p}, \mathbb{U}) > 0$ for $\mathbf{p} \succeq \mathbf{0}$. Then the convergence property of the fixed-point iteration follows from Theorem 5.3.

Proof of Theorem 5.2: The key step to the proof is to establish the convergence property of the dual network power \mathbf{q} via nonlinear Perron-Frobenius theory. Define the mapping $f^{(2)} : \mathbb{R}_+^{K \times 1} \rightarrow \mathbb{R}_+^{K \times 1}$ as

$$f_k^{(2)}(\mathbf{q}) = \min_{\mathbf{u}_k} \left(\frac{\beta_k \mathbf{u}_k^\dagger (\sum_{j \neq k} q_j \boldsymbol{\Sigma}_{j,k} + w_k \mathbf{I}) \mathbf{u}_k}{\mathbf{u}_k^\dagger \boldsymbol{\Sigma}_{k,k} \mathbf{u}_k} \right), \quad \forall k. \quad (5.24)$$

$f^{(2)}(\mathbf{q})$ is the point-wise minimum of an affine mapping. Thus, $f^{(2)}(\mathbf{q})$ is a concave self-mapping of \mathbf{q} . Also, we have $f_k^{(2)}(\mathbf{q}) > 0$ for $\mathbf{q} \succeq \mathbf{0}$. Define the norm $\|\cdot\|_{\text{DN}}$ on $\mathbb{R}_+^{K \times 1}$ as: $\|\mathbf{q}\|_{\text{DN}} = (1/\bar{P}) \sum_k \sigma_k |q_k|$. Then applying Theorem 5.3, we can show that the normalized fixed-point iteration $\hat{f}_k^{(2)}(\mathbf{q}[\ell + 1]) = (1/\|f_k^{(2)}(\mathbf{q}[\ell])\|_{\text{DN}}) f_k^{(2)}(\mathbf{q}[\ell])$ converges geometrically fast to the optimal solution of the following conditional eigenvalue problem

$$\frac{1}{\zeta^*} \mathbf{q}^* = \left(f^{(2)}(\mathbf{q}^*) \frac{1}{\bar{P}} \boldsymbol{\sigma}^\top \right) \mathbf{q}^*. \quad (5.25)$$

Following the same line of argument, the convergence property of the primal network power \mathbf{p} can be proven. Then the alternate optimization given by *Algorithm 5.2* converges geometrically fast to the optimal solution of (5.16).

Table 5.1: Algorithm 5.1–Decentralized algorithm to compute the optimal solution under fixed beamformer

- For a given \mathbb{U} , initialize arbitrary $\mathbf{p}[0] \in \mathbb{R}_{++}^{K \times 1}$ such that $\mathbf{w}^\top \mathbf{p}[0] \leq \bar{P}$.

1. Update power $\mathbf{p}[\ell + 1]$: $\forall k$

$$p_k[\ell + 1] = \frac{\beta_k \sigma_k}{c_{k,k}(\mathbb{U})} + \sum_{j \neq k} p_k[\ell] \log \left(1 + \frac{\beta_k p_j[\ell] c_{k,j}(\mathbb{U})}{p_k[\ell] c_{k,k}(\mathbb{U})} \right).$$

2. Normalize $\mathbf{p}[\ell + 1]$:

$$\mathbf{p}[\ell + 1] \leftarrow \frac{\bar{P}}{\mathbf{w}^\top \mathbf{p}[\ell + 1]} \mathbf{p}[\ell + 1].$$

Table 5.2: Algorithm 5.2–Decentralized algorithm to compute the optimal solution for (5.16)

- Initialize arbitrary $\mathbf{p}[0] \in \mathbb{R}_{++}^{K \times 1}$, $\mathbf{q}[0] \in \mathbb{R}_{++}^{K \times 1}$ and $\mathbf{u}_k[0] \in \mathbb{C}^{N \times 1}$ for $k = 1, \dots, K$ such that $\|\mathbf{u}_k[0]\| = 1, \forall k$, $\mathbf{w}^\top \mathbf{p}[0] \leq \bar{P}$, and $\boldsymbol{\sigma}^\top \mathbf{q}[0] \leq \bar{P}$.

1. Update dual network power $\mathbf{q}[\ell + 1]$:

$$q_k[\ell + 1] = \left(\frac{\beta_k}{\Gamma_k^{\text{DN}}(\mathbf{q}[\ell], \mathbb{U}[\ell])} \right) q_k[\ell] \quad \forall k.$$

2. Normalize $\mathbf{q}[\ell + 1]$:

$$\mathbf{q}[\ell + 1] \leftarrow \frac{\bar{P}}{\boldsymbol{\sigma}^\top \mathbf{q}[\ell + 1]} \mathbf{q}[\ell + 1].$$

3. Update transmit beamformer $\mathbb{U}[\ell + 1]$: $\forall k$

$$\mathbf{u}_k[\ell + 1] = \mathcal{P} \left\{ \left(\sum_{j \neq k} q_j[\ell + 1] \boldsymbol{\Sigma}_{j,k} + w_k \mathbf{I} \right)^{-1} \boldsymbol{\Sigma}_{k,k} \right\},$$

where $\mathcal{P}\{\cdot\}$ is the operator that computes the dominant eigenvector of a matrix.

4. Update primal network power $\mathbf{p}[\ell + 1]$:

$$p_k[\ell + 1] = \left(\frac{\beta_k}{\Gamma_k^{\text{PN}}(\mathbf{p}[\ell], \mathbb{U}[\ell + 1])} \right) p_k[\ell] \quad \forall k.$$

5. Normalize $\mathbf{p}[\ell + 1]$:

$$\mathbf{p}[\ell + 1] \leftarrow \frac{\bar{P}}{\mathbf{w}^\top \mathbf{p}[\ell + 1]} \mathbf{p}[\ell + 1].$$

Chapter 6

Efficient Algorithm Design Being Aware of Large System Structure

6.1 Introduction

To benefit from the available and increasing spatial degrees of freedom, multicell networks exploit different forms of intercell cooperation to operate the system in an interference-aware manner [83]. Due to practical constraints such as limited feedback [1] and the finite capacity of the backhaul [37], beamforming level coordination and efficient power control strategies are favored over data level cooperation and nonlinear precoding approaches [120, 124] to effectively scale up the system performance. Considering these practical constraints, two characteristics are appealing to joint beamforming and power control algorithms design: distributed computation and fast-convergent algorithms with low complexity. The desired distributed feature addresses system scalability, and the distributed algorithm only relies on local channel state information (CSI) which can be obtained by uplink measurement in a time division duplex (TDD) system or through user feedback in a frequency division duplex (FDD) system. On the other hand, simple algorithms possessing fast convergence rate are attractive in that they reduce the message passing overhead and alleviate the finite backhaul constraint.

The algorithm design is intimately related to the system performance metric

of interest. Different system performance metrics reflect different design priorities. One common approach is to maximize the sum rate of the system. However, due to the non-convexity of the problem, numerically finding the optimal solution is challenging and the design of distributed algorithms that can compute the global optimal solution efficiently is still open, e.g., see [83,155,159–161] and the references therein. It is known that two specific problem formulations admit global optimal solutions: the transmit power minimization subject to signal-to-interference-plus-noise ratio (SINR) constraints, and the maximization of minimum SINR subject to power constraints. The former problem whose priority is energy saving has been addressed extensively in the literature and efficient algorithms have been proposed for both the single cell and multicell systems [85,121,122,146,150,151,162–165]. The analysis of single cell downlink relies on the well-known uplink-downlink duality [121,122,150,164,165] which is readily interpreted by the Lagrange duality in convex optimization. In [151], the duality is observed for the MIMO multiuser ad hoc network setting, and in [85], the duality is extended to the multicell setting.

The literature for the latter problem which aims to enforce the fairness level of the system is comparatively less. The max-min SINR problem was first addressed in [166] using an extended coupling matrix approach, and a centralized algorithm was proposed in [164], which involves an increased dimension matrix computation. A reformulation of the max-min problem is analyzed in [156] by conic programming and a heuristic algorithm is provided. Recently, the problem was studied in [155] using a nonlinear Perron-Frobenius theory [149], and a distributed algorithm was proposed that exhibits the distributed power control (DPC) structure in [162]. The DPC-like structure is independent of parameter configuration, thus enabling the application of the power control module in [162] already used in practical cellular systems. The approach [155] is extended to the MIMO downlink in [167] wherein the convergence of a heuristic algorithm in [156] is proved. Herein, we extend the analysis in [155,167] to the multicell setting with multiple serving users per cell. The duality between primal and dual network is derived and characterized by the Perron-Frobenius theory. A distributed algorithm is also proposed which possesses geometrically fast convergence rate.

The designed algorithm, though converging to the optimal solution, requires instantaneous power update within the coordinated cluster through backhaul. This instantaneous information exchange may become prohibitive when the number of transmit antennas at base station as well as the serving users per cell grow large. In such emerging large-scale multiple antenna systems [168–170], the backhaul capability may turn into the bottleneck. In order to alleviate this problem and to enable simplified design that utilizes only the statistical channel information, additional tools from random matrix theory [171, 172] are to be leveraged. The large system analysis for linear receiver design in the uplink was initiated in [173], and the notion of effective interference and effective bandwidth was proposed. In [174], asymptotic analysis for the transmit power minimization problem is carried out. The approaches in [175] and [176] decouple beamforming and power control by assuming zero-forcing or regularized zero-forcing beamformers [177]. The analysis in [178] examines the max-min SINR problem from the transmit power minimization perspective, and compares several cooperation strategies by assuming a two-cell model with homogeneous channel setting. In this chapter, we perform large system analysis for the max-min SINR problem in a general multicell setting. Utilizing tools developed from random matrix theory, the deterministic equivalents [172, 179] for the dual network SINR and for the primal network SINR are established. These asymptotic approximations are used to compute the asymptotic power which only relies on statistical channel information. Intuitively, in a large-scale multiple antenna system, the optimal powers for different users would approach different deterministic values and the obtained power can be utilized for optimal beamformer design with local CSI. Moreover, by using nonlinear Perron-Frobenius theory and random matrix theory, we observe an effective network for the dual network and an effective network for the primal network, which capture the characteristic of the power control effect in the large system setting. The established effective network is further leveraged to provide a distributed algorithm with fast convergence rate.

To summarize, the contributions of this chapter are three-fold: 1) analysis and algorithm design for joint optimal beamforming and power control in a fi-

nite multicell system to maximize the minimum weighted SINR, 2) the established effective network to characterize the algebraic structure of the power control problem in the large system setting, and 3) low complexity algorithm design which requires no instantaneous backhaul exchange. All these contributions lead to efficient methodologies to design algorithms for the large-scale coordinated multicell downlink. The chapter is organized as follows. Section 6.2 presents the system model. The finite system analysis is provided in Section 6.3. Section 6.4 carries out large system analysis and derives the asymptotic solution. Numerical results are presented in Section 6.5. Finally, Section 6.6 concludes the chapter.

Notations in this chapter are presented as follows. Boldface upper-case letters denote matrices, boldface lower-case letters denote vectors, and italics denote scalars. The Perron-Frobenius eigenvalue of a nonnegative matrix \mathbf{F} is denoted as $\rho(\mathbf{F})$. Let $\mathbf{x}(\mathbf{F})$ and $\mathbf{y}(\mathbf{F})$ denote the Perron (right) and left eigenvectors of \mathbf{F} associated with $\rho(\mathbf{F})$ respectively. $\text{Tr}(\mathbf{A})$ denotes the trace of the matrix \mathbf{A} , and $\text{diag}(\mathbf{a})$ denotes the diagonal matrix having the vector \mathbf{a} on its diagonal. Let $(f(\mathbf{a}))_m$ denote the m th element of a function vector $f(\mathbf{a})$. Let $\mathbf{a} \circ \mathbf{b} \triangleq (a_1b_1, \dots, a_Mb_M)^\top$ (the Schur product). Let \mathbb{C} , \mathbb{R}_+ , and \mathbb{R}_{++} represent the set of complex numbers, the set of nonnegative real numbers, and the set of positive real numbers respectively. Let $(\cdot)^\top$ and $(\cdot)^\dagger$ denote the transpose operation and conjugate transpose operation respectively. $\|\cdot\|$ denotes the Euclidean norm for vectors and spectral norm for matrices, and $\xrightarrow{a.s.}$ denotes almost sure convergence.

6.2 System Model

Consider a coordinated multicell downlink formulated by J coordinating base stations utilizing the same carrier frequency. Each base station is equipped with N transmit antennas and serves K users simultaneously. Herein, the focus is on the base station side interference coordination, and each user is assumed to have a single antenna. The received signal $y_{j,k}$ for user k in cell j is written as

$$y_{j,k} = \sum_{l=1}^J \mathbf{h}_{l,j,k}^\dagger \mathbf{x}_l + z_{j,k} \quad (6.1)$$

where $\mathbf{h}_{l,j,k} \in \mathbb{C}^{N \times 1}$ denotes the channel vector from cell l towards user k in cell j , $\mathbf{x}_l \in \mathbb{C}^{N \times 1}$ is the transmitted signal vector of cell l , and $z_{j,k}$ characterizes the additive white noise effect and any intercell interference not included in the coordinated cluster for user k in cell j , which is distributed as $\mathcal{CN}(0, \sigma_{j,k})$ with $\sigma_{j,k} \in \mathbb{R}_{++}$.

Linear beamforming strategy is assumed at the base station, and thus the transmit signal vector \mathbf{x}_j for cell j can be expressed as $\mathbf{x}_j = \sum_{k=1}^K \mathbf{x}_{j,k} = \sum_{k=1}^K \sqrt{\frac{p_{j,k}}{N}} s_{j,k} \mathbf{u}_{j,k}$, where $\mathbf{x}_{j,k} \in \mathbb{C}^{N \times 1}$ represents the signal intended for stream k of cell j , $s_{j,k}$ and $\frac{p_{j,k}}{N}$ denote the information signal and the transmit power for that stream, and $\mathbf{u}_{j,k} \in \mathbb{C}^{N \times 1}$ denotes the normalized transmit beamformer for user k in cell j , i.e., $\|\mathbf{u}_{j,k}\|^2 = 1$. The SINR for user k in cell j can be written as

$$\Gamma_{j,k}^{\text{PN}} \triangleq \text{SINR}_{j,k}^{\text{PN}} = \frac{\frac{p_{j,k}}{N} |\mathbf{h}_{j,j,k}^\dagger \mathbf{u}_{j,k}|^2}{\sum_{(l,i) \neq (j,k)} \frac{p_{l,i}}{N} |\mathbf{h}_{l,j,k}^\dagger \mathbf{u}_{l,i}|^2 + \sigma_{j,k}} \quad (6.2)$$

where the superscript $(\cdot)^{\text{PN}}$ represents the primal downlink network. Let $w_{j,k}$ denote the weight associated with $p_{j,k}$ for user k in cell j illustrating different power prices, and denote $\beta_{j,k}$ as the priority factor associated with $\Gamma_{j,k}^{\text{PN}}$ for user k in cell j demonstrating diverse service priorities. Then the max-min problem under weighted sum power constraint¹ can be written as follows

$$\begin{aligned} & \text{maximize} && \min_{j,k} \frac{\Gamma_{j,k}^{\text{PN}}}{\beta_{j,k}} \\ & \text{subject to} && \sum_{j,k} w_{j,k} \frac{p_{j,k}}{N} \leq \bar{P}, \quad p_{j,k} > 0, \quad \|\mathbf{u}_{j,k}\|^2 = 1 \\ & \text{variables :} && p_{j,k}, \mathbf{u}_{j,k}. \end{aligned} \quad (6.3)$$

The problem (6.3) appears non-convex at first, but can be transformed into a second-order cone program [60] by applying methods similar to that in [156], which admits a global optimal solution. However, employing standard convex optimization methods to find the optimal solution typically requires centralized computation and incurs a fair amount of parameter tuning and message passing overhead that may not be practical in wireless networks. Thus in Section 6.3, we will employ

¹The weighted sum power constraint implies that multiple base stations form a coordinated cluster to jointly perform power control in order to achieve the desired fairness level for users in the cluster.

nonlinear Perron-Frobenius theory to propose DPC-like algorithm [162] that does not require parameter tuning and has geometrically-fast convergence rate. Then in Section 6.4, algorithms that are even simpler and more practical for systems with a large number of transmit antennas and users will be presented by performing an asymptotic analysis.

6.3 Finite System Analysis

This section is devoted to finite system analysis when N and K are not asymptotically large. Section 6.3.1 reformulates problem (6.3) to exploit its analytic structure. Section 6.3.2 establishes the network duality via a Perron-Frobenius characterization, and provides a geometrically-fast convergent algorithm to compute the optimal solution.

6.3.1 Problem Reformulation

The problem formulation in (6.3) essentially regards an interference network with JK users. However, the formulation in terms of the channel $\mathbf{h}_{l,j,k}$ and the link gain $|\mathbf{h}_{l,j,k}^\dagger \mathbf{u}_{l,i}|^2$ does not easily lead to amenable analysis. In order to construct the $JK \times JK$ cross channel interference matrix, consider the matrix $\mathbf{G} \in \mathbb{R}_{++}^{JK \times JK}$ with subscripts m and n , whose entry can be written as

$$G_{m,n} = |\mathbf{h}_{\lceil \frac{n}{K} \rceil, \lceil \frac{m}{K} \rceil, m-K \lfloor \frac{m}{K} \rfloor}^\dagger \mathbf{u}_{\lceil \frac{n}{K} \rceil, n-K \lfloor \frac{n}{K} \rfloor}|^2 \quad (6.4)$$

where $\lceil \cdot \rceil$ and $\lfloor \cdot \rfloor$ denote the ceil and floor operation respectively. Thus the channel $\mathbf{h}_{l,j,k}$ can be represented with subscripts m and n : $\mathbf{h}_{m,n} \triangleq \mathbf{h}_{\lceil \frac{n}{K} \rceil, \lceil \frac{m}{K} \rceil, m-K \lfloor \frac{m}{K} \rfloor}$. Moreover, define the power vector $\mathbf{p} \in \mathbb{R}_{++}^{JK \times 1}$ as $p_m \triangleq p_{\lceil \frac{m}{K} \rceil, m-K \lfloor \frac{m}{K} \rfloor}$, and the beamforming matrix as $\mathbb{U} \triangleq (\mathbf{u}_1, \dots, \mathbf{u}_{JK})$ with $\mathbf{u}_m \triangleq \mathbf{u}_{\lceil \frac{m}{K} \rceil, m-K \lfloor \frac{m}{K} \rfloor}$. The general formulation in (6.4) can be easily interpreted through two special cases: a) $J = 1$, K arbitrary and b) $K = 1$, J arbitrary. The former case refers to a single cell downlink with K interfering users, while the latter case corresponds to an ad hoc interference network setting with J transmitter-receiver pairs or a multicell setting with one user served per cell. By the formulation of \mathbf{G} , the cross channel

interference matrix, denoted by $\mathbf{F} \in \mathbb{R}_+^{JK \times JK}$ can be obtained by

$$F_{m,n} = \begin{cases} 0, & \text{if } m = n \\ G_{m,n}, & \text{if } m \neq n. \end{cases} \quad (6.5)$$

Similarly, the weight vector $\mathbf{w} \in \mathbb{R}_+^{JK \times 1}$, the priority vector $\boldsymbol{\beta} \in \mathbb{R}_+^{JK \times 1}$, and the noise vector $\boldsymbol{\sigma} \in \mathbb{R}_+^{JK \times 1}$ can be defined by: $w_m \triangleq w_{\lceil \frac{m}{K} \rceil, m-K \lfloor \frac{m}{K} \rfloor}$, $\beta_m \triangleq \beta_{\lceil \frac{m}{K} \rceil, m-K \lfloor \frac{m}{K} \rfloor}$, and $\sigma_m \triangleq \sigma_{\lceil \frac{m}{K} \rceil, m-K \lfloor \frac{m}{K} \rfloor}$. From the aforementioned mapping, if we denote the SINR vector as $\boldsymbol{\Gamma}^{\text{PN}} \in \mathbb{R}_+^{JK \times 1}$ with $\Gamma_m^{\text{PN}} \triangleq \Gamma_{\lceil \frac{m}{K} \rceil, m-K \lfloor \frac{m}{K} \rfloor}^{\text{PN}}$, and the auxiliary vector $\mathbf{g} \in \mathbb{R}_+^{JK \times 1}$ with $\mathbf{g} \triangleq \left(\frac{1}{G_{1,1}}, \dots, \frac{1}{G_{JK,JK}} \right)^\top$, then the optimization problem (6.3) can be readily reformulated as follows:

$$\begin{aligned} & \text{maximize} && \min_m \frac{\Gamma_m^{\text{PN}}(\mathbf{p}, \mathbb{U})}{\beta_m} = \frac{\frac{1}{N} p_m}{\left(\text{diag}(\boldsymbol{\beta} \circ \mathbf{g}) \left(\frac{1}{N} \mathbf{F} \mathbf{p} + \boldsymbol{\sigma} \right) \right)_m} \\ & \text{subject to} && \frac{1}{N} \mathbf{w}^\top \mathbf{p} \leq \bar{P}, \quad \mathbf{p} > 0, \quad \|\mathbf{u}_m\|^2 = 1 \\ & \text{variables :} && \mathbf{p}, \mathbb{U}. \end{aligned} \quad (6.6)$$

It can be shown that solving (6.6) is equivalent to solving (6.3). The compact formulation in (6.6) introduces a nonnegative matrix $\text{diag}(\boldsymbol{\beta} \circ \mathbf{g}) (\mathbf{F} + (1/\bar{P}) \boldsymbol{\sigma} \mathbf{w}^\top)$, whose algebraic structure helps in establishing the network duality and is pursued next.

6.3.2 Network Duality and Algorithm Design

The analytic structure in (6.6) is similar to the formulation in [167] for the single cell multiuser downlink scenario. In [167], the uplink-downlink duality is proved by a geometric programming formulation and the Lagrange duality. Herein, we provide a network duality interpretation for the max-min based multi-cell scenario via Perron-Frobenius characterization.

For any given beamforming matrix \mathbb{U} , a simpler optimization problem for (6.6) can be formulated by only optimizing the power solution. It is known that at optimality, the weighted SINR for different users are the same, and the weighted power constraint becomes tight [155]. Now if we explicitly make the dependence on \mathbb{U} and denote the optimal weighted SINR as $\tau^*(\mathbb{U})$, then the optimal power

solution satisfies [155, 167]:

$$\frac{1}{\tau^*(\mathbb{U})} \frac{\mathbf{p}^*(\mathbb{U})}{N} = \text{diag}(\boldsymbol{\beta} \circ \mathbf{g}(\mathbb{U})) (\mathbf{F}(\mathbb{U}) + (1/\bar{P})\boldsymbol{\sigma}\mathbf{w}^\top) \frac{\mathbf{p}^*(\mathbb{U})}{N}. \quad (6.7)$$

From (6.7), it can be shown from nonnegative matrix theory [180] that $\frac{\mathbf{p}^*(\mathbb{U})}{N}$ is the Perron (right) eigenvector (up to a scaling factor) of the nonnegative matrix $\text{diag}(\boldsymbol{\beta} \circ \mathbf{g}(\mathbb{U})) (\mathbf{F}(\mathbb{U}) + (1/\bar{P})\boldsymbol{\sigma}\mathbf{w}^\top)$, namely, $\frac{\mathbf{p}^*(\mathbb{U})}{N} = \frac{N\bar{P}\mathbf{x}(\text{diag}(\boldsymbol{\beta} \circ \mathbf{g}(\mathbb{U}))(\mathbf{F}(\mathbb{U}) + (1/\bar{P})\boldsymbol{\sigma}\mathbf{w}^\top))}{\mathbf{w}^\top \mathbf{x}(\text{diag}(\boldsymbol{\beta} \circ \mathbf{g}(\mathbb{U}))(\mathbf{F}(\mathbb{U}) + (1/\bar{P})\boldsymbol{\sigma}\mathbf{w}^\top))}$, and $\tau^*(\mathbb{U})$ is related to its spectral radius by the following:

$$\tau^*(\mathbb{U}) = \frac{1}{\rho(\text{diag}(\boldsymbol{\beta} \circ \mathbf{g}(\mathbb{U})) (\mathbf{F}(\mathbb{U}) + (1/\bar{P})\boldsymbol{\sigma}\mathbf{w}^\top))}. \quad (6.8)$$

Now, in order to establish the network duality, consider the hypothesized dual uplink network by construction. Denote the dual network transmit power solution $\mathbf{q} \in \mathbb{R}_{++}^{JK \times 1}$ as $q_m \triangleq q_{\lceil \frac{m}{K} \rceil, m - K \lfloor \frac{m}{K} \rfloor}$, where $\frac{q_{j,k}}{N}$ with subscripts j and k denotes the reciprocal uplink transmit power for user k in cell j . Let the weight vector \mathbf{w} in the primal network be the noise vector in the dual network, and conversely let the noise vector $\boldsymbol{\sigma}$ in the primal network be the weight vector in the dual network. Then the max-min problem for the dual network given receive beamforming matrix \mathbb{U} can be formulated as

$$\begin{aligned} & \text{maximize} \quad \min_m \frac{\Gamma_m^{\text{DN}}(\mathbf{q}, \mathbb{U})}{\beta_m} = \frac{\frac{1}{N} q_m(\mathbb{U})}{\left(\text{diag}(\boldsymbol{\beta} \circ \mathbf{g}(\mathbb{U})) \left(\frac{1}{N} \mathbf{F}^\top(\mathbb{U}) \mathbf{q}(\mathbb{U}) + \mathbf{w} \right) \right)_m} \\ & \text{subject to} \quad \frac{1}{N} \boldsymbol{\sigma}^\top \mathbf{q}(\mathbb{U}) \leq \bar{P}, \quad \mathbf{q}(\mathbb{U}) > 0 \\ & \text{variables :} \quad \mathbf{q}(\mathbb{U}) \end{aligned} \quad (6.9)$$

where the superscript $(\cdot)^{\text{DN}}$ denotes the dual uplink network. By leveraging the following properties of nonnegative matrices [180]: $\rho(\mathbf{A}) = \rho(\mathbf{A}^\top)$ and $\rho(\mathbf{A}\mathbf{B}) = \rho(\mathbf{B}\mathbf{A})$, the optimal solution for (6.9) equals $\frac{1}{\rho(\text{diag}(\boldsymbol{\beta} \circ \mathbf{g}(\mathbb{U})) (\mathbf{F}^\top(\mathbb{U}) + (1/\bar{P})\boldsymbol{\sigma}\mathbf{w}^\top))}$. Comparing with the optimal solution for the primal network in (6.8), the network duality is observed by employing \mathbf{F}^\top as the cross channel interference matrix for the dual network and reversing the role of \mathbf{w} and $\boldsymbol{\sigma}$. Thus the optimal power solution given \mathbb{U} is the left eigenvector of the nonnegative matrix $\text{diag}(\boldsymbol{\beta} \circ \mathbf{g}(\mathbb{U})) (\mathbf{F}(\mathbb{U}) + (1/\bar{P})\boldsymbol{\sigma}\mathbf{w}^\top)$, namely, $\frac{\mathbf{q}^*(\mathbb{U})}{N} = \frac{N\bar{P}\mathbf{y}(\text{diag}(\boldsymbol{\beta} \circ \mathbf{g}(\mathbb{U}))(\mathbf{F}(\mathbb{U}) + (1/\bar{P})\boldsymbol{\sigma}\mathbf{w}^\top))}{\boldsymbol{\sigma}^\top \mathbf{y}(\text{diag}(\boldsymbol{\beta} \circ \mathbf{g}(\mathbb{U}))(\mathbf{F}(\mathbb{U}) + (1/\bar{P})\boldsymbol{\sigma}\mathbf{w}^\top))}$. Note that since the network duality holds for any given \mathbb{U} , the achievable SINR regions of the max-min problem are the same for both the primal network and the dual network.

The motivation for establishing the dual network is to exploit the decoupled property of the receive beamformer optimization and to utilize the optimized received beamformer as the optimal transmit beamformer for each user. The optimal beamforming matrix \mathbb{U}^* depends on the power vector \mathbf{q} , and for any given \mathbf{q} , the optimal beamformer $\mathbf{u}_m^*(\mathbf{q})$ can be obtained by

$$\mathbf{u}_m^*(\mathbf{q}) = \arg \min_{\mathbf{u}_m} \frac{\mathbf{u}_m^\dagger (\sum_{n \neq m} \frac{q_n}{N} \mathbf{h}_{m,n} \mathbf{h}_{m,n}^\dagger + w_m \mathbf{I}) \mathbf{u}_m}{\mathbf{u}_m^\dagger \mathbf{h}_{m,m} \mathbf{h}_{m,m}^\dagger \mathbf{u}_m} \quad (6.10)$$

which can be readily solved and is known to be the minimum variance distortionless response (MVDR) beamformer which is given by:

$$\mathbf{u}_m^*(\mathbf{q}) = \frac{(\sum_{n \neq m} \frac{q_n}{N} \mathbf{h}_{m,n} \mathbf{h}_{m,n}^\dagger + w_m \mathbf{I})^{-1} \mathbf{h}_{m,m}}{\|(\sum_{n \neq m} \frac{q_n}{N} \mathbf{h}_{m,n} \mathbf{h}_{m,n}^\dagger + w_m \mathbf{I})^{-1} \mathbf{h}_{m,m}\|}. \quad (6.11)$$

Therefore, the optimal solution for the beamformers, the power of the dual network, and the power of the primal network can be written as: $\mathbf{u}_m^* = \mathbf{u}_m^*(\mathbf{q}^*)$, $\mathbf{q}^* = \mathbf{q}^*(\mathbb{U}^*)$, and $\mathbf{p}^* = \mathbf{p}^*(\mathbb{U}^*)$. The optimal solution is of analytical interest. In order to derive a fast algorithm to compute the optimal solution in a distributed manner, we employ nonlinear Perron-Frobenius theory and propose the algorithm given in Table 6.1, referred to as *Algorithm 6.1* for the multicell scenario. It exhibits the DPC-like structure as in [155, 167] for the single cell scenario. The convergence property of *Algorithm 6.1* is discussed in the following theorem.

Theorem 6.1. *Starting from any initial point $\mathbf{q}[0]$, $\mathbf{p}[0]$, and $\mathbb{U}[0]$, the $\mathbf{q}[\kappa]$, $\mathbf{p}[\kappa]$, and $\mathbb{U}[\kappa]$ in *Algorithm 6.1* converges geometrically fast to the optimal solution \mathbf{q}^* , \mathbf{p}^* , and \mathbb{U}^* .*

Proof. The proof is given in Appendix J. □

Remark: Distributed algorithms utilizing only local CSI and requiring limited backhaul exchange are important for practical implementation issues. *Algorithm 6.1* is distributed in the sense that the iterative update (step 1, 3, 4 of *Algorithm 6.1*) can be independently performed for each individual user at each base station. In addition, each base station only employs local CSI, which can be directly obtained in a TDD system or acquired by user feedback in a FDD

system. The normalization procedure (step 2 and 5 of *Algorithm 6.1*), however, requires a central computation of $\mathbf{w}^\top \mathbf{p}[\kappa]$ and $\boldsymbol{\sigma}^\top \mathbf{q}[\kappa]$. This procedure can be made distributed by gossip algorithms [181] and power update through the backhaul.

Hitherto, an algorithm for computing the optimal solution to (6.3) is established. In Section 6.5, we provide numerical results that support and confirm its fast convergence property. Furthermore, with minimal parameter exchange and configuration, this algorithm is practical in a finite system. However, in a large-scale system when both N and K become large, the instantaneous power update across the coordinated cluster limits its practical implementation. Therefore, a lower complexity algorithm is needed in large-scale systems and is studied next in Section 6.4.

6.4 Large System Analysis

This section is devoted to a large system analysis² when both the number of transmit antennas N and the number of serving users per cell K go to infinity while the ratio (load factor) $\lim \frac{K}{N}$ remains bounded, i.e., the notation $N \rightarrow \infty$ denotes that both N and K become large, while $\liminf \frac{K}{N} > 0$ and $\limsup \frac{K}{N} < \infty$. In this large-scale system setting, for a given channel realization, the amount of instantaneous power update through the limited backhaul can be impractically large and thus impacts the system performance. A key question is whether it is possible to design a non-iterative algorithm to compute the beamformer and still achieve some form of optimal egalitarian fairness. Herein, the optimality is in the asymptotic sense. This means that, if the power \mathbf{p} and \mathbf{q} in the large system converge to some deterministic values that only rely on statistical channel information, then these deterministic values can be a priori calculated, stored, and updated only when the channel statistics change. Thereafter, the beamforming matrix ought to be non-iteratively computed using these slowly updated power values and the available instantaneous local CSI.

This idea of practical implementation for large systems will be studied by

²The large system analysis for a single cell downlink is examined in [182].

addressing two problems related to (6.3). Firstly, different users in the multicell network have potentially different weights, different priorities, different noise powers, and more importantly, different large-scale channel effects which may consist of path loss, shadowing, and antenna gain. Thus, to maintain the max-min fairness across users, the powers for different users would converge to different deterministic values in the large system setting. One key issue is to establish the asymptotic optimality for both the dual network power \mathbf{q} and primal network power \mathbf{p} . Another key issue is to design distributed algorithm to compute these deterministic values.

In Section 6.3, no specific channel models are assumed. Now for amenable analysis, the transformed notation using subscripts m and n will be still employed and the following channel model is further assumed:

$$\mathbf{h}_{m,n} = \sqrt{d_{m,n}} \tilde{\mathbf{h}}_{m,n} \quad (6.12)$$

where $d_{m,n}$ represents the large-scale channel effect and illustrates the statistical channel information. The $\tilde{\mathbf{h}}_{m,n}$ denotes the normalized CSI whose elements are independent and identically distributed as $\mathcal{CN}(0, 1)$. This assumption corresponds to the practical setting where the antenna elements equipped at each base station are placed sufficiently apart. Herein, independent channel assumption is employed and the analysis with the general correlated channel model [183–187] is left for future work. Employing this channel model, the asymptotic analysis for the dual network and primal network is carried out in Section 6.4.1 and Section 6.4.2, respectively.

6.4.1 Asymptotic Analysis for the Dual Network

The large system analysis for the dual network is examined first to derive the asymptotic dual network power, which is utilized for beamformer design. One key step is to study the asymptotic behavior of the dual network SINR, whose

expression is given by using the optimal MVDR beamformer as follows:

$$\begin{aligned}\Gamma_m^{\text{DN}}(\mathbf{q}) &= \frac{q_m}{N} \mathbf{h}_{m,m}^\dagger \left(\sum_{n \neq m} \frac{q_n}{N} \mathbf{h}_{m,n} \mathbf{h}_{m,n}^\dagger + w_m \mathbf{I} \right)^{-1} \mathbf{h}_{m,m} \\ &= \frac{q_m d_{m,m}}{N} \tilde{\mathbf{h}}_{m,m}^\dagger \left(\sum_{n \neq m} \frac{q_n d_{m,n}}{N} \tilde{\mathbf{h}}_{m,n} \tilde{\mathbf{h}}_{m,n}^\dagger + w_m \mathbf{I} \right)^{-1} \tilde{\mathbf{h}}_{m,m} \quad \forall m.\end{aligned}\quad (6.13)$$

Since each instantaneous CSI is random, the instantaneous SINR in (6.13) is a random variable in quadratic form. Moreover, since the dual network power and large scale channel effects are diverse across users, if we define the random matrix $\tilde{\mathbf{H}}_m$ as $\tilde{\mathbf{H}}_m \tilde{\mathbf{H}}_m^\dagger \triangleq \sum_{n \neq m} \frac{q_n d_{m,n}}{N} \tilde{\mathbf{h}}_{m,n} \tilde{\mathbf{h}}_{m,n}^\dagger$, then the random matrix $\tilde{\mathbf{H}}_m$ possesses a variance profile [179, 188]. The asymptotic approximation for $\Gamma_m^{\text{DN}}(\mathbf{q})$ is given in the following lemma.

Lemma 6.1. *The instantaneous random variable $\Gamma_m^{\text{DN}}(\mathbf{q})$ can be approximated by a deterministic quantity³ $\gamma_m^{\text{DN}}(\mathbf{q})$ such that $\Gamma_m^{\text{DN}}(\mathbf{q}) - \gamma_m^{\text{DN}}(\mathbf{q}) \xrightarrow{a.s.} 0$ as the system dimension $N \rightarrow \infty$. Also, $\gamma_m^{\text{DN}}(\mathbf{q})$ is described by the following fixed-point equation:*

$$\gamma_m^{\text{DN}}(\mathbf{q}) = \frac{q_m d_{m,m}}{w_m + \frac{1}{N} \sum_{n \neq m} \frac{q_n q_m d_{m,n} d_{m,m}}{q_m d_{m,m} + q_n d_{m,n} \gamma_m^{\text{DN}}(\mathbf{q})}} \quad \forall m.\quad (6.14)$$

Proof. The proof is given in Appendix K. □

From Lemma 6.1, we know that $\gamma_m^{\text{DN}}(\mathbf{q})$ becomes more accurate when increasing the system dimension, and is asymptotically tight for $\Gamma_m^{\text{DN}}(\mathbf{q})$. For further analysis, an auxiliary vector $\phi \in \mathbb{R}_{++}^{JK \times 1}$ is defined with $\phi_m(\mathbf{q}) \triangleq \frac{\gamma_m^{\text{DN}}(\mathbf{q})}{q_m d_{m,m}}$, $\forall m$. Then from Lemma 6.1, the fixed-point equation for $\phi_m(\mathbf{q})$ can be written as

$$\phi_m(\mathbf{q}) = \frac{1}{w_m + \frac{1}{N} \sum_{n \neq m} \frac{q_n d_{m,n}}{1 + q_n d_{m,n} \phi_m(\mathbf{q})}} \quad \forall m.\quad (6.15)$$

From (6.15), it is easy to see that \mathbf{q} and ϕ are coupled and their relationship only depends on the statistical channel information reflected in $d_{m,n}$. Designing

³Note that we present the asymptotic behavior of $\Gamma_m^{\text{DN}}(\mathbf{q})$ with a given power vector \mathbf{q} , not with the instantaneous optimal power vector \mathbf{q}^* . The instantaneous optimal power vector is a function of channel and thus complicates standard large system analysis. Bounding techniques trying to investigate this issue are conducted in [178]. In this chapter, iterative method is used to compute the asymptotically optimal power. This comment carries over to the following lemmas.

algorithms to compute \mathbf{q} and $\phi(\mathbf{q})$ is of primary interest and one common approach is to examine the conditional convergence property of \mathbf{q} and ϕ separately.

The convergence property of ϕ given \mathbf{q} is relatively easy to establish since it does not involve any constraint. Given any $\hat{\mathbf{q}}$ satisfying the dual network power constraint, the algorithm to compute the corresponding $\hat{\phi}(\hat{\mathbf{q}})$ is given in Table 6.2 and is referred to as *Algorithm 6.2* whose convergence property is given below.

Lemma 6.2. *For a given $\hat{\mathbf{q}}$, starting from any initial $\hat{\phi}[0]$, the $\hat{\phi}[\ell]$ in Algorithm 6.2 converges to the unique solution⁴ of the fixed-point equation (6.15).*

Proof. The proof is given in Appendix K. □

Now consider the convergence property of \mathbf{q} given ϕ . Combining (6.14) and (6.15) yields the equivalent fixed-point equation for $\gamma_m^{\text{DN}}(\mathbf{q}) = \frac{q_m d_{m,m}}{w_m + \frac{1}{N} \sum_{n \neq m} \frac{q_n d_{m,n}}{1 + q_n d_{m,n} \phi_m(\mathbf{q})}}$.

Thus the additive effect of $\frac{1}{N} \sum_{n \neq m} \frac{q_n d_{m,n}}{1 + q_n d_{m,n} \phi_m(\mathbf{q})}$ can be seen as the asymptotically equivalent interference and is regarded as effective interference in [173]. In the sequel, we construct the *effective dual network* to draw further insight for the power control problem.

Firstly, the following power control problem conditioned on $\hat{\phi}$ is constructed by considering the weighted power constraint:

$$\begin{aligned} & \text{maximize} && \min_m \frac{\hat{q}_m d_{m,m}}{\beta_m \left(w_m + \frac{1}{N} \sum_{n \neq m} \frac{\hat{q}_n d_{m,n}}{1 + \hat{q}_n d_{m,n} \hat{\phi}_m} \right)} \\ & \text{subject to} && \frac{1}{N} \boldsymbol{\sigma}^\top \hat{\mathbf{q}} \leq \bar{P}, \quad \hat{\mathbf{q}} > 0 \\ & \text{variables :} && \hat{\mathbf{q}}. \end{aligned} \tag{6.16}$$

Then, by defining the vector $\mathbf{e}^{\text{DN}} \triangleq \left(\frac{1}{d_{1,1}}, \dots, \frac{1}{d_{JK,JK}} \right)^\top$ and the nonnegative matrix $\mathbf{E}^{\text{DN}}(\hat{\mathbf{q}})$ as

$$E_{m,n}^{\text{DN}}(\hat{\mathbf{q}}) = \begin{cases} 0, & \text{if } m = n \\ \frac{d_{m,n}}{1 + \hat{q}_n d_{m,n} \hat{\phi}_m}, & \text{if } m \neq n \end{cases} \tag{6.17}$$

⁴The existence of the solution can be shown by employing the same method as in the proof of Theorem 6.1 in [172] and the proof of Theorem 1 in [186].

the objective function in (6.16) can be expressed compactly as the following: $\frac{\hat{q}_m}{(\text{diag}(\boldsymbol{\beta} \circ \mathbf{e}^{\text{DN}}) (\frac{1}{N} \mathbf{E}^{\text{DN}}(\hat{\mathbf{q}}) \hat{\mathbf{q}} + \mathbf{w}))_m}$, whose algebraic structure leads to the following eigenvalue problem in terms of the power $\hat{\mathbf{q}}^*$ and weighted asymptotic SINR ζ^* :

$$\frac{\hat{\mathbf{q}}^*}{\zeta^*} = \text{diag}(\boldsymbol{\beta} \circ \mathbf{e}^{\text{DN}}) (\mathbf{E}^{\text{DN}}(\hat{\mathbf{q}}^*) + (1/\bar{P}) \mathbf{w} \boldsymbol{\sigma}^T) \frac{\hat{\mathbf{q}}^*}{N}. \quad (6.18)$$

By comparing with (6.7), we can see that $\mathbf{E}^{\text{DN}}(\hat{\mathbf{q}})$ can be regarded as the effective cross channel interference matrix and the effective dual network can be characterized by the nonnegative matrix $\text{diag}(\boldsymbol{\beta} \circ \mathbf{e}^{\text{DN}}) (\mathbf{E}^{\text{DN}}(\hat{\mathbf{q}}) + (1/\bar{P}) \mathbf{w} \boldsymbol{\sigma}^T)$. Note that in the finite system setting, the cross channel interference matrix \mathbf{F} is independent of the power. However, for the large system setting, $\mathbf{E}^{\text{DN}}(\hat{\mathbf{q}})$ and $\hat{\mathbf{q}}$ are interdependent. In the following, we employ nonlinear Perron-Frobenius theory to propose a distributed algorithm to compute $\hat{\mathbf{q}}^*$ given $\hat{\boldsymbol{\phi}}$, which is given in Table 6.3 and is referred to as *Algorithm 6.3*.

Theorem 6.2. *For a given $\hat{\boldsymbol{\phi}}$, starting from any initial $\hat{\mathbf{q}}[0]$, the $\hat{\mathbf{q}}[\ell]$ in Algorithm 6.3 converges geometrically fast to the optimal solution $\hat{\mathbf{q}}^*(\hat{\boldsymbol{\phi}})$ of (6.16).*

Proof. The proof is given in Appendix J. □

After establishing the convergence properties of computing $\hat{\boldsymbol{\phi}}(\hat{\mathbf{q}})$ in *Algorithm 6.2* and $\hat{\mathbf{q}}^*(\hat{\boldsymbol{\phi}})$ in *Algorithm 6.3*, both *Algorithm 6.2* and *Algorithm 6.3* can be combined using alternate optimization to compute an asymptotically local optimal solution $\boldsymbol{\phi}(\hat{\mathbf{q}}^*)$ and $\hat{\mathbf{q}}^*$. The asymptotically optimal dual network power is used to design the asymptotically optimal beamformer in (6.11). The procedure to derive the asymptotically optimal primal network power requires $\hat{\mathbf{q}}^*$ and $\boldsymbol{\phi}(\hat{\mathbf{q}}^*)$, and is pursued next.

6.4.2 Asymptotic Analysis for the Primal Network

Similar procedure for analyzing the dual network can be applied to the primal network in order to examine the asymptotically optimal transmit power $\hat{\mathbf{p}}^*$. From the analysis in Section 6.3, the primal network SINR is given as

$$\Gamma_m^{\text{PN}}(\mathbf{p}) = \frac{\frac{p_m d_{m,m}}{N} |\tilde{\mathbf{h}}_{m,m}^\dagger \mathbf{u}_m^*|^2}{\sum_{n \neq m} \frac{p_n d_{m,n}}{N} |\tilde{\mathbf{h}}_{m,n}^\dagger \mathbf{u}_n^*|^2 + \sigma_m}. \quad (6.19)$$

The asymptotic approximation of $\Gamma_m^{\text{PN}}(\mathbf{p})$ is presented in the following lemma.

Lemma 6.3. *The instantaneous random variable $\Gamma_m^{\text{PN}}(\mathbf{p})$ can be approximated by a deterministic quantity $\gamma_m^{\text{PN}}(\mathbf{p})$ such that $\Gamma_m^{\text{PN}}(\mathbf{p}) - \gamma_m^{\text{PN}}(\mathbf{p}) \xrightarrow{a.s.} 0$ as the system dimension $N \rightarrow \infty$. Also, $\gamma_m^{\text{PN}}(\mathbf{p})$ is described by the following fixed-point equation:*

$$\gamma_m^{\text{PN}}(\mathbf{p}) = \frac{p_m d_{m,m} \frac{\phi_m^2(\mathbf{q})}{-\phi'_m(\mathbf{q})}}{\sigma_m + \frac{1}{N} \sum_{n \neq m} \frac{p_n d_{m,n} \phi'_m(\mathbf{q})}{(1+q_m d_{m,m} \phi_m(\mathbf{q}))^2 \phi'_n(\mathbf{q})}} \quad \forall m \quad (6.20)$$

$$\text{where } \phi'_m(\mathbf{q}) = \frac{-\phi_m(\mathbf{q})}{w_m + \frac{1}{N} \sum_{n \neq m} \frac{q_n d_{m,n}}{(1+q_n d_{m,n} \phi_m(\mathbf{q}))^2}} \quad \forall m.$$

Proof. The proof is given in Appendix K. \square

We can see from (6.20) that the effective interference in the primal network equals the following: $\frac{1}{N} \sum_{n \neq m} \frac{p_n d_{m,n} \phi'_m(\mathbf{q})}{(1+q_m d_{m,m} \phi_m(\mathbf{q}))^2 \phi'_n(\mathbf{q})}$. In order to establish the *effective primal network*, we consider the following constructed power control problem conditioned on $\hat{\mathbf{q}}$ and $\hat{\phi}$:

$$\begin{aligned} & \text{maximize} \quad \min_m \frac{\hat{p}_m d_{m,m} \frac{\hat{\phi}_m^2}{-\hat{\phi}'_m}}{\beta_m \left(\sigma_m + \frac{1}{N} \sum_{n \neq m} \frac{\hat{p}_n d_{m,n} \hat{\phi}'_m}{(1+\hat{q}_m d_{m,m} \hat{\phi}_m)^2 \hat{\phi}'_n} \right)} \\ & \text{subject to} \quad \frac{1}{N} \mathbf{w}^T \hat{\mathbf{p}} \leq \bar{P}, \quad \hat{\mathbf{p}} > 0 \\ & \text{variables :} \quad \hat{\mathbf{p}}. \end{aligned} \quad (6.21)$$

Then, by defining the vector $\mathbf{e}^{\text{PN}} \triangleq \left(\frac{-\hat{\phi}'_1}{d_{1,1} \hat{\phi}_1^2}, \dots, \frac{-\hat{\phi}'_{JK}}{d_{JK,JK} \hat{\phi}_{JK}^2} \right)^T$ and the nonnegative matrix \mathbf{E}^{PN} as

$$E_{m,n}^{\text{PN}} = \begin{cases} 0, & \text{if } m = n \\ \frac{d_{m,n} \hat{\phi}'_m}{(1+\hat{q}_m d_{m,m} \hat{\phi}_m)^2 \hat{\phi}'_n}, & \text{if } m \neq n \end{cases} \quad (6.22)$$

the objective function in (6.21) can be expressed compactly as the following:

$\frac{\hat{p}_m}{\left(\text{diag}(\beta \circ \mathbf{e}^{\text{PN}}) \left(\frac{1}{N} \mathbf{E}^{\text{PN}} \hat{\mathbf{p}} + \sigma \right) \right)_m}$, whose algebraic structure leads to the following eigenvalue problem in terms of the power $\hat{\mathbf{p}}^*$ and weighted asymptotic SINR ζ^* :

$$\frac{\hat{\mathbf{p}}^*}{\zeta^*} = \text{diag}(\beta \circ \mathbf{e}^{\text{PN}}) \left(\mathbf{E}^{\text{PN}} + (1/\bar{P}) \sigma \mathbf{w}^T \right) \hat{\mathbf{p}}^*. \quad (6.23)$$

By comparing with (6.7), we can see that \mathbf{E}^{PN} can be regarded as the effective cross channel interference matrix and the effective primal network can be characterized

by the nonnegative matrix $\text{diag}(\boldsymbol{\beta} \circ \mathbf{e}^{\text{PN}}) (\mathbf{E}^{\text{PN}} + (1/\bar{P})\boldsymbol{\sigma}\mathbf{w}^{\text{T}})$. Compared with the effective dual network, \mathbf{E}^{PN} is not dependent on $\hat{\mathbf{p}}$. In the following, we employ Perron-Frobenius theory to propose a distributed algorithm to compute $\hat{\mathbf{p}}^*$ given $\hat{\mathbf{q}}$ and $\hat{\boldsymbol{\phi}}$, which is given in Table 6.4 and is referred to as *Algorithm 6.4*.

Theorem 6.3. *For given $\hat{\mathbf{q}}$ and $\hat{\boldsymbol{\phi}}$, starting from any initial $\hat{\mathbf{p}}[0]$, the $\hat{\mathbf{p}}[\ell]$ in *Algorithm 6.4* converges geometrically fast to the optimal solution $\hat{\mathbf{p}}^*(\hat{\mathbf{q}}, \hat{\boldsymbol{\phi}})$ of (6.21).*

Proof. The proof is given in Appendix J. □

Now, by combining *Algorithm 6.2*, *Algorithm 6.3*, and *Algorithm 6.4* that have respectively treated $\hat{\boldsymbol{\phi}}$, $\hat{\mathbf{q}}$ and $\hat{\mathbf{p}}$ separately, a single timescale algorithm is given in Table 6.5 and is referred to as *Algorithm 6.5*. Even though this algorithm that computes the asymptotic power is iterative, it only requires statistical channel information and thus the asymptotic power is updated at a slower timescale. Then for each instantaneous time, the asymptotic primal network power $\hat{\mathbf{p}}^*$ is used for the downlink transmission, and the asymptotic dual network power $\hat{\mathbf{q}}^*$ is employed to non-iteratively obtain the instantaneous beamforming matrix $\hat{\mathbf{U}}^*$ with local CSI as $\hat{\mathbf{u}}_m^*(\hat{\mathbf{q}}^*) = \frac{(\sum_{n \neq m} \frac{\hat{q}_n^*}{N} \mathbf{h}_{m,n} \mathbf{h}_{m,n}^\dagger + w_m \mathbf{I})^{-1} \mathbf{h}_{m,m}}{\|(\sum_{n \neq m} \frac{\hat{q}_n^*}{N} \mathbf{h}_{m,n} \mathbf{h}_{m,n}^\dagger + w_m \mathbf{I})^{-1} \mathbf{h}_{m,m}\|}$. In this way, by leveraging the asymptotic property in the large scale system, no instantaneous power update is required in the coordinated cluster to jointly optimize power control and beamformer.

Discussion of Complexity: It is important to note that even though *Algorithm 6.1* and *Algorithm 6.5* are both discrete time algorithms, their operating timescales as well as the implementation complexities are vastly different (we use indices κ and ℓ to differentiate them). In *Algorithm 6.1*, the power update is on the order of milliseconds to track the instantaneous channel effect. Thus, this algorithm requires a large amount of instantaneous power update to compute the optimal solution. In contrast, the power update in *Algorithm 6.5* relies only on statistical channel information. Therefore, this algorithm operates on the order of tens of seconds or more (at the same timescale as the variation of the long-term channel statistics) and thus the implementation complexity is greatly reduced.

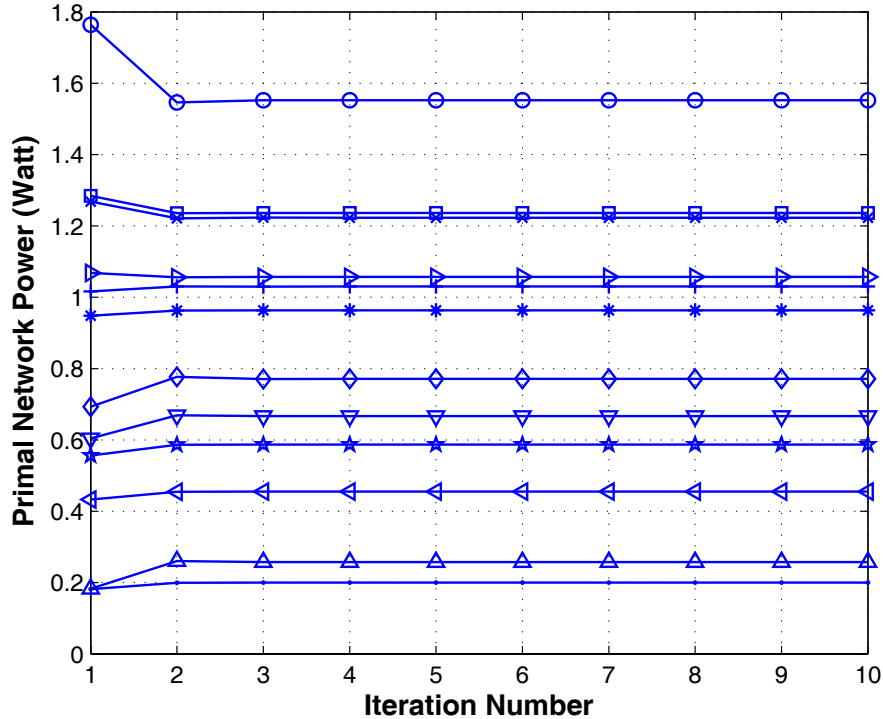


Figure 6.1: Convergence plot of the primal network power in a finite system setting employing Algorithm 6.1: ($N = 4$, $K = 4$, $J = 3$, $\bar{P} = 10$ Watt). Different marker types represent different users.

6.5 Numerical Results

In this section, we conduct a numerical study to support the analysis. We consider a three-cell cluster, i.e., $J = 3$, wherein the three base stations jointly perform power control and coordinated beamforming. The path loss (in dB) model in [111] is assumed with $15.3 + 37.6 \log_{10} d$ for distance d in meters and a log-normal shadowing with standard deviation of 8 dB is employed. The noise power spectral density is set to -162 dBm/Hz. The radius of each base station is set to be 1.5 km, and a 15 dBi antenna gain is assumed. For illustration purpose, the coordinated cluster is subject to a total power constraint, i.e., $\mathbf{w} = \mathbf{1}$, and each user possesses the same priority of service, i.e., $\beta = 1$. The total power constraint \bar{P} is assumed to equal 10 Watt.

Firstly, a finite system setting is considered. Each base station is assumed

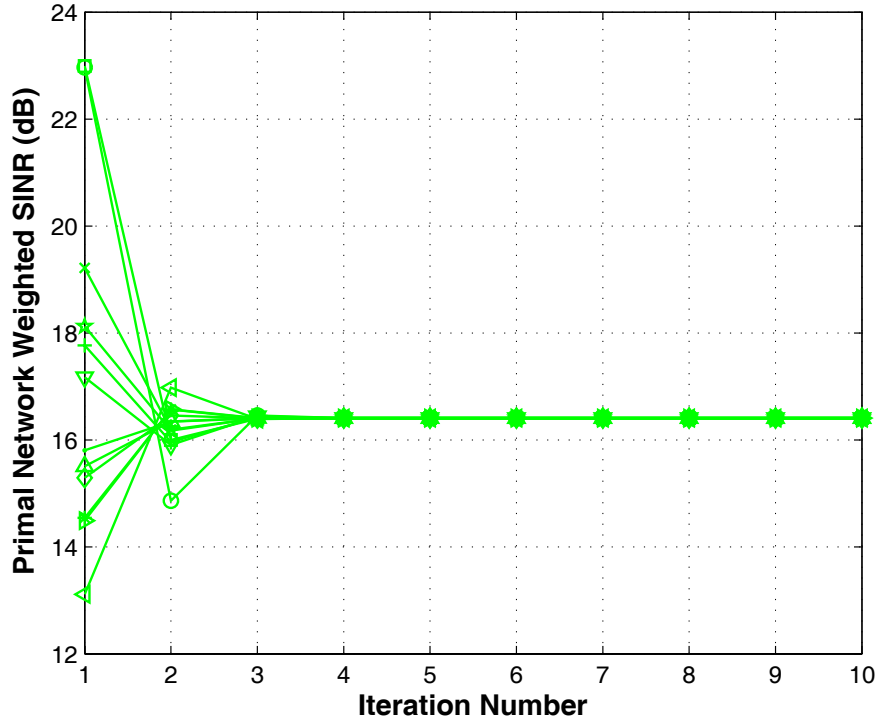


Figure 6.2: Convergence plot of the primal network weighted SINR in a finite system setting employing Algorithm 6.1: ($N = 4$, $K = 4$, $J = 3$, $\bar{P} = 10$ Watt). Different marker types represent different users.

to be equipped with $N = 4$ antennas and serves $K = 4$ randomly located users simultaneously. For one channel realization, the coordinated cluster utilizes *Algorithm 6.1* to iteratively obtain the optimal beamformer and optimal power. Fig. 6.1 demonstrates the convergence plot of the primal network power for different users. It is observed that for this channel realization, the power converges to its optimal value within 3 runs of iteration. This demonstrates the geometrically fast convergent property of *Algorithm 6.1*. Extensive numerical evaluations show that it converges typically within 5 runs of iteration for different channel realizations. In Fig. 6.2, the convergence plot of the primal network weighted SINR for different users is shown. Since the system metric of the coordinated cluster is to maintain fairness across users, each user's optimal SINR ($\mathbf{w} = \mathbf{1}$) would converge to the same value for a given channel realization, which is verified in Fig. 6.2.

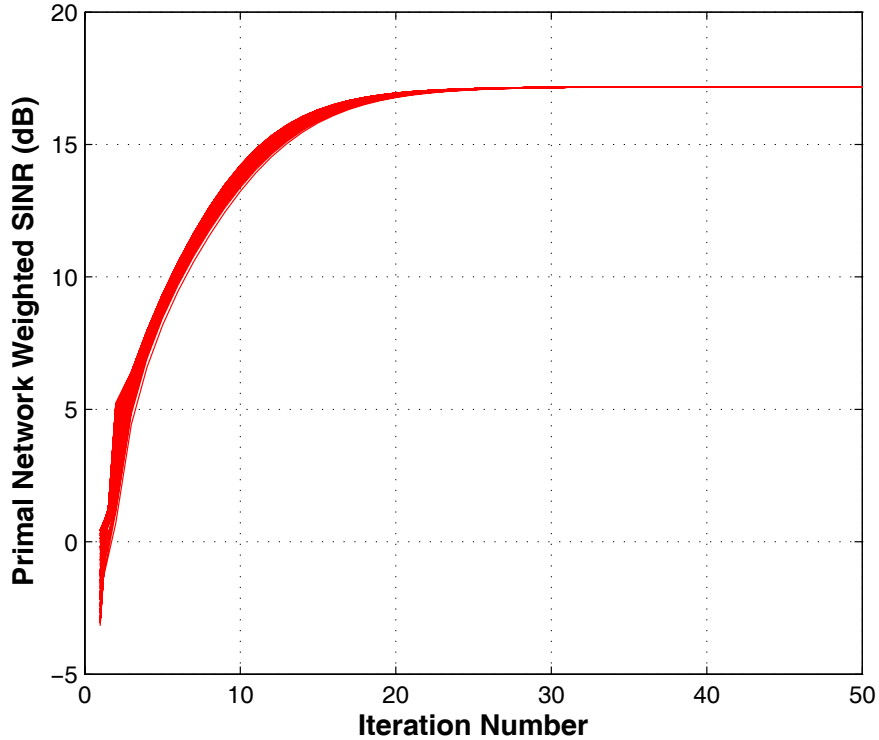


Figure 6.3: Convergence plot of the primal network weighted SINR in a large system setting employing Algorithm 6.5: ($N = 50$, $K = 40$, $J = 3$, $\bar{P} = 10$ Watt). The SINR for different users are not differentiated, but use the same line style for illustration.

Next, a large system setting is considered with $N = 50$ and $K = 40$. For a given geometry, the asymptotic SINR of the primal network is of interest, whose convergence plot is shown in Fig. 6.3 by employing *Algorithm 6.5*. The SINR's of each user are not differentiated, and uses the same line of type for illustration. Note that the converged value does not depend on the channel realization. However, it depends on the user geometry, namely the large scale channel effects, which means different user geometries would lead to different deterministic equivalents for the optimal SINR in the large system. Fig. 6.4 considers the use of asymptotic result. The asymptotic primal network power is utilized for downlink transmission, and the asymptotic dual network power is leveraged to non-iteratively determine the instantaneous beamformer. The achieved SINR's for different users using the deter-

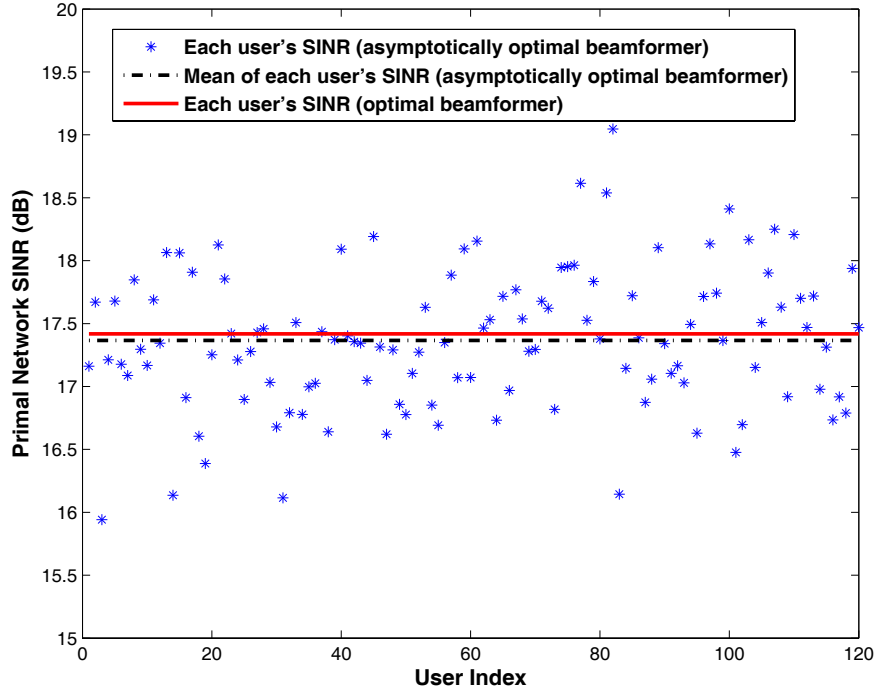


Figure 6.4: The achieved primal network SINR for each individual user using the asymptotically optimal beamformer in a large system setting for one channel realization: ($N = 50$, $K = 40$, $J = 3$, $\bar{P} = 10$ Watt). The mean of the achieved SINR using asymptotically optimal beamformer averaged over users and the the achieved SINR using the optimal beamformer are illustrated for comparison.

mined beamformer are shown, along with their mean and the achieved SINR using the optimal beamformer obtained via *Algorithm 6.1*, for one channel realization. It is observed that the SINR's of different users employing the asymptotically optimal beamformer fluctuate around the optimal one, with the mean close to the optimal SINR. Therefore, by using *Algorithm 6.5* to obtain the asymptotically optimal beamformer, the max-min fairness across users can be achieved in the asymptotic sense.

Finally, in Fig. 6.5, we consider the use of the asymptotic result in a finite system with $N = 4$ and $K = 3$ and demonstrate the comparison of the average SINR using optimal beamformer and the asymptotically optimal beamformer with respect to the variation of the total power constraint \bar{P} . Herein, the averaging is

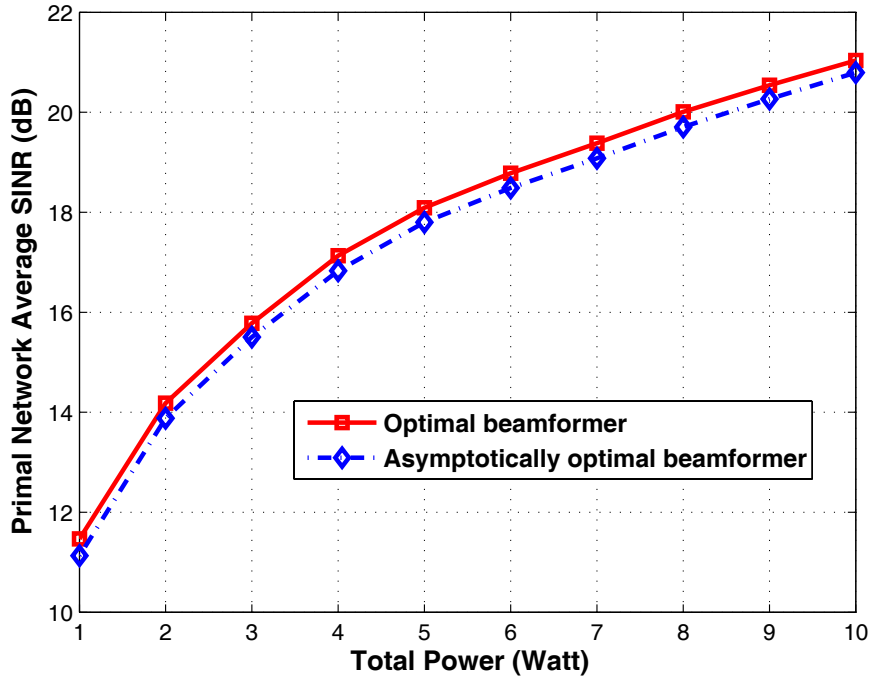


Figure 6.5: Comparison of the average achieved primal network SINR using asymptotically optimal beamformer and the optimal beamformer in a finite system setting with respect to different values of the power constraint \bar{P} : ($N = 4$, $K = 3$, $J = 3$).

over the user geometries, and for a given user geometry, different channel realizations are drawn. It can be seen from Fig. 6.5 that the performance of applying asymptotic result holds well for finite system setting. Accordingly, in a practical system with limited backhaul constraint, the asymptotically optimal power and beamformer can be developed and leveraged to reduce the implementation complexity and approach the optimal performance in the asymptotic sense.

6.6 Conclusion

In this chapter, we consider a joint optimization of beamforming and power control in a coordinated multicell downlink and employ the max-min formulation to enforce egalitarian fairness across users. The network duality is interpreted via a nonlinear Perron-Frobenius theoretic characterization and utilized to design a dis-

tributed algorithm to obtain the optimal solution. The iterative algorithm requires instantaneous power update through the limited backhaul and does not scale well in a large system setting. In order to design an algorithm that only utilizes channel statistics, we leverage random matrix theory to derive deterministic equivalents for the optimal SINR expression, and utilize the nonlinear Perron-Forbenius theory to establish the notion of effective network and propose a fast convergent algorithm. The asymptotically optimal solution enables a non-iterative approach to compute the instantaneous beamformer and thus requires no instantaneous information exchange across the coordinated cluster.

The text of this chapter, in part, is a reprint of the paper [189], Y. Huang, C. W. Tan, and B. D. Rao, “Joint beamforming and power control in coordinated multicell: max-min duality, effective network and large system transition”, *IEEE Transactions on Wireless Communications, minor revision, revised*, 2012. The dissertation author is the primary researcher and author, and the co-authors listed in these publications contributed to or supervised the research which forms the basis of this chapter.

6.7 Appendices

6.7.1 Appendix J

Proof of Theorem 6.1: The key step to the proof is to establish the convergence property of the dual network power \mathbf{q} via a nonlinear Perron-Frobenius theory in [167]. The relationship between \mathbf{q}^* and the optimal weighted SINR τ^* is of interest, and can be obtained by substituting the optimal MVDR beamformer:

$$\frac{q_m^*}{N\tau^*} = \frac{\beta_m}{\mathbf{h}_{m,m}^\dagger (\sum_{n \neq m} \frac{q_n^*}{N} \mathbf{h}_{m,n} \mathbf{h}_{m,n}^\dagger + w_m \mathbf{I})^{-1} \mathbf{h}_{m,m}} \quad \forall m. \quad (6.24)$$

Thus the mapping $\mathcal{I}^{(1)}(\cdot) : \mathbb{R}_+^{JK \times 1} \rightarrow \mathbb{R}_+^{JK \times 1}$ can be defined by the following equation: $\mathcal{I}_m^{(1)}(\mathbf{q}^*) \triangleq \frac{\beta_m}{\mathbf{h}_{m,m}^\dagger (\sum_{n \neq m} \frac{q_n^*}{N} \mathbf{h}_{m,n} \mathbf{h}_{m,n}^\dagger + w_m \mathbf{I})^{-1} \mathbf{h}_{m,m}}$. It can be shown using the same technique in [167] that $\mathcal{I}^{(1)}(\cdot)$ is a concave self-mapping of \mathbf{q}^* . Also, for the dual network, the weighted sum power constraint $\frac{1}{N} \boldsymbol{\sigma}^\top \mathbf{q}^* = \bar{P}$ induces a norm

on $\mathbb{R}_+^{JK \times 1}$ defined by $\|\mathbf{q}^*\|_{\text{DN}} \triangleq (N/\bar{P}) \sum_m \sigma_m q_m^*$. By applying [149, Theorem 1], starting from any initial point $\mathbf{q}[0]$, the fixed-point iteration (step 1 and step 2 of *Algorithm 6.1*) converges geometrically fast to the optimal solution \mathbf{q}^* for the eigenvalue problem (6.24). The optimal beamforming matrix \mathbb{U}^* is unique and can be computed by substituting the optimal dual network power \mathbf{q}^* into the MVDR beamformer (6.11) for each user (step 3 of *Algorithm 6.1*). For the primal network power \mathbf{p} , the induced norm on $\mathbb{R}_+^{JK \times 1}$ is established by the weighted power constraint $\frac{1}{N} \mathbf{w}^\top \mathbf{p}^* = \bar{P}$ as: $\|\mathbf{p}^*\|_{\text{PN}} \triangleq (N/\bar{P}) \sum_m w_m p_m^*$. Therefore, by using the same line of argument for the dual network with the optimal beamforming matrix \mathbb{U}^* , the fixed-point iteration (step 4 and step 5 of *Algorithm 6.1*) converges geometrically fast to the optimal solution \mathbf{p}^* for the eigenvalue problem (6.7) with any initial point $\mathbf{p}[0]$. This completes the proof of Theorem 6.1.

Proof of Theorem 6.2: For a given $\hat{\phi}$, the nonlinear eigenvalue problem in (6.18) enables us to define the mapping $\mathcal{I}^{(3)}(\cdot) : \mathbb{R}_+^{JK \times 1} \rightarrow \mathbb{R}_+^{JK \times 1}$ as: $\mathcal{I}_m^{(3)}(\hat{\mathbf{q}}) \triangleq \frac{\beta_m}{d_{m,m}} \left(w_m + \frac{1}{N} \sum_{n \neq m} \frac{\hat{q}_n d_{m,n}}{1 + \hat{q}_n d_{m,n} \hat{\phi}_m} \right)$. Since the function $\frac{x}{1+x}$ is strictly concave in $x \in \mathbb{R}_{++}$, the mapping $\mathcal{I}_m^{(3)}(\hat{\mathbf{q}})$ is a summation of strictly concave functions in $\hat{\mathbf{q}}$ and thus is a concave self-mapping in $\hat{\mathbf{q}}$. Then using the norm $\|\mathbf{q}\|_{\text{DN}}$ and applying [149, Theorem 1], the fixed-point iteration (step 1 and 2 of *Algorithm 6.3*) converges geometrically fast to $\hat{\mathbf{q}}^*(\hat{\phi})$ for the eigenvalue problem (6.18).

Proof of Theorem 6.3: For given $\hat{\phi}$ and $\hat{\mathbf{q}}$, the eigenvalue problem in (6.23) enables us to define the mapping $\mathcal{I}^{(4)}(\cdot) : \mathbb{R}_+^{JK \times 1} \rightarrow \mathbb{R}_+^{JK \times 1}$ as: $\mathcal{I}_m^{(4)}(\hat{\mathbf{p}}) \triangleq \frac{-\hat{\phi}_m \beta_m}{\hat{\phi}_m^2 d_{m,m}} \left(\sigma_m + \frac{1}{N} \sum_{n \neq m} \frac{\hat{p}_n d_{m,n} \hat{\phi}'_m}{(1 + \hat{q}_m d_{m,n} \hat{\phi}_m)^2 \hat{\phi}'_n} \right)$. It can be easily seen that the mapping $\mathcal{I}_m^{(4)}(\hat{\mathbf{p}})$ is affine, thus it is a concave self-mapping in $\hat{\mathbf{p}}$. Then using the norm $\|\mathbf{p}\|_{\text{PN}}$ and applying [149, Theorem 1], the fixed-point iteration (step 1 and 2 of *Algorithm 6.4*) converges geometrically fast to $\hat{\mathbf{p}}^*(\hat{\phi}, \hat{\mathbf{q}})$ for the eigenvalue problem (6.23).

6.7.2 Appendix K

Useful Results from Random Matrix Theory: We reproduce the following theorem [174, 178, 188] that will be employed to prove Lemma 6.1 and Lemma 6.3.

Theorem 6.4. (Theorem 2 in [188]) Consider an $\tilde{N} \times \tilde{n}$ random matrix $\mathbf{Y} = (Y_{i,j})_{i=1, j=1}^{\tilde{N}, \tilde{n}}$ where the entries are given by: $Y_{i,j} = \frac{\tilde{\sigma}_{i,j}}{\sqrt{\tilde{n}}} X_{i,j}$, the $X_{i,j}$ being independent and identically distributed (i.i.d.), with the following assumptions hold:

A1: The complex random variables $X_{i,j}$ are i.i.d. with $\mathbb{E}[X_{i,j}] = 0$, $\mathbb{E}[X_{i,j}^2] = 0$, $\mathbb{E}[|X_{i,j}|^2] = 1$, and $\mathbb{E}[|X_{i,j}|^8] < \infty$.

A2: There exists a real number $\tilde{\sigma}_{\max} < \infty$ such that: $\sup_{\tilde{n} \geq 1} \max_{\substack{1 \leq i \leq \tilde{N} \\ 1 \leq j \leq \tilde{n}}} |\tilde{\sigma}_{i,j}| \leq \tilde{\sigma}_{\max}$.

There exists a deterministic $\tilde{N} \times \tilde{N}$ matrix-valued function

$$\Psi(z) = \text{diag}(\psi_1(z), \dots, \psi_{\tilde{N}}(z))$$

analytic in $\mathbb{C} - \mathbb{R}_+$ such that:

$$\frac{1}{\tilde{N}} \text{Tr}(\mathbf{Y}\mathbf{Y}^\dagger - z\mathbf{I}_{\tilde{N}})^{-1} - \frac{1}{\tilde{N}} \text{Tr}(\Psi(z)) \xrightarrow{a.s.} 0 \quad \text{for } z \in \mathbb{C} - \mathbb{R}_+ \quad (6.25)$$

whose elements are the unique solutions of the deterministic system of $\tilde{N} + \tilde{n}$ equations:

$$\begin{aligned} \psi_i(z) &= \frac{-1}{z \left(1 + \frac{1}{\tilde{n}} \sum_{j=1}^{\tilde{n}} \tilde{\sigma}_{i,j}^2 \tilde{\psi}_j(z)\right)} \quad \text{for } 1 \leq i \leq \tilde{N} \\ \tilde{\psi}_j(z) &= \frac{-1}{z \left(1 + \frac{1}{\tilde{n}} \sum_{i=1}^{\tilde{N}} \tilde{\sigma}_{i,j}^2 \psi_i(z)\right)} \quad \text{for } 1 \leq j \leq \tilde{n} \end{aligned} \quad (6.26)$$

such that $\frac{1}{\tilde{N}} \text{Tr}(\Psi(z))$ is the Stieltjes transform [171] of a probability measure.

Proof of Lemma 6.1: The technique to establish the deterministic equivalent for $\gamma_m^{\text{DN}}(\mathbf{q})$ lies in the asymptotic behavior of the empirical distribution of the eigenvalue for $\left(\sum_{n \neq m} \frac{q_n d_{m,n}}{N} \tilde{\mathbf{h}}_{m,n} \tilde{\mathbf{h}}_{m,n}^\dagger + w_m \mathbf{I}\right)^{-1}$. This uplink problem for the equal power system has been addressed in [173], and the general treatment using the notion of variance profiles for random matrices is provided in [188]. Applying [190, Lemma 2.7] yields the following:

$$\gamma_m^{\text{DN}}(\mathbf{q}) - \frac{q_m d_{m,m}}{N} \text{Tr} \left(\left(\sum_{n \neq m} \frac{q_n d_{m,n}}{N} \tilde{\mathbf{h}}_{m,n} \tilde{\mathbf{h}}_{m,n}^\dagger + w_m \mathbf{I} \right)^{-1} \right) \xrightarrow{a.s.} 0. \quad (6.27)$$

Since the separable variance profile for the Gram matrix $\sum_{n \neq m} \frac{q_n d_{m,n}}{N} \tilde{\mathbf{h}}_{m,n} \tilde{\mathbf{h}}_{m,n}^\dagger$ is characterized by the optimal power q_n and the large-scale channel effects $d_{m,n}$,

there exist a deterministic equivalent for the Stieltjes transform [171] of this Gram matrix. In order to invoke Theorem 6.4, the channel model needs to satisfy the two assumptions (i.e., $A1$ and $A2$) described above. Note that the channel model in (6.12) constitutes a special case of the channel model assumed in [179, 188], therefore the matrices considered satisfy the two necessary assumptions. Employing Theorem 6.4 generates the fixed-point equation for $\gamma_m^{\text{DN}}(\mathbf{q})$ in (6.14).

Proof of Lemma 6.2: For a given $\hat{\mathbf{q}}$, define the following mapping: $\mathcal{I}_m^{(2)}(\hat{\phi}_m) \triangleq \frac{1}{w_m + \frac{1}{N} \sum_{n \neq m} \frac{\hat{q}_n d_{m,n}}{1 + \hat{q}_n d_{m,n} \hat{\phi}_m}}$. The idea for proving this lemma is to use the standard interference function framework [146]. It is straightforward to check that the positivity and monotonicity conditions in [146] hold for $\mathcal{I}_m^{(2)}(\hat{\phi}_m)$. Also, for all $\varepsilon > 1$, we have $\frac{1}{\frac{w_m}{\varepsilon} + \frac{1}{N} \sum_{n \neq m} \frac{\hat{q}_n d_{m,n}}{\varepsilon + \hat{q}_n d_{m,n} \varepsilon \hat{\phi}_m}} > \frac{1}{w_m + \frac{1}{N} \sum_{n \neq m} \frac{\hat{q}_n d_{m,n}}{1 + \hat{q}_n d_{m,n} \varepsilon \hat{\phi}_m}}$, which establishes the scalability condition in [146]. Since the mapping is a standard interference function, the convergence result follows from [146], thus completing the proof of Lemma 6.2.

Proof of Lemma 6.3: The expression for $\Gamma_m^{\text{PN}}(\mathbf{p})$ is given in (6.19), and the optimal beamformer \mathbf{u}_m^* is the MVDR beamformer in (6.11). The asymptotic approximations for $\frac{1}{N} |\tilde{\mathbf{h}}_{m,m}^\dagger \mathbf{u}_m^*|^2$ and $\frac{1}{N} |\tilde{\mathbf{h}}_{m,m}^\dagger \mathbf{u}_n^*|^2$ need to be determined. The expression for $\frac{1}{N} |\tilde{\mathbf{h}}_{m,m}^\dagger \mathbf{u}_m^*|^2$ can be further expanded as

$$\frac{1}{N} |\tilde{\mathbf{h}}_{m,m}^\dagger \mathbf{u}_m^*|^2 = \frac{\left(\frac{1}{N} \tilde{\mathbf{h}}_{m,m}^\dagger \left(\sum_{n \neq m} \frac{q_n d_{m,n}}{N} \tilde{\mathbf{h}}_{m,n} \tilde{\mathbf{h}}_{m,n}^\dagger + w_m \mathbf{I} \right)^{-1} \tilde{\mathbf{h}}_{m,n} \right)^2}{\frac{1}{N} \tilde{\mathbf{h}}_{m,m}^\dagger \left(\sum_{n \neq m} \frac{q_n d_{m,n}}{N} \tilde{\mathbf{h}}_{m,n} \tilde{\mathbf{h}}_{m,n}^\dagger + w_m \mathbf{I} \right)^{-2} \tilde{\mathbf{h}}_{m,n}}. \quad (6.28)$$

Employing Theorem 6.4, the numerator of (6.28) converges almost surely to $\phi_m^2(\mathbf{q})$. In order to obtain the deterministic equivalent for the denominator, the dependence of $\phi_m(\mathbf{q})$ on the noise variance w_m can be made explicit, i.e., $\phi_m(\mathbf{q}) = \phi_m(\mathbf{q}, x)|_{x=w_m}$. Then, by employing the differential of the Stieltjes transform of the Gram matrix $\sum_{n \neq m} \frac{q_n d_{m,n}}{N} \tilde{\mathbf{h}}_{m,n} \tilde{\mathbf{h}}_{m,n}^\dagger$ and applying Theorem 6.4, the denominator of (6.28) converges almost surely to $-\phi'_m(\mathbf{q}) \triangleq -\frac{\partial}{\partial x} \phi_m(\mathbf{q}, x)|_{x=w_m}$, which can be shown to be: $\phi'_m(\mathbf{q}) = \frac{-\phi_m(\mathbf{q})}{w_m + \frac{1}{N} \sum_{n \neq m} \frac{q_n d_{m,n}}{(1 + q_n d_{m,n} \phi_m(\mathbf{q}))^2}}$.

The expression for $\frac{1}{N}|\tilde{\mathbf{h}}_{m,m}^\dagger \mathbf{u}_n^*|^2$ can be further expanded as

$$\begin{aligned} & \frac{1}{N}|\tilde{\mathbf{h}}_{m,m}^\dagger \mathbf{u}_n^*|^2 \\ &= \frac{\frac{1}{N}\tilde{\mathbf{h}}_{m,m}^\dagger \left(\sum_{j \neq n} \frac{q_j d_{n,j}}{N} \tilde{\mathbf{h}}_{n,j} \tilde{\mathbf{h}}_{n,j}^\dagger + w_n \mathbf{I} \right)^{-1} \tilde{\mathbf{h}}_{n,n} \tilde{\mathbf{h}}_{n,n}^\dagger \left(\sum_{j \neq n} \frac{q_j d_{n,j}}{N} \tilde{\mathbf{h}}_{n,j} \tilde{\mathbf{h}}_{n,j}^\dagger + w_n \mathbf{I} \right)^{-1} \tilde{\mathbf{h}}_{m,m}}{\frac{1}{N}\tilde{\mathbf{h}}_{n,n}^\dagger \left(\sum_{j \neq n} \frac{q_j d_{n,j}}{N} \tilde{\mathbf{h}}_{n,j} \tilde{\mathbf{h}}_{n,j}^\dagger + w_n \mathbf{I} \right)^{-2} \tilde{\mathbf{h}}_{n,n}}. \end{aligned} \quad (6.29)$$

Following the same line of argument, the denominator of (6.29) converges almost surely to $-\phi'_n(\mathbf{q})$. For the numerator of (6.29), since $\tilde{\mathbf{h}}_{m,m}$ and the Gram matrix $\sum_{j \neq n} \frac{q_j d_{n,j}}{N} \tilde{\mathbf{h}}_{n,j} \tilde{\mathbf{h}}_{n,j}^\dagger$ are not independent, the numerator of (6.29) is transformed into the following equivalent form by matrix inversion lemma:

$$\begin{aligned} & \frac{\frac{1}{N}\tilde{\mathbf{h}}_{m,m}^\dagger \left(\sum_{j \neq m,n} \frac{q_j d_{n,j}}{N} \tilde{\mathbf{h}}_{n,j} \tilde{\mathbf{h}}_{n,j}^\dagger + w_n \mathbf{I} \right)^{-1} \tilde{\mathbf{h}}_{n,n} \tilde{\mathbf{h}}_{n,n}^\dagger \left(\sum_{j \neq m,n} \frac{q_j d_{n,j}}{N} \tilde{\mathbf{h}}_{n,j} \tilde{\mathbf{h}}_{n,j}^\dagger + w_n \mathbf{I} \right)^{-1} \tilde{\mathbf{h}}_{m,m}}{\left(1 + \frac{q_m d_{m,m}}{N} \tilde{\mathbf{h}}_{m,m}^\dagger \left(\sum_{j \neq m,n} \frac{q_j d_{n,j}}{N} \tilde{\mathbf{h}}_{n,j} \tilde{\mathbf{h}}_{n,j}^\dagger + w_n \mathbf{I} \right)^{-1} \tilde{\mathbf{h}}_{m,m} \right)^2} \end{aligned} \quad (6.30)$$

By employing the rank-1 perturbation lemma [191] and Theorem 6.4, the numerator of (6.30) converges almost surely to $-\phi'_m(\mathbf{q})$, and the denominator of (6.30) converges almost surely to $(1 + q_m^* d_{m,m} \phi_m(\mathbf{q}))^2$. Combining the aforementioned results yields the fixed-point equation for $\gamma_m^{\text{PN}}(\mathbf{p})$ in (6.20). This completes the proof of Lemma 6.3.

Table 6.1: Algorithm 6.1–Max-min weighted SINR for multicell downlink

-
- Initialize arbitrary $\mathbf{p}[0] \in \mathbb{R}_{++}^{JK \times 1}$, $\mathbf{q}[0] \in \mathbb{R}_{++}^{JK \times 1}$ and $\mathbf{u}_m[0] \in \mathbb{C}^{N \times 1}$ for $m = 1, \dots, JK$ such that $\|\mathbf{u}_m[0]\| = 1, \forall m$, $\frac{1}{N} \mathbf{w}^\top \mathbf{p}[0] \leq \bar{P}$, and $\frac{1}{N} \boldsymbol{\sigma}^\top \mathbf{q}[0] \leq \bar{P}$.

1. Update dual network power $\mathbf{q}[\kappa + 1]$:

$$q_m[\kappa + 1] = \left(\frac{\beta_m}{\Gamma_m^{\text{DN}}(\mathbf{q}[\kappa], \mathbb{U}[\kappa])} \right) q_m[\kappa] \quad \forall m.$$

2. Normalize $\mathbf{q}[\kappa + 1]$:

$$\mathbf{q}[\kappa + 1] \leftarrow \frac{N\bar{P}}{\boldsymbol{\sigma}^\top \mathbf{q}[\kappa + 1]} \mathbf{q}[\kappa + 1].$$

3. Update transmit beamforming matrix $\mathbb{U}[\kappa + 1]$:

$$\mathbf{u}_m[\kappa + 1] = \frac{(\sum_{n \neq m} \frac{q_n[\kappa+1]}{N} \mathbf{h}_{m,n} \mathbf{h}_{m,n}^\dagger + w_m \mathbf{I})^{-1} \mathbf{h}_{m,m}}{\|(\sum_{n \neq m} \frac{q_n[\kappa+1]}{N} \mathbf{h}_{m,n} \mathbf{h}_{m,n}^\dagger + w_m \mathbf{I})^{-1} \mathbf{h}_{m,m}\|} \quad \forall m.$$

4. Update primal network power $\mathbf{p}[\kappa + 1]$:

$$p_m[\kappa + 1] = \left(\frac{\beta_m}{\Gamma_m^{\text{PN}}(\mathbf{p}[\kappa], \mathbb{U}[\kappa + 1])} \right) p_m[\kappa] \quad \forall m.$$

5. Normalize $\mathbf{p}[\kappa + 1]$:

$$\mathbf{p}[\kappa + 1] \leftarrow \frac{N\bar{P}}{\mathbf{w}^\top \mathbf{p}[\kappa + 1]} \mathbf{p}[\kappa + 1].$$

Table 6.2: Algorithm 6.2–Computation of $\hat{\phi}$ given $\hat{\mathbf{q}}$

-
- Initialize arbitrary $\hat{\phi}[0] \in \mathbb{R}_{++}^{JK \times 1}$ with a given $\hat{\mathbf{q}}$.
 - Update $\hat{\phi}[\ell + 1]$:

$$\hat{\phi}_m[\ell + 1] = \frac{1}{w_m + \frac{1}{N} \sum_{n \neq m} \frac{\hat{q}_n d_{m,n}}{1 + \hat{q}_n d_{m,n} \hat{\phi}_m[\ell]}} \quad \forall m.$$

Table 6.3: Algorithm 6.3–Computation of $\hat{\mathbf{q}}$ given $\hat{\phi}$

-
- Initialize arbitrary $\hat{\mathbf{q}}[0] \in \mathbb{R}_{++}^{JK \times 1}$ with a given $\hat{\phi}$ such that $\frac{1}{N} \boldsymbol{\sigma}^\top \hat{\mathbf{q}}[0] \leq \bar{P}$.
1. Update dual network power $\hat{\mathbf{q}}[\ell + 1]$:

$$\hat{q}_m[\ell + 1] = \frac{\beta_m}{d_{m,m}} \left(w_m + \frac{1}{N} \sum_{n \neq m} \frac{\hat{q}_n[\ell] d_{m,n}}{1 + \hat{q}_n[\ell] d_{m,n} \hat{\phi}_m} \right) \quad \forall m.$$

2. Normalize $\hat{\mathbf{q}}[\ell + 1]$:

$$\hat{\mathbf{q}}[\ell + 1] \leftarrow \frac{N\bar{P}}{\boldsymbol{\sigma}^\top \hat{\mathbf{q}}[\ell + 1]} \hat{\mathbf{q}}[\ell + 1].$$

Table 6.4: Algorithm 6.4–Computation of $\hat{\mathbf{p}}$ given $\hat{\mathbf{q}}$ and $\hat{\phi}$

-
- Initialize arbitrary $\hat{\mathbf{p}}[0] \in \mathbb{R}_{++}^{JK \times 1}$ with given $\hat{\mathbf{q}}$ and $\hat{\phi}$ such that $\frac{1}{N} \mathbf{w}^\top \hat{\mathbf{p}}[0] \leq \bar{P}$.

1. Update primal network power $\hat{\mathbf{p}}[\ell + 1]$:

$$\hat{p}_m[\ell + 1] = \frac{-\hat{\phi}'_m \beta_m}{\hat{\phi}_m^2 d_{m,m}} \left(\sigma_m + \frac{1}{N} \sum_{n \neq m} \frac{\hat{p}_n[\ell] d_{m,n} \hat{\phi}'_m}{(1 + \hat{q}_m d_{m,m} \hat{\phi}_m)^2 \hat{\phi}'_n} \right) \quad \forall m.$$

2. Normalize $\hat{\mathbf{p}}[\ell + 1]$:

$$\hat{\mathbf{p}}[\ell + 1] \leftarrow \frac{N \bar{P}}{\mathbf{w}^\top \hat{\mathbf{p}}[\ell + 1]} \hat{\mathbf{p}}[\ell + 1].$$

Table 6.5: Algorithm 6.5–Computation of $\hat{\mathbf{p}}$ and $\hat{\mathbf{q}}$ for multicell downlink

-
- Initialize arbitrary $\hat{\boldsymbol{\phi}}[0] \in \mathbb{R}_{++}^{JK \times 1}$, $\hat{\mathbf{p}}[0] \in \mathbb{R}_{++}^{JK \times 1}$, and $\hat{\mathbf{q}}[0] \in \mathbb{R}_{++}^{JK \times 1}$ such that $\frac{1}{N} \mathbf{w}^\top \hat{\mathbf{p}}[0] \leq \bar{P}$, and $\frac{1}{N} \boldsymbol{\sigma}^\top \hat{\mathbf{q}}[0] \leq \bar{P}$.

1. Update dual network power $\hat{\mathbf{q}}[\ell + 1]$:

$$\hat{q}_m[\ell + 1] = \frac{\beta_m}{d_{m,m}} \left(w_m + \frac{1}{N} \sum_{n \neq m} \frac{\hat{q}_n[\ell] d_{m,n}}{1 + \hat{q}_n[\ell] d_{m,n} \hat{\phi}_m[\ell]} \right) \quad \forall m.$$

2. Normalize $\hat{\mathbf{q}}[\ell + 1]$:

$$\hat{\mathbf{q}}[\ell + 1] \leftarrow \frac{N \bar{P}}{\boldsymbol{\sigma}^\top \hat{\mathbf{q}}[\ell + 1]} \hat{\mathbf{q}}[\ell + 1].$$

3. Update $\hat{\boldsymbol{\phi}}[\ell + 1]$:

$$\hat{\phi}_m[\ell + 1] = \frac{\beta_m}{d_{m,m} \hat{q}_m[\ell + 1]} \quad \forall m.$$

4. Update primal network power $\hat{\mathbf{p}}[\ell + 1]$:

$$\begin{aligned} \hat{p}_m[\ell + 1] &= \frac{-\hat{\phi}'_m[\ell + 1] \beta_m}{\hat{\phi}_m^2[\ell + 1] d_{m,m}} \\ &\times \left(\sigma_m + \frac{1}{N} \sum_{n \neq m} \frac{\hat{p}_n[\ell] d_{m,n} \hat{\phi}'_m[\ell + 1]}{(1 + \hat{q}_m[\ell + 1] d_{m,m} \hat{\phi}_m[\ell + 1])^2 \hat{\phi}'_n[\ell + 1]} \right) \quad \forall m. \end{aligned}$$

5. Normalize $\hat{\mathbf{p}}[\ell + 1]$:

$$\hat{\mathbf{p}}[\ell + 1] \leftarrow \frac{N \bar{P}}{\mathbf{w}^\top \hat{\mathbf{p}}[\ell + 1]} \hat{\mathbf{p}}[\ell + 1].$$

Chapter 7

Concluding Remarks

This dissertation investigates several novel techniques and system design issues for next generation wireless networks and advocates the concept of situational aware wireless networks. The algorithmic issues and analytical studies related to feedback, power control and beamforming have been investigated. The objective of this dissertation is two-fold. Firstly, by exploring the aforementioned research topics in this dissertation, several open problems related to feedback, power control and beamforming have been tackled, and a number of novel design mechanisms has been proposed and studied in a theoretical manner. Secondly, each of the aforementioned research topics has addressed situational awareness from a different perspective. More specifically, Chapter 2 designs adaptive feedback based on spectral channel statistics (being aware of channel attributes); Chapter 3 designs heterogeneous partial feedback based on user densities across cells (being aware of user attributes); The scheduling policy utilized in Chapter 3 and Chapter 4 leverages the diverse statistics of the users' channels to maintain user fairness and obtain multiuser diversity gain (being aware of channel attributes and user attributes); The algorithm design in Chapter 5 employs the spatial channel statistics (being aware of channel attributes); Chapter 6 proposes to design efficient algorithm based on the large system structure (being aware of system attributes). In the sequel, we discuss some possible future research directions for each of the aforementioned research topics, enabled by the theoretical and algorithmic developments presented in this dissertation.

1. In Chapter 2, the explicit feedback assumption is used to analyze the adaptive feedback with channel estimation error and feedback delay. Practical scenarios may incorporate the effect of finite-rate quantization [192–195]. Some initial study examining the impact of quantized feedback and quantizer design can be found in [196]. Instead of quantizing order statistics to minimize the mean-squared error [197, 198], the approach in [196] optimizes the quantizer design to maximize the sum rate. The impact of quantized feedback under the framework in Chapter 2 is studied separately. From a practical point of view, it would be great interest to consider all these imperfections in a joint manner.
2. Chapter 3 and Chapter 4 employ the CDF-based scheduling policy to decouple each user's rate to provide analytical insight. In order to guarantee that each user is equiprobable to be scheduled, the equal weight is used for the CDF-based scheduling policy. In a general system setting, each user may have different QoS requirement, which may correspond to different weights in the CDF-based scheduling policy. Some initial study examining the weighted CDF-based scheduling policy in a relay-assisted downlink can be found in [199]. It is an interesting problem to consider the design of partial feedback in a relay-assisted system under the weighted CDF-based scheduling policy and draw theoretical relationship with the proportional-fair scheduling policy. Furthermore, Chapter 3 considers a generic multicell SISO network and Chapter 4 considers a single cell multi-antenna network and utilizes random beamforming as the transmission scheme. Some initial study examines random beamforming and receiver design in a distributed antenna system [200–203] can be found in [204]. A possible research direction is to extend the techniques in both Chapter 3 and Chapter 4 to a centralized multicell MIMO network and a distributed multicell MIMO network.
3. In Chapter 5, the weighted sum power constraint is employed for algorithm design in a multiuser MISO network. Application scenarios including the ad hoc network and the device-to-device network [205, 206] may involve individual power constraint [207, 208]. A potential research problem along the

direction of Chapter 5 is to investigate decentralized algorithm design under the individual power constraint.

4. Chapter 6 proposes to compute asymptotic power based on statistical channel information and thus the instantaneous beamformer can be obtained in a non-iterative manner. When performing large system analysis in Chapter 6, an independent channel with asymmetric large-scale channel effects for different users is assumed. This corresponds to the scenario when transmit antennas are placed far apart. A general system setting may involve correlation among antennas [183–186]. Some initial study examining the transmit-side channel correlation in power minimization algorithm design can be found in [209]. It would be interesting to jointly consider the practical issues such as channel correlation, channel estimation error, and pilot contamination for efficient algorithm design.

This dissertation advocates the concept of situational aware wireless networks by mainly focusing on PHY and MAC layer issues. Solving the aforementioned research problems related to feedback, power control and beamforming are useful first steps in the vision of situational aware wireless networks. Lastly, we would like to briefly comment on the framework of situational aware wireless networks. The proposed methods and algorithm design in this dissertation focus on the awareness of situations (channel, user and system). Such awareness can be achieved by leveraging learning in the wireless ecosystem. In current wireless system, there is no learning based on the gathered wireless data and thus there is no efficient data base to utilize the history of the wireless networks. Proper utilization of history can certainly give rise to a superior Bayesian prior for parameter setting and system design. The overall architecture of such systems, the components, and mechanism by which learning will take place are still very unclear and are needed so that there is a basis for future development, evaluation and integration. Cognition [210] as a way to deal with the challenges of future wireless networks has been suggested in various forms: cognitive radios [211, 212], self-organizing networks [213, 214], biologically inspired networks [215–217], etc. However, there remain many unanswered questions and it is important to consider

all the players in a wireless ecosystem in a coherent manner¹, namely the end user, infra-structure providers and content providers. Increasing the innate abilities of each of the participants is clearly going to be important in meeting the needs of the future wireless systems, but this is not enough. There is need for synergy among all the participants to make maximal use of these abilities. In order to achieve this synergy, there is a need for enhanced situational awareness at all levels and an ability to learn and adapt.

¹A conceptual framework to leverage a swarm of mobile users to collaboratively obtain situational aware wireless data can be found in [218].

Bibliography

- [1] D. J. Love, R. W. Heath, V. K. N. Lau, D. Gesbert, B. D. Rao, and M. Andrews, “An overview of limited feedback in wireless communication systems,” *IEEE J. Sel. Areas Commun.*, vol. 26, no. 8, pp. 1341–1365, Oct. 2008.
- [2] C. Y. Wong, R. S. Cheng, K. B. Letaief, and R. D. Murch, “Multiuser OFDM with adaptive subcarrier, bit, and power allocation,” *IEEE J. Sel. Areas Commun.*, vol. 17, no. 10, pp. 1747–1758, Oct. 1999.
- [3] J. Jang and K. B. Lee, “Transmit power adaptation for multiuser OFDM systems,” *IEEE J. Sel. Areas Commun.*, vol. 21, no. 2, pp. 171–178, Feb. 2003.
- [4] D. Kivanc, G. Li, and H. Liu, “Computationally efficient bandwidth allocation and power control for OFDMA,” *IEEE Trans. Wireless Commun.*, vol. 2, no. 6, pp. 1150–1158, Nov. 2003.
- [5] Z. Shen, J. G. Andrews, and B. L. Evans, “Adaptive resource allocation in multiuser OFDM systems with proportional rate constraints,” *IEEE Trans. Wireless Commun.*, vol. 4, no. 6, pp. 2726–2737, Nov. 2005.
- [6] H. Zhu and J. Wang, “Chunk-based resource allocation in OFDMA systems—part I: chunk allocation,” *IEEE Trans. Commun.*, vol. 57, no. 9, pp. 2734–2744, Sept. 2009.
- [7] H. Hashemi, “The indoor radio propagation channel,” *Proc. IEEE*, vol. 81, no. 7, pp. 943–968, Jul. 1993.
- [8] L. J. Greenstein, V. Erceg, Y. S. Yeh, and M. V. Clark, “A new path-gain/delay-spread propagation model for digital cellular channels,” *IEEE Trans. Veh. Technol.*, vol. 46, no. 2, pp. 477–485, May 1997.
- [9] C. Cheon, G. Liang, and H. L. Bertoni, “Simulating radio channel statistics for different building environments,” *IEEE J. Sel. Areas Commun.*, vol. 19, no. 11, pp. 2191–2200, Nov. 2001.

- [10] A. Algans, K. I. Pedersen, and P. E. Mogensen, "Experimental analysis of the joint statistical properties of azimuth spread, delay spread, and shadow fading," *IEEE J. Sel. Areas Commun.*, vol. 20, no. 3, pp. 523–531, Apr. 2002.
- [11] H. Asplund, A. A. Glazunov, A. F. Molisch, K. I. Pedersen, and M. Steinbauer, "The COST 259 directional channel model-part II: macrocells," *IEEE Trans. Wireless Commun.*, vol. 5, no. 12, pp. 3434–3450, Dec. 2006.
- [12] S. Yarkan and H. Arslan, "Exploiting location awareness toward improved wireless system design in cognitive radio," *IEEE Commun. Mag.*, vol. 46, no. 1, pp. 128–136, Jan. 2008.
- [13] A. F. Molisch, L. J. Greenstein, and M. Shafi, "Propagation issues for cognitive radio," *Proc. IEEE*, vol. 97, no. 5, pp. 787–804, May. 2009.
- [14] Y. Huang and B. D. Rao, "On using a priori channel statistics for cyclic prefix optimization in OFDM," in *Proc. IEEE Wireless Communications and Networking Conference (WCNC)*, Mar. 2011, pp. 1460–1465.
- [15] R. Knopp and P. A. Humblet, "Information capacity and power control in single-cell multiuser communications," in *Proc. IEEE International Conference on Communications (ICC)*, Jun. 1995, pp. 331–335.
- [16] P. Viswanath, D. N. C. Tse, and R. Laroia, "Opportunistic beamforming using dumb antennas," *IEEE Trans. Inf. Theory*, vol. 48, no. 6, pp. 1277–1294, Jun. 2002.
- [17] S. Sanayei and A. Nosratinia, "Opportunistic downlink transmission with limited feedback," *IEEE Trans. Inf. Theory*, vol. 53, no. 11, pp. 4363–4372, Nov. 2007.
- [18] V. Hassel, D. Gesbert, M. S. Alouini, and G. E. Oien, "A threshold-based channel state feedback algorithm for modern cellular systems," *IEEE Trans. Wireless Commun.*, vol. 6, no. 7, pp. 2422–2426, Jul. 2007.
- [19] J. Chen, R. Berry, and M. Honig, "Limited feedback schemes for downlink OFDMA based on sub-channel groups," *IEEE J. Sel. Areas Commun.*, vol. 26, no. 8, pp. 1451–1461, Oct. 2008.
- [20] M. Pugh and B. D. Rao, "Reduced feedback schemes using random beamforming in MIMO broadcast channels," *IEEE Trans. Signal Process.*, vol. 58, no. 3, pp. 1821–1832, Mar. 2010.
- [21] S. Sesia, I. Toufik, and M. Baker, *LTE—The UMTS Long Term Evolution*, 2nd ed. Wiley, 2011.

- [22] B. C. Jung, T. W. Ban, W. Choi, and D. K. Sung, "Capacity analysis of simple and opportunistic feedback schemes in OFDMA systems," in *Proc. International Symposium on Communications and Information Technologies (ISCIT)*, Oct. 2007, pp. 203–208.
- [23] J. Y. Ko and Y. H. Lee, "Opportunistic transmission with partial channel information in multi-user OFDM wireless systems," in *Proc. IEEE Wireless Communications and Networking Conference (WCNC)*, Mar. 2007, pp. 1318–1322.
- [24] J. G. Choi and S. Bahk, "Cell-throughput analysis of the proportional fair scheduler in the single-cell environment," *IEEE Trans. Veh. Technol.*, vol. 56, no. 2, pp. 766–778, Mar. 2007.
- [25] Y. J. Choi and S. Bahk, "Partial channel feedback schemes maximizing overall efficiency in wireless networks," *IEEE Trans. Wireless Commun.*, vol. 7, no. 4, pp. 1306–1314, Apr. 2008.
- [26] K. Pedersen, T. Kolding, I. Kovacs, G. Monghal, F. Frederiksen, and P. Mogenssen, "Performance analysis of simple channel feedback schemes for a practical OFDMA system," *IEEE Trans. Veh. Technol.*, vol. 58, no. 9, pp. 5309–5314, Nov. 2009.
- [27] J. Leinonen, J. Hamalainen, and M. Juntti, "Performance analysis of downlink OFDMA resource allocation with limited feedback," *IEEE Trans. Wireless Commun.*, vol. 8, no. 6, pp. 2927–2937, Jun. 2009.
- [28] S. Donthi and N. Mehta, "Joint performance analysis of channel quality indicator feedback schemes and frequency-domain scheduling for LTE," *IEEE Trans. Veh. Technol.*, vol. 60, no. 7, pp. 3096–3109, Sept. 2011.
- [29] S. Hur and B. D. Rao, "Sum rate analysis of a reduced feedback OFDMA downlink system employing joint scheduling and diversity," *IEEE Trans. Signal Process.*, vol. 60, no. 2, pp. 862–876, Feb. 2012.
- [30] Y. Huang and B. D. Rao, "Environmental-aware heterogeneous partial feedback design in a multiuser OFDMA system," in *Proc. Asilomar Conference on Signals, Systems, and Computers*, Nov. 2011, pp. 970–974.
- [31] P. Piantanida, G. Matz, and P. Duhamel, "Outage behavior of discrete memoryless channels under channel estimation errors," *IEEE Trans. Inf. Theory*, vol. 55, no. 9, pp. 4221–4239, Sept. 2009.
- [32] V. Lau, W. K. Ng, and D. S. W. Hui, "Asymptotic tradeoff between cross-layer goodput gain and outage diversity in OFDMA systems with slow fading and delayed CSIT," *IEEE Trans. Wireless Commun.*, vol. 7, no. 7, pp. 2732–2739, Jul. 2008.

- [33] T. Wu and V. Lau, "Design and analysis of multi-user SDMA systems with noisy limited CSIT feedback," *IEEE Trans. Wireless Commun.*, vol. 9, no. 4, pp. 1446–1450, Apr. 2010.
- [34] S. Akoum and R. W. Heath, "Limited feedback for temporally correlated MIMO channels with other cell interference," *IEEE Trans. Signal Process.*, vol. 58, no. 10, pp. 5219–5232, Oct. 2010.
- [35] Q. Ma and C. Tepedelenlioglu, "Practical multiuser diversity with outdated channel feedback," *IEEE Trans. Veh. Technol.*, vol. 54, no. 4, pp. 1334–1345, Jul. 2005.
- [36] A. Kuhne and A. Klein, "Throughput analysis of multi-user OFDMA-systems using imperfect CQI feedback and diversity techniques," *IEEE J. Sel. Areas Commun.*, vol. 26, no. 8, pp. 1440–1450, Oct. 2008.
- [37] E. Dahlman, S. Parkvall, and J. Skold, *4G LTE/LTE-Advanced for Mobile Broadband*. Academic Press, 2011.
- [38] Ericsson, "System-level evaluation of OFDM - further consideration," 3GPP, TSG-RAN WG1R1-031303, Tech. Rep., Nov. 2003.
- [39] H. Song, R. Kwan, and J. Zhang, "Approximations of EESM effective SNR distribution," *IEEE Trans. Commun.*, vol. 59, no. 2, pp. 603–612, Feb. 2011.
- [40] S. N. Donthi and N. B. Mehta, "An accurate model for EESM and its application to analysis of CQI feedback schemes and scheduling in LTE," *IEEE Trans. Wireless Commun.*, vol. 10, no. 10, pp. 3436–3448, Oct. 2011.
- [41] L. Wan, S. Tsai, and M. Almgren, "A fading-insensitive performance metric for a unified link quality model," in *Proc. IEEE Wireless Communications and Networking Conference (WCNC)*, Apr. 2006, pp. 2110–2114.
- [42] J. Fan, Q. Yin, G. Y. Li, B. Peng, and X. Zhu, "Adaptive block-level resource allocation in OFDMA networks," *IEEE Trans. Wireless Commun.*, vol. 10, no. 11, pp. 3966–3972, Nov. 2011.
- [43] G. D. Forney Jr and G. Ungerboeck, "Modulation and coding for linear Gaussian channels," *IEEE Trans. Inf. Theory*, vol. 44, no. 6, pp. 2384–2415, Oct. 1998.
- [44] N. Al-Dhahir and J. M. Cioffi, "Optimum finite-length equalization for multicarrier transceivers," *IEEE Trans. Commun.*, vol. 44, no. 1, pp. 56–64, Jan. 1996.
- [45] S. H. Muller-Weinfurtner, "Coding approaches for multiple antenna transmission in fast fading and OFDM," *IEEE Trans. Signal Process.*, vol. 50, no. 10, pp. 2442–2450, Oct. 2002.

- [46] M. R. McKay, P. J. Smith, H. A. Suraweera, and I. B. Collings, “On the mutual information distribution of OFDM-based spatial multiplexing: exact variance and outage approximation,” *IEEE Trans. Inf. Theory*, vol. 54, no. 7, pp. 3260–3278, Jul. 2008.
- [47] M. Eslami and W. A. Krzymien, “Net throughput maximization of per-chunk user scheduling for MIMO-OFDM downlink,” *IEEE Trans. Veh. Technol.*, vol. 60, no. 9, pp. 4338–4348, Nov. 2011.
- [48] R. McEliece and W. E. Stark, “Channels with block interference,” *IEEE Trans. Inf. Theory*, vol. 30, no. 1, pp. 44–53, Jan. 1984.
- [49] M. Médard and R. G. Gallager, “Bandwidth scaling for fading multipath channels,” *IEEE Trans. Inf. Theory*, vol. 48, no. 4, pp. 840–852, Apr. 2002.
- [50] C. Chen and L. Wang, “A unified capacity analysis for wireless systems with joint multiuser scheduling and antenna diversity in nakagami fading channels,” *IEEE Trans. Commun.*, vol. 54, no. 3, pp. 469–478, Mar. 2006.
- [51] J. Jiang, R. Buehrer, and W. Tranter, “Antenna diversity in multiuser data networks,” *IEEE Trans. Commun.*, vol. 52, no. 3, pp. 490–497, Mar. 2004.
- [52] Z. Chen, J. Yuan, and B. Vucetic, “Analysis of transmit antenna selection/maximal-ratio combining in rayleigh fading channels,” *IEEE Trans. Veh. Technol.*, vol. 54, no. 4, pp. 1312–1321, Jul. 2005.
- [53] Y. Huang and B. D. Rao, “Asymptotic analysis of a partial feedback OFDMA system employing spatial, spectral, and multiuser diversity,” in *Proc. IEEE International Conference on Acoustics, Speech and Signal Processing (ICASSP)*, Mar. 2012, pp. 3221–3224.
- [54] Q. Zhou and H. Dai, “Asymptotic analysis on the interaction between spatial diversity and multiuser diversity in wireless networks,” *IEEE Trans. Signal Process.*, vol. 55, no. 8, pp. 4271–4283, Aug. 2007.
- [55] Y. Huang and B. D. Rao, “Analysis of a MIMO OFDMA heterogeneous feedback system employing joint scheduling and spatial diversity in Nakagami fading channels,” in *Proc. IEEE International Conference on Communications (ICC)*, Jun. 2012, pp. 4673–4677.
- [56] H. A. David and H. N. Nagaraja, *Order Statistics*, 3rd ed. Wiley-Interscience, 2003.
- [57] M. Abramowitz and I. A. Stegun, *Handbook of Mathematical Functions with Formulas, Graphs, and Mathematical Tables*. Dover, 1972.

- [58] M. Sharif and B. Hassibi, "On the capacity of MIMO broadcast channels with partial side information," *IEEE Trans. Inf. Theory*, vol. 51, no. 2, pp. 506–522, Feb. 2005.
- [59] A. H. Nuttall, "Some integrals involving the Q-function," Naval Underwater Systems Center, Tech. Rep., Apr. 1972.
- [60] S. P. Boyd and L. Vandenberghe, *Convex Optimization*. Cambridge Univ Pr, 2004.
- [61] Y. Yu, "On log-concavity of the generalized Marcum Q function," *Arxiv Preprint*, 2011. [Online]. Available: arXiv:1105.5762
- [62] M. K. Simon, *Probability Distributions Involving Gaussian Random Variables: A Handbook For Engineers and Scientists*. Springer Netherlands, 2002.
- [63] Y. Huang and B. D. Rao, "Performance analysis of heterogeneous feedback design in an OFDMA downlink with partial and imperfect feedback," *IEEE Trans. Signal Process.*, 2012, accepted, to appear.
- [64] I. S. Gradshteyn and I. M. Ryzhik, *Tables of Integrals, Series and Products*, 7th ed., D. Zwillinger and A. Jeffrey, Eds. Academic Press, 2007.
- [65] P. Billingsley, *Probability and Measure*, 3rd ed. John Wiley & Sons, 1995.
- [66] H. Finner and M. Roters, "Log-concavity and inequalities for Chi-square, F and Beta distributions with applications in multiple comparisons," *Statistica Sinica*, vol. 7, pp. 771–788, 1997.
- [67] R. Madan, J. Borran, A. Sampath, N. Bhushan, A. Khandekar, and T. Ji, "Cell association and interference coordination in heterogeneous LTE-A cellular networks," *IEEE J. Sel. Areas Commun.*, vol. 28, no. 9, pp. 1479–1489, Dec. 2010.
- [68] A. Damnjanovic, J. Montojo, Y. Wei, T. Ji, T. Luo, M. Vajapeyam, T. Yoo, O. Song, and D. Malladi, "A survey on 3GPP heterogeneous networks," *IEEE Wireless Commun.*, vol. 18, no. 3, pp. 10–21, Jun. 2011.
- [69] A. Damnjanovic, J. Montojo, J. Cho, H. Ji, J. Yang, and P. Zong, "UE's role in LTE advanced heterogeneous networks," *IEEE Commun. Mag.*, vol. 50, no. 2, pp. 164–176, Feb. 2012.
- [70] D. López-Pérez, X. Chu, and I. Guvenc, "On the expanded region of picocells in heterogeneous networks," *IEEE J. Sel. Top. Signal Process.*, vol. 6, no. 3, pp. 281–294, Jun. 2012.

- [71] V. Chandrasekhar, J. Andrews, and A. Gatherer, "Femtocell networks: a survey," *IEEE Commun. Mag.*, vol. 46, no. 9, pp. 59–67, Sept. 2008.
- [72] J. G. Andrews, H. Claussen, M. Dohler, S. Rangan, and M. C. Reed, "Femtocells: past, present, and future," *IEEE J. Sel. Areas Commun.*, vol. 30, no. 3, pp. 497–508, Apr. 2012.
- [73] A. Barbieri, A. Damnjanovic, T. Ji, J. Montojo, Y. Wei, D. Malladi, O. Song, and G. Horn, "LTE femtocells: system design and performance analysis," *IEEE J. Sel. Areas Commun.*, vol. 30, no. 3, pp. 586–594, Apr. 2012.
- [74] D. Soldani and S. Dixit, "Wireless relays for broadband access," *IEEE Commun. Mag.*, vol. 46, no. 3, pp. 58–66, Mar. 2008.
- [75] Y. Yang, H. Hu, J. Xu, and G. Mao, "Relay technologies for WiMAX and LTE-advanced mobile systems," *IEEE Commun. Mag.*, vol. 47, no. 10, pp. 100–105, Oct. 2009.
- [76] L. Sanguinetti, A. A. D'Amico, and Y. Rong, "A tutorial on the optimization of amplify-and-forward MIMO relay systems," *IEEE J. Sel. Areas Commun.*, vol. 30, no. 8, pp. 1331–1346, Sept. 2012.
- [77] H. S. Dhillon, R. K. Ganti, F. Baccelli, and J. G. Andrews, "Modeling and analysis of K-tier downlink heterogeneous cellular networks," *IEEE J. Sel. Areas Commun.*, vol. 30, no. 3, pp. 550–560, Apr. 2012.
- [78] M. Z. Win, P. C. Pinto, and L. A. Shepp, "A mathematical theory of network interference and its applications," *Proc. of the IEEE*, vol. 97, no. 2, pp. 205–230, Feb. 2009.
- [79] G. Boudreau, J. Panicker, N. Guo, R. Chang, N. Wang, and S. Vrzic, "Interference coordination and cancellation for 4G networks," *IEEE Commun. Mag.*, vol. 47, no. 4, pp. 74–81, Apr. 2009.
- [80] N. Ksairi, P. Bianchi, P. Ciblat, and W. Hachem, "Resource allocation for downlink cellular OFDMA systems-part I: optimal allocation," *IEEE Trans. Signal Process.*, vol. 58, no. 2, pp. 720–734, Feb. 2010.
- [81] K. Son, S. Lee, Y. Yi, and S. Chong, "REFIM: a practical interference management in heterogeneous wireless access networks," *IEEE J. Sel. Areas Commun.*, vol. 29, no. 6, pp. 1260–1272, Jun. 2011.
- [82] H. Zhang, L. Venturino, N. Prasad, P. Li, S. Rangarajan, and X. Wang, "Weighted sum-rate maximization in multi-cell networks via coordinated scheduling and discrete power control," *IEEE J. Sel. Areas Commun.*, vol. 29, no. 6, pp. 1214–1224, Jun. 2011.

- [83] D. Gesbert, S. Hanly, H. Huang, S. Shitz, O. Simeone, and W. Yu, "Multi-cell MIMO cooperative networks: a new look at interference," *IEEE J. Sel. Areas Commun.*, vol. 28, no. 9, pp. 1380–1408, Dec. 2010.
- [84] M. Sawahashi, Y. Kishiyama, A. Morimoto, D. Nishikawa, and M. Tanno, "Coordinated multipoint transmission/reception techniques for LTE-advanced," *IEEE Wireless Commun.*, vol. 17, no. 3, pp. 26–34, Jun. 2010.
- [85] H. Dahrouj and W. Yu, "Coordinated beamforming for the multicell multi-antenna wireless system," *IEEE Trans. Wireless Commun.*, vol. 9, no. 5, pp. 1748–1759, May 2010.
- [86] R. Bhagavatula and R. W. Heath, "Adaptive limited feedback for sum-rate maximizing beamforming in cooperative multicell systems," *IEEE Trans. Signal Process.*, vol. 59, no. 2, pp. 800–811, Feb. 2011.
- [87] V. R. Cadambe and S. A. Jafar, "Interference alignment and degrees of freedom of the K user interference channel," *IEEE Trans. Inf. Theory*, vol. 54, no. 8, pp. 3425–3441, Aug. 2008.
- [88] C. Suh, M. Ho, and D. Tse, "Downlink interference alignment," *IEEE Trans. Commun.*, vol. 59, no. 9, pp. 2616–2626, Sept. 2011.
- [89] Z. Luo and S. Zhang, "Dynamic spectrum management: complexity and duality," *IEEE J. Sel. Top. Signal Process.*, vol. 2, no. 1, pp. 57–73, Feb. 2008.
- [90] Y. Huang and B. D. Rao, "Awareness of channel statistics for slow cyclic prefix adaptation in an OFDMA system," *IEEE Wireless Commun. Lett.*, vol. 1, no. 4, pp. 332–335, Aug. 2012.
- [91] E. L. Hahne, "Round-robin scheduling for max-min fairness in data networks," *IEEE J. Sel. Areas Commun.*, vol. 9, no. 7, pp. 1024–1039, Sept. 1991.
- [92] D. Park, H. Seo, H. Kwon, and B. G. Lee, "Wireless packet scheduling based on the cumulative distribution function of user transmission rates," *IEEE Trans. Commun.*, vol. 53, no. 11, pp. 1919–1929, Nov. 2005.
- [93] S. Patil and G. De Veciana, "Measurement-based opportunistic scheduling for heterogenous wireless systems," *IEEE Trans. Commun.*, vol. 57, no. 9, pp. 2745–2753, Sept. 2009.
- [94] F. Kelly, "Charging and rate control for elastic traffic," *Eur. Trans. Telecommun.*, vol. 8, no. 1, pp. 33–37, Jan. 1997.

- [95] A. Jalali, R. Padovani, and R. Pankaj, "Data throughput of CDMA-HDR a high efficiency-high data rate personal communication wireless system," in *Proc. IEEE Vehicular Technology Conference (VTC)*, May 2000, pp. 1854–1858.
- [96] G. Caire, R. Muller, and R. Knopp, "Hard fairness versus proportional fairness in wireless communications: the single-cell case," *IEEE Trans. Inf. Theory*, vol. 53, no. 4, pp. 1366–1385, Apr. 2007.
- [97] Y. Huang and B. D. Rao, "Heterogeneous partial feedback design in heterogeneous OFDMA cellular networks," in *Proc. IEEE International Conference on Communications (ICC)*, Jun. 2012, pp. 2462–2466.
- [98] J. Galambos, *The Asymptotic Theory of Extreme Order Statistics*. Wiley, 1978.
- [99] G. Song and Y. Li, "Asymptotic throughput analysis for channel-aware scheduling," *IEEE Trans. Commun.*, vol. 54, no. 10, pp. 1827–1834, Oct. 2006.
- [100] T. Yoo, N. Jindal, and A. Goldsmith, "Multi-antenna downlink channels with limited feedback and user selection," *IEEE J. Sel. Areas Commun.*, vol. 25, no. 7, pp. 1478–1491, Sept. 2007.
- [101] D. Gesbert and M. Kountouris, "Rate scaling laws in multicell networks under distributed power control and user scheduling," *IEEE Trans. Inf. Theory*, vol. 57, no. 1, pp. 234–244, Jan. 2011.
- [102] A. Tajer and X. Wang, "Information exchange limits in cooperative MIMO networks," *IEEE Trans. Signal Process.*, vol. 59, no. 6, pp. 2927–2942, Jun. 2011.
- [103] H. J. Bang, D. Gesbert, and P. Orten, "On the rate gap between multi- and single-cell processing under opportunistic scheduling," *IEEE Trans. Signal Process.*, vol. 60, no. 1, pp. 415–425, Jan. 2012.
- [104] Y. Huang and B. D. Rao, "Sum rate analysis of one-pico-inside OFDMA network with opportunistic scheduling and selective feedback," *IEEE Signal Process. Lett.*, vol. 19, no. 7, pp. 383–386, Jul. 2012.
- [105] Y. Isukapalli and B. D. Rao, "Packet error probability of a transmit beamforming system with imperfect feedback," *IEEE Trans. Signal Process.*, vol. 58, no. 4, pp. 2298–2314, Apr. 2010.
- [106] Y. Huang and B. D. Rao, "A unified analysis of CDF-based distributed scheduling in a heterogeneous multicell," in *Proc. Asilomar Conference on Signals, Systems, and Computers*, Nov. 2012, pp. 1–5.

- [107] G. Casella and R. L. Berger, *Statistical Inference*. Duxbury Press, 2001.
- [108] S. M. Berman, "Limiting distribution of the maximum term in sequences of dependent random variables," *The Annals of Mathematical Statistics*, vol. 33, no. 3, pp. 894–908, 1962.
- [109] J. Pickands, "Moment convergence of sample extremes," *The Annals of Mathematical Statistics*, vol. 39, no. 3, pp. 881–889, Jun. 1968.
- [110] Y. Huang and B. D. Rao, "On rate scaling laws with CDF-based distributed scheduling in multicell networks," in *Proc. International Symposium on Information Theory and its Applications (ISITA)*, Oct. 2012, pp. 511–515.
- [111] 3GPP, "TS 36.201 V10.0.0 - LTE Physical Layer - General Description (Release 10)," 3GPP, Tech. Rep., 2010.
- [112] R. Elliott, "A measure of fairness of service for scheduling algorithms in multiuser systems," in *Proc. IEEE CCECE*, vol. 3, May 2002, pp. 1583–1588.
- [113] L. Yang and M. S. Alouini, "Performance analysis of multiuser selection diversity," *IEEE Trans. Veh. Technol.*, vol. 55, no. 6, pp. 1848–1861, Nov. 2006.
- [114] Y. Huang and B. D. Rao, "An analytical framework for heterogeneous partial feedback design in heterogeneous multicell OFDMA networks," *IEEE Trans. Signal Process.*, 2012, accepted, to appear.
- [115] Y. Tokgoz and B. D. Rao, "The effect of imperfect channel estimation on the performance of maximum ratio combining in the presence of cochannel interference," *IEEE Trans. Veh. Technol.*, vol. 55, no. 5, pp. 1527–1534, Sept. 2006.
- [116] E. Bjornson, D. Hammarwall, and B. Ottersten, "Exploiting quantized channel norm feedback through conditional statistics in arbitrarily correlated MIMO systems," *IEEE Trans. Signal Process.*, vol. 57, no. 10, pp. 4027–4041, Oct. 2009.
- [117] H. Stark and J. W. Woods, *Probability and Random Processes with Applications to Signal Processing*, 3rd ed. Pearson Education, Inc., 2002.
- [118] J. C. Roh and B. D. Rao, "Transmit beamforming in multiple-antenna systems with finite rate feedback: A VQ-based approach," *IEEE Trans. Inf. Theory*, vol. 52, no. 3, pp. 1101–1112, Mar. 2006.
- [119] T. Yoo and A. Goldsmith, "On the optimality of multiantenna broadcast scheduling using zero-forcing beamforming," *IEEE J. Sel. Areas Commun.*, vol. 24, no. 3, pp. 528–541, Mar. 2006.

- [120] G. Caire and S. Shamai, "On the achievable throughput of a multiantenna Gaussian broadcast channel," *IEEE Trans. Inf. Theory*, vol. 49, no. 7, pp. 1691–1706, Jul. 2003.
- [121] P. Viswanath and D. N. C. Tse, "Sum capacity of the vector Gaussian broadcast channel and uplink-downlink duality," *IEEE Trans. Inf. Theory*, vol. 49, no. 8, pp. 1912–1921, Aug. 2003.
- [122] S. Vishwanath, N. Jindal, and A. Goldsmith, "Duality, achievable rates, and sum-rate capacity of Gaussian MIMO broadcast channels," *IEEE Trans. Inf. Theory*, vol. 49, no. 10, pp. 2658–2668, Oct. 2003.
- [123] W. Yu and J. M. Cioffi, "Sum capacity of Gaussian vector broadcast channels," *IEEE Trans. Inf. Theory*, vol. 50, no. 9, pp. 1875–1892, Sept. 2004.
- [124] H. Weingarten, Y. Steinberg, and S. Shamai, "The capacity region of the Gaussian multiple-input multiple-output broadcast channel," *IEEE Trans. Inf. Theory*, vol. 52, no. 9, pp. 3936–3964, Sept. 2006.
- [125] W. Zhang and K. B. Letaief, "MIMO broadcast scheduling with limited feedback," *IEEE J. Sel. Areas Commun.*, vol. 25, no. 7, pp. 1457–1467, Sept. 2007.
- [126] T. Tang, R. W. Heath, S. Cho, and S. Yun, "Opportunistic feedback for multiuser MIMO systems with linear receivers," *IEEE Trans. Commun.*, vol. 55, no. 5, pp. 1020–1032, May 2007.
- [127] T. Y. Al-Naffouri, A. F. Dana, and B. Hassibi, "Scaling laws of multiple antenna group-broadcast channels," *IEEE Trans. Wireless Commun.*, vol. 7, no. 12, pp. 5030–5038, Dec. 2008.
- [128] H. Wang and T. Kirubarajan, "Random unitary beamforming with partial feedback for MISO downlink transmission using multiuser diversity," *IEEE Trans. Signal Process.*, vol. 55, no. 7, pp. 3380–3389, Jul. 2007.
- [129] Y. Kim, J. Yang, and D. Kim, "A closed form approximation of the sum rate upperbound of random beamforming," *IEEE Commun. Lett.*, vol. 12, no. 5, pp. 365–367, May 2008.
- [130] K. Park, Y. Ko, and M. Alouini, "Accurate approximations and asymptotic results for the sum-rate of random beamforming for multi-antenna gaussian broadcast channels," in *Proc. IEEE Vehicular Technology Conference (VTC)*, Apr. 2009, pp. 1–6.
- [131] S. H. Moon, S. R. Lee, and I. Lee, "Sum-rate capacity of random beamforming for multi-antenna broadcast channels with other cell interference," *IEEE Trans. Wireless Commun.*, vol. 10, no. 8, pp. 2440–2444, Aug. 2011.

- [132] Y. Huang and B. D. Rao, "Closed form sum rate of random beamforming," *IEEE Commun. Lett.*, vol. 16, no. 5, pp. 630–633, Mar. 2012.
- [133] H. Yang, P. Lu, H. Sung, and Y. Ko, "Exact sum-rate analysis of MIMO broadcast channels with random unitary beamforming," *IEEE Trans. Commun.*, vol. 59, no. 11, pp. 2982–2986, Nov. 2011.
- [134] P. Svedman, S. K. Wilson, L. J. Cimini Jr, and B. Ottersten, "A simplified opportunistic feedback and scheduling scheme for OFDM," in *Proc. IEEE Vehicular Technology Conference (VTC)*, vol. 4, May 2004, pp. 1878–1882.
- [135] P. Svedman, S. Wilson, L. J. Cimini, and B. Ottersten, "Opportunistic beamforming and scheduling for OFDMA systems," *IEEE Trans. Commun.*, vol. 55, no. 5, pp. 941–952, May 2007.
- [136] M. Fakhereddin, M. Sharif, and B. Hassibi, "Reduced feedback and random beamforming for OFDM MIMO broadcast channels," *IEEE Trans. Commun.*, vol. 57, no. 12, pp. 3827–3835, Dec. 2009.
- [137] Y. Huang and B. D. Rao, "Performance analysis of random beamforming with heterogeneous users," in *Proc. Conference on Information Sciences and Systems (CISS)*, Mar. 2012, pp. 1–5.
- [138] K. Joag-Dev and F. Proschan, "Negative association of random variables with applications," *The Annals of Statistics*, vol. 11, no. 1, pp. 286–295, Mar. 1983.
- [139] S. I. Resnick, "Tail equivalence and its applications," *Journal of Applied Probability*, pp. 136–156, 1971.
- [140] Y. Huang and B. D. Rao, "Random beamforming with heterogeneous users and selective feedback: individual sum rate and individual scaling laws," *IEEE Trans. Wireless Commun.*, 2012, submitted.
- [141] M. Chiang, P. Hande, T. Lan, and C. W. Tan, *Power Control in Wireless Cellular Networks*. NOW Publishers, 2008, vol. 2, no. 4.
- [142] C. Chuah, D. Tse, J. Kahn, and R. Valenzuela, "Capacity scaling in MIMO wireless systems under correlated fading," *IEEE Trans. Inf. Theory*, vol. 48, no. 3, pp. 637–650, Mar. 2002.
- [143] A. Tulino, A. Lozano, and S. Verdu, "Impact of antenna correlation on the capacity of multiantenna channels," *IEEE Trans. Inf. Theory*, vol. 51, no. 7, pp. 2491–2509, Jul. 2005.
- [144] S. Kandukuri and S. Boyd, "Optimal power control in interference-limited fading wireless channels with outage-probability specifications," *IEEE Trans. Wireless Commun.*, vol. 1, no. 1, pp. 46–55, Jan. 2002.

- [145] J. Papandriopoulos, J. Evans, and S. Dey, "Optimal power control for Rayleigh-faded multiuser systems with outage constraints," *IEEE Trans. Wireless Commun.*, vol. 4, no. 6, pp. 2705–2715, Nov. 2005.
- [146] R. D. Yates, "A framework for uplink power control in cellular radio systems," *IEEE J. Sel. Areas Commun.*, vol. 13, no. 7, pp. 1341–1347, Sept. 1995.
- [147] S. Ghosh, B. D. Rao, and J. R. Zeidler, "Outage-efficient strategies for multiuser MIMO networks with channel distribution information," *IEEE Trans. Signal Process.*, vol. 58, no. 12, pp. 6312–6324, Dec. 2010.
- [148] C. W. Tan, "Optimal power control in Rayleigh-fading heterogeneous networks," in *IEEE INFOCOM*, Apr. 2011, pp. 2552–2560.
- [149] U. Krause, "Concave Perron-Frobenius theory and applications," *Nonlinear Analysis*, vol. 47, no. 3, pp. 1457–1466, 2001.
- [150] F. Rashid-Farrokhi, K. J. R. Liu, and L. Tassiulas, "Transmit beamforming and power control for cellular wireless systems," *IEEE J. Sel. Areas Commun.*, vol. 16, no. 8, pp. 1437–1450, Oct. 1998.
- [151] B. Song, R. L. Cruz, and B. D. Rao, "Network duality for multiuser MIMO beamforming networks and applications," *IEEE Trans. Commun.*, vol. 55, no. 3, pp. 618–630, Mar. 2007.
- [152] Y. Huang, C. W. Tan, and B. D. Rao, "Multicell network duality with instantaneous and statistical channel information: a nonlinear Perron-Frobenius characterization," in *Proc. Conference on Information Sciences and Systems (CISS)*, Mar. 2012, pp. 1–6.
- [153] A. Annamalai, C. Tellambura, and V. K. Bhargava, "Simple and accurate methods for outage analysis in cellular mobile radio systems—a unified approach," *IEEE Trans. Commun.*, vol. 49, no. 2, pp. 303–316, Feb. 2001.
- [154] Y. Huang, C. W. Tan, and B. D. Rao, "Cooperative beamforming in multiuser MIMO networks: fast SINR fairness algorithms," in *Proc. IEEE Global Communications Conferences (Globecom)*, Dec. 2012, pp. 1–6.
- [155] C. W. Tan, M. Chiang, and R. Srikant, "Maximizing sum rate and minimizing MSE on multiuser downlink: optimality, fast algorithms and equivalence via max-min SINR," *IEEE Trans. Signal Process.*, vol. 59, no. 12, pp. 6127–6143, Dec. 2011.
- [156] A. Wiesel, Y. C. Eldar, and S. Shamai, "Linear precoding via conic optimization for fixed MIMO receivers," *IEEE Trans. Signal Process.*, vol. 54, no. 1, pp. 161–176, Jan. 2006.

- [157] A. F. Molisch, "A generic model for MIMO wireless propagation channels in macro- and microcells," *IEEE Trans. Signal Process.*, vol. 52, no. 1, pp. 61–71, Jan. 2004.
- [158] Y. Huang, C. W. Tan, and B. D. Rao, "Outage balancing in multiuser MISO networks: network duality and algorithms," in *Proc. IEEE Global Communications Conferences (Globecom)*, Dec. 2012, pp. 1–6.
- [159] M. K. Karakayali, G. J. Foschini, and R. A. Valenzuela, "Network coordination for spectrally efficient communications in cellular systems," *IEEE Trans. Wireless Commun.*, vol. 13, no. 4, pp. 56–61, Aug. 2006.
- [160] S. S. Christensen, R. Agarwal, E. Carvalho, and J. Cioffi, "Weighted sum-rate maximization using weighted MMSE for MIMO-BC beamforming design," *IEEE Trans. Wireless Commun.*, vol. 7, no. 12, pp. 4792–4799, Dec. 2008.
- [161] L. Venturino, N. Prasad, and X. Wang, "Coordinated linear beamforming in downlink multi-cell wireless networks," *IEEE Trans. Wireless Commun.*, vol. 9, no. 4, pp. 1451–1461, Apr. 2010.
- [162] G. J. Foschini and Z. Miljanic, "A simple distributed autonomous power control algorithm and its convergence," *IEEE Trans. Veh. Technol.*, vol. 42, no. 4, pp. 641–646, Nov. 1993.
- [163] E. Visotsky and U. Madhow, "Optimum beamforming using transmit antenna arrays," in *IEEE Veh. Technol. Conf. (VTC)*, vol. 1, Jul. 1999, pp. 851–856.
- [164] M. Schubert and H. Boche, "Solution of the multiuser downlink beamforming problem with individual SINR constraints," *IEEE Trans. Veh. Technol.*, vol. 53, no. 1, pp. 18–28, Jan. 2004.
- [165] W. Yu, "Uplink-downlink duality via minimax duality," *IEEE Trans. Inf. Theory*, vol. 52, no. 2, pp. 361–374, Feb. 2006.
- [166] W. Yang and G. Xu, "Optimal downlink power assignment for smart antenna systems," in *IEEE Int. Conf. Acoust., Speech and Signal Process. (ICASSP)*, vol. 6, May 1998, pp. 3337–3340.
- [167] D. W. H. Cai, T. Q. S. Quek, and C. W. Tan, "A unified analysis of max-min weighted SINR for MIMO downlink system," *IEEE Trans. Signal Process.*, vol. 59, no. 8, pp. 3850–3862, Feb. 2011.
- [168] T. L. Marzetta, "Noncooperative cellular wireless with unlimited numbers of base station antennas," *IEEE Trans. Wireless Commun.*, vol. 9, no. 11, pp. 3590–3600, Nov. 2010.

- [169] J. Jose, A. Ashikhmin, T. L. Marzetta, and S. Vishwanath, "Pilot contamination and precoding in multi-cell TDD systems," *IEEE Trans. Wireless Commun.*, vol. 10, no. 8, pp. 2640–2651, Aug. 2011.
- [170] F. Rusek, D. Persson, B. K. Lau, E. G. Larsson, T. L. Marzetta, O. Edfors, and F. Tufvesson, "Scaling up MIMO: opportunities and challenges with very large arrays," *IEEE Signal Process. Mag.*, 2012. [Online]. Available: arXiv:1201.3210
- [171] A. M. Tulino and S. Verdú, *Random Matrix Theory and Wireless Communications*. Foundations and Trends in Communications and Information Theory, 2004.
- [172] R. Couillet and M. Debbah, *Random Matrix Methods for Wireless Communications*. Cambridge Univ Pr, 2011.
- [173] D. N. C. Tse and S. V. Hanly, "Linear multiuser receivers: effective interference, effective bandwidth and user capacity," *IEEE Trans. Inf. Theory*, vol. 45, no. 2, pp. 641–657, Mar. 1999.
- [174] S. Lakshminaryana, J. Hoydis, M. Debbah, and M. Assaad, "Asymptotic analysis of distributed multi-cell beamforming," in *IEEE Personal Indoor and Mobile Radio Communications (PIMRC)*, Sept. 2010, pp. 2105–2110.
- [175] H. Huh, A. M. Tulino, and G. Caire, "Network MIMO with linear zero-forcing beamforming: large system analysis, impact of channel estimation and reduced-complexity scheduling," *IEEE Trans. Inf. Theory*, vol. 58, no. 5, pp. 2911–2934, May 2012.
- [176] S. Wagner, R. Couillet, M. Debbah, and D. Slock, "Large system analysis of linear precoding in correlated MISO broadcast channels under limited feedback," *IEEE Trans. Inf. Theory*, vol. 58, no. 7, pp. 4509–4537, Jul. 2012.
- [177] C. B. Peel, B. M. Hochwald, and A. L. Swindlehurst, "A vector-perturbation technique for near-capacity multiantenna multiuser communication-part I: channel inversion and regularization," *IEEE Trans. Commun.*, vol. 53, no. 1, pp. 195–202, Jan. 2005.
- [178] R. Zakhour and S. V. Hanly, "Base station cooperation on the downlink: large system analysis," *IEEE Trans. Inf. Theory*, vol. 58, no. 4, pp. 2079–2106, Apr. 2012.
- [179] W. Hachem, P. Loubaton, and J. Najim, "Deterministic equivalents for certain functionals of large random matrices," *Ann. Appl. Probab.*, vol. 17, no. 3, pp. 875–930, 2007.

- [180] A. Berman and R. Plemmons, *Nonnegative Matrices in the Mathematical Sciences*. New York: Academic, 1979.
- [181] S. Boyd, A. Ghosh, B. Prabhakar, and D. Shah, "Randomized gossip algorithms," *IEEE Trans. Inf. Theory*, vol. 52, no. 6, pp. 2508–2530, Jun. 2006.
- [182] Y. Huang, C. W. Tan, and B. D. Rao, "Asymptotic analysis of max-min weighted SINR in multiuser downlink," in *Proc. Conference on Information Sciences and Systems (CISS)*, Mar. 2012, pp. 1–5.
- [183] J. Dumont, W. Hachem, S. Lasaulce, P. Loubaton, and J. Najim, "On the capacity achieving covariance matrix for Rician MIMO channels: an asymptotic approach," *IEEE Trans. Inf. Theory*, vol. 56, no. 3, pp. 1048–1069, Mar. 2010.
- [184] G. Taricco and E. Riegler, "On the ergodic capacity of correlated Rician fading MIMO channels with interference," *IEEE Trans. Inf. Theory*, vol. 57, no. 7, pp. 4123–4137, Jul. 2011.
- [185] C. Artigue and P. Loubaton, "On the precoder design of flat fading MIMO systems equipped with MMSE receivers: a large-system approach," *IEEE Trans. Inf. Theory*, vol. 57, no. 7, pp. 4138–4155, Jul. 2011.
- [186] R. Couillet, M. Debbah, and J. W. Silverstein, "A deterministic equivalent for the analysis of correlated MIMO multiple access channels," *IEEE Trans. Inf. Theory*, vol. 57, no. 6, pp. 3493–3514, Jun. 2011.
- [187] J. Zhang, C. K. Wen, S. Jin, X. Gao, and K. K. Wong, "On capacity of large-scale MIMO multiple access channels with distributed sets of correlated antennas," *IEEE J. Sel. Areas Commun.*, 2012. [Online]. Available: arXiv:1209.5513
- [188] A. Kammoun, M. Kharouf, W. Hachem, and J. Najim, "A central limit theorem for the SINR at the LMMSE estimator output for large-dimensional signals," *IEEE Trans. Inf. Theory*, vol. 55, no. 11, pp. 5048–5063, Nov. 2009.
- [189] Y. Huang, C. W. Tan, and B. D. Rao, "Joint beamforming and power control in coordinated multicell: max-min duality, effective network and large system transition," *IEEE Trans. Wireless Commun.*, 2012, minor revision, revised.
- [190] Z. D. Bai and J. W. Silverstein, "No eigenvalue outside the support of the limiting spectral distribution of large dimensional sample covariance matrices," *Ann. Probab.*, vol. 26, no. 1, pp. 316–345, 1998.
- [191] J. W. Silverstein and Z. D. Bai, "On the empirical distribution of eigenvalues of a class of large dimensional random matrices," *Journal of Multivariate Analysis*, vol. 54, no. 2, pp. 175–192, 1995.

- [192] A. P. T. Lau and F. R. Kschischang, "Feedback quantization strategies for multiuser diversity systems," *IEEE Trans. Inf. Theory*, vol. 53, no. 4, pp. 1386–1400, Apr. 2007.
- [193] Y. Al-Harhi, A. H. Tewfik, and M. S. Alouini, "Multiuser diversity with quantized feedback," *IEEE Trans. Wireless Commun.*, vol. 6, no. 1, pp. 330–337, Jan. 2007.
- [194] H. Shirani-Mehr and G. Caire, "Channel state feedback schemes for multiuser MIMO-OFDM downlink," *IEEE Trans. Commun.*, vol. 57, no. 9, pp. 2713–2723, Sept. 2009.
- [195] O. Ozdemir and M. Torlak, "Optimum feedback quantization in an opportunistic beamforming scheme," *IEEE Trans. Wireless Commun.*, vol. 9, no. 5, pp. 1584–1593, May 2010.
- [196] Y. Huang and B. D. Rao, "Sum rate analysis and quantizer design for a quantized heterogeneous feedback MIMO OFDMA downlink," in *Proc. Asilomar Conference on Signals, Systems, and Computers*, Nov. 2012, pp. 1–5.
- [197] P. P. Gandhi, "Optimum quantization of order statistics," *IEEE Trans. Signal Process.*, vol. 45, no. 9, pp. 2153–2159, Sept. 1997.
- [198] V. Misra, V. K. Goyal, and L. R. Varshney, "Distributed scalar quantization for computing: high-resolution analysis and extensions," *IEEE Trans. Inf. Theory*, vol. 57, no. 8, pp. 5298–5325, Aug. 2011.
- [199] A. H. Nguyen, Y. Huang, and B. D. Rao, "Weighted CDF-based scheduling for an OFDMA relay downlink with partial feedback," in *Proc. Asilomar Conference on Signals, Systems, and Computers*, Nov. 2012, pp. 1–5.
- [200] A. Saleh, A. Rustako, and R. Roman, "Distributed antennas for indoor radio communications," *IEEE Trans. Commun.*, vol. 35, no. 12, pp. 1245–1251, Dec. 1987.
- [201] K. Kerpez, "A radio access system with distributed antennas," *IEEE Trans. Veh. Technol.*, vol. 45, no. 2, pp. 265–275, May 1996.
- [202] H. Zhu, "Performance comparison between distributed antenna and microcellular systems," *IEEE J. Sel. Areas Commun.*, vol. 29, no. 6, pp. 1151–1163, Jun. 2011.
- [203] R. Heath, T. Wu, Y. Kwon, and A. Soong, "Multiuser MIMO in distributed antenna systems with out-of-cell interference," *IEEE Trans. Signal Process.*, vol. 59, no. 10, pp. 4885–4899, Oct. 2011.

- [204] Y. Huang and B. D. Rao, "Opportunistic beamforming in a downlink distributed antenna system with linear receivers," in *Proc. International Conference on Signal Processing and Communications (SPCOM)*, Jul. 2012, pp. 1–5.
- [205] K. Doppler, M. Rinne, C. Wijting, C. Ribeiro, and K. Hugl, "Device-to-device communication as an underlay to LTE-advanced networks," *IEEE Commun. Mag.*, vol. 47, no. 12, pp. 42–49, Dec. 2009.
- [206] G. Fodor, E. Dahlman, G. Mildh, S. Parkvall, N. Reider, G. Miklós, and Z. Turányi, "Design aspects of network assisted device-to-device communications," *IEEE Commun. Mag.*, vol. 50, no. 3, pp. 170–177, Mar. 2012.
- [207] W. Yu and T. Lan, "Transmitter optimization for the multi-antenna downlink with per-antenna power constraints," *IEEE Trans. Signal Process.*, vol. 55, no. 6, pp. 2646–2660, Jun. 2007.
- [208] D. W. H. Cai, T. Q. S. Quek, C. W. Tan, and S. H. Low, "Max-min SINR coordinated multipoint downlink transmission-duality and algorithms," *IEEE Trans. Signal Process.*, vol. 60, no. 10, pp. 5384–5395, Oct. 2012.
- [209] Y. Huang, C. W. Tan, and B. D. Rao, "Large system analysis of power minimization in multiuser MISO downlink with transmit-side channel correlation," in *Proc. International Symposium on Information Theory and its Applications (ISITA)*, Oct. 2012, pp. 240–244.
- [210] R. W. Thomas, D. H. Friend, L. A. DaSilva, and A. B. MacKenzie, "Cognitive networks: adaptation and learning to achieve end-to-end performance objectives," *IEEE Commun. Mag.*, vol. 44, no. 12, pp. 51–57, Dec. 2006.
- [211] J. Mitola III and G. Q. Maguire Jr, "Cognitive radio: making software radios more personal," *IEEE Pers. Commu.*, vol. 6, no. 4, pp. 13–18, Aug. 1999.
- [212] S. Haykin, "Cognitive radio: brain-empowered wireless communications," *IEEE J. Sel. Areas Commun.*, vol. 23, no. 2, pp. 201–220, Feb. 2005.
- [213] C. Prehofer and C. Bettstetter, "Self-organization in communication networks: principles and design paradigms," *IEEE Commun. Mag.*, vol. 43, no. 7, pp. 78–85, Jul. 2005.
- [214] S. Dixit, E. Yanmaz, and O. K. Tonguz, "On the design of self-organized cellular wireless networks," *IEEE Commun. Mag.*, vol. 43, no. 7, pp. 86–93, Jul. 2005.
- [215] E. Bonabeau, M. Dorigo, and G. Theraulaz, *Swarm Intelligence: From Natural to Artificial Systems*. Oxford University Press, 1999.

- [216] S. Camazine, J. L. Deneubourg, N. R. Franks, J. Sneyd, G. Theraula, and E. Bonabeau, *Self-Organization in Biological Systems*. Princeton University Press, 2003.
- [217] F. Dressler and O. Akan, “Bio-inspired networking: from theory to practice,” *IEEE Commun. Mag.*, vol. 48, no. 11, pp. 176–183, Nov. 2010.
- [218] Y. Huang, F. Lu, and B. D. Rao, “Swarm of mobile phones: towards learning large-scale channel map,” UCSD, Tech. Rep., 2010, Qualcomm Innovation Fellowship 2010 Finalist.